BOWEN VOLUME
PART TWO

American Journal of Science

Established in 1818 by Benjamin Silliman

EDITORS
CHESTER R. LONGWELL - JOHN RODGERS

ASSOCIATE EDITORS

REGINALD A. DALY — A. F. BUDDINGTON
CAMBRIDGE, MASS. — PRINCETON, N. J.

CARL O. DUNBAR — RICHARD F. FLINT
HENRY MARGENAU — HAROLD G. CASSIDY
HORACE WINCHELL — G. EVELYN HUTCHINSON
NEW HAVEN, CONN.

LEASON H. ADAMS — WILMOT H. BRADLEY
WASHINGTON, D. C.

WILLIAM H. TWENHOFEL — HOWEL WILLIAMS
ORLANDO, FLORIDA — BERKELEY, CALIF.

FREDERICK J. ALCOCK — CECIL E. TILLEY
OTTAWA, CANADA — CAMBRIDGE, ENGLAND

GEORGE GAYLORD SIMPSON — ADOLPH KNOPF
NEW YORK, N. Y. — STANFORD, CALIF.

STERLING TOWER
NEW HAVEN, CONNECTICUT
1952

PAYNE & LANE, *Printers*, New Haven, Conn.

Printed in the United States of America

American Journal of Science

Established in 1818 by Benjamin Silliman

EDITORS

CHESTER R. LONGWELL - JOHN RODGERS

ASSOCIATE EDITORS

REGINALD A. DALY, CAMBRIDGE, MASS. — A. F. BUDDINGTON, PRINCETON, N. J.

CARL O. DUNBAR — RICHARD F. FLINT

HENRY MARGENAU — HAROLD G. CASSIDY

HORACE WINCHELL — G. EVELYN HUTCHINSON

NEW HAVEN, CONN.

LEASON H. ADAMS — WILMOT H. BRADLEY

WASHINGTON, D. C.

WILLIAM H. TWENHOFEL, ORLANDO, FLORIDA — HOWEL WILLIAMS, BERKELEY, CALIF.

FREDERICK J. ALCOCK, OTTAWA, CANADA — CECIL E. TILLEY, CAMBRIDGE, ENGLAND

GEORGE GAYLORD SIMPSON, NEW YORK, N. Y. — ADOLPH KNOPF, STANFORD, CALIF.

BOWEN VOLUME

PART TWO

NEW HAVEN, CONNECTICUT

1952

TABLE OF CONTENTS

PART ONE

List of Systems Investigated at Geophysical Laboratory
Leason H. Adams 1

The Differentiation of a Composite Aplite from the Priblof Islands, Alaska ..... *Tom. F. W. Barth* 27

Chemical Petrology of Some Metamorphosed Adirondack Gabbroic, Syenitic and Quartz Syenitic Rocks
A. F. Buddington 37

Relations between Composition and Indices of Refraction in Natural Plagioclase ..... *F. Chayes* 85

Two New Crystalline Phases of the Anorthite Composition, $CaO \cdot Al_2O_3 \cdot 2SiO_2$ ..... *G. L. Davis and O. F. Tuttle* 107

The Symmetry Change in the High-Temperature Alkali-Feldspar Series ..*Gabrielle Donnay* and *J. D. H. Donnay* 115

On the Granulites of Lapland ..... *Pentti Eskola* 133

Orthopyroxenes of the Bushveld Type, Ion Substitutions, and Changes in Unit Cell Dimensions ..... *H. H. Hess* 173

Twinning Frequency in Feldspar Phenocrysts from a Quartz Latite Sill at Sierra Blanca, Texas ..... *Earl Ingerson* 189

Significance of Variation in the High-Low Inversion of Quartz
M. L. Keith and *O. F. Tuttle* 203

Japanese Twins of Quartz ..... *S. Kozu* 281

Thermochemistry of Plagioclase and Alkali Feldspars
F. C. Kracek and *K. J. Neuvonen* 293

PART TWO

The Effect of Temperature on the Symmetry of High Temperature Soda-Rich Feldspars *Wm. S. MacKenzie* 319

The System H_2O—Na_2O—SiO_2 at 400° C.
G. W. Morey and *J. M. Hesselgesser* 343

Heat of Formation of Merwinite and Monticellite
K. J. Neuvonen 373

The Chemistry of the Keweenawan Lavas ..... *Paul Niggli* 381

The System Diopside—Forsterite—Anorthite
E. F. Osborn and *D. B. Tait* 413

A Reconnaissance of Liquidus Relations in the System $K_2O \cdot 2SiO_2$—FeO—SiO_2 ..... *Edwin Roedder* 435

Leucite, Potash Nepheline, and Clinopyroxene from Volcanic Lavas from Southwestern Uganda and Adjoining Belgian Congo ..... *Th. G. Sahama* 457

The System FeO—Al_2O_3—SiO_2
J. F. Schairer and *Kenzo Yagi* 471

Single-Crystal Measurements on Paracelsian .... *J. V. Smith* 513

Temperature Scales and Silicate Research .... *R. B. Sosman* 517

Some Trends of Basaltic Magma in Limestone Syntexis
C. E. Tilley 529

The Angle between the *a*-Axis and the Trace of the Rhombic Section on the {010}-Pinacoid in the Plagioclases
George Tunell 547

Optical Studies on Alkali Feldspars ..... *O. F. Tuttle* 553

The MgO—Al_2O_3—SiO_2—H_2O System and the Related Metamorphic Facies ..... *H. S. Yoder, Jr.* 569

American Journal of Science
Bowen Volume
PART TWO

THE EFFECT OF TEMPERATURE ON THE SYMMETRY OF HIGH-TEMPERATURE SODA-RICH FELDSPARS

WM. SCOTT MACKENZIE

ABSTRACT. X-ray and optical data show that natural anorthoclase and synthetic soda-rich feldspars, triclinic at room temperature, acquire monoclinic symmetry on heating. On cooling the reverse process takes place. The experimental results suggest that there are two triclinic forms of synthetic high albite and adjacent feldspars. The temperature at which the symmetry becomes monoclinic differs in the two forms and there are slight differences in the X-ray powder diffraction patterns at room temperature.

The inversion temperatures of natural anorthoclases may prove useful in geologic thermometry.

INTRODUCTION

THE dry-melt studies of Schairer and Bowen (1935) and of Schairer (1950) and the hydrothermal studies of Bowen and Tuttle (1950) indicate that the alkali feldspars form a complete series of solid solutions of the type with a minimum temperature of melting. The change of symmetry at about $Or_{35}Ab_{65}$[1] (Donnay and Donnay, 1952) has introduced a difficulty since there is no apparent discontinuity in the liquidus curve of the series, and a solid solution series involving a change in symmetry is unknown in other silicate systems. The possibility of a transformation from triclinic to monoclinic symmetry in the case of high albite was investigated by Tuttle and Bowen (1950) by means of differential heating curves, but no evidence of a heat effect was found. In the same communication it is reported that G. L. Davis, from careful examination of the X-ray powder spectra of samples at elevated temperatures, concluded that there was no clear evidence of such an inversion. In spite of these inconclusive results, Tuttle and Bowen were of the opinion that the possibility still exists of a non-quenchable, order-disorder transformation, which would result in a gradual change in cell constants with increasing temperature to monoclinic symmetry.

[1] All compositions are given as weight per cent.

In order to test this belief, the triclinic members of the alkali feldspar series were investigated at elevated temperatures by X-ray and optical methods. The details of the methods used and the results obtained are described in the following pages. These results confirm the belief, held by Tuttle and Bowen, that a gradual change in cell constants to monoclinic symmetry does take place with rising temperature for the triclinic members of the alkali feldspar series.[2] In addition, a few synthetic plagioclases have been investigated in order to find the effect of lime on the temperature at which the transformation to monoclinic symmetry takes place and also to find whether the high-temperature sodic-plagioclases crystallized with monoclinic symmetry.

Only homogeneous materials were used for this study, and in cases where unmixing to two phases occurred in the natural minerals these were homogenized by heating at 900° C. for 24 hours.

X-RAY EXPERIMENTAL METHODS

A high-temperature furnace, suitable for mounting on a Philips back-reflection X-ray spectrometer, was used for the X-ray investigations. The furnace was a modification by G. L. Davis of the apparatus described by Birks and Friedman (1947). The thermocouple had been calibrated by Davis using the following fixed points on the temperature scale; CsCl transition point, 479° C.; KCl melting point, 770° C.; K_2SO_4 transition point, 588° C., and melting point 1076° C. The sample to be studied, ground to a few microns in particle size, was pressed into a fine mesh of platinum wire mounted on a sheet of platinum, through which a small hole carried the 10 per cent Rh lead of the Pt-10 per cent Rh thermocouple. The platinum wire mesh served both to retain the sample on the flat sample holder and to ensure a more even temperature distribution through the sample. The thermocouple junction was made at the center of the sample, the platinum sheet constituting the Pt element of the junction. In addition to measurements at elevated temperature one measurement was made below room temperature and this was accomplished by filling the space in the furnace below the sample with solid CO_2.

In an accompanying paper, Donnay and Donnay show that

[2] Dr. Laves independently found the transformation to monoclinic symmetry by extinction angle measurements on natural anorthoclases using a high-temperature stage on the petrographic microscope. (Personal communication to Dr. Bowen.)

a useful criterion for determining the symmetry of an alkali feldspar is the separation or coincidence of the 111 and $1\bar{1}1$ reflections in X-ray powder diffraction patterns. In the case of monoclinic symmetry only one reflection representing both 111 and $1\bar{1}1$ is observed. For the present investigation the absolute readings of the interplanar spacings were neglected, the difference in the spacings of the (111) and ($1\bar{1}1$) planes being used as a measure of the amount of departure from monoclinic symmetry. It was found that in the case of triclinic alkali feldspars the 111 and $1\bar{1}1$ reflections converge gradually with increasing temperature and finally coincide, the coincidence persisting when heating is carried to still higher temperatures. Only by single crystal X-ray studies at elevated temperatures can it be shown that the symmetry becomes truly monoclinic as distinct from pseudo-monoclinic symmetry.

At room temperature the peaks produced on the spectrometer charts by the (111) and ($1\bar{1}1$) planes are uniquely resolved in the triclinic members of the alkali feldspar series from $Or_{30}Ab_{70}$ to $Or_{20}Ab_{80}$. With increasing content of albite the 111 reflection merges into the $1\bar{3}0$ reflection until, in pure albite, it is completely obscured. However, with an increase in temperature, the 111 reflection becomes completely resolved and its angular separation from the $1\bar{1}1$ reflection can be measured. This is also the case for the plagioclases used in this study, i.e., from Ab to $Ab_{70}An_{30}$. The $11\bar{2}$ and $1\bar{1}2$ reflections might have been used in place of 111 and $1\bar{1}1$. The disadvantage, however, is that $11\bar{2}$ is part of a peak consisting of several reflections at room temperature for all compositions between Or_{35} Ab_{65} and Ab. The value of $2\theta_{111} - 2\theta_{1\bar{1}1}$ (CuK_α) is .875° for synthetic albite (Donnay and Donnay, 1952) so that only a small angle need be scanned at each temperature. The recorder of the X-ray spectrometer was adjusted so that two peaks having this angular difference were approximately two inches apart and the Geiger counter scanning speed set to give a change in 2θ of .25° per minute. Figure 1 shows the variation, with temperature, of the distance between the 111 and $1\bar{1}1$ reflections for two synthetic feldspar compositions.

Although the surface of the powder sample used was only 10 x 15 mm., the heating element must of necessity also be fairly small, so that the temperature distribution over the surface cannot be considered uniform, especially at high temperatures. This becomes clear when synthetic albite (m.p. 1118°

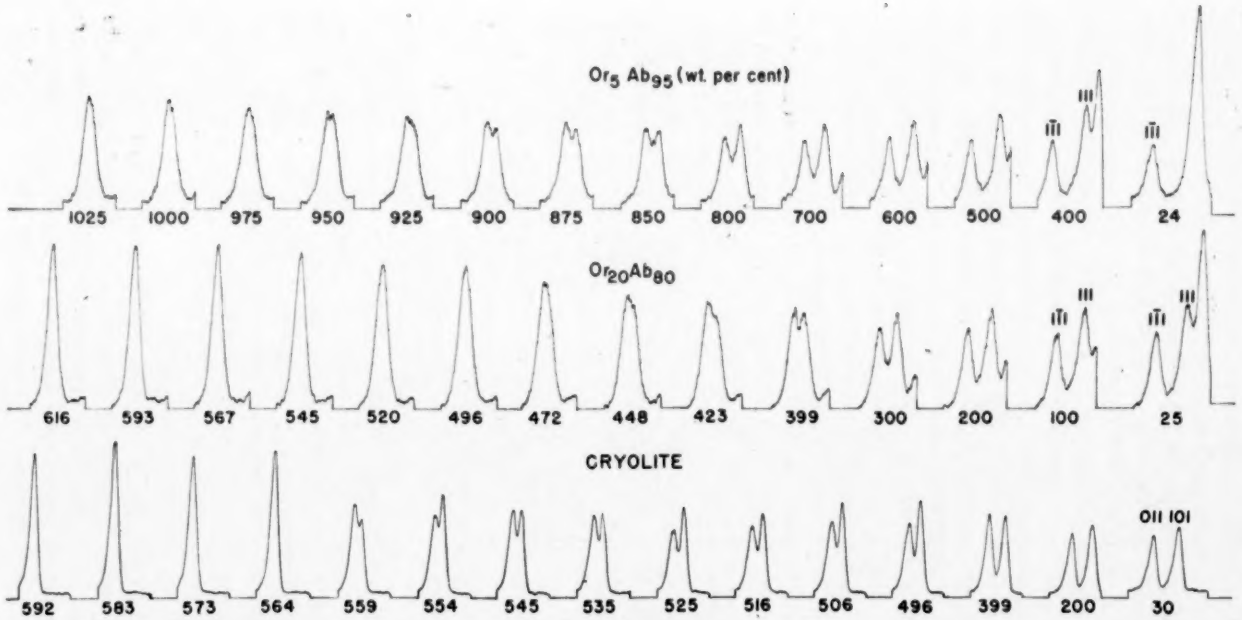

Fig. 1. X-ray diffraction charts of two synthetic feldspars crystallized at 800° C. and 1000 kg/cm² pressure of H_2O showing the gradual convergence of the 111 and 1$\bar{1}$1 reflections with rise in temperature. For comparison the convergence of the 011 and 101 reflections of cryolite with rise in temperature is shown. Under each pair of peaks, or single peak when the two converge, the temperature in degrees centigrade at which the record was made is given.

± 3° C.), prepared hydrothermally, can be seen to have melted in small patches on the surface of the specimen although the maximum temperature recorded by the thermocouple was only 1075° C. The accuracy of the temperature measurements in the region of 560° C. was checked at intervals during the course of the investigation by determining the inversion temperature of a sample of cryolite from Ivigtut, West Greenland. The inversion temperature of this sample has been accurately determined to be 562.7°—563.0° C. (Keith and Tuttle, 1952) by the method of differential heating curves. It is estimated that the error in temperature measurement at this temperature is about ± 5°, but it would be difficult to estimate the error in the region of 1000° C. A rough check on the reproducibility of the temperature measurements was made by using two variacs in series so that the temperature could be accurately set by the second variac. The temperatures recorded by the thermocouple were marked on the dial of the second variac and by using the same settings of the variac for successive runs it was found that the temperatures were within 5° C. of the marked temperature. The error of measurement of the position of a peak is somewhat less than 0.01° in 2θ except where two peaks overlap with a consequent displacement of the maximum of each peak.

The method used to determine the inversion temperature was as follows. For each feldspar composition studied the difference in 2θ of the 111 and $1\bar{1}1$ reflections was plotted against temperature from the lowest temperature at which the two peaks were discernible up to the highest temperature at which they were still clearly resolved from each other. The smooth curve obtained by joining the points so obtained was extrapolated to zero angular difference, the point of intersection with the zero line representing the temperature at which the 111 and $1\bar{1}1$ reflections should coincide. This temperature has been taken as the inversion temperature. The values of $2\theta_{111} - 2\theta_{1\bar{1}1}$ measured at different temperatures are given in table 1 for all the synthetic feldspar compositions studied, and these values are plotted in figure 2. The reproducibility of the measurements can be seen from these results in which the average angular difference in duplicate measurements is .015°.

Whether this gradual change resulting in a structure with monoclinic symmetry can be classed as an inversion may be a

matter of some doubt; however, for the present discussion it is convenient to describe it as such. Since the alkali feldspars form a solid solution series there should be a range of temperature within which both the triclinic and monoclinic forms are stable if this is a true inversion. Only one temperature, which probably lies within this inversion interval, has actually been determined, and when the term "inversion temperature" is used in the subsequent discussion, it is to be understood that this refers to one point within the supposed two-crystal region. The accuracy of the present determinations of this temperature for those compositions which invert below 600° C. is estimated to be about ± 10° C. In the region of 1000° C. the error in the determinations may be of the order of ± 30° C. but this seemingly large error does not influence the nature of the general relations at these temperatures.

From figure 1 it can be seen that when the 111 and $1\bar{1}1$ peaks merge to form a single peak, there is a gradual increase

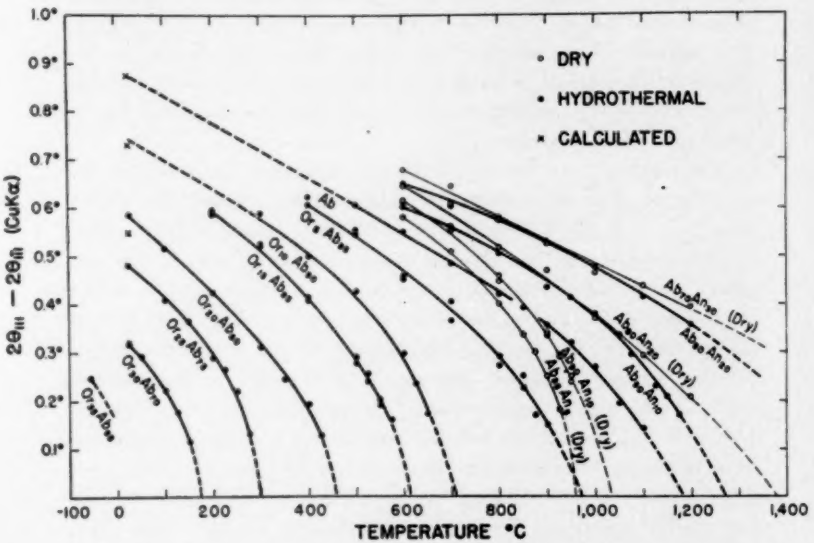

Fig. 2. The difference in 2θ of the 111 and $1\bar{1}1$ reflections of synthetic feldspars plotted against temperature. The curves for the hydrothermally crystallized materials are drawn in heavier lines than those for "dry" crystallization. The crosses indicate the calculated values of $2\theta_{111} - 2\theta_{1\bar{1}1}$ from the data obtained at room temperature by Donnay and Donnay (1952).

in the height of the single peak, owing to the addition of the 111 and $1\bar{1}1$ reflections with increasing temperature up to a temperature above which the peak height remains constant; the decreasing peak width becomes constant at about the same temperature. Slight variations in peak height and width are to be expected, but these do not obscure the general trend. The inversion temperature of $Or_{20}Ab_{80}$ has been determined to be 460° C. by the method of extrapolating to zero angular difference the 111 and $1\bar{1}1$ reflections as described above, and in figure 1 it can be seen that the peak height continues to increase with increasing temperature up to 567° C. after which it remains fairly constant. It was thought that the temperature at which the peak reached a constant height, or a constant width at half-height, might be used as an indication of the upper temperature of the two-crystal region. But it was found that the values so obtained were not as reproducible as those obtained by the method described above, and for this reason the figures are not quoted.

OPTICAL METHODS

For the optical investigation of the change of symmetry, the crystal to be studied was contained in a small silica glass vessel placed in an electric furnace. The furnace was suitable for mounting on the stage of a petrographic microscope, its upper and lower surfaces being cooled by chambers through which water was circulating. Convection currents of air through the furnace were prevented by covering the hole through which the crystal was to be observed with a thin silica glass cover slip. The temperature of the crystal was measured by means of a Pt-10 per cent Rh thermocouple, the leads of which were passed through holes drilled in the wall of the silica glass container. In this way the thermocouple junction was kept very close to the crystal to ensure accurate measurement of the temperature of the crystal.

The criterion used for determining the temperature of inversion was the disappearance on heating and reappearance on cooling of the fine albite twinning lamellae. Since this could be done only with crystals in which the twinning was easily observed, only natural anorthoclases lent themselves to investigation in this manner. For temperatures up to about 230° C. cottonseed oil was suitable as an immersion medium. For

TABLE 1

$2\theta_{111}-2\theta_{1\bar{1}1}$ (Cu K_α) For Synthetic Feldspars at Various Temperatures

Crystallized hydrothermally P_{H_2O} = 1000 kg/cm²; T = 800° C.

$Or_{35}Ab_{65}$	—56° C.								
	.247								
$Or_{30}Ab_{70}$	24° C.	50° C.	100° C.	125° C.	150° C.				
	.317	.292	.222	.177	.115				
$Or_{25}Ab_{75}$	24° C.	100° C.	150° C.	200° C.	225° C.	250° C.	275° C.		
	.482	.410	.365	.290	.265	.220	.132		
$Or_{20}Ab_{80}$	26° C.	100° C.	200° C.	300° C.	350° C.	400° C.	425° C.		
	.587	.517	.425	.310	.245	.192	.127		
$Or_{15}Ab_{85}$	200° C.	300° C.	400° C.	500° C.	525° C.	550° C.	575° C.		
	.595	.527	.415	.290	.257	.202	.160		
	.587	.510	.407	.277	.240	.190	...		
$Or_{10}Ab_{90}$	300° C.	400° C.	500° C.	600° C.	625° C.	650° C.			
	.587	.500	.427	.297	.235	.172			
Or_5Ab_{95}	400° C.	500° C.	600° C.	700° C.	800° C.	850° C.	875 C.	900° C.	
	.607	.555	.460	.405	.290	.252	....	.150	
	.622	.545	.452	.365	.272	.227	.170	.150	
Ab	500° C.	600° C.	700° C.	800° C.	900° C.	950° C.	1000° C.	1050° C.	1100° C.
	.605	.552	.485	.420	.355	.320	.270	.195	.142

TABLE 1 (*Cont.*)

$2\theta_{111}-2\theta_{1\bar{1}1}$ (Cu K_α) For Synthetic Feldspars at Various Temperatures

Crystallized hydrothermally P_{H_2O} = 1000 kg/cm²; T = 800° C.

$Ab_{90}An_{10}$	600° C.	700° C.	800° C.	900° C.	950° C.	1000° C.	1050° C.	1075° C.	1125° C.	1150° C.	1175° C.
	.602	.562	.505	.435	.415	.380	.335	.292	.230	.210	.170
$Ab_{80}An_{20}$	600° C.	700° C.	800° C.	900° C.	1000° C.	1100° C.	1200° C.				
	.650	.607	.575	.530	.477	.415	.355				
$Or_{10}Ab_{80}An_{10}$	500° C.	600° C.	700° C.	800° C.	850° C.	900° C.					
	.477	.435	.397	.320	.290	.272					
$Or_{10}Ab_{70}An_{20}$	600° C.	700° C.	800° C.	900° C.	1000° C.	1100° C.					
	.555	.502	.455	.405	.345	.245					
$Or_{20}Ab_{70}An_{10}$	300° C.	350° C.	400° C.	450° C.	500° C.	550° C.					
	.515	.487	.425	.387	.325	.267					

Crystallized dry

$Ab_{95}An_5$	600° C.	700° C.	800° C.	850° C.	875° C.	900° C.	925° C.				
	.582	.510	.400	.335	.300	.250	.182				
$Ab_{90}An_{10}$	600° C.	700° C.	800° C.	850° C.	900° C.	925° C.	950° C.				
	.612	.532	.447	.392	.335	.290	.250				
	.615	.530	.460	...	.340	...	.240				
$Ab_{80}An_{20}$	600° C.	700° C.	800° C.	900° C.	1000° C	1100° C.	1200° C.				
	.645	.605	.520	.470	.370	.292	.207				
$Ab_{70}An_{30}$	600° C.	700° C.	800° C.	900° C.	1000° C.	1100° C.	1200° C.				
	.680	.642	.580	.527	.465	.437	.395				

observations at higher temperatures (001) cleavage fragments were ground to a wedge shape and both surfaces polished to obviate the necessity of an immersion medium. The object of using a wedge shape was to make the crystal easy to handle during polishing, and yet have it thin enough at one end to make the twinning lines appear as sharply as possible under the microscope.

The inversion temperature was determined by raising and lowering the temperature of the sample several times and recording the temperatures at which the fine twinning disappeared and reappeared. Coarse twinning lamellae were found to persist at temperatures above that at which fine lamellae disappeared. The disappearance of the fine lamellae was chosen as an indication of monoclinic symmetry. In table 2 a range of temperature is given for the inversion of two of the natural crystals studied, the higher temperature being that at which the fine twinning disappeared on heating and the lower temperature that at which it reappeared on cooling. From the gradual nature of the change of symmetry shown by the X-ray investigations it might be expected that it would not be possible by optical methods to fix accurately a single temperature for the inversion. For this reason and since only natural minerals were suitable for study by this method, the X-ray data have been used in the subsequent discussion.

In most of the crystals studied it was found that on lowering the temperature from some value above the inversion temperature the fine twinning lines reappeared in the crystal in the same position which they had occupied before heating. In one case, however, a twin lamella, which had not been apparent on first observing the crystal at room temperature, made its appearance on lowering the temperature from above the inversion temperature. In another case when a (001) cleavage fragment, which had been carefully polished by Dr. J. W. Greig of this laboratory to give an optically flat surface on both sides, was heated to 950° C., well above the inversion temperature, striations developed parallel to the trace of the (010) cleavage. These were at first mistaken for fine twinning still persisting above the inversion temperature, but on subsequent examination at room temperature in a liquid, it was found that the microscopic twinning had been competely destroyed and the surface of the crystal was no longer optically

TABLE 2

Inversion Temperatures of Feldspars

(a) Synthetic materials

Hydrothermally crystallized at 800° C. and $P_{H_2O} = 1000$ *kg/cm²*		*Dry crystallized*	
Composition	*Inversion temperature ° C. X-ray*	*Composition*	*Inversion Temp.° C. X-ray*
$Or_{80}Ab_{70}$	175°	$Ab_{95}An_5$	960°
$Or_{25}Ab_{75}$	300°	$Ab_{90}An_{10}$	1035°
$Or_{20}Ab_{80}$	460°	$Ab_{80}An_{20}$	1380°
$Or_{15}Ab_{85}$	615°		
$Or_{10}Ab_{90}$	710°		
Or_5Ab_{95}	970°		
Ab	1180°		
$Ab_{90}An_{10}$	1270°		
$Ab_{80}An_{20}$	> 1500°		
$Or_{10}Ab_{80}An_{10}$	1230°		
$Or_{10}Ab_{70}An_{20}$	1370°		
$Or_{20}Ab_{70}An_{10}$	675°		

(b) Natural feldspars of anorthoclase type

Composition	*Locality*	*Inversion temperature ° C. X-ray*	*optics*
$Or_{21.7}Ab_{66.8}An_{1.8}$	Grande Caldeira I., Azores	100	...
$Or_{28.1}Ab_{61.8}An_{10.1}$	Mt. Kenya, East Africa	140	...
$Or_{23.8}Ab_{75.5}An_{1.2}$	Victoria, Australia	360	...
$Or_{22.0}Ab_{69.5}An_{7.8}$	Ropp, Nigeria	540	555 – 580
$Or_{23.4}Ab_{68.2}An_{8.8}$	Mt. Anakie, Australia	575	560 – 590
$Or_{17.9}Ab_{82.2}An_{19.9}$	Mt. Erebus, Antarctica	600	...

flat but was traversed by a series of ridges parallel to the trace of (010). The indication here appears to be that the crystallographic reorientation, necessitated by the change to monoclinic symmetry, destroyed the flat surface, but it is not certain why the twinning did not reappear in this particular feldspar.

Further optical study of the effect of heat on the twinning may afford more information on the relation between composition or crystallization history and the presence or absence of either albite or pericline twinning in feldspars of anorthoclase type.

RESULTS

The inversion temperatures of both natural and synthetic feldspars were determined by the X-ray method. The synthetic materials were of two types: those crystallized "dry" by Dr. Schairer, and those crystallized hydrothermally by Dr. Tuttle from glasses prepared by Dr. Schairer. A considerable difference was found in the inversion temperatures of both the members of the plagioclase series and of the alkali series depending on the method of crystallization. The inversion temperatures of the synthetic feldspars studied are given in table 2 together with those obtained from six natural feldspars of anorthoclase type by the X-ray method and, in two cases, by the optical method.

In figure 3 the inversion temperatures of the hydrothermal synthetic alkali feldspars have been plotted against composition and a smooth curve drawn through the points. No natural feldspars are included in this diagram, but if the inversion temperature of the two natural minerals which contain less than 2 per cent An are plotted against their (Ab + An) content, the points fall very close to the curve. A ternary diagram, to which reference will be made later, has been constructed (fig. 6), showing the relation between composition and inversion temperature of the natural minerals and hydrothermal synthetic crystals.

Only material which is completely crystalline or nearly so can be used to measure accurately the difference in 2θ between the 111 and $1\bar{1}1$ reflections, since these planes, even at best, do not give strong X-ray reflections. Except in the case of albite, the plagioclase series in the compositional range studied may be obtained "dry" and hydrothermally in well crystallized

form. The alkali feldspars cannot be completely crystallized "dry" (Schairer, 1950) with the result that peaks, sufficiently well resolved for accurate measurements, were not obtained on the powder patterns. From the runs which were made, however, it appears that these "dry" crystallized alkali feldspars invert to monoclinic symmetry at lower temperatures than do the hydrothermally crystallized materials of the same composition. The data for hydrothermally crystallized synthetic feldspars given in tables 1 and 2 were obtained from samples crystallized under only one set of conditions, viz. at 800° C. and P_{H_2O} = 1000 kg/cm².

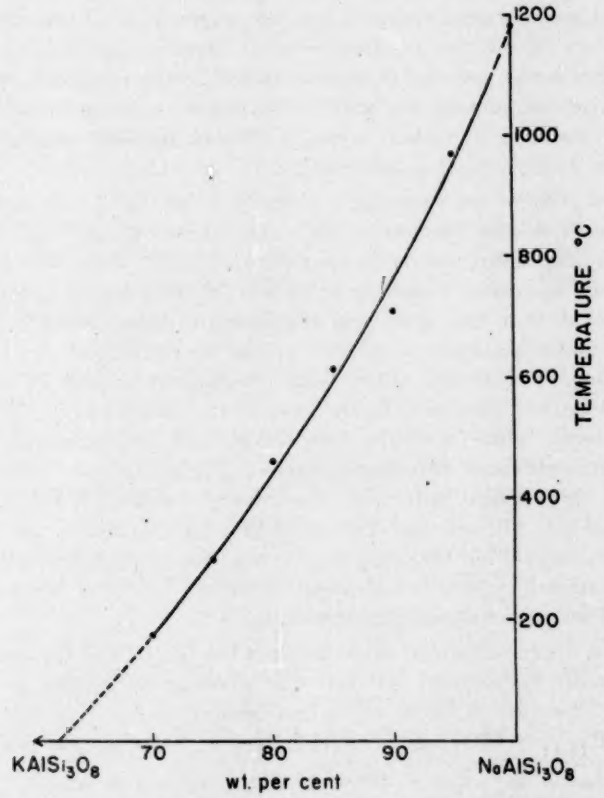

Fig. 3. Curve showing the variation in inversion temperature with composition of synthetic alkali feldspars crystallized hydrothermally at 800° C. and 1000 kg/cm².

The first synthetic plagioclases investigated were those crystallized in the "dry" way by Dr. Schairer. It was found that plagioclases of composition $Ab_{95}An_5$ and $Ab_{90}An_{10}$ inverted to monoclinic symmetry at a lower temperature than hydrothermally crystallized albite. On the other hand $Ab_{80}An_{20}$ inverted at a higher temperature than such albite. This suggests that there was some difference between albite crystallized hydrothermally and that crystallized "dry." Samples of albite crystallized "dry" are not sufficiently well crystallized for investigation by this method, and therefore glasses of composition $Ab_{90}An_{10}$ and $Ab_{80}An_{20}$ were crystallized at 800° C. and 1000 kg/cm^2 pressure of water vapor, and the inversion temperatures obtained were compared with those of the "dry" crystals. From the position of the curves obtained from the hydrothermal material it can be seen that the regular increase in inversion temperature with decreasing Or content, which has been noted in the alkali series, continues into the plagioclase series with increasing An content.

Since there are very slight differences in the X-ray powder patterns of the hydrothermally crystallized plagioclase feldspars, depending on the temperature at which they were crystallized (personal communication by Dr. Bowen), it might be expected that the inversion temperatures also would differ. Except in the case of albite, all the hydrothermal synthetic samples used in this study were crystallized at 800° C. and 1000 kg/cm^2 pressure. In the case of the alkali feldspar series this temperature is above the solvus and consequently the crystals obtained were homogeneous. The solvus has, however, been determined only for the binary system $KAlSi_3O_8$—$NaAlSi_3O_8$ (Bowen and Tuttle, 1950). In the case of the ternary composition $Or_{20}Ab_{70}An_{10}$ it was found that two phases crystallized at 800° C. Heating at 1030° C. for a few hours rendered this material homogeneous.

The difference which exists between the "dry" and the hydrothermally crystallized material was investigated further in two ways. Samples of albite which had been crystallized at 800° C. and $P_{H_2O} = 1000$ kg/cm^2 were heated at 1030° C. for periods of 1 and 5 days and at 1080° C. for 7 days. The curves, Nos. 1-4 in figure 4a, were obtained by plotting the values of $2\theta_{111} - 2\theta_{1\bar{1}1}$ against temperature for these samples. The values obtained are given in table 3. A curve for "dry" albite has

been estimated from the position of the curves for the "dry" plagioclases (fig. 2) and part of this has been drawn as a dashed line in the figure 4a. Curve No. 5 is the change in $2\theta_{111} - 2\theta_{1\bar{1}1}$ with temperature for a sample of Amelia albite which had been heated at 1055° C. for 10 weeks. Although the value of the inversion temperature for each of these samples has not been noted, it is clear that there is a gradual lowering of the inversion temperature toward the estimated value for "dry" albite. The amount by which the inversion temperature is lowered is dependent on the temperature and duration of the heat treatment. It is probable that if the hydrothermal material were heated at a temperature just below its melting point for sufficient time its inversion temperature would correspond to that of the "dry" material.

The second approach to the question of the difference in inversion temperature between the "dry" and the hydrothermal material crystallized at 800° C. was made by crystallizing albite hydrothermally at 700° C., 950° C., and 1025° C.[3] In figure 4b the curves for $2\theta_{111} - 2\theta_{1\bar{1}1}$ plotted against temperature are shown for these samples of albite along with that of the albite crystallized at 800° C. It can be seen that the curves for the samples crystallized at 950° C. and 1025° C. fall close together as do the curves for the material crystallized at 700° C. and 800° C., but the curves for the two high-temperature samples have steeper slopes than do those for the lower temperature material. The difference between the position of the curve for the two samples crystallized at 950° C. and 1025° C. can probably be accounted for by errors both in temperature measurement and in measuring the position of the peaks. The same is probably true of the two lower temperature curves. It would appear then that albite crystallized hydrothermally above some temperature between 800° C. and 950° C. is similar to "dry" albite as far as the inversion temperature is concerned. Below this temperature the material which crystallizes has been loosely described in the preceding pages as "hydrothermally crystallized" since all compositions were crystallized at the same temperature and pressure. It is likely that in the plagioclase series and in the alkali series a similar relation holds although

[3] The pressures at which albite could be crystallized hydrothermally at these temperatures were obtained from the equilibrium curve of the system $NaAlSi_3O_8$—H_2O determined by Goranson (1938, p. 84). These are given in table 3.

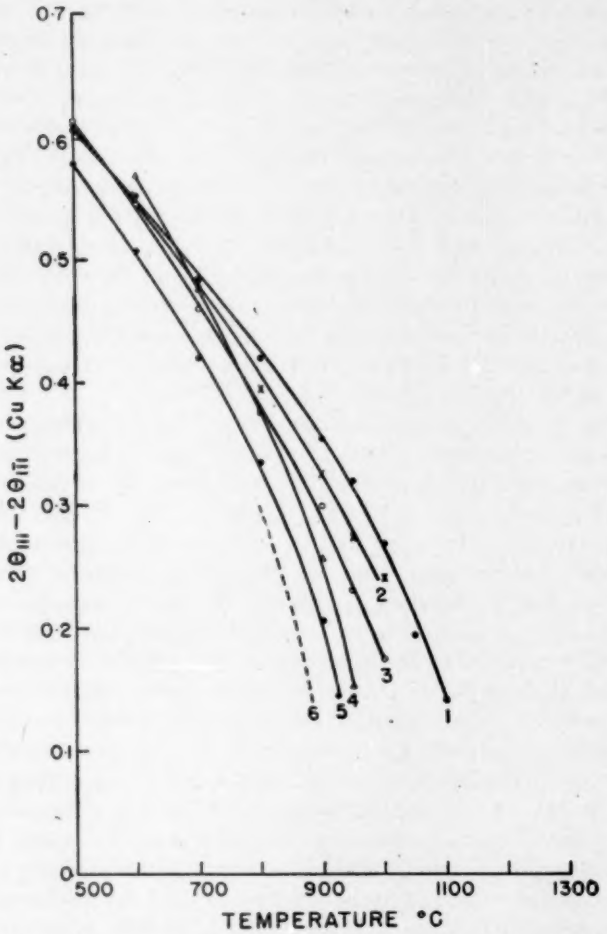

Fig. 4. Curves showing the change of $2\theta_{111} - 2\theta_{1\bar{1}1}$ with temperature for different samples of high albite.

(a) Curves 1-4 are for synthetic albite crystallized at 800° C.; P_{H_2O} = 1000 kg/cm².
Curve 1 — sample unheated
Curve 2 — sample heated for 1 day at 1030° C.
Curve 3 — sample heated for 5 days at 1030° C.
Curve 4 — sample heated for 7 days at 1080° C.
Curve 5 — Amelia albite heated for 10 weeks at 1055° C.
Curve 6 — represents a possible position for the curve for "dry" albite and is deduced from the position of the curves for the "dry" plagioclases in figure 2.

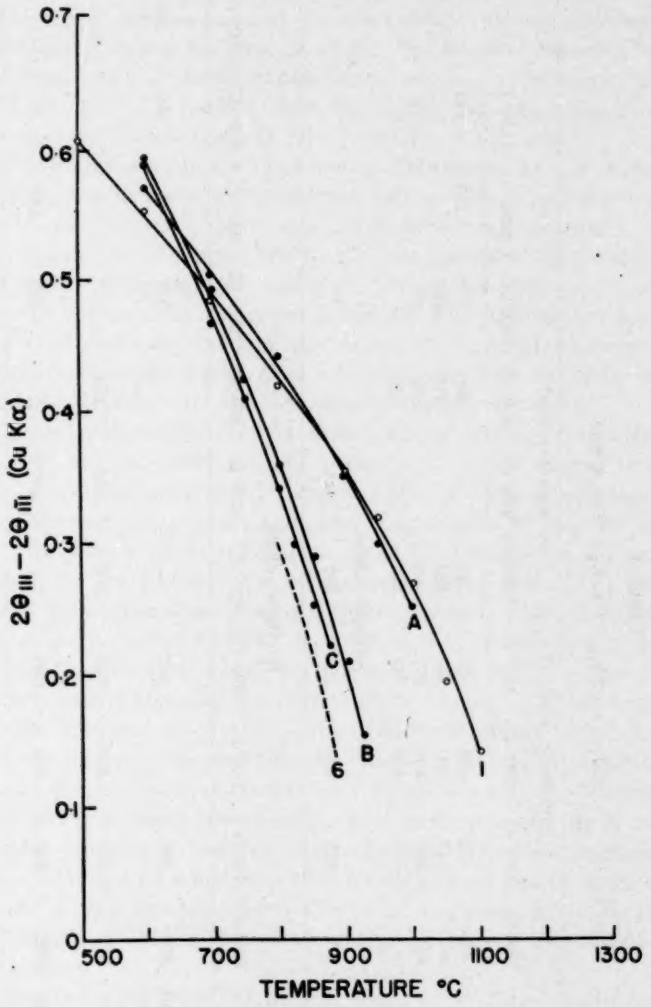

(b) Curves 1 and 6 are as in figure 4a.

Curve A — crystallized at 700° C. and $P_{H_2O} = 1000$ kg/cm².

Curve B — crystallized at 950° C. and $P_{H_2O} = 350$ kg/cm².

Curve C — crystallized at 1025° C. and $P_{H_2O} = 140$ kg/cm².

Table 3

$2\theta_{111} - 2\theta_{1\bar{1}1}$ (Cu K_α) For Albite

	Synthetic albite P_{H_2O} = 1000 kg/cm²; 800° C.										
	500° C.	600° C.	700° C.	800° C.	900° C.	925° C.	950° C.	1000° C.	1050° C.	1100° C.	
Unheated	.605	.552	.485	.420	.355	...	.320	.270	.195	.142	...
Htd. 1 day at 1030° C.	.607	.547	.480	.395	.325	...	.275	.242	...	...	...
Htd. 5 days at 1030° C.	.612	.545	.460	.377	.300	...	.232	.175	...	...	...
Htd. 7 days at 1080° C.	...	.567	.475	.375	.257	...	.152	...	...	...	...
	Amelia albite										
Htd. 10 weeks at 1055° C.	.577	.507	.420	.335	.207	.145	...	...	...	...	...

	Synthetic albite										
	600° C.	700° C.	750° C.	800° C.	825° C.	850° C.	875° C.	900° C.	925° C.	950° C.	1000° C.
Crystallized at 700° C. and P_{H_2O} = 1000 kg/cm²	.570	.505	...	.442	...	...	...	.352	...	.300	.252
Crystallized at 950° C. and P_{H_2O} = 350 kg/cm²	.587	.467	.410	.342	.300	.253	.223	...	...	...	...
Crystallized at 1025° C. and P_{H_2O} = 140 kg/cm²	.592	.492	.425	.360	...	.290	...	.210	.155	...	...

the effect of heating materials crystallized at 800° C., or, of crystallizing compositions at different temperatures, has been investigated only in the case of albite. The gradual lowering by heat treatment of the inversion temperature of albite crystallized at 800° C. implies that there may be all gradations between the "hydrothermal form" and the "dry form."

The temperature of the inversion, as determined by the X-ray method, thus appears to depend not only on the temperature of crystallization but also on any subsequent heat treatment. It is probable that a similar lowering of the inversion temperature will result when natural feldspars are heated for prolonged periods, but no data are as yet available. The preliminary heat treatment necessary for homogenization of the unmixed natural feldspars was purposely kept of short duration in order to minimize the effect on the inversion temperature.

X-ray spectrometer charts were made of albite, crystallized at 800° C. and 1000 kg/cm^2 pressure of water vapor, both unheated and heated for 7 days at 1080° C. The charts were made at room temperature and covered a range of 2θ from 60° to 10°. Only very slight differences could be detected on the two charts. On the basis of the difference in 2θ of the $(\bar{1}32)$ and $(1\bar{3}1)$ planes the albite prepared hydrothermally at 800° C. and subsequently heated at 1080° C. for 7 days is identical with that of "dry" albite (see Tuttle and Bowen, 1950, fig. 5). The unheated hydrothermally prepared albite shows a significantly smaller value for $2\theta_{\bar{1}32} - 2\theta_{1\bar{3}1}$ than the "dry" material, but it is still considerably larger than the value for natural low albite. It can be said with assurance that there is a slight difference between "dry" and hydrothermal albite on the basis of the X-ray powder patterns as well as on the basis of inversion temperatures. It might be noted here that no differences can be detected in the X-ray spectrometer patterns of high-sanidine (Tuttle, 1951) and sanidine although the optical properties show distinct differences.

The fact that "dry" albite and albite crystallized hydrothermally at 1025° C. invert to monoclinic symmetry at a temperature below the melting point, whereas albite crystallized hydrothermally at 800° C. melts before becoming monoclinic, leaves some doubt as to the true equilibrium relations of the inversion. The alkali feldspar equilibrium diagram for a pressure of water vapor of 1000 kg/cm^2 (Bowen and Tuttle, 1950)

has been modified in the light of the data obtained for the inversion temperatures of compositions crystallized at 800° C. and $P_{H_2O} = 1000$ kg/cm^2 (fig. 5). The two-crystal field is enclosed in dashed lines since its limits have not been determined; indeed, its existence has not been proved. The diagram may require slight alteration if it can be shown that the inversion temperatures of the equilibrium forms of the various compositions differ appreciably from those which have been determined. It is probable that the natural minerals are similar to what has been called the "hydrothermal form." Further work may elucidate the differences between these two types of synthetic albite and contiguous feldspars of the alkali and plagioclase series and their relation to the natural minerals.

THE INVERSION AND ITS PETROLOGICAL IMPLICATIONS

The gradual change to monoclinic symmetry which takes place with change in temperature must be contrasted with that which occurs in cryolite (fig. 1). In the case of the cryolite inversion a preliminary gradual change takes place in the value of $2\theta_{101} - 2\theta_{011}$, with increase in temperature, up to the

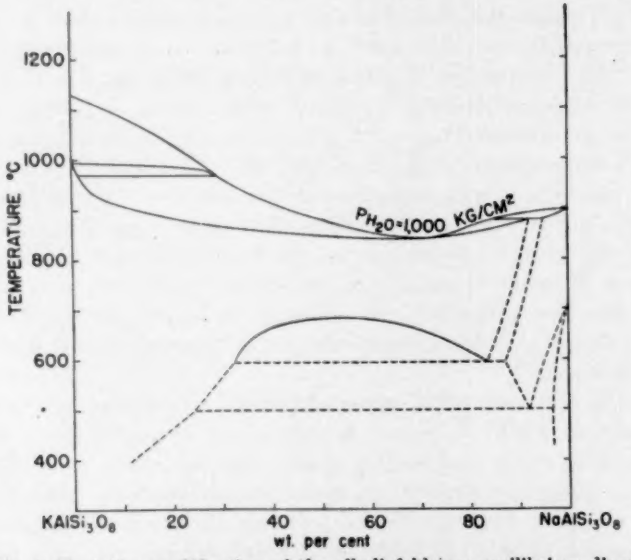

Fig. 5. Tentative modification of the alkali feldspar equilibrium diagram from Bowen and Tuttle (1950) in the light of the present data.

temperature of the inversion when a sudden discontinuity occurs. A measurable heat effect occurs at the inversion temperature of cryolite (Keith and Tuttle, 1952), so that it was desirable to determine whether or not a heat effect accompanied the feldspar inversion. Differential heating curves were run on samples of four natural anorthoclase feldspars. The sensitivity of the equipment used was checked by determining the inversion temperature of a sample of quartz, and the galvanometer gave a scale deflection of about 3 feet for the quartz inversion which has a heat of transformation of 4.8 calories per gram (Kelly, 1949, p. 153). With this sensitive apparatus no definite evidence of a discontinuity in the differential thermal curves of the natural feldspars was found.

Figure 6 shows part of the ternary diagram $KAlSi_3O_8$—$NaAlSi_3O_8$—$CaAl_2Si_2O_8$ in which are plotted the natural and hydrothermal synthetic compositions studied. The inversion temperatures are noted beside each point, the values in parentheses being obtained by extrapolation of the $2\theta_{111}$ — $2\theta_{1\bar{1}1}$ curves to temperatures above the liquidus. Sufficient data are not yet available to draw even approximate isotherms for the inversion temperatures. In addition, the temperatures given are not known to be the equilibrium inversion temperatures. A dashed line which divides the area into two fields is shown. This line has been drawn using the liquidus temperature data determined for the "dry" system (Franco and Schairer, 1951) and separates those compositions whose inversion temperature lies above the liquidus from those whose inversion temperature lies below the liquidus for the "dry" system. It is certain that the liquidus temperatures for water vapor pressures of 1000 kg/cm^2 will be lower, so that the dashed curve would be displaced downwards and thus narrow the field of compositions whose inversion temperature lies below the liquidus for the hydrothermal system. However, this dashed line gives a rough approximation to the division between the two fields. It would be desirable to have some criterion by which the temperature of crystallization could be related to the inversion temperature for the naturally occurring high-temperature soda-rich feldspars.

The cross-hatched or tartan appearance of the twinning generally seen in anorthoclase crystals on examination in thin section under a petrographic microscope is often sufficiently

characteristic to identify the mineral as anorthoclase. Since the natural crystals investigated here are from lavas or other high temperature environments, it is probable that they crystallized above their inversion temperatures. It is tentatively suggested that the cross-hatched appearance of natural anorthoclase crystals results from the fact that they crystallized with monoclinic symmetry, and, in the process of cooling, become triclinic.[4] From the data presented here, it seems likely that potash-bearing high-

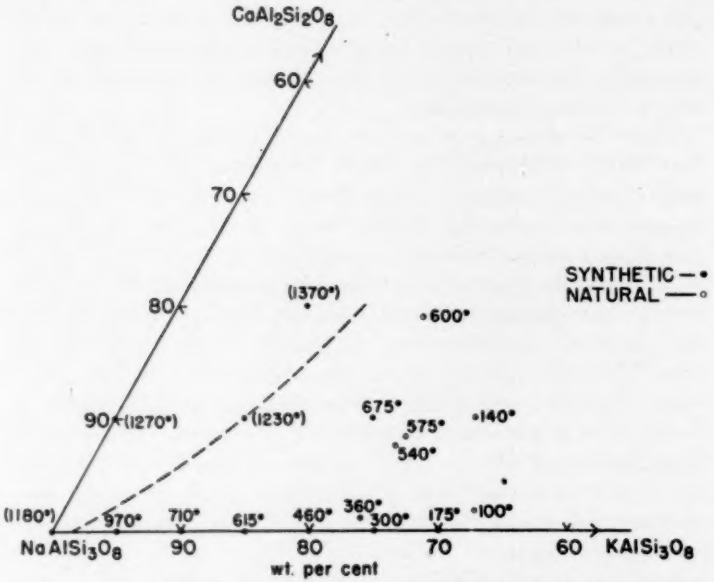

Fig. 6. The inversion temperatures of natural and synthetic feldspars (800° C.; P_{H_2O} =1000 kg/cm²) plotted in part of the ternary diagram $KAlSi_3O_8$—$NaAlSi_3O_8$—$CaAl_2Si_2O_8$. The temperatures in parentheses are above the liquidus for the "dry" system for the compositions to which they refer. For explanation see text.

$Or_{31.7}Ab_{66.8}An_{1.9}$	Grande Caldeira, Azores. (analyst: J. H. Scoon).
$Or_{28.1}Ab_{61.8}An_{10.1}$	Mt. Kenya, East Africa. (Mountain, 1925).
$Or_{23.2}Ab_{75.5}An_{1.3}$	Victoria, Australia. (Kracek and Neuvonen, 1952).
$Or_{23.0}Ab_{69.5}An_{7.5}$	Ropp, Nigeria. (J. R. F. Joyce and P. M. Game, 1952).
$Or_{23.4}Ab_{68.3}An_{8.3}$	Mt. Anakie, Australia. (Edwards, 1938).
$Or_{17.0}Ab_{63.2}An_{19.9}$	Mt. Erebus, Antarctica. (Mountain, 1925).

[4] Laves (1950, p. 550) concludes that "the well known cross-grating twinning of microcline can be explained only by the assumption that such microcline originally crystallized as a modification with true monoclinic symmetry."

temperature albite or oligoclase crystallized with triclinic symmetry with the result that the twinning is clearly defined and the cross-hatched appearance is absent. Only a small amount of an analysed high-temperature plagioclase was available for study. This was the plagioclase, from a rhyolite from Nathrop, Colorado, on which the alkalis had been determined by Mr. J. H. Scoon, of Cambridge, England, and the composition found to to be $Or_{7.7}Ab_{81.2}An_{11.1}$. The small amount of material available was sufficient to determine that the inversion temperature would be about 1250° C., which is very near the liquidus for this composition in the "dry" system (Franco and Schairer, 1951). It is probable that this feldspar crystallized with triclinic symmetry and the absence of cross-hatched twinning, when examined under the petrographic microscope, confirms this view.

It is possible that the relations between the varieties of potash feldspar may also be clarified by the X-ray method described here. Microcline can be distinguished from orthoclase by the presence of two peaks representing 111 and $1\bar{1}1$, only one peak representing both 111 and $1\bar{1}1$ being present in the X-ray powder diffraction pattern of orthoclase. The triclinic character of microcline is more clearly shown, however, by the presence of two peaks between 2θ values of 23.0° and 24.0° (Cu radiation), since these peaks have a greater angular separation and greater intensity than 111 and $1\bar{1}1$. These peaks are probably due to the 130 and $1\bar{3}0$ reflections. Many of the problems related to inversions in general may be elucidated by the study of the changes produced in X-ray spectrometer patterns with change in temperature.

ACKNOWLEDGMENTS

This research was carried out at the Geophysical Laboratory during the tenure of a Fellowship of the Carnegie Institution of Washington. The writer is grateful to Dr. L. H. Adams, Director of the Laboratory, for the opportunity afforded to work there, and to Professor C. E. Tilley of the University of Cambridge, who made this arrangement possible. He also wishes to express his sincere gratitude to Dr. O. F. Tuttle, at whose suggestion and under whose guidance the work was carried out, for his constant advice and encouragement. The author is also indebted to Dr. J. F. Schairer for providing both synthetic glasses and the "dry" crystals required for this investigation

and to Drs. N. L. Bowen and O. F. Tuttle for making both synthetic and natural analyzed feldspars available for this study. To the other members of the staff of the Geophysical Laboratory, particularly Drs. N. L. Bowen, J. W. Greig, G. L. Davis, H. S. Yoder, and G. Donnay, the writer is deeply indebted for their assistance and many helpful suggestions.

References

Birks, L. S., and Friedman, H., 1947. A high temperature X-ray diffraction apparatus: Rev. Sci. Instr., vol. 18, pp. 576-580.

Bowen, N. L., and Tuttle, O. F., 1950. The system $NaAlSi_3O_8$—$KAlSi_3O_8$—H_2O: Jour. Geology, vol. 58, pp. 489-511.

Donnay, G., and Donnay, J. D. H., 1952. The symmetry change in the high-temperature alkali-feldspar series: Am. Jour. Sci., present vol.

Edwards, A. B., 1938. The tertiary rocks of central Victoria: Geol. Soc. London Quart. Jour., vol. 94, pp. 243-320.

Franco, R. R., and Schairer, J. F., 1951. Liquidus temperatures in mixtures of the feldspars of soda, potash, and lime: Jour. Geology, vol. 59, pp. 259-267.

Goranson, R. W., 1938. Silicate-water systems: phase equilibria in the $NaAlSi_3O_8$—H_2O and $KAlSi_3O_8$—H_2O systems at high temperatures and pressures: Am. Jour. Sci., 5th Ser., vol. 35A, pp. 71-91.

Joyce, J. R. F., and Game, P. M., 1952. Note on anorthoclase from Nigeria: British Museum (Nat. Hist.) Mineralogy, 1, 3 (in press).

Keith, M. L., and Tuttle, O. F., 1952. Significance of variation in the high-low inversion of quartz: Am. Jour. Sci., present vol.

Kelly, K. K., 1949. Contributions to the data on theoretical metallurgy: U. S. Bur. Mines Bull. 476.

Kracek, F. C., and Neuvonen, K. J., 1952. Thermochemistry of plagioclase and alkali feldspars: Am. Jour. Sci., present vol.

Laves, F., 1950. The lattice and twinning of microcline and other potash feldspars: Jour. Geology, vol. 58, pp. 548-571.

Mountain, E. D., 1925. Potash oligoclase from Mt. Erebus, Antarctic, and anorthoclase from Mt. Kenya, East Africa: Mineralog. Mag., vol. 20, pp. 331-345.

Schairer, J. F., 1950. The alkali-feldspar join in the system $NaAlSiO_4$—$KAlSiO_4$—SiO_2: Jour. Geology, vol. 58, pp. 512-517.

———, and Bowen, N. L., 1935. Preliminary report on equilibrium-relations between feldspathoids, alkali feldspars and silica: Am. Geophys. Union Trans., 16th Ann. Meeting, pp. 325-328.

Tuttle, O. F., 1951. Studies in feldspar equilibria at the Geophysical Laboratory, Washington: Mineralog. Mag., vol. 29, pp. 757-758.

———, and Bowen, N. L., 1950. High-temperature albite and contiguous feldspars: Jour. Geology, vol. 58, pp. 572-583.

Geophysical Laboratory
Carnegie Institution of Washington
Washington, D. C.

Department of Mineralogy and Petrology
University of Cambridge
England

THE SYSTEM H_2O—Na_2O—SiO_2 AT 400° C.

GEORGE W. MOREY and JAMES M. HESSELGESSER

ABSTRACT. A method and an apparatus have been devised which have made possible the analyses of coexisting gas and liquid phases in the system H_2O—Na_2O—SiO_2 at 400° C. and at pressures up to 2500 bars. The isothermal polybaric saturation curves—both gaseous and liquid—of quartz, sodum disilicate, and sodium metasilicate have been determined, and the melting pressure of $Na_2O \cdot 2SiO_2$ found to be 2200 bars. The boundary curve G + L + quartz + sodium disilicate is continuous and does not intersect the crtical end-point curve, and probably the boundary curve G + L + sodium disilicate + sodium metasilicate has a similar relationship. There are probably two critical regions surrounded by critical curves, one of which is represented by (G = L) + $Na_2O \cdot SiO_2$, the other by (G = L) + $Na_2O \cdot 2SiO_2$, although the possibility has not been excluded that these two critical curves intersect, giving rise to a double critical end-point (G = L) + $Na_2O \cdot SiO_2$ + $Na_2O \cdot 2SiO_2$. There is also a critical region represented by (G = L) + Qtz.

INTRODUCTION

THE complete solubility curve of a salt in water covers the entire composition and temperature range from the melting point of ice to the melting point of the salt. When the melting point of the salt is high, the vapor pressure of the saturated solutions may reach high values, and the solubility of the solid in the gas may become so great as to be not only of theoretical interest but also of practical importance (Morey and Hesselgesser, 1951*a*, 1951*b*). There is almost no experimental knowledge of such systems, and the present study is an introduction to an almost new field. This field is important to geochemistry. Knowledge about systems containing water at high temperature and pressure is essential to understanding the mechanism of rock formation, and knowledge about the gas compositions which may coexist with aqueous silicate melts under high pressure is essential to understanding the genesis of vein minerals, pegmatite deposits, and pneumatolytic processes in general.

The first study of a water—silicate system was that by Morey and Fenner (1917) of H_2O—K_2SiO_3—SiO_2. In that system the solubility curves of K_2SiO_3 and $K_2Si_2O_5$ in water are continuous, and there is no intersection of the critical surface by the solubility surface, except in the region in which quartz is the solid phase. The vapor pressures of the saturated solutions are small, and there is no significant solubility of K_2O and SiO_2 in the gas. Attempts to work out the system H_2O—Na_2O—SiO_2 in a similar manner were unsuccessful, and further work on

the silicate systems was long delayed, chiefly because of the necessity of studying the anhydrous systems before the introduction of water.

The compounds $Na_2O \cdot SiO_2$ and $Na_2O \cdot 2SiO_2$, prepared hydrothermally, were described by Morey (1914), and the binary system $Na_2O \cdot SiO_2$—SiO_2 was worked out by Morey and Bowen (1924). Later Kracek (1930) extended the study to the orthosilicate, $2Na_2O \cdot SiO_2$. In 1938 Morey and Ingerson described some work on the lowering of the melting point of $Na_2O \cdot 2SiO_2$ by water up to 133 bars pressure. That work indicated that the vapor pressure of a saturated solution of sodium disilicate increased rapidly with decreasing temperature. Other experiments by Morey and Ingerson (Adams, 1941) showed that both $Na_2O \cdot SiO_2$ and $Na_2O \cdot 2SiO_2$ at lower temperatures had retrograde solubility curves with intersection of the critical curve by the solubility curve at practically the critical temperature of water. In the same publication the first mention was made of the method and apparatus used in the present study. Freidman (1950) made some experiments at the temperature of this work, 400° C., with results somewhat different from those of this paper. His method of study did not include direct determination of the pressure in separation and analysis of both gas and liquid, which may account for the differences observed. He confirmed the retrograde solubility of sodium disilicate.

METHOD AND APPARATUS

The method of study was as follows: A sodium silicate glass or crystalline mixture of known composition was placed in a loosely covered platinum crucible which rested on a pedestal inside a high pressure vessel or bomb. This was attached to the pressure line (fig. 1) and the furnace raised around it. When up to the desired temperature, water was pumped into the hot bomb until the desired pressure was reached. The temperature and pressure were held constant—usually overnight, sometimes for 2 or 3 days—after which the valve connecting the bomb with the pressure line was closed, the furnace lowered, the bomb cooled and opened. On cooling the gas had condensed to a liquid, which was weighed and analyzed. Some gas condensed in the crucible, and this was poured off, weighed and analyzed. The material left in the crucible, which was all

crystals, all liquid, or a mixture of crystals and liquid,[1] also was weighed and analyzed. These three analyses gave the amount and compositions of the coexisting phases, and the amount of water injected into the bomb.

The apparatus is shown diagrammatically in figure 1. It consists of a pump, which pumps distilled water into a pressure line, which includes a pressure reservoir, a pressure measuring and regulating apparatus, and a bomb containing the charge, and suitable valves. The pump, made by the American Instrument Company, is rated at 2000 bars, but it has been used for higher pressures. For higher pressures, a pressure intensifier, not shown, has been used with the pump. This effects a multiplication of pressure of 10 to 1, so that at pressure of 3000 bars the pump pressure is only 300 bars. In using the intensifier the pressure usually is first pumped up to 1000-1500 bars with the pump working directly into the system, after which the intensifier is introduced into the line by a system of valves. The purpose of the pressure reservoir is to increase the volume of the system so that each stroke of

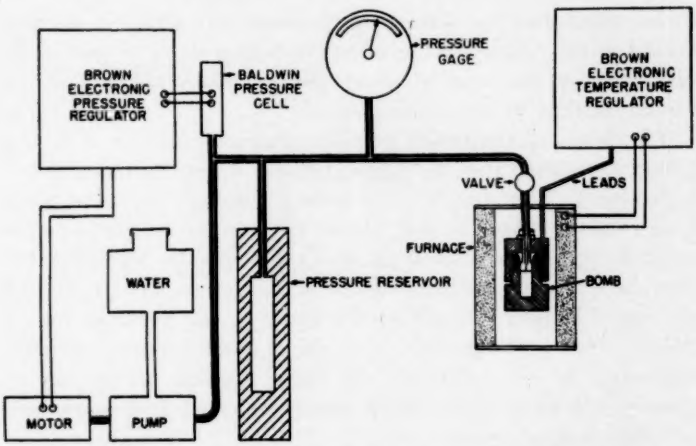

Fig. 1. Diagrammatic representation of the apparatus. Water is pumped into a pressure line in which there is a pressure regulator, a pressure gage, a reservoir, a bomb container, the charge, and suitable valves. The bomb hangs in a furnace with automatic temperature control.

[1]This can be expressed more briefly by the objectionable expression "liquid and/or crystals;" we commonly refer to it as the "andor," and it will be so designated subsequently.

the pump does not have so much effect. The reservoir used for pressures up to 1500 bars has a volume of 2240 cc.; for higher pressures, 250 cc.

The earlier form of the pressure controller, described in a preceding paper (Morey and Hesselgesser, 1951*a*), was a Bourdon gage which maintained constant pressure by means of a light and photocell. In the later work a Baldwin Fluid Pressure Cell, the sensitive elements of which are two Baldwin Strain Gages, was used in connection with a special Brown Electronic Indicating Potentiometer. The instrument had a pressure range up to 3300 bars, and a high sensitivity. Pressures were measured on 10-inch Bourdon type pressure gages, made by the Ashcroft Instrument Company, and calibrated against a dead-weight gage.

The temperature of the Nichrome-wound furnace is regulated by a Brown Electronic Indicating Contact Controller. The regulating thermocouple, either iron-constantan or chromel-alumel, was placed in a hole drilled in the cap of the bomb to the level of the top of the chamber, as shown in figure 2. An auxiliary winding, controlled by a separate Variac, was so adjusted that the bottom of the bomb was a degree warmer than the top. Temperatures were determined by a platinum: platinum 10 per cent rhodium couple placed in a position similar to that of the control couple.

The bomb is connected with the pressure line by a hollow plunger, as indicated in figure 1, and shown in more detail in figure 2. The stem is long enough so that the cone joint connection is about 3 cm. above the top of the furnace. A suitable system of valves enables the bomb to be connected with the pressure line or to blow off to the air. At the end of the run the valve connecting the bomb to the pressure line is closed. After cooling there may be a small residual pressure remaining in the bomb, so the valve opening to the air is opened and whatever is blown out is collected and considered in subsequent analyses.

The pressure vessels and bombs used in this work were similar to that described by Morey and Ingerson (1937), with the differences that the continuous thread is in two diameters, a convenience for putting on and removing the cap, and that the plunger has a longitudinal hole for admitting water and is elongated to connect with the pressure apparatus. Several dif-

ferent types of closure were used. The simplest is a flat silver disc pierced through the middle and used with a flat plunger. This is the easiest to use, but cannot be used for long runs or for pressures over 500 bars. A second type of closure is that described by Morey and Ingerson (1937), and Morey (1914). This will hold 1000 bars but at higher pressures there is danger of it leaking during the cooling.

For high pressures, the closure shown in figure 2 has proven most satisfactory. It makes use of the internal pressure to maintain the seal. The head of the plunger fits inside the

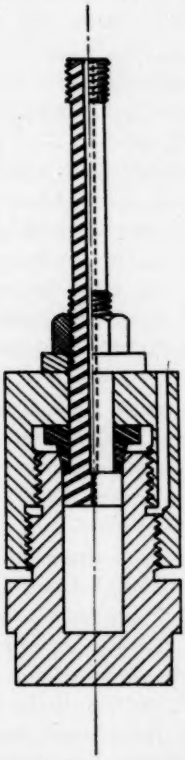

Fig. 2. The bomb assembly. This consists of a body and a hollow plunger held in place by a follower washer and the cap. The sealing washer is between the head of the plunger and the follower. The initial seal is made by tightening the nut which bears on the top of the cap, but as pressure builds up it makes the seal by compression of the sealing washer between the follower and the head of the plunger.

chamber of the bomb. A follower washer made with a slight taper, held in place by the cap, fits over the stem of the plunger, and the lower-¼ inch fits inside the chamber of the bomb. A washer ⅛-inch thick fits over the stem of the plunger and is compressed between the head of the plunger and the follower. The washers usually are of silver, but copper and aluminum washers have been used. The initial closure has been made by screwing down the nut bearing on the top of the cap; the final closure, by the action of the pressure in the interior of the bomb. The area of the head of the plunger is 0.60 square inch, that of the silver washer, 0.30 square inch, so that the pressure on the washer is twice the internal pressure. This closure has never leaked, even when subjected to wide changes in pressure and temperature.

Most of the bombs were made of Inconel X, which withstands the corrosive action of highly alkaline gases better than stainless steel. Several stainless steel bombs failed by having a hole drilled through them overnight. For example, if 5 grams $Na_2O \cdot SiO_2$ are heated at 400° C. with 100 bars water pressure, the gas will contain about 10 per cent Na_2O and will drill a hole in a 303 stainless steel bomb overnight. A study made by the National Bureau of Standards showed that failure was due to stress corrosion, and that the fracture took place across the grains. Several Inconel X bombs have failed from the chemical action of alkaline gases under more drastic conditions. A study made by the International Nickel Company showed that failure was caused by intergranular corrosion.

The platinum crucibles were 17.5 mm. in diameter at the top, tapering to 16 mm. at the bottom, and usually 15 mm. high. This size holds about 5 grams of powdered silicate, and when larger charges were needed, a higher crucible was used. The desired amount of glass of known composition was put in the weighed crucible, loosely covered with a silver disc, and placed in the bomb, resting on a silver pedestal of such height that the crucible was at the top of the chamber, and the bomb was then assembled. The loose cover was to prevent any of the powder from being blown out when water was let into the bomb and this usually was further prevented by about 1 ml. of water placed in the bomb initially, which served to sinter the loose powder. The assembled bomb was attached to the pressure line by means of a standard cone fitting, the regulating and

reading thermocouples inserted, and the furnace raised around the bomb. When it was up to temperature, water was pumped in to the desired pressure.

After a run was over, the valve connecting the bomb with the pressure line was closed, the furnace dropped, and the bomb cooled in air for about 10 minutes, by which time its temperature had fallen to about 250° C. Then the bomb was immersed in water up to the cap and cooled to about 70°. It was then taken off the pressure line and the cap and plunger removed. Most of what was gas at high temperature had condensed on the walls of the bomb outside of the crucible. It was removed with a pipette, weighed and analyzed. Several examples are given in table 2.

If the amount of glass put into the crucible was greater than that which corresponds to the solubility in gas, some remained as crystals, or liquid plus crystals, or liquid only. When there was a liquid at the temperature of the experiment it cooled to a more or less hard glass. The extra gas condensed in the crucible was poured off, the "andor" remaining in the crucible was weighed, examined with the petrographic microscope for the pressure of crystals, and analyzed. Except with mixtures having a $SiO_2/(Na_2O + SiO_2)$ ratio of less than 0.62, the crucible containing the "andor" usually was placed in a large covered crucible and heated. It then puffed up into a pumicious mass. When a small amount of quartz was present it could be quantitatively separated and weighed by heating in a pressure cooker at about 15 pounds steam pressure after adding enough NaOH solution to bring the SiO_2-ratio to 0.4. A systematic error in all of the liquid compositions is caused by some of the condensed gas penetrating the upper layers of the liquid. When the SiO_2-ratio is greater than 0.66, the error probably is small. In such mixtures the liquid forms a hard glass from which the last drops of condensed gas can be soaked up with filter paper strips, and the surface of the glass is not sticky. But with mixtures increased in metasilicate the liquid becomes a stiff paste, and there is enough penetration of the surface to make it sticky. The amount of this error probably is not large, but it is not possible to make allowance for it.

On top of the "andor" was some condensed gas which had had the opportunity to react with it. This extra gas usually weighed 1-2 grams, and was analyzed separately. Since it is

condensed gas which has reacted with "andor" its composition will be intermediate between the reacting phases, and hence the amount of reaction can be calculated. This calculation was made both from the Na_2O—content and the SiO_5—content, and the agreement between these two gives an idea of the precision of the experiment.

The formulae used in these calculations are:—

$$G = \frac{Ex - Na_2O}{x - x'} = \frac{Ey - SiO_2}{y - y'}$$

in which E is weight of extra gas which includes both the condensed gas and what has dissolved from the "andor"; G the weight of condensed gas, x and y the weight fractions Na_2O and SiO_2 in the "andor"; x′ and y′, the weight fractions Na_2O and SiO_2 in the gas; and Na_2O and SiO_2, the weights of these oxides found in the E grams of extra gas.

For the gas of table 2 (1) this gives:—

$$\frac{1.104(.192) - .0453}{.192 - .019} \quad \text{and} \quad \frac{1.104(.508) - 0.1152}{.500 - .037}$$

which give for the weight of gas 0.963 g. and 0.943 g., respectively; mean 0.953 g.; material dissolved by the gas, 0.151 g.

In some experiments no liquid was formed; the mixture was in the region gas plus solid. In such experiments the amount of condensed gas remaining in the interstices between the crystals was calculated in the same manner from the gas composition, the composition of the crystals and the gross composition. An example is the gas of table 2 (8) in equilibrium $Na_2O \cdot SiO_2$ crystals: —

$$\frac{2.76(.5035) - 0.6598}{.5035 - .242} \quad \text{and} \quad \frac{2.76(.4965) - .2693}{.4965 - .084}$$

which give for the weight of gas 2.791 g. and 2.609 g., respectively; mean 2.73; material dissolved by the gas, 0.03 g.

The sum of the weights of condensed gas weighed directly, and calculated from the extra gas and the gas condensed in interstices between crystals, gives the total weight of gas. The free volume of the bombs depends on the type of closure used, the volume of the crucible and pedestal, and of crystals or liquid. The density of the liquid is not known, and the amount of liquid is different in different runs. However, an approxi-

mate volume can be calculated, and from it and the weight of gas, an approximate density of the gas can be calculated. Several densities so calculated are given in table 2.

The sum of Na_2O and SiO_2 found in the analyses of gas, the extra gas, and the "andor," was compared with the amounts of Na_2O and SiO_2 put in. There was always some shortage. The usual shortage was less than 0.1 g. each of Na_2O and SiO_2; when the shortage was large the run was usually rejected. A small part of the shortage was due to reaction with the bomb. Part was due to migration of Na_2O and SiO_2 back into the pressure line. An estimate of the amount of this loss was made in a large number of runs by inserting a valve between the main valve block and the bomb, thus retaining all the material in the stem and tubing up to the valve. With mixtures high in SiO_2 (.66 or more) the amount in the stem was less than 10 mg. but with mixtures of composition near the metasilicate it amounted to as much as 30 mg. This is a negligible error.

In these experiments the pressure is fixed and known, and the amount of water used was determined by the pressure. This amount could be ascertained by subtracting from the total weight of gas plus extra gas plus "andor," the weight of sodium silicate taken. It was rarely convenient to use more than 7 grams of silicate, and the amount of water usually was over 50 per cent.

The sodium silicate mixtures were powdered glasses, except for the $Na_2O \cdot SiO_2$ melt, which always crystallized. Most of these were made from Laboratory stock of Na_2CO_3 and SiO_2, but some were commercial glasses obtained from the Philadelphia Quartz Company. Mixtures of the desired percentage of SiO_2 were obtained by mixing stock glasses, powdered to pass 40-mesh screens, and mixed by several screenings. Mixtures higher in Na_2O than sodium metasilicate were made of $Na_2O \cdot SiO_2$ and a stock of solution of NaOH, which contained 35 per cent of Na_2O, was weighed from a weight burette.

The method of working and the general consistency of the results are illustrated by several examples in tables 1 and 2. Table 1 gives the sequence of compositions of gas and liquid at 1000 bars with increasing amounts of sodium disilicate glass. With successively 1, 2, and 2.5 grams both the water content and the SiO_2 content of the liquid decrease. When 2.8

grams were added the liquid (which cooled to a hard glass) contained a small amount of disilicate crystals, and it was assumed that the composition of the liquid of the three-phase triangle gas + saturated solution + $Na_2O \cdot 2SiO_2$ (G + L + Di) is the mean of the liquids with 2.5 and 2.8 grams. This procedure was used in establishing all of the liquid compositions. The gas composition was taken as the mean of the gases in the same two experiments.

Table 2 (1) and (2) give the details of two of the runs of table 1. First is given the amount of disilicate glass used, the temperature and the pressure. Next is given the weight of the gas removed from the bomb with a pipette, and its composition. In all cases the composition is given in terms of weight fractions H_2O, Na_2O, and SiO_2, followed by the ratio $SiO_2/(Na_2O+SiO_2)$, in square brackets. Then is given the weight of the liquid, or "andor." This was in the bottom of the crucible and was a hard glass without crystals. Next is the extra gas. This had condensed inside the loosely covered crucible, where it had had opportunity to react with the liquid (hydrous glass). The amount of condensed gas was calculated on the assumption that the liquid poured off was a mixture of condensed gas and dissolved liquid, and the agreement between the amounts calculated on the basis of the amount of Na_2O and in the amount of SiO_2 is satisfactory. The difference between the total weight and the weight of condensed gas is the weight of the liquid dissolved, 0.111 g. Next is given the

TABLE 1

Sequence of Gas and Liquid Compositions Determining the Liquid of the Three-phase Triangle G + L + Na_2O at 400°, 1000 Bars, Using Sodium Disilicate Glass [0.66 SiO_2].

All compositions are given in weight fractions. In mixtures containing all three components, the weight fractions are given in the order (H_2O, Na_2O; SiO_2), and this is usually followed by the weight ratio $SiO_2/(Na_2O + SiO_2)$ in square brackets.

Weight glass (grams)	Condition	Gas	Liquid
1	Liquid only	(0.957; .017; .026) [.62]	(0.368; .169; .463) [.733]
2	Liquid only	(0.944; .019; .037) [.66]	(0.308; .192; .500) [.732]
2.5	Liquid only	(0.944; .020; .036) [.64]	(0.265; .215; .520) [.708]
2.8	Liquid + Di	(0.956; .018; .026) [.59]	(0.254; .279; .517) [.693]

TABLE 2

Details of Some Typical Experiments

(1)		
2.0 g. (.34; .66) at 400°, 1000 bars		
Condensed gas weighed directly		11.60 g.
Composition (.944; .019; .037) [.66]		
Liquid; no crystals	1.513 g.	
Composition (.308; .192; .500) [.723]		
Extra gas 1.104 g.		
Na_2O 0.0453 g. = 0.963 g. gas		
SiO_2 0.1152 g. = 0.943 g. gas		0.953
Total weight of gas		12.56
Density (free volume = 16.4 ml.)	.766	
Total weight H_2O = 12.21 = 0.859 wt. fraction		
(2)		
2.8 g. (.34; .66) at 400°, 1000 bars		
Condensed gas weighed directly		10.925 g.
Composition (.956; .018; .026) [.62]		
Liquid + few $Na_2O \cdot 2SiO_2$	2.795	
Composition (.254; .229; .517) [.693]		
Extra gas, 0.639 g.		
Na_2O: 0.0639 g. = 0.391 g. gas		
SiO_2 0.1318 g. = 0.402 g. gas		0.396 g.
Total weight of gas		11.321
Density (free volume 14.9 ml.)	0.76	
Total H_2O = 11.56 g. = 0.805 wt. fraction		
(3)		
Condensed gas weighed directly		7.66 g.
Composition (.881; .049; .070) [.592]		
Liquid; no crystals	3.44 g.	
Composition (.315; .211; .474) [.691]		
Extra gas, 2.35 g.		
Na_2O: 0.1432 g. = 2.271 g. gas		
SiO_2: 0.2384 g. = 2.170 g. gas		2.17 g.
Total gas		9.83 g.
Density (free volume = 10.4 ml.)	0.945	
Total wt. H_2O = 9.93 g. = 0.739 wt. fraction		

TABLE 2 (*Cont.*)

Details of Some Typical Experiments

(4)		
5.0 g. (.34; .66), 400°, 2000 bars		
Condensed gas weighed directly		8.02 g.
Composition (.853; .059; .088) [.599]		
Liquid, trace $Na_2O \cdot 2SiO_2$ crystals 4.69 g.		
Composition (.312; .224; .464) [.675]		
Extra gas, 1.94 g.		
Na_2O: 0.0829 g. = 2.13 g. gas		
SiO_2: 0.2308 g. = 1.78 g. gas.....		1.78 g.
Total gas		9.80 g.
Density (free volume 10.4 ml.)	0.942	
Total wt. H_2O = 9.65 g. = 0.659 wt. fraction		
(5)		
2 g. (.26; .74), 400°, 247 bars		
Condensed gas weighed directly		2.50 g.
Composition (.997; .002; .001) [.37]		
Liquid; no crystals	2.36 g.	
Composition (.229; .200; .571) [.741]		
Extra gas, 0.47 g.		
Na_2O: O.0352 g. = 0.335 g. gas		
SiO_2: 0.1004 g. = 0.321 g. gas		0.328 g.
Total gas		2.828 g.
Density (free volume = 17 ml.)	0.166	
Total wt. H_2O = 3.366 g. = 0.631 wt. fraction		
(6)		
5 g. (.255; .745), 400°, 2000 bars		
Condensed gas weighed directly		6.30 g.
Composition (.728; .161; .111) [.721]		
Liquid no crystals	4.06 g.	
Composition (.318; .161; .521) [.764]		
Extra gas, 0.83 g.		
Na_2O: 0.0645 = 0.813 g. gas		
SiO_2 0.1631 = 0.829 g. gas		0.82 g.
Total gas		7.12 g.
Density (free volume = 9.6 ml.)	0.742	
Total wt. H_2O = 6.482 = 0.565 wt fraction		

TABLE 2 (*Cont.*)
Details of Some Typical Experiments

(7)		
1.5 g. (.44; .56) at 400° C., 700 bars		
Condensed gas weighed directly		11.185 g.
Composition (.955; .025; .020) [.45]		
Condensed gas + $Na_2O \cdot 2SiO_2$ crystals	0.90 g.	
Na_2O: 0.2509 g. = gas		
SiO_2: 0.4724 g. = 0.429 g. gas		0.432 g.
Extra gas, 1.445 g.		
Na_2O: 0.0964 g. = 1.220 g. gas		
SiO_2: 0.1281 g. = 1. 256 g. gas		1.238 g.
Total weight of gas		12.855 g.
Density (free volume = 17 ml.)	0.756	
Total weight H_2O = 12.04 g. = 0.889 wt. fraction		
(8)		
6 g. (.7; .3), 400° C., 2000 bars		
Condensed gas weighed directly		11.27 g.
Composition (.674; .242; .084) [.257]		
Condensed gas with $Na_2O \cdot SiO_2$ crystals, 2.56 g.		
Na_2O: 0.7847 = 1.005 g. gas		
SiO_2: 0.6135 = 1.017 g. gas		1.01 g.
Extra gas, 2.76		
Na_2O: 0.6598 = 2.791		
SiO_2: 0.2693 = 2.669.....		2.73
Total gas		15.01 g.
Density (free volume = 11 ml.)	1.36	
Total weight H_2O = 12.04 g. = 0.889 wt. fraction.		

total weight of gas, the sum of that weighed directly and the extra gas, and its approximate density. This is obtained by dividing the total weight of gas by the free volume of the bomb. The last line gives the total weight of water in the bomb and its weight fraction.

Table 2 (3) and (4) give similar details for two runs at 2000 bars. In (4) the weight of gas calculated from the Na_2O is high and was discarded. This discrepancy would be explained by some loss of Na_2O.

Table 2 (5) is a run with glass near the disilicate-quartz boundary, at a pressure near the boundary pressure, but with too little solid present to give crystals, and (6) is a similar one at 2000 bars. Each of these is in a bivariant region above the three-phase pressure.

Table 2 (6) and (7) are experiments in which no liquid is formed; the mixtures were both in the field of gas plus crystals, and in each case the crystals were large and well formed with many crystal faces. There was some condensed gas held in the interstices between the crystals after the supernatant liquid was poured out of the crucible, and the amount of gas was calculated as shown. The calculated density of gas in (8), 1.36, is noteworthy.

THEORETICAL DISCUSSION

The complete system.—The results here presented consist of a series of isothermal polybaric saturation curves at 400° C. The complete representation of this system, with two composition variables, pressure, and temperature, would require a hyperprism of four dimensions. In such a hyperprism the liquid solubility or saturation regions of each solid phase would be represented by a hypersurface and the corresponding gaseous solubility regions by a second hypersurface. The intersection of the two liquid saturation hypersurfaces would give a boundary curve in four-dimensional space between the two saturation regions. The complete representation of the system requires consideration of the critical hypersurface which, stably or metastably, joins the critical points of the three components. It is known that this critical hypersurface is intersected by saturation hypersurfaces, at which points the gaseous and liquid surfaces fold into each other, and this intersection is a critical end-point curve. In this paper the critical end-point curves will be mentioned only briefly.

A section through the hyperprism at constant temperature gives a triangular prism with the composition triangle as base, pressure as ordinate. The experimental results may be considered as a determination of the pressure necessary to dissolve in each Na_2O—SiO_2 mixture enough water to lower its melting point to 400° C., the identification of any crystals, and the analyses of the gaseous and liquid phases. The melting point of $Na_2O \cdot SiO_2$ is 1089°, of the eutectic between $Na_2O \cdot$

SiO_2 and $Na_2O \cdot 2SiO_2$, 846°, of $Na_2O \cdot 2SiO_2$, 874° and of the eutectic between $Na_2O \cdot 2SiO_2$ and quartz, 793°. It was convenient to make a series of runs at constant pressure, increasing the amounts of sodium silicate added until the compositions of the gas and saturated solution of the three-phase triangle G + L + S could be determined.

The isothermal isobaric section.—The discussion of these experiments is aided by figure 3 which is a diagrammatic representation of a projection of a section at constant pressure through a solid model representing the relations at constant temperature between pressure and composition; that is, through the $(P\text{-}X\text{-}Y)_T$ model. Part of the side Na_2O—SiO_2 is indicated, and Di represents the composition of $Na_2O \cdot 2SiO_2$. The broken lines E L_1 and E L_2 are the saturation curves of quartz and of $Na_2O \cdot 2SiO_2$, metastable except at the points L_1 and L_2. These are points of the three-phase triangles $G_1 - L_1$ —Qtz and G_2 —L_2 — Di, and represent invariant equilibrium at constant pressure and temperature. The portions of the saturation curves E L_1 and E L_2 represent solutions of vapor pressure lower than that of the diagram; the prolongations of these curves represent pressures higher than that of the diagram. The curve L_1 L_2 represents solutions unsaturated with respect to solid at this temperature and pressure.

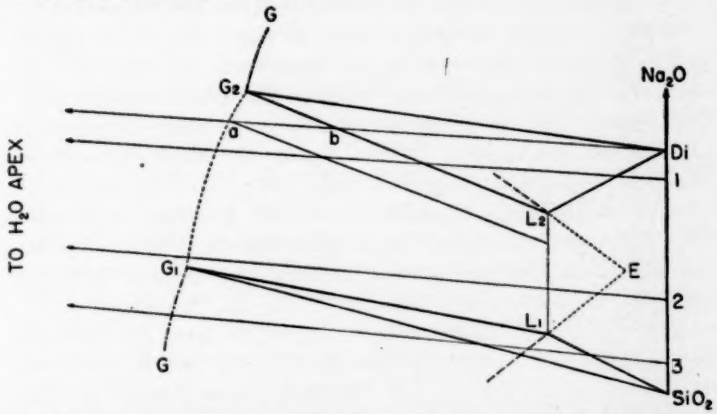

Fig. 3. Diagrammatic representation of part of a section at constant pressure through a solid model representing the relations between pressure and composition at constant temperature. On part of the side Na_2O—SiO_2 is indicated the composition of sodium disilicate, Di. The lines 1, 2, 3 go to the H_2O apex.

The lines H_2O—Di, H_2O—1, H_2O—2 and H_2O—3 join the H_2O—apex with mixtures on the side Na_2O—SiO_2 of the indicated composition. The gross composition of every ternary mixture which can be formed by adding H_2O to the given Na_2O—SiO_2 mixture will be on this line, and when both a gaseous and a liquid phase are formed the line joining their compositions cuts the line from the H_2O-apex at a point corresponding to the percentage of water injected.

When a small amount of disilicate is put into the crucible it will all be dissolved by the gas. If just enough is added to give a liquid, the gas will have a composition indicated by *a* on the line H_2O—Di and the liquid will be on the curve L_1 L_2, as indicated by the tie-line. If more disilicate is added, the gas composition follows the curve G_1 G_2, the liquid the curve L_1 L_2, until the gross composition *b* is reached. The liquid has now reached the composition L_2, crystalline sodium disilicate is formed, and the coexisting phases now are fixed in composition. If the original silicate mixture was of composition 1, there would be the same sequence of phases, $G \rightarrow G + L \rightarrow G + L +$ Di, but more of the mixture would have to be added before the three-phase triangle was entered; that is, the percentage of the water is less. If the mixture had the composition 2, no crystalline phase could be obtained; a mixture of this composition forms only unsaturated solution at this temperature and pressure.

With a mixture of composition 3, the sequence of phases will be different. The mixture will pass from the region of unsaturated gas to that of gas + quartz. The line G G_1 represents the solubility of SiO_2 in gases of changing Na_2O—content, in equilibrium with quartz. In this region the Na_2O dissolves in the gas in greater proportion than SiO_2, leaving crystalline quartz. With larger amounts of 3, the three-phase triangle $G + L_1 +$ Qtz is reached, liquid of composition L_1 is formed, and the phases become of fixed composition, their proportions changing as more solid is added.

The three-phase triangle $G + L_2 +$ Di is entered from a region of $G + L_1$, at the point where the tie-line H_2O—Di or H_2O—1 cuts the side G_2 L_2. The three-phase triangle $G + L_1 +$ Qtz is entered from a region of G + Qtz, at the point where the tie-line H_2O—3 cuts the side G_1—SiO_2. In the first case the phase sequence is $G \rightarrow G + L \rightarrow G + L +$ crystals; in the second it is $G \rightarrow G +$ crystals $\rightarrow G + L +$ crystals.

If the area of the three-phase triangle $G_1 + L_1 +$ quartz is calculated, writing the compositions of the phases in this order, the area will be found to have a positive sign, and it is circumscribed clockwise. If the area of the three-phase triangle $G_2 + L_2 +$ Di is calculated, writing the phases in the same order, the area will be found to have a negative sign, and the three-phase triangle will be circumscribed counterclockwise. In general, a three-phase area of positive sign will result from a phase sequence G → G + crystals → G + L + crystals, and one of negative sign will form a phase sequence G → G + L → G + L + crystals.

EXPERIMENTAL RESULTS

Preliminary work had indicated that the second critical end-point curve of sodium disilicate probably is below 400° C. and accordingly 400° was chosen as a desirable temperature for the first isotherm. The saturation pressures at 400° over much of the system are greater than at higher temperatures; consequently the effect of the gaseous solubility is more important. The summarized results of the various saturation curves are given in tables 3 to 6, and shown in figures 4 to 6. Figure 7 shows the isothermal polybaric saturation curves, both gas and liquid. It will be discussed in more detail subsequently.

The boundary, sodium disilicate—quartz.—The coexistence of G + L + Di + Qtz is an invariant point at constant temperature. It represents the point at 400° of the boundary between the regions of $Na_2O \cdot 2SiO_2$ and quartz, which starts at the eutectic in the binary system at 793° C. and 0.793 SiO_2. Its coordinates are p = 240 bars; gas (0.998, 0.001, 0.001) [0.37]; liquid (0.229, 0.200, 0.571) [0.741]. At 233 bars there was no liquid, only gas, crystalline disilicate and quartz. At 247 bars the phases were gas, solution, and a trace of quartz; the experimental details are given in table 2 (5). The pressure at the invariant point is taken as the mean of 233 and 247, or 240 bars, and gas and liquid compositions are assumed to be the same as at 247 bars. The density of the gas is 0.165; that of water at the same temperature and pressure is 0.152. The ratio $SiO_2/(Na_2O + SiO_2)$, 0.741, is essentially the same as at the binary eutectic.

The isothermal polybaric saturation curve of quartz.—As the pressure of water is increased at 400° above that of the

boundary between disilicate and quartz, the composition of both the gas and the liquid in equilibrium with quartz changes. The three-phase triangle G + L + Qtz is of positive area, and the sequence of the phases as the amount of sodium silicate is increased is G → G + Qtz → G + L + Qtz. In other words, a small amount of sodium silicate, say of ratio 0.76, is all dissolved by the steam. When more silicate is added, the ratio $SiO_2/(Na_2O + SiO_2)$ in the gas is smaller than in the liquid, Na_2O is extracted, and some SiO_2 is left behind as quartz. With still more silicate, liquid is formed, and the mixture enters the three-phase triangle G + L + Qtz. On further increase in the amount of silicate, the compositions of gas and liquid remain fixed and the proportions of gas, liquid and solid change. At lower pressures the difference between the $SiO_2/(Na_2O + SiO_2)$ ratio of gas and liquid is larger than at higher pressures; at 400° it is 0.37 at 240 bars, and 0.72 at 2000 bars, not very different from the ratio in the liquid, 0.76. This was found to be true in every case. At low pressure sodium oxide is extracted by the gas, but as pressure is increased the SiO_2—ratio in the gas approaches that in the liquid. The same effect was found with albite (Morey and Hesselgesser, 1951*b*).

The gaseous and liquid composition of the three-phase equilibrium at 400° C. are given in table 3 and shown graphically in figure 4. The ordinate is pressure in bars. The first pair of curves gives the weight fraction of H_2O in gas and liquid; the middle pair, the weight fraction SiO_2 in gas and liquid; and the

TABLE 3

Composition of Gas and Liquid of the Three-phase Triangle with Quartz at 400° C.

Pressure	Gas				Liquid			
				SiO_2				SiO_2
bars	H_2O	Na_2O	SiO_2	$Na_2O + SiO_2$	H_2O	Na_2O	SiO_2	$Na_2O + SiO_2$
240	.998	.001	.001	.5	.229	.200	.571	.741
400	.992	.003	.005	.58	.242	.195	.563	.743
700	.968	.012	.020	.63	.251	.192	.559	.746
800	.960	.013	.027	.68	.261	.186	.553	.748
1000	.950	.016	.034	.68	.270	.183	.547	.75
1200	.913	.027	.060	.69	.277	.181	.542	.75
1600	.88	.035	.085	.71	.281	.179	.540	.75
2000	.84	.045	.115	.72	.318	.161	.521	.76
2500	.77	.062	.168	.73	.35	.156	.494	.76

third pair, the ratio $SiO_2/(Na_2O + SiO_2)$ in gas and liquid.

At the highest pressure used, 2500 bars, the gas and liquid are still far apart in composition. Table 2 (6) gives details of a determinative run. Five grams of 0.745 glass were taken, and a total of 6.48 g. H_2O or 56.5 per cent was injected, and the weights and compositions of the condensed gas (solution in the bomb outside of the crucible), the liquid solution (glass) in the bottom of the crucible, and the extra gas poured out of the crucible are given. The glass contained a small amount, less than 0.1 per cent, of quartz.

At a sufficiently high pressure the gas and liquid will become identical in composition and the critical end-point will be reached. This line will extend into the P-T-X-Y hyperprism,

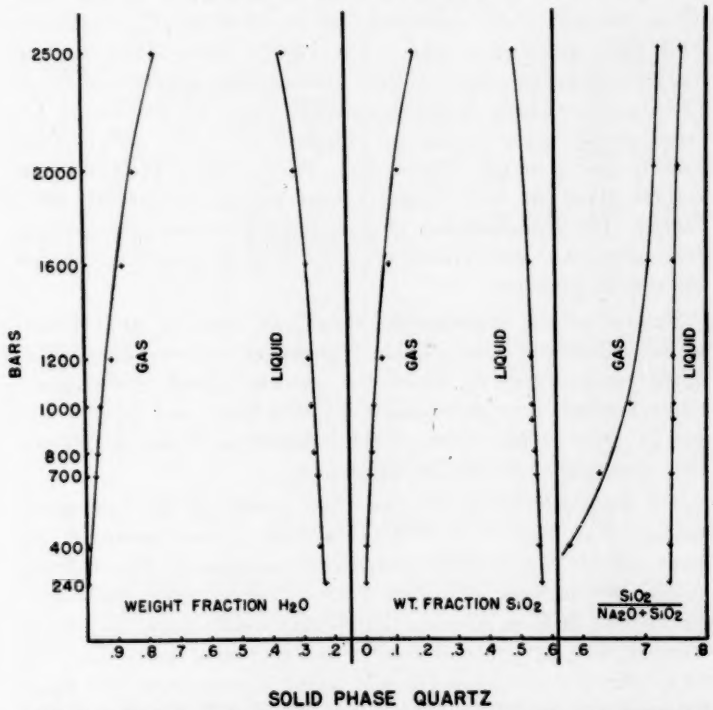

Fig. 4. The gas and liquid saturation curves of quartz. The ordinate; pressure in bars. The first pair of curves gives the weight fraction of H_2O in gas and liquid, in equilibrium with quartz; the second pair, the weight fraction of SiO_2 in gas and liquid; and the third pair the ratio $SiO_2/(Na_2O + SiO_2)$ in gas and liquid.

from the first critical end-point in the system H_2O—SiO_2, which is practically identical with the critical point of water; and will end at the second critical end-point in the system H_2O—SiO_2, if such an end-point exists. The critical end-point line at 400° will be at pressures greater than 2500 bars.

The isothermal polybaric saturation curve of sodium disilicate. (*a*) *Negative side.* As the pressure of water increases at 400° above the boundary between sodium disilicate and quartz, the composition of both gas and liquid in equilibrium with disilicate change. At each pressure the three-phase triangle gas + solution + disilicate is of negative area, and the phase sequence as the quantity of sodium silicate is increased is G → G + L → G + L + Di. Two thousand bars is not enough to obtain a liquid on the join H_2O—disilicate, but at 2250 bars 7 grams of a 0.63 glass gave no crystals, gas (.806; .081; .113) [.584], liquid (.339; .224; .437) [.661]. The melting pressure of $Na_2O \cdot 2SiO_2$ accordingly is taken as 2200 bars. At 2500 bars the same charge gave a gas of composition (.77; .093; .135) [.588] and a liquid (.347; .222; .431) [.66]. With 6 g. of a 0.66 glass the liquid composition was (.445; .170; .385) [.695]. The compositions of gas and liquid are approaching each other, and the critical region will be met with on further increase in pressure.

Several of the experimental details of tables 1 and 2 refer to this saturation curve. Table 1 gives the sequence of gas and liquid compositions by which the gas and liquid of the three-phase triangle were determined at 1000 bars, and table 2 (1) and (2) give details of two of the experiments. Table 2, (3) and (4), give similar details for 2000 bars.

The compositions of the gases and liquids of the three-phase triangle G + L + Di at 400° C. and at various pressures are given in table 4, and shown graphically in figure 5. The ordinate is pressure in bars. The first pair of curves gives the weight fraction of H_2O in gas and liquid; the middle pair, the weight fraction SiO_2 in gas and liquid; and the third pair, the ratio $SiO_2/(Na_2O + SiO_2)$ in gas and liquid. Comparison with figure 4 shows that at 2000 bars, gas and liquid are farther apart than in the saturation curve of quartz. The gas saturation curve of quartz shows a much greater decrease in water and increase in SiO_2 from 1000 to 2000 bars than does the disilicate curve; and

the ratio of $SiO_2/(Na_2O + SiO_2)$ in gas and liquid is little changed with increase in pressure.

(*b*) ***Positive side.*** The three-phase triangle G + L + Di which goes from the boundary G + L + M + Di is of positive area, and the sequence of phases as the amount of sodium silicate is increased is G → G + Di → G + L + Di. This liquid curve was difficult to determine. The gas which condensed inside the crucible reacted rapidly with crystals and the liquid reaction product was a pasty mass. It was hard to tell when liquid began to form and to separate the extra gas, and successive experiments under the same conditions were much less concordant than on the negative side of the disilicate curve or even of the metasilicate curve.

The end-points of this curve are the metasilicate-disilicate

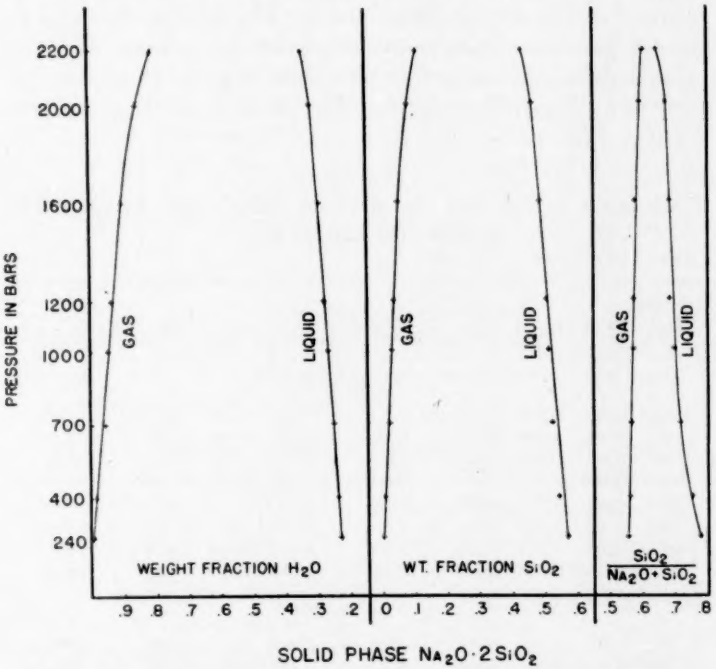

Fig. 5. The gas and liquid saturation curves of $Na_2O \cdot 2SiO_2$. The ordinate is pressure in bars. The first pair of curves gives the weight fraction H_2O of gas and liquid in equilibrium with $Na_2O \cdot 2SiO_2$; the second pair, the weight fraction of SiO_2 of gas and liquid; and the third pair the ratio $SiO_2/(Na_2O + SiO_2)$ in gas and liquid.

boundary, at 380 bars, discussed subsequently, and the congruent saturation curve of $Na_2O \cdot 2SiO_2$, at 2200 bars. The coordinates of the curve are in table 4 b. Experiments were made at 400 and 500 bars, but the results were too discordant to interpret. At higher pressures the results are somewhat better, and the points given are the mean of several experiments.

The boundary, sodium metasilicate-sodium disilicate.—The coexistence of gas, liquid, $Na_2O \cdot SiO_2$ and $Na_2O \cdot 2SiO_2$ is an invariant point at constant temperature. It represents the point at 400° of the boundary between the regions of $Na_2O \cdot SiO_2$ and $Na_2O \cdot 2SiO_2$, which starts at the eutectic in the binary system at 846° and 0.621 SiO_2.

This invariant (T) point, and the univariant curves leading from it, were difficult to locate. At 360 bars and at lower pressures all mixtures from .60 to .64 SiO_2 give only gas + crystals. At 400 bars there is an undoubted formation of liquid with 4 g. of a mixture containing 0.52 SiO_2; with 2 g. the phases are gas + $Na_2O \cdot SiO_2$ + $Na_2O \cdot 2SiO_2$. The pressure at the univariant

TABLE 4

Composition of Gas and Liquid of the Three-phase Triangle with Sodium Disilicate at 400° C.

Pressure	Gas				Liquid			
				SiO_2				SiO_2
bars	H_2O	Na_2O	SiO_2	$Na_2O + SiO_2$	H_2O	Na_2O	SiO_2	$Na_2O + SiO_2$
				a. Negative Side				
240	0.998	0.001	0.001	0.5	0.229	0.200	0.571	0.741
400	0.987	0.006	0.007	0.56	0.242	0.202	0.556	0.733
700	0.965	0.015	0.020	0.57	0.263	0.207	0.530	0.719
1000	0.946	0.023	0.031	0.58	0.271	0.210	0.519	0.712
1200	0.933	0.028	0.039	0.58	0.280	0.210	0.510	0.708
1600	0.903	0.040	0.057	0.59	0.293	0.214	0.493	0.697
2000	0.858	0.056	0.086	0.60	0.310	0.216	0.474	0.687
2200	0.806	0.076	0.118	0.61	0.340	0.224	0.436	0.661
				b. Positive Side				
380	0.96	0.027	0.013	0.32	0.265	0.294	0.441	0.600
700	0.932	0.044	0.024	0.35	0.272	0.281	0.447	0.614
1000	0.907	0.054	0.039	0.42	0.292	0.266	0.442	0.624
1600	0.836	0.077	0.087	0.53	0.315	0.247	0.438	0.640
2000	0.823	0.077	0.100	0.58	0.333	0.231	0.436	0.654
2200	0.806	0.074	0.120	0.61	0.340	0.224	0.436	0.661

(T) point is accordingly assumed to be 380 ± 20 bars. The compositions of the gaseous and liquid phases were estimated by extrapolation of the curves for G ± L + $Na_2O \cdot SiO_2$ down to 380 bars.

The isothermal polybaric saturation curve of $Na_2O \cdot SiO_2$. This saturation curve at 900° C. goes from the boundary with disilicate at 380 bars to the melting pressure of sodium metasilicate, if a critical region is not met with first. Our experiments go only to 2500 bars, and only two runs were made at that pressure; in one of these were no crystals, in the other only a few. The gas composition given for this pressure (0.61, 0.197, 0.193) [.497] is in part an extrapolation; the runs agreed in the $SiO_2/(Na_2O + SiO_2)$ ratio but the percentages of H_2O were far apart and one was disregarded. The liquid composition (0.427, 0.268, 0.305) [.532] is the average of the two runs. The water content and the $SiO_2/(Na_2O + SiO_2)$ ratios of gas and liquid are approaching each other, and it is probable that a critical region is not far distant. A water pressure which will melt sodium disilicate will not melt metasilicate. The experimental details are given in table 5 and shown graphically in figure 6.

The saturation curve is of negative area and the phase sequence is G → G + L → G + L + S. At the lower pressures it was hard to determine the first appearance of crystals, but at higher pressures the liquid of the three-phase equilibrium could be determined with more certainty. Work with this material was stopped because of its extremely corrosive action on the bombs, even on bombs made of Inconel X.

The more alkaline regions.—The regions containing more Na_2O than corresponds to the metasilicate (.5035; .4965) have not been cleared up. Sodium orthosilicate has the comopsition (.6737; .3263) but it was never found in any of the experiments. Mixtures containing 0.30 SiO_2 are in the divariant region of gas + crystalline metasilicate from 400 to 2000 bars; table 4 gives a summary of gas compositions at various pressures in equilibrium with $Na_2O \cdot SiO_2$ with an original composition containing 0.30 SiO_2. The ratio $SiO_2/Na_2O + SiO_2$ increases from 0.1 at low pressure to 0.26 at 2000 bars; at low pressure Na_2O is extracted; at high pressure the material is practically dissolved as such. Details of the experiments at 2000

bars are in table 2, example 8. This gas has a content of dissolved $Na_2O + SiO_2$ of 32.6 per cent, and a density of 1.35. It will eat through ¾ inch of stainless steel overnight, and even Inconel X cannot withstand its corrosive action for long. Stainless steel fails by stress corrosion, Inconel X by intergranular corrosion. It was because of this extremely corrosive nature of these highly alkaline gases that the studies have not been pushed to the critical end-point curve, which cannot be far away.

When 5 g. of a mixture containing 0.10 SiO_2 was heated at 100 bars, it was in the region of gas + metasilicate; the gas composition was (0.583, 0.410, 0.007) [.016]. The high-pressure steam extracted most of the Na_2O, leaving metasilicate crystals; the density of the gas was 0.49, that of the H_2O at the same temperature and pressure is 0.38. When 5 g. of the same mixture was heated at 1200 bars, there were no crystals. The composition of the gas was (0.756; .225; .020) [.083], that of the mixture of the liquid and condensed gas in the crucible, (0.722; .223; .053) [0.196]. The proportions of gas and liquid are unknown, but the possible range of the proportion is limited by the known behaviour of the mixture containing 0.30 SiO_2. If the proportion is 6 gas: 4 liquid, the liquid composition would be (0.679; .221; .108) [0.33] which is about the highest probable proportion. In any case, liquid and gas are approaching each other in composition, and a point on the critical surface is not far distant.

Several runs were made with NaOH at 80 bars. Lump NaOH

TABLE 5

Composition of Gas and Liquid of the Three-phase Triangle with Sodium Metasilicate at 400° C.

Pressure	Gas				Liquid			
bars	H_2O	Na_2O	SiO_2	$\frac{SiO_2}{Na_2O+SiO_2}$	H_2O	Na_2O	SiO_2	$\frac{SiO_2}{Na_2O+SiO_2}$
380	.96	.027	.013	.320	.265	.294	.441	.600
500	.94	.040	.020	.336	.289	.290	.421	.594
700	.91	.057	.033	.365	.308	2.86	.406	.587
1000	.86	.087	.053	.380	.333	.282	.385	.577
1200	.79	.127	.083	.395	.347	.280	.373	.571
1600	.76	.138	.102	.425	.366	.279	.355	.559
2000	.68	.174	.146	.458	.403	.270	.327	.547
(2500)	.61	.197	.193	(.497)	.427	.268	.305	.532

was put into the crucible, and analyses made as usual. On cooling, the condensed gas usually formed a mush of $NaOH \cdot H_2O$ crystals. The average gas composition was (.503, .497), the mixed condensed gas + liquid in the crucible (.492; .518), or gas, 0.641 NaOH, condensed gas + liquid, 0.668 NaOH. There is no way of estimating the proportion of condensed gas in the mixture.

The isothermal polybaric saturation curve.—This is shown in figure 7. Consider again the complete representation by means of the hyperprism X-Y-P-T. The consideration of this may be simplified by a separate consideration of the X-Y-T prism and the X-Y-P prism, which by transformation through a fourth dimension unite to form the hyperprism. The X-Y-T prism is similar to the triangular prism commonly used to represent

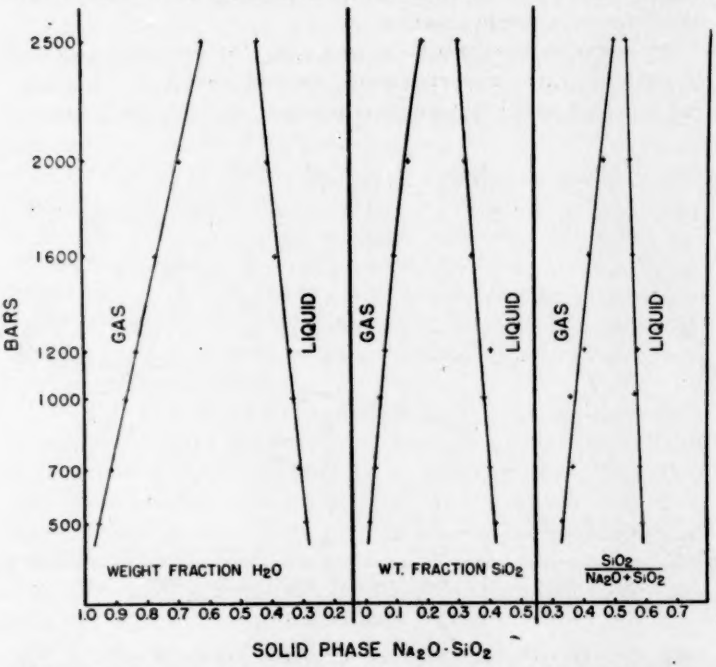

Fig. 6. The gas and liquid saturation curves of $Na_2O \cdot SiO_2$. The ordinate is pressure in bars. The first pair of curves gives the weight fraction of H_2O of gas and liquid in equilibrium with $Na_2O \cdot SiO_2$; the second pair the weight fraction of SiO_2 of gas and liquid; and the third pair the ratio $SiO_2/(Na_2O + SiO_2)$ in gas and liquid.

phase equilibrium relations in the ternary systems, except that it is two-leaved. We commonly think of the liquid leaf, which gives the compositions of the liquids which can coexist with crystalline phases. But when the compositions of the coexisting gas phases must be considered, there must be a second leaf or set of surfaces representing the compositions of those gases. The pressures of these saturated solutions will not be constant but will range between wide limits. A second triangular prism must be considered, the X-Y-P prism. This, of course, must also be two-leaved, and composition is the connecting link between the two prisms. If a given composition is chosen, a perpendicular at the composition will give in the X-Y-T prism the melting point of that mixture, in the X-Y-P prism the vapor pressure of that saturated solution, or the pressure of water plus the dissolved material which must be developed to liquify the mixture at the temperature in question.

At every temperature there is a range of pressures required to melt the various compositions, so that an $(X\text{-}Y\text{-}P)_T$ model can be constructed for each temperature, and the projection of

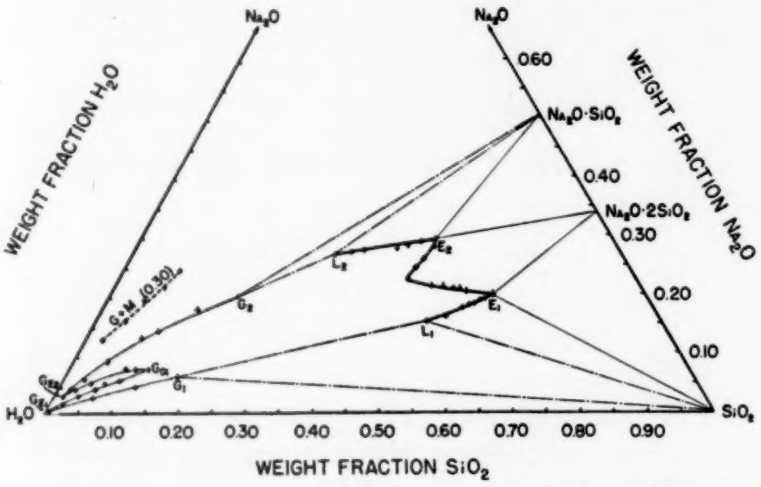

Fig. 7. The isothermal polybaric saturation curves at 400° C. The curve E_1L_1 is the liquid saturation curve of quartz; GE_1G_1 the coexisting saturation curve; and the triangle $G_1L_1SiO_2$ is the three-phase triangle at 2500 bars. E_1E_2 and G_1G_2 are the gas and liquid saturation curves of $Na_2O{\cdot}2SiO_2$. E_2L_2 and GE_2G_2 are the saturation curves of $Na_2O{\cdot}SiO_2$, and G_2L_2 $Na_2O{\cdot}SiO_2$ is the three-phase triangle at 2500 bars.

such model on the base will give a representation of the results of this study. Figure 7 is such a projection at 400° C.

The intersection of the saturation curves of quartz and disilicate is at E_1; the pressure at this point is 240 bars. The coexisting gas is at G_{E_1}. The curve E_1 L_1 is the isothermal polybaric saturation curve of quartz, and along it pressure increases to 2500 bars. G_1—L_1—SiO_2 is the three-phase triangle at 2500 bars.

The curve E_1 E_2 is the liquid saturation curve of sodium disilicate, and G_{E_1} G_{Di} G_{E_2} is the coexisting gaseous saturation curve. Liquid of the ratio of $SiO_2/(Na_2O + SiO_2)$ of sodium disilicate, [0.66], is in equilibrium with a gas containing a larger proportion of Na_2O, of ratio [.61]. The three-phase triangle at this pressure is gas—sodium disilicate—liquid so that the point of maximum water content, the point of tangency of a line parallel to the side Na_2O—SiO_2, will not be exactly 0.66 but will be displaced to be on the line G—$Na_2O \cdot 2SiO_2$. This will be at a ratio of about 0.65. This gas contains less dissolved material than that in equilibrium with the liquid saturation curve of quartz at the same pressure.

E_2 is the point on the boundary between metasilicate and disilicate, and from it the saturation curve of metasilicate rises to the three-phase triangle at 2500 bars. G_2—M—L_2 is the three-phase triangle at this pressure. Gas and liquid are approaching each other, and the critical end-point curve probably would be reached in another thousand bars. It is noteworthy that the melting pressure of sodium metasilicate is greater than that of sodium disilicate.

The line G + M (0.30) represents the gases in equilibrium with metasilicate crystals at pressures up to 2000 bars, with an initial silica ratio of 0.3 (table 6). A higher pressure than 2000 bars is necessary to obtain a liquid with this composition. A mixture with a silica ratio of 0.10 was in the region gas + metasilicate crystals at 100 bars, and the gas contained 42 per cent dissolved material. At 1200 bars unsaturated liquid was obtained.

When the system as a whole is considered it is evident that some such results are inevitable. Sodium metasilicate and sodium disilicate are surrounded by a critical curve, representing the intersection of the critical hypersurface joining the critical points of the three components by the saturation hypersurface.

The metasilicate critical region will extend toward the side H_2O—Na_2O, which it cannot reach. Similarly, the boundary between disilicate and quartz is a continuous curve which does not intersect a critical curve. The disilicate and the metasilicate critical regions thus will be surrounded by closed curves. These curves either may be separate closed curves, or they may intersect, giving rise to upper and lower double critical end-points. Which of these possibilities represents the facts cannot be said for certain until other work which is under way can be completed, but at present it seems probable that the critical surface is not intersected by the boundary G + L + metasilicate + disilicate. Each critical region will then be surrounded by a closed curve. These critical regions are remarkable in that the temperature difference across them is so small. The first critical end-point on the join G + L + Di cannot be much above 374°, with a pressure near 212 bars, and the second critical end-point must be below 400°, with a pressure greater than 2250 bars. The end-point on the join G + L + M must be at a higher pressure, possibly a higher temperature. It may be true in general that systems of the type water-salt which show critical end-points will have similar relationships between the first and second critical end-points, namely, a small difference in temperature and a very great difference in pressure.

Other work on this system is under way, at both higher and lower temperatures and will be reported before long.

TABLE 6

Composition of Gases in Equilibrium with Crystalline Sodium Metasilicate at 400° C.

The original charge was 5 g. of a (0.7:0.3) mixture.

Pressure bars	H_2O	Na_2O	SiO_2	$\frac{SiO_2}{Na_2O + SiO_2}$
400	0.871	0.115	0.014	0.11
700	0.852	0.121	0.027	0.18
1000	0.799	0.156	0.045	0.22
1200	0.754	0.191	0.055	0.23
1600	0.712	0.213	0.075	0.26
2000	0.674	0.242	0.084	0.26

References

Adams, L. H., 1941. Report of the Director of the Geophysical Laboratory: Carnegie Inst. Washington Year Book 40.

Friedman, I., 1950. Immiscibility in the system H_2O—Na_2—SiO_2: Am. Chemical Soc. Jour., vol. 72, pp. 4570-4574.

Kracek, F. C., 1930. The system sodium oxide—silica: Phys. Chemical Jour., vol. 34, pp. 1583-1595.

Morey, G. W., 1914. New crystalline silicates of potassium and sodium, their preparation and general properties: Am. Chemical Soc. Jour., vol. 36, pp. 215-230.

———, and Bowen, N. L., 1924. The binary system sodium metasilicate—silica: Physical Chem. Jour., vol. 28, pp. 1167-1179.

———, and Fenner, C. N., 1917. The ternary system H_2O—K_2SiO_3—SiO: Am. Chemical Soc. Jour., vol. 39, pp. 1173-1229.

———, and Hesselgesser, J. M., 1951*a*. The solubility of quartz and some other substances in superheated steam at high pressures: Am. Soc. Mechanical Engineers Trans., vol. 74, pp. 865-876.

———, and ———, 1951*b*. The solubility of some minerals in superheated steam at high pressures: Econ. Geology, vol. 46, pp. 821-835.

———, and Ingerson, Earl, 1937. A bomb for use in hydrothermal experimentation: Am. Mineralogist, vol. 22, pp. 1121-1122.

———, and ———, 1958. The system, water—sodium disilicate: Am. Jour. Sci., 5th ser., vol. 35A, pp. 217-225.

Geophysical Laboratory
Carnegie Institution of Washington
Washington, D. C.

HEAT OF FORMATION OF MERWINITE AND MONTICELLITE

K. J. NEUVONEN

ABSTRACT. The heats of formation of merwinite $Ca_3Mg(SiO_4)_2$ and monticellite $CaMgSiO_4$ have been measured by means of solution calorimetry. Natural merwinite from Crestmore, California, and natural monticellite from Magnet Cove, Arkansas, were used for the measurements. The results, corrected for theoretical compositions of the two minerals, are for merwinite $\Delta H = -57{,}020 \pm 380$ cal/mole and for monticellite $\Delta H = -27{,}560 \pm 140$ cal/mole. The values account for the heat of formation of the two silicates at 25° C. from quartz, calcium oxide, and magnesium oxide (prepared through dehydrating magnesium hydroxide 2.5 hours at 1425° C.).

IN connection with a general research program of obtaining numerical data for the thermal quantities of rock-making silicates, the simple and complex orthosilicates of magnesium and calcium are of considerable importance. For pure magnesium orthosilicate (forsterite), the heat of formation from the component oxides has been measured by Torgeson and Sahama (1948) and for pure calcium orthosilicate (β) by King (1951). The values given by these authors are $\Delta H_{Mg_2SiO_4} = -15{,}120 \pm 210$ cal/mole and $\Delta H_{Ca_2SiO_4} = -30{,}190 \pm 230$ cal/mole, respectively.

In the system Mg_2SiO_4 —Ca_2SiO_4, two additional orthosilicates occur, merwinite $Ca_3Mg(SiO_4)_2$ and monticellite $CaMgSiO_4$. Both are typical constituents of limestone contact zones. In order to establish the stability relations of the silicate constituents of dolomitic limestones, it seems very desirable to produce data for the heats of formation of these two complex calcium magnesium orthosilicates. In the present paper, heats of formation of merwinite and monticellite are given from the component oxides at 25° C. For that purpose, a specimen of natural merwinite from Crestmore, California, was placed at the author's disposal by Dr. F. W. Foshag, of the U. S. National Museum, Washington, D. C. A natural monticellite from Magnet Cove, Arkansas, was obtained from the collections of the Institute of Geology, University of Helsinki, Finland. High temperature heat content data for these two minerals will be given on a later occasion. The materials available of the minerals in question are, unfortunately, too scanty to allow low temperature calorimetric work. Accordingly, esti-

mates of the entropies can not be made at present. No previous work dealing with the thermal properties of merwinite and monticellite has been published.

The measurements were done by means of solution calorimetry using an acid mixture of 20 per cent by weight hydrochloric acid and 5 per cent by weight hydrofluoric acid at a temperature of 75° C. The apparatus and experimental procedure have been fully described by Sahama and Neuvonen (1951) and by Neuvonen (1952).

The specimens were crushed and ground down to a suitable grain size. The powdered materials were subjected to mineral separation by centrifuging in Clerici solution several times. The purities of the final products to be analyzed were tested under the microscope in immersion liquids of approximately the same indices of refraction as the minerals in question. By counting a large number of grains, a rough idea of the amount of impurities was obtained. According to the estimations made in that way, the merwinite sample used contained ca. 0.4 per cent of foreign material. The monticellite sample was virtually 100 per cent pure. The physical properties of the two minerals are as follows:

	Merwinite Crestmore, Calif.	Monticellite Magnet Cove, Ark.
α	1.702	1.651
β	1.710	1.657
γ	1.723	1.664
2V (Universal stage)	76°(+)	72°(—)
$c \wedge a$	36°	—
$d_4^{20°}$ (pycnometer)	3.316	3.269

The chemical composition of merwinite is given in table 1 and that of monticellite in table 2.

In calculating the composition of merwinite, titania and alumina were combined with silica, ferric iron was converted to ferrous iron, and water was neglected.

In calculating the composition of monticellite, ferric iron was converted to ferrous iron and water was neglected. The result was reduced to 100 per cent.

For obtaining the heat of solution of merwinite in the acid

mixture, six runs were made. The results are summarized in table 3.

The average value for the heat of solution of merwinite given in table 3 must still be corrected to correspond to the ideal

TABLE 1

Analysis of Merwinite from Crestmore, Calif. Analyst H. B. Wiik.

	Theoretical composition of $Ca_3Mg(SiO_4)_2$	Weight per cent found	Atomic proportions multiplied by 10,000		Calculated composition. Weight per cent	
SiO_2	36.54	35.58	Si	5924	$Ca_3Mg(SiO_4)_2$	99.03
TiO_2	....	0.08	Ti	4	Fe_2SiO_4	0.60
Al_2O_3	....	0.35	Al	69	Mg_2SiO_4	0.33
Fe_2O_3	....	0.07	Fe^{3+}	9	Mn_2SiO_4	0.03
FeO	....	0.36	Fe^{2+}	50		
MnO	....	0.02	Mn	3	Total	99.99
MgO	12.27	12.34	Mg	3061		
CaO	51.19	50.69	Ca	9039		
H_2O+	....	0.44	OH	488		
H_2O-	....	0.00				
Total	100.00	99.88				

TABLE 2

Analysis of Monticellite from Magnet Cove, Ark. Analyst K. J. Neuvonen.

	Theoretical composition of $CaMgSiO_4$	Weight per cent found	Atomic proportions multiplied by 10,000		Calculated composition. Weight per cent	
SiO_2	38.39	35.96	Si	5987	$CaMgSiO_4$	82.25
TiO_2	....	0.00	Fe^{3+}	213	Ca_2SiO_4	7.01
Al_2O_3	....	0.00	Fe^{2+}	685	Fe_2SiO_4	9.08
Fe_2O_3	....	1.70	Mn	165	Mn_2SiO_4	1.66
FeO	....	4.92	Mg	5298		
MnO	....	1.17	Ca	6118	Total	100.00
MgO	25.77	21.36	OH	755		
CaO	35.84	34.31				
H_2O+	....	0.68				
H_2O-	....	0.00				
Total	100.00	100.10				

TABLE 3

Heat of Solution of Merwinite from Crestmore, Calif., in the Acid Mixture Used. Not Corrected for Chemical Composition.

	Weight of sample dissolved gram	Heat of solution cal/gram
Run No. 1.	0.5038	−584.18
2.	0.5128	−585.08
3.	0.5235	−585.38
4.	0.5115	−586.19
5.	0.5077	−586.28
6.	0.5454	−587.74
	Average: −585.81 ± 1.00 cal/gram	

composition of $Ca_3Mg(SiO_4)_2$. On making the correction it is assumed that the heat of solution measured equals the sum of heats of solution of the compounds listed in the fifth column of table 1. This assumption neglects the heat of formation of the solid solution from the simple orthosilicates. The error introduced thereby is considered negligible for purposes of correction. Accordingly, the heat of solution of merwinite, corrected for the contents of Fe_2SiO_4, Mg_2SiO_4, and Mn_2SiO_4 in solid solution, may be calculated from the relationship

$$-585.81 = 0.9903 \cdot \Delta H + 0.0060 \cdot \Delta H_{Fe} + 0.0033 \cdot \Delta H_{Mg} + 0.0003 \cdot \Delta H_{Mn} \cdot$$

In this equation, ΔH_{Fe}, ΔH_{Mg}, and ΔH_{Mn} denote the heats of solution of the corresponding simple orthosilicates, respectively, and ΔH denotes the heat of solution of merwinite corrected for the orthosilicates mentioned. On the basis of two preliminary heat of solution experiments made on pure synthetic fayalite, ΔH_{Fe} was estimated to −373.5 cal/gram. ΔH_{Mg} was computed from the heats of solution of magnesium oxide and quartz in the acid mixture, given by Neuvonen (1952) and from the heat of formation of forsterite given by Torgeson and Sahama (1948). The value obtained is ΔH_{Mg} = −634.3 cal/gram. On the basis of the data given by Sahama and Torgeson (1949) the heat of solution of manganese orthosilicate was estimated to −68,900 cal/mole corresponding to ΔH_{Mn} = −341.2 cal/gram. Substituting these figures in the equation above yields ΔH = −587.07 cal/gram. This value must still be corrected for the 0.44 per cent water

shown by the analysis of table 1. Using the value of $^{+}30.38$ cal/gram for the heat of solution of liquid water in the acid mixture (reaction VI below) and $^{+}79.71$ cal/gram for the latent heat of fusion of ice as given by Osborne (1939) yields

$$\Delta H_{\text{Merwinite}} = -590.15 \text{ cal/gram or}$$
$$= -193{,}970 \text{ cal/mole.}$$

To this value an uncertainty of ± 350 calories must be added.

For obtaining the heat of solution of monticellite in the acid mixture, six runs were made. The results are summarized in table 4.

TABLE 4

Heat of Solution of Monticellite from Magnet Cove, Ark., in the Acid Mixture. Not Corrected for Chemical Composition.

	Weight of sample dissolved gram	Heat of solution cal/gram
Run No. 1.	0.2080	−554.48
2.	0.2350	−554.63
3.	0.2908	−554.90
4.	0.2680	−555.30
5.	0.3592	−555.82
6.	0.3372	−556.01
	Average:	−555.19 ± 0.52 cal/gram

The average value for the heat of solution of monticellite given in table 4 was corrected for chemical composition of the mineral in the same way as before. The correction was computed according to the relationship

$$-555.19 = 0.8225 \cdot \Delta H + 0.0701 \cdot \Delta H_{Ca} + 0.0908 \cdot \Delta H_{Fe} + 0.0166 \cdot \Delta H_{Mn}.$$

The values for ΔH_{Fe} and ΔH_{Mn} have been given above. ΔH_{Ca} was calculated on the basis of the heat of formation of Ca_2SiO_4 (β) from calcium oxide and quartz given by King (1951) and from the heats of solution of calcium oxide and quartz in the acid mixture mentioned below. The computation yields $\Delta H_{Ca} = -594.3$ cal/gram. Substituting these figures in the equation above yields $\Delta H = -576.24$ cal/gram or, corrected for the 0.68 per cent water shown by the analysis,

$$\Delta H_{\text{Monticellite}} = -580.94 \text{ cal/gram or}$$
$$= -90{,}890 \text{ cal/mole.}$$

To this value an uncertainty of ± 100 calories must be added.

The reactions for evaluating the heat of formation of merwinite are as follows:

I $Ca_3Mg(SiO_4)_2$(merwinite, 25°C.) + 20HF(sol., 75°C.) → $3CaF_2$(sol., 75°C.) + MgF_2(sol., 75°C.) + $2H_2SiF_6$ (sol., 75°C.) + $8H_2O$(sol., 75°C.)

II SiO_2(quartz, 25°C.) + 6HF(sol., 75°C.) → H_2SiF_6 (sol., 75°C.) + $2H_2O$(sol., 75°C.)

III CaO(cryst., 25°C.) + 2HF(sol., 75°C.) → CaF_2(sol., 75°C.) + H_2O(sol., 75°C.)

IV $Mg(OH)_2$(brucite, 25°C.) + 2HF(sol., 75°C.) → MgF_2 (sol., 75°C.) + $2H_2O$(sol., 75°C.)

V MgO(cryst., 25°C., magnesium hydroxide dehydrated 2.5 hours at 1425°C.) + H_2O(liquid, 25°C.) → $Mg(OH)_2$(brucite, 25°C.)

VI H_2O(liquid, 25°C.) → H_2O(sol., 75°C.)

VII $3CaO$(cryst., 25°C.) + MgO(cryst., 25°C., magnesium hydroxide dehydrated 2.5 hours at 1425°C.) + $2SiO_2$ (quartz, 25°C.) → $Ca_3Mg(SiO_4)_2$(merwinite, 25°C.).

$$\Delta H_{VII} = -\Delta H_I + 2\Delta H_{II} + 3\Delta H_{III} + \Delta H_{IV} + \Delta H_V - \Delta H_{VI}.$$

The value for ΔH_I was mentioned above, *viz.*:

$$\Delta H_I = -193{,}970 \pm 350 \text{ cal.}$$

The values for the heats of the reactions II-IV and VI have been given by Neuvonen (1952). They were obtained with the same apparatus and in similar experimental conditions. The figures are listed below:

$$\Delta H_{II} = -\ 33{,}400 \pm 30 \text{ cal.}$$
$$\Delta H_{III} = -\ 49{,}570 \pm 30$$
$$\Delta H_{IV} = -\ 25{,}850 \pm 70$$
$$\Delta H_{VI} = +\ \ 550 \pm 15$$

The heat of reaction V, taken from Taylor and Wells (1938), amounts to

$$\Delta H_V = -\ 9{,}080 \pm 30 \text{ cal.}$$

Substituting these figures in the equation for the heat of reaction VII yields

$$\Delta H_{VII} = -57{,}020 \pm 380 \text{ cal/mole.}$$

This value gives the heat of formation of $Ca_3Mg(SiO_4)_2$ (merwinite) from the component oxides at 25° C.

For evaluating the heat of formation of monticellite, the following reaction is considered:

VIII $CaMgSiO_4$(monticellite, 25° C.) + 10HF(sol., 75° C.) → CaF_2(sol., 75° C.) + MgF_2(sol., 75° C.) + H_2SiF_6 (sol., 75° C.) + $4H_2O$(sol., 75° C.)

Combining reaction VIII with reactions II-VI yields

IX CaO(cryst., 25°C.) + MgO(cryst., 25°C., magnesium hydroxide dehydrated 2.5 hours at 1425°C.) + SiO_2 (quartz, 25°C.) → $CaMgSiO_4$(monticellite, 25°C.)

with the corresponding heat of reaction

$$\Delta H_{IX} = -\Delta H_{VIII} + \Delta H_{II} + \Delta H_{III} + \Delta H_{IV} + \Delta H_{V} - \Delta H_{VI}.$$

Substituting the values given for the heats of the reactions mentioned yields

$$\Delta H_{IX} = -27{,}560 \pm 140 \text{ cal/mole.}$$

This value gives the heat of formation of $CaMgSiO_4$ (monticellite) from the component oxides at 25° C.

The author expresses his gratitude to Dr. F. W. Foshag for the merwinite specimen used and to Mr. H. B. Wiik for making the analysis of merwinite.

References

King, E. G., 1951. Heats of formation of crystalline orthosilicate, tricalcium silicate and zinc orthosilicate: Am. Chemical Soc. Jour., vol. 73, pp. 656-658.

Neuvonen, K. J., 1952. Thermochemical investigation of the åkermanite-gehlenite series: Comm. géol. Finlande Bull. 158.

Osborne, N. S., 1939. Heat of fusion of ice. A revision: Nat. Bur. Standards Jour. Research, vol. 23, pp. 643-646.

Sahama, Th. G., and Neuvonen, K. J., 1951. A solution calorimeter for silicates: Soc. géol. Finlande Comptes rendus, no. 24.

———, and Torgeson, D. R., 1949. Thermochemical study of the stability relation of geikielite and ilmenite in rocks: U. S. Bur. Mines Rept. Inv. 4407.

Taylor, Kenneth, and Wells, L. S., 1938. Studies of heat of solution of calcium and magnesium oxides and hydroxides: Nat. Bur. Standards Jour. Research, vol. 21, pp. 133-149.

Torgeson, D. R., and Sahama, Th. G., 1948. A hydrofluoric acid solution calorimeter and the determination of the heats of formation of Mg_2SiO_4, $MgSiO_3$, and $CaSiO_3$: Am. Chemical Soc. Jour., vol. 70, pp. 2156-2160.

Institute of Geology
Helsinki, Finland

THE CHEMISTRY OF THE KEWEENAWAN LAVAS

PAUL NIGGLI

ABSTRACT. Research by various authors and especially by T. M. Broderick and Henry R. Cornwall has done much to clarify the chemistry of the Keweenawan lavas. Calculations and graphic representations based on molecular units instead of weight percentages are carried out in the present paper with a view to clarifying the differentiation tendencies in these basic magmas. It is pointed out that the formation of the so-called pegmatite layers can be regarded as the first indications of a differentiation tending toward the development of a spilitic to keratophyric association.

THE papers by T. M. Broderick (1935) on differentiation in lavas of the Michigan Keweenawan and Henry R. Cornwall (1951) on differentiation in lavas of the Keweenawan series and the origin of the copper deposits of Michigan are a most valuable contribution on the chemical, mineralogical, and genetic relations of these basic lavas. In the book *Die jungen Eruptivgesteine des mediterranen Orogens*, Vol. I, [quoted hereafter as B and N] an attempt was made to compare typical examples of basic magmatic rock provinces. It seems appropriate to add the example of the Keweenawan lavas to this investigation. It will be necessary for comparative purposes to use the same system of calculations (Niggli values and molecular norms), and this will furnish an opportunity of seeing whether such calculations are able in any way to supplement the detailed discussions given by Broderick and Cornwall.

Cornwall classifies the rocks as follows:

ophites: mainly basalts and andesites (fine-grained also called trap)
glomeroporphyrites: basalts, andesites, dacites
porphyrites: basalts, andesites, dacites
melaphyres: basalts, andesites, dacites, rhyodacites
felsites: rhyolites
aplitic differentiate in dykes: granodiorite aplite
pegmatitic facies of basalts (often called dolerites): partly albite-diabases or spilites

On the top of many flows is often an amygdaloidal zone; the base of the flows is in many cases chilled.

In the two papers we find analyses of the following regions or flows:

Greenstone flow (G): 13 analyses (Broderick); 7 analyses (Cornwall); total, 20 analyses
Kearsage flow (K): 8 analyses (Broderick)
Cape Spencer flow (Sp): 5 analyses (Broderick)
"Big" Trap (T): 6 analyses (Cornwall)
Diabase sill (Lake Huron, Ontario) (Si): 4 analyses (Broderick)

To these 43 analyses Broderick adds 16 further analyses from different localities: 3 analyses of the Mt. Bohemian gabbro—gabbro aplite series (B), 5 melaphyres (M), 2 glomeroporphyrites (Gl), 3 felsites (F), 1 weathered felsite porphyrite (FP), 1 porphyrite (P), 1 ophite (O). We shall use the numbers given in the two papers, so that the special localities can easily be found. All the 59 analyses were recalculated.

The rocks belong in the main to the following chemically defined magma types (see table 1):

miharaitic, c-gabbroid to hawaiitic (20 analyses)
gabbrodioritic to melagabbrodioritic (18 analyses)
(normal)—gabbroid (6 analyses)

TABLE 1

Magma Types of the Keweenawan Lavas

Miharaitic and c-gabbroic	Si 1, 2; M 3091 G 253, average 3132, 3134, 3148, 3150 K average 3117, 3119, 3121 Sp 5; O 3095
Hawaiitic (to gabbrodioritic)	G 3144; T 1370; Sp 7, 8, 9
Gabbroic	G 453, 3152, 3154; T 1522, 1716; Gl 3110
Gabbrodioritic	Si 3 G 3136, 3138, 3142, 3146 K 3115, 3123 T 1399, 1413; Sp 6; M 3106
Melagabbrodioritic (to gabbrodioritic)	M 3129; G 149, 604, 3140 T 1501; B 3163, 3166 to sodalamprosyenitic
Gabbrodioritic to sodalamprosyenitic	Gl 3103
Sodalamprosyenitic	K 3113; P 3170
Mugearitic	M 3127, 3104; FP 3169
Pyroxengabbroic	G 297; K 3112
Ariégitic	G 559
Si-gabbrodioritic	Si 4
Moyitic	G 26
Granitic	B 3161
Alcaligranitic	F 3156, 3159

In addition, some compositions tend toward natronlamproitic and mugearitic and, in isolated cases, toward pyroxenegabbroid to ariegitic.

As the Niggli values and magma types of many basic rocks are given in B and N, an accurate comparison between these and the chemistry of basic lavas contained in other differentiation series can at once be undertaken. As in the previous work, a number of characteristic average and individual values, independent of the classification according to magma types, will be given for the Keweenawan series (table 2). They cover approximately the whole range and will be compared with the Hawaiian lavas contained in table 3 taken from another statistical investigation. These tables and the graphical presentation in figures 1*a* and 1*b* clearly indicate the existing differences.

	si	al	fm	c	alk
Basic lavas of the Hawaiian Islands	60-160	4.5-32	30-80	10-32	2.5-24
Part between si 100-130	100-130	14-30	33-55	19-30	3-22
Basic lavas of the Keweenawan (without aplites, felsites, etc.), general	100-171	16-26	35-55	9-40	3-17
Main part between si 100-130	100-130	16-25	40-55	17.5-35	3-12.5

Although the lack of analyses of olivine-rich rocks in the Keweenawan series may be fortuitous, it cannot be doubted that the lavas of the Hawaiian Islands contain the si-poorer members. In the same si interval the Hawaiian lavas are often

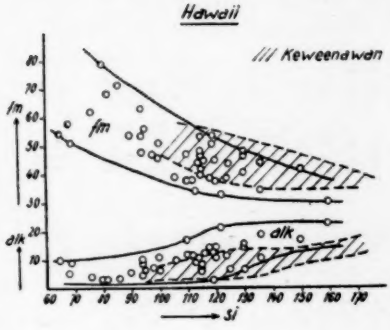

Fig. 1a

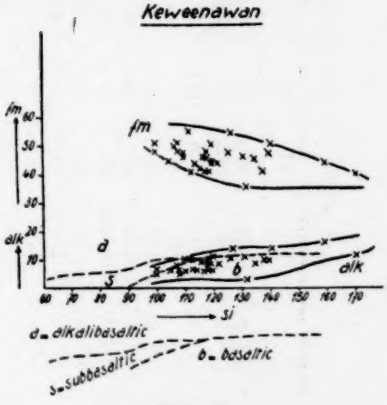

Fig. 1b

TABLE 2

Characteristic Average Values and Single Types of the Keweenawan Lavas

	si	al	fm	c	alk	k	mg	Related to:
I a	118	18	48	27.5	6.5	0.1 -0.2	0.6 -0.65	Sp 9, 8, 7
I b	117	21.5	46	26.5	6	0.1	0.6	Si 1
II a	105-120	23.5	44.5	26	6	~0.1	0.5 -0.55	G average, 3132, 3148, 3150, 3134, K average, 3117, 3119, 3121
II b	~114	23	43.5	27.5	6	0.1 -0.2	0.5 -0.6	Si 2, M 3091
II c	116	21	42	28	9	0.04	0.4	G 253
II d	118-138	23	41	26	10	0.1	0.45	G 3142, Sp 6
III a	~122	24	44	23.5	8.5	0.1 -0.2	0.4 -0.5	G 3146, K 3123
III b	119	25	41	25.5	8.5	0.1 -0.2	0.4	G 3138, 3144
III c	~120	24	44	21	11	~0.1	~0.5	M 3106, K 3115
IV a	118-135	21.5	45.5	24.5	8.5	0.0 -0.35	0.3 -0.5	T 1413, Sp 5
IV b	107	17.5	50	24.5	8	0.1 -0.3	0.4 -0.5	G 453, T 1501
IV c	126	16.5	47.5	25.5	10.5	0.1	0.3	G 3140
IV d	131	20.5	46.5	22	11	0.2	0.4	G 3136
V a	100-108	21.5	51	22.5	5	0.1	0.6	G 3152, 3154
V b	100-108	22.5	48	23	6.5	~0.1	0.5 -0.6	T 1716, 1522, Gl 3110, O 3095
VI a	112	18	55	17	10	0.4 -0.5	0.3 -0.4	B 3166
VI b	110-140	23.5	47.5	19	10	0.15-0.3	0.35-0.55	Gl 3103, Si 3, T 1399, G 149
VI c	~120	20.5	50.5	18	11	0.1 -0.4	0.35-0.5	B 3163, M 3129, G 604, K 3113
VI d	141	20.5	50.5	15	14	0.1 -0.2	~0.4	M 3104
VII	127	22	54.5	9.5	14	0.1 -0.2	0.4 -0.5	P 3170
VIII a	110	19	46	29	6	0-0.15	0.35-0.55	G 559, T 1370
VIII b	113	19	41	33.5	6.5	0.2	0.4 -0.5	G 247
VIII c	132	22	35.5	39.5	3	0.1	0.4	K 3112 (has undergone secondary changes, altered)
IX a	171	25.5	40	23	11.5	0.1	0.3	Si 4
IX b	160	26	44	14.5	16	0.2 -0.3	0.4 -0.6	FP 3169, M 3127

noticeably richer in alk and quite often poorer in fm. This signifies (B and N, pp. 181, 206) that in the Hawaiian Islands alkali basalts and subbasalts occur in significant amounts beside the normal basalts. In the si-alk diagram the boundary lines (dotted in fig. 1*b*) between normal basalts, alkali basalts and subbasalts, as given in B and N, are so placed that relatively few analyses from Keweenawan lie outside the area of normal basalts and subbasalts. And these few lie near the boundary line. The c-gabbroid, hawaiitic, miharaitic, melagabbrodioritic, and gabbroid magma types are common to both provinces; but the interpacific island province contains other magma types besides, such as hornblenditic, kaulaitic, ankaratritic, essexitic, polzenitic. In addition the mugearitic types from Hawaii are richer in alk.

Chemically the lavas of the Keweenawan series are closely related to certain ophiolites of the mediterranean orogenic area (B and N). Details and particular differentiation trends can best be brought out by means of the molecular base and molecular norm. Their calculation is considerably simpler than that of the CIPW values used by the authors of the Keweenawan papers. The norm to be calculated is not based on weight percentages but on equivalent unit compounds in a basic rock cell containing a total of 100 atoms of Si,Al,Fe,Mg, Mn,Ca,Na,K,Ti,P. In each unit of a "compound" the sum of these elements is 1 and this unit is symbolized by the same abbreviations (written in capital letters) as those used by CIPW. The atomic proportions already required for deriving the Niggli values can be used to calculate the basis compounds, or norm-mineral compounds. For example:

$$\begin{aligned} SiO_2 &= (1\ Si) = 1\ Q \\ K\ Al\ SiO_4 &= (1\ K + 1\ Al + Si) = 3\ Kp \\ K\ Al\ Si_3O_8 &= (1\ K + 1\ Al + 3\ Si) = 5\ Or, \end{aligned}$$

and this gives the equation $3\ Kp + 2\ Q = 5\ Or$. This closely approximates the weight-per cent relations which are as follows:

$$2.64\ gr\ Kp + 2.05\ gr\ Q = 4.645\ gr\ Or.$$

When use is made of the stoichiometric relationships, the transformation of a given percentage composition of these unit compounds to others can easily be effected. Hence we

TABLE 3

Lava Types from Hawaiian Islands

	si	al	fm	c	alk	k	mg	Examples from:
1 a	115-130	18	48.5	27	6.5	0.02-0.2	0.4 -0.7	Hawaii, Oahu, Necker I., Nihoa, Niihau,
1 b	115-130	21	47	25.5	6.5	~0.1	~0.55	Kahoolawe
2 a	125	23	44	26.5	6.5	0.1 -0.2	0.35-0.6	Oahu, Hawaii, Maui, Lauai
2 b	115	23	40	28.5	8.5	0.1 -0.2	0.35-0.6	
2 c	115	21.5	42	29.5	7	0.1 -0.2	0.36-0.6	
3 a	136	22.5	44.5	22.5	10.5	0.1	0.5 -0.6	Oahu, Hawaii
3 c	120	21	45	23	11	0.2	0.4	
4 a	115	17.5	53.5	23	6	~0.1	0.6 -0.8	Oahu, Hawaii, Nihoa
4 b	119	17	54	26	3	0.1	0.5	
5 a	112	27	38	23.5	11.5	0.1 -0.2	0.3 -0.45	Oahu, Hawaii, Kauai, Maui, Niihau
5 b	113	27	34.5	28.5	9.5	0.2	0.4	
6 a	100	19	51	24	6	0.1 -0.2	0.5 -0.7	Oahu, Hawaii, Kauai, Maui, Niihau
6 b	90	17.5	54	23	5.5	0.1 -0.2	0.5 -0.7	
6 c	95	14	56	23.5	6.5	0.1 -0.2	0.5 -0.7	
6 d	76	10.5	62	23.5	4	0.1 -0.2	0.5 -0.7	
6 e	82	8	68.5	20.5	3	0.1 -0.2	0.7 -0.8	
7 a	94	14.5	63	18	4.5	usually	0.65-0.8	Oahu, Hawaii, Kauai, Maui, Necker I.,
7 b	86	10	71.5	15	3.5	0.1 -0.2	0.65-0.8	La Pérouse
7 c	80	6	79	12	3		0.65-0.8	

TABLE 8 (*Cont.*)

Lava Types from Hawaiian Islands

	si	al	fm	c	alk	k	mg	Examples from:
8 a	98	19	47	27	7	0.1 -0.2	0.4 -0.65	Hawaii, Maui, Necker I., Niihau
8 b	100	16	46	27	11	~0.2	~0.45	
9 a	124	23	39	26.5	11.5	0.1 -0.2	0.3 -0.5	Hawaii, Oahu
9 b	106	23	39	28	10	0.1 -0.2	0.3 -0.5	
10	118	24	39	22.5	14.5	0.2 -0.3	0.4	Maui
11 a	114	20	44.5	25	10.5	0.15-0.36	0.4 -0.5	Hawaii, Oahu, Maui, Gardner Rock
11 b	116	23.5	45	19	12.5	~0.2	0.4 -0.5	
11 c	110	22	47.5	19	11.5	~0.2	0.4 -0.5	
12 a	120	26	38	21.5	14.5	0.2 -0.1	~0.4	Maui, Necker I.
12 b	110	23	38	22	17	0.2 -0.1	~0.4	
12 c	122	24.5	33	21	21.5	0.2 -0.1	~0.4	
13 a	130	24	41	19	16	0.2	0.3 -0.4	Hawaii, Oahu, Maui
13 b	150	24	42	17	17	0.25	0.25	
14 a	130	28.5	37.5	19.5	14.5	~0.2	~0.3 -0.4	Hawaii, Maui
14 b	136	27	35	19	19	~0.2	~0.3 -0.4	
14 c	160	31	30.5	15.5	23	~0.2	~0.3 -0.4	
15 a	94	15	53.5	22	9.5	0.1 -0.2	0.5 -0.6	Hawaii, Oahu, Maui
15 b	119	14	51	22	13	0.1 -0.2	0.5 -0.6	
15 c	94	19.5	48	22.5	10	0.1 -0.2	0.5 -0.6	
16 a	68	10	58	27	5	0.1 -0.2	0.65-0.7	Oahu, Kauai
16 b	69	13	51	27	9	0.1 -0.2	0.65-0.7	
16 c	65	10.5	54	25.5	10	0.1 -0.2	0.65-0.7	

first calculate a molecular base, and from this the norm. Normally the following basic compounds are contained in igneous rocks:

$K\ Al\ SiO_4$	$Na\ Al\ SiO_4$	$Ca\ Al_2O_4$	Mg_2SiO_4	Fe_2SiO_4
3 Kp	3 Ne	3 Cal	3 Fo	3 Fa
Fe_2SiO_5	Ca_2SiO_4	TiO_2	$Ca_3P_2O_8$	SiO_2
3 Fs	3 Cs	1 Ru	5 Cp	1 Q

The sum of Kp + Ne + Cal is called L; the sum of Fo + Fa + Fs + Cs is called M'; the sum of Ru + Cp is called Acc.

$$Q + L + M' + Acc = 100.$$

If we combine M' + Acc to form M, the distribution of the compounds to Q + L + M = 100 can be plotted in a triangle. By recalculation of the sum of L to 100 the distribution of K-, Na-, Ca-alumosilicates can be shown in a second triangle $K\ Al\ SiO_4$-$Na\ Al\ SiO_4$-$Ca\ Al_2\ O_4$ or K, Na, Ca respectively. This is important for showing the molecular relations of the normative feldspars.

A third triangle Mg-Fe-Ca serves for the M'-compounds (example given Fo + [Fa + Fs] + Cs = 100) and indicates the possible molecular composition of olivines and pyroxenes.

For the construction of the latter two triangles the following ratios are convenient:

$$\pi = \frac{Cal}{Cal + Kp + Ne} = \frac{An}{An + Or + Ab}$$

$$k = \frac{K_2O}{HNa_2O + K_2O}, \text{ in many cases } = \frac{Kp}{Kp + Ne} \text{ or } \frac{Or}{Or + Ab}$$

$$mg = \frac{Mg}{Mg + Fe\ (+\ Mn)}, \text{ and often (if no spinels are used)}$$

$$= \frac{Fo}{Fo + Fa + Fs} \quad \gamma = \frac{Cs}{Cs + Fo + Fa + Fs}.$$

As the molecular norm (calculation of which from the molecular base is a matter of minutes) is not widely used in the United States, we give a comparative table containing both the weight percentage norm and molecular norm of some Hawaiian and Keweenawan rocks (tables 4a and 4b). The calculation is based on the same principles of distribution in both cases. These tables show that the molecular norms very closely approach the weight percentage norms and that they

can well be substituted for these. There are, however, some differences:

1. Compounds of norm minerals with high density (e.g., Mt, Hm, Ilm) have somewhat smaller molecular values and the distribution resembles that according to volume percentages as obtained directly from measurements on thin sections. That is no shortcoming, but an advantage.
2. The CIPW norms given by Cornwall are not calculated to the sum of 100 (CO_2, water, etc., are neglected). In the molecular norms the sum calculated is always 100 in spite of the omission of CO_2, H_2O, etc. This constitutes a further advantage especially for comparative purposes.
3. In view of the degree of accuracy of the chemical analyses and of the measurements made on thin sections, it seems useless to calculate the compositions to two decimal points. Thus the molecular norms have always been given to the nearest 0.X or 0.X5.

No one who has made chemical analyses or measurements on thin sections will, on studying these examples, doubt that the molecular norms are in every way as characteristic of the normative mineral composition as the weight percentage norms. They possess the great advantage of being easily transformable into other mineral assemblages, the usual stoichiometric formulae and equations being all that are required for the purpose. Only one example need be quoted here. If the ideal composition of biotite is to be derived from olivine and orthoclase, the equation is as follows:

$$K\,Al\,Si_3O_8 + 3/2(Mg,Fe)_2SiO_4 + 1\,H_2O = Si_3AlO_{10}(OH)_2(Mg,Fe)_3K + 3/2\,SiO_2$$

$$5\,Or + 4.5\,(Fo + Fa)\,(+ H_2O) = 8\,Bi + 3/2\,Q.$$

If in rock G 453, for example, with Or = 9.15 and (Fo + Fa) = 9.40 the entire Or-content were contained in biotite, the required amount of olivine would be obtained by rule of three as follows:

$$5 : 4.5 = 9.15 : x \qquad x = 8.25$$

y of biotite is derived from

$$5 : 8 = 9.15 : y \qquad y = 14.65$$

TABLE 4a

CIPW Norms and Molecular Norms of Some Rocks of Keweenawan

		Ap Cp	Ilm	Mt	Or	Ab	An	Augite (Wollast.)	Olivine	Q	Remainder	
G 253		0.67	5.02	4.87	1.11	30.92	23.07	26.01	4.62	—	3.80	weight % (CIPW—norm)
		0.8	3.8	3.7	1.5	33.65	24.3	26.5	5.75	—	—	molecular norm
G 297	Pegmatitic facies of basalts	0.67	3.80	5.57	5.56	18.86	24.19	37.88	—	0.42	2.91	weight % (CIPW—norm)
		0.4	3.0	4.2	5.5	21.15	25.65	39.55	—	0.55	—	molecular norm
G 149		1.01	5.17	5.57	10.56	28.82	17.24	26.23	—	2.40	3.14	weight % (CIPW—norm)
		0.9	4.0	4.1	11.35	31.85	18.4	26.0	—	3.4	—	molecular norm
G 453	(Cornwall)	1.34	5.32	5.57	8.90	18.86	21.68	27.02	7.92	—	4.40	weight % (CIPW—norm)
		1.0	4.2	4.3	9.15	21.65	23.35	26.95	9.40	—	—	molecular norm
G 604	Basalt (chill zone)	0.67	3.80	6.73	15.57	18.86	20.02	29.91	0.76	—	3.97	weight % (CIPW—norm)
		0.4	3.0	5.1	16.35	21.35	20.85	31.50	1.45	—	—	molecular norm
G 26	Aplite	—	1.67	4.64	21.13	28.30	9.45	14.06	—	18.54	2.22	weight % (CIPW—norm)
		0.3	1.2	3.5	22.15	31.15	9.65	14.35	—	17.7	—	molecular norm
Ophite (953-1097 feet) (Broderick)		0.27	2.13	2.78	1.67	16.24	35.31	24.80	13.27	—	0.18 Cc	weight % (CIPW—norm)
		0.3	1.6	2.1	1.5	17.65	36.35	26.75	13.60	—	—	molecular norm
Pinkish dolerite 3136 (Broderick)		0.74	5.17	5.10	8.34	28.82	16.68	31.00	—	1.68	0.9 Cc	weight % (CIPW—norm)
		0.2	3.8	3.8	8.5	32.0	18.0	32.45	—	1.25	—	molecular norm

TABLE 4b

CIPW Norms and Molecular Norms of Some Rocks of Hawaii

	Ap Cp	Ilm	Mt	Hm	Or	Ab	An	Ne	Augite	Olivine	Q	
"Pikritbasalt"	0.67	4.56	6.03	—	2.22	7.34	20.57	3.12	29.93	23.88	—	weight % (CIPW—norm)
Pakaoa Hill, Haleakala	0.5	3.4	4.4	—	2.3	7.65	20.5	4.05	30.8	26.4	—	molecular norm
"Andesite"	2.02	—	14.52	—	9.45	34.06	25.85	3.12	6.05	5.39	—	weight % (CIPW—norm)
Kahaku Cliff, Haleakala	1.7	4.8	5.9	—	9.7	37.3	22.5	3.3	9.6	5.2	—	molecular norm
"Andesite"	2.0	7.45	6.5	—	13.90	25.15	18.07	7.10	14.82	4.86	—	weight % (CIPW—norm)
Rest House, Haleakala	1.5	5.6	4.6	—	14.3	26.05	18.3	8.85	15.7	5.1	—	molecular norm

A biotite variant of the molecular norm can therefore be calculated for G 453 containing 14.65 Bi. Thus 9.4 — 8.25 = 1.15. Ol would remain over, but 2.75 Q would be simultaneously liberated. Also 1.15 (Fo + Fa) requires 1/3(1.15 Q) to form pyroxene, i.e., 0.4 approximately, so that the usual molecular norm

Or	Ol	Qz	
9.15	9.40	—	$\Sigma = 18.55$

can be converted into the following biotite variant:

Bi	Hy + En	Qz	
14.65	1.55	2.35	$\Sigma = 18.55$

The other values remain unaffected by this change. Therefore if biotite had been formed instead of Or, the norm (biotite variant) would no longer contain olivine but 2.35 per cent Qz + 14.65 per cent Bi instead and 1.55 per cent more Aug.

Table 5 contains the values of Q, L, M′, Cp, Ru, π, k, γ, mg, and the sums Acc = Cp + Mt + Ilm ± Hm for 34 analyses of Keweenawan lavas. In addition the values of Alkf = Or + Ab; An, Ol = (Fo + Fa) or Q of the molecular norms, and the corresponding Niggli values are given. In figures 2, *a*, *b*, *c* the projection points of these and of the remaining 25 analyses are plotted in the three triangles. A direct comparison with the numerous similar presentations in B and N is thus made possible. In addition figures 3*a*, 3*b*, and 3*c* show a new presentation after Burri of the composition of the Palisade diabases based on analyses that were published by F. Walker and J. V. Lewis. In the Q L M diagram P indicates the ideal composition of pyroxene, F that of the feldspars. Straight lines in the Q L M diagram (fig. 2*a*) emerging from some particularly frequent compositions of basic magmas have the following significance:

Line leading to		1	:	enrichment of pyroxene
"	"	2	:	enrichment of olivine
"	"	3	:	enrichment of accessories
"	"	4	:	enrichment of feldspar
"	"	5	:	enrichment of alkali feldspar and quartz in the proportions found in many aplites.

These relationships at once make clear the general trend of

the differentiation diagram (fig. 3*a*) of the Palisade diabase and indicate that a gravitative separation of olivine and perhaps of augite took place.

The point Ol_2 in figure 2*c* marks the composition of an olivine with Fo 60 Fa 40, or of an ortho-augite E 60 Hy 40. Di is the composition of iron-free diopside and Aug that of ordinary augites which frequently resemble diopside in composition. Straight lines connecting these points with certain rock compositions therefore indicate the change in composition of residual melts when these minerals crystallize. The first olivines will be considerably richer in Mg and correspond, for instance, to Ol_1 in figure 2*c*. Hence the shape of the field of the Palisade diabases given in figure 3*b* confirms the fact that a crystallization differentiation of Mg-rich constituents took place at the outset.

For saturated lavas the Na corner in figure 2*b* corresponds to normative Ab, while the K corner is that of normative Or and the Ca corner that of normative An. Starting from plagioclases with about An 60 and a small content of Or, crystallization differentiation will produce changes in the residual melt corresponding to the lines 1→5 according to whether and how much Or enters the relatively basic plagioclase. In the Palisade diabases k is generally larger in basic rocks than in the corresponding members of the Keweenawan series.

We will now use our method of presentation to illustrate more clearly certain features of the Keweenawan lavas. The Greenstone group is the one for which most chemical analyses exist. Broderick determined the mean compositions of cores at various depths of the lava mass which is about 1300 feet thick. (The depths are given in feet below the top of amygdaloid and andesite.) Cornwall has given data especially on the dolerites from the central parts which he calls the pegmatitic facies and which contain both ophitic and doleritic layers. The si-al-fm-c-alk values are plotted in figure 4 in relation to depth (the values on the right correspond to positions nearest the roof). The values are derived from average analyses and lie on horizontal lines corresponding to the depths. Cornwall's values for individual members of the pegmatitic facies are represented as points at the appropriate places (the depths have been recalculated to Broderick's scale). Broderick's dolerite analyses have been similarly treated. The main dia-

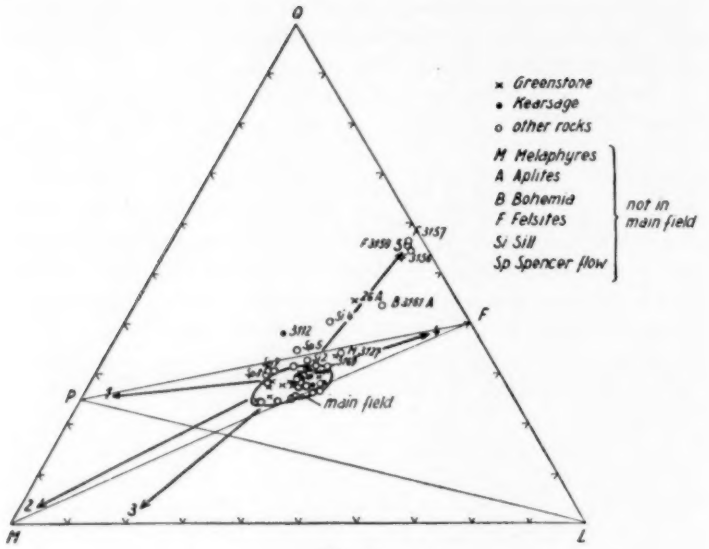
O
F
P
M
L
1
2
3
main field
× Greenstone
• Kearsage
o other rocks
M Melaphyres
A Aplites
B Bohemia
F Felsites
Si Sill
Sp Spencer flow
not in main field

Fig. 2a

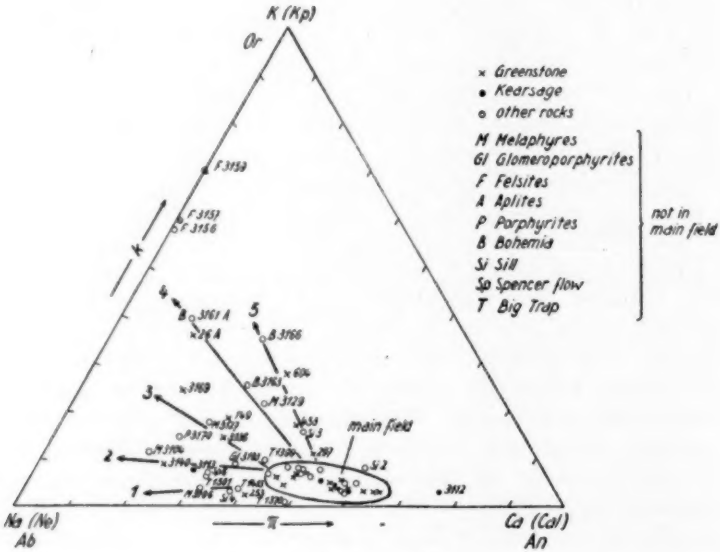
K (Kp)
Or
Na (Ne)
Ab
Ca (Cal)
An
main field
× Greenstone
• Kearsage
o other rocks
M Melaphyres
Gl Glomeroporphyrites
F Felsites
A Aplites
P Porphyrites
B Bohemia
Si Sill
Sp Spencer flow
T Big Trap
not in main field

Fig. 2b

gram is simple in character and shows that in the section containing the pegmatitic layers si and alk are somewhat higher while fm, c, and al are somewhat lower. The points corresponding to the 5 pegmatitic facies (G 559, G 453, G 297, G 253, G 149) and to the pinkish dolerites (Broderick, nos. 3136 and 3140) show that the si values vary from 105 to somewhat over 130. Thus fm is only slightly higher in the pegmatitic bands than in the ophitic layers. However, al is generally distinctly lower than the mean values, while c is higher than the latter in the deeper pegmatitic layers and lower in the upper ones. The reverse applies to alk, for it does not tend to rise until the upper differentiation bands are reached. If we call the zone from 116 feet down to 665 feet the *critical zone*, we see that it contains a differentiation in bands or layers which affects si, fm, alk and particularly c and al. The average of the pegmatitic facies (inset figure on the right) differs from the total average of the rather uniform ophites in having low al, higher c, alk, and si. The variation of the chief and average rocks is on the whole not very different from that of the Kearsage flow (fig. 5) concerning which no individual analyses are available. Only individual analyses exist of the Big Trap. In figure 6 they

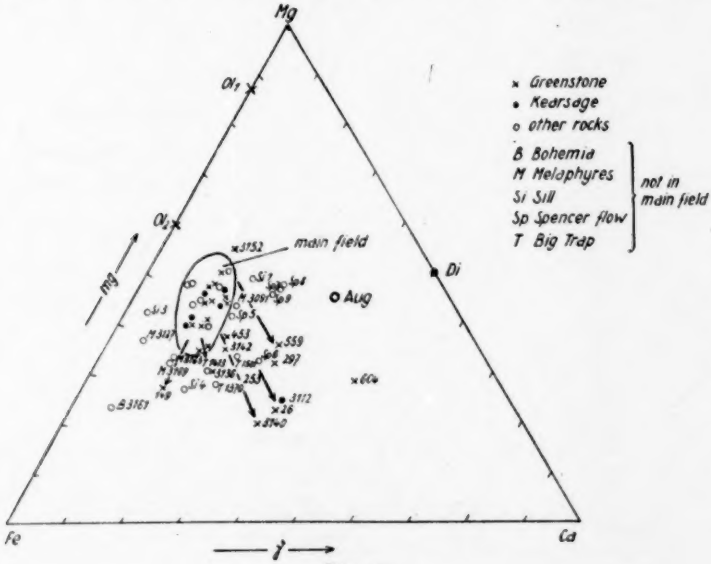

Fig. 2c

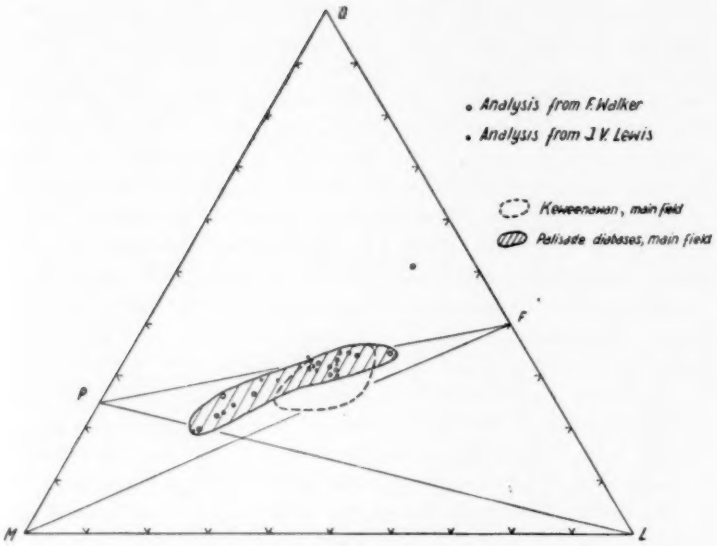
Q
F
P
M
L
• Analysis from F. Walker
• Analysis from J.V. Lewis
Keweenawan, main field
Palisade diabases, main field

Fi. 3a

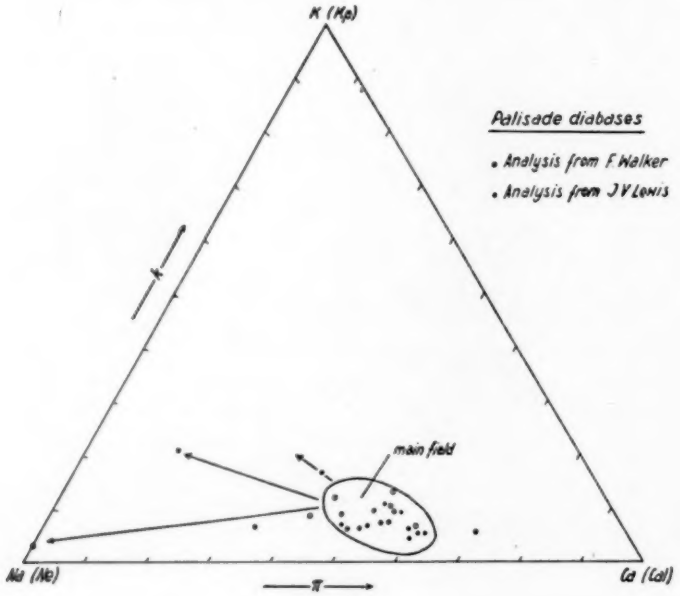
K (Kp)
Na (Ne)
Ca (Col)
main field
Palisade diabases
• Analysis from F. Walker
• Analysis from J.V. Lewis

Fig. 3b

are marked with a P when derived from pegmatitic layers or with an N, when the corresponding rocks were designated as andesites or basalts. Connections have been drawn between the last-named points only, so that here again it becomes evident that the P facies does not differ greatly in si, fm, and alk from the normal rocks though c is higher and al lower.

The calculation of the base and molecular norm together with the graphic representation provides further information concerning these relationships. Table 6 contains data concerning the Greenstone flow. G_{MO} refers to the fundamental values of an average of the ophites 3144, 3132, 3152, 3154, 3150, 3148; G_{M} to the total average calculated by Broderick; G 3144 are the values of an individual ophite from the critical zone; G_{PM} applies to an average of the pegmatitic facies 3140, 3136, 297, 149, 253, 559, 453; G 604 refers to the chilled facies and G 26 to the aplite.

In the graphic presentation of the molecular norms (fig. 7)

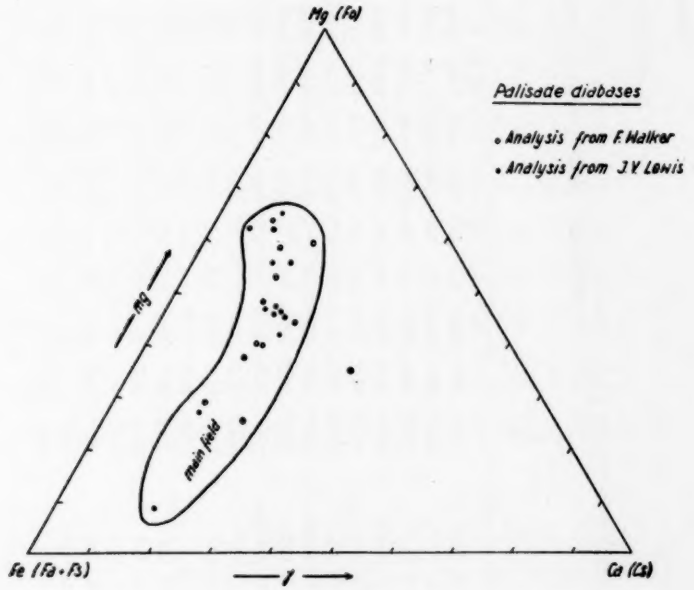

Fig. 3c

TABLE 5

Keweenawan Lavas

	Molecular Base									Molecular Norm					Niggli Values				
	Q	L	M	Cp	Ru	π	k	γ	mg	Erz Ap.	Alkf.	An	Ol	Q	si	al	fm	c	alk
K 3112	37.9	28.6	32.0	0.5	1.0	0.76	0.11	0.36	0.38	9.9	11.15	36.5	—	16.55	132	22	35.5	39.5	3
O 3095	28.3	36	34.4	0.3	1.0	0.58	0.07	0.13	0.56	6.6	24.8	35.15	5.55	—	106	22.5	47.5	24	6
G 3152	27.5	33.4	38.0	0.3	0.8	0.65	0.08	0.13	0.63	4.0	19.15	36.35	13.60	—	100	21.5	52	22.5	4
K 3119	29.2	37.4	32.2	0.3	0.9	0.56	0.10	0.15	0.55	6.6	27.7	34.65	3.2	—	111	24	44	25	7
K average	30.7	36.6	31.3	0.4	1.0	0.53	0.12	0.16	0.52	7.5	28.5	32.5	—	2.0	118	23	44.5	25.5	7
Si 1	31.6	33.5	34.5	0.1	0.3	0.58	0.11	0.19	0.60	2.9	23.5	32.35	—	0.25	117	21.5	46	26.5	6
G 3132	29.9	35.7	32.9	0.4	1.1	0.59	0.08	0.16	0.54	7.1	24.15	35.35	—	1.15	111	23	44.5	26.5	6
T 1522	26.6	38.6	33.0	0.4	1.4	0.60	0.12	0.08	0.52	11.65	25.8	38.5	0.8	—	100	24	47	23	6
G average	29.6	36.9	32.0	0.4	1.1	0.55	0.11	0.14	0.52	5.7	27.5	34.0	4.4	—	112	23.5	45	25	6.5
G 559	27.3	31.3	39.6	0.3	1.5	0.48	0.13	0.30	0.51	5.9	27.0	25.15	8.0	—	109	18.5	44	31	6.5
G 297	28.5	31.4	38.2	0.4	1.5	0.49	0.21	0.31	0.46	7.6	26.65	25.65	—	0.55	113	19	41	33.5	6.5
Sp 8	30.0	29.8	39.6	—	0.6	0.49	0.15	0.25	0.64	3.0	25.35	24.35	2.05	—	117	18	48	28	6
G 453	25.2	32.5	39.2	1.0	2.1	0.43	0.30	0.20	0.47	9.5	30.80	23.35	9.4	—	105	18.5	49.5	25	7
G 253	27.6	35.7	34.0	0.8	1.9	0.41	0.04	0.26	0.39	8.3	35.15	24.3	5.75	—	116	21	42	28	9
G 3138	30.2	39.3	28.9	0.2	1.4	0.48	0.12	0.17	0.42	7.3	34.15	31.35	—	0.05	120	25	41.5	25	8.5
K 3115	28.0	40.7	29.9	0.4	1.0	0.43	0.12	0.12	0.53	8.9	38.8	29.0	4.95	—	116	24.5	44	21.5	10
Gl 3103	26.5	40.5	31.4	0.4	1.2	0.36	0.19	0.09	0.53	8.9	43.15	24.35	11.0	—	115	23	48	18	11
Si 3	31.5	39.8	28.1	0.1	0.5	0.45	0.28	0.04	0.44	4.8	36.5	29.85	1.6	—	126	25	47.5	18	9.5

TABLE 5 (*Cont.*)

Keweenawan Lavas

	Molecular Base									Molecular Norm					Niggli Values				
	Q	L	M	Cp	Ru	π	k	γ	mg	Erz Ap.	Alkf.	An	Ol	Q	si	al	fm	c	alk
M 3129	27.2	37.6	32.7	0.7	1.8	0.35	0.33	0.12	0.45	12.1	40.85	21.85	—	0.8	118	21.5	49	19	10.5
G 604	28.0	35.1	35.0	0.4	1.5	0.36	0.43	0.12	0.54	8.5	37.7	20.85	1.45	—	119	20	52	18.5	9.5
T 1399	26.2	39.5	32.0	0.6	1.7	0.41	0.17	0.11	0.49	11.8	38.8	27.0	3.85	—	111	23	47.5	20	9.5
B 3163	28.6	35.7	33.0	0.9	1.8	0.30	0.36	0.13	0.38	11.6	41.65	17.85	—	2.7	125	20	50.5	18.5	11
Sp 6	31.8	37.2	30.1	—	0.9	0.32	0.10	0.28	0.45	8.85	42.55	20.0	—	4.35	138	22.5	40	26	11.5
G 149	30.4	36.9	29.8	0.9	2.0	0.30	0.26	0.14	0.32	9.0	43.2	18.4	—	3.4	135	22	47	19	12
K 3113	27.4	38.7	32.0	0.5	1.4	0.29	0.11	0.12	0.47	11.85	46.0	18.5	—	0.85	124	21.5	49	17.5	12
T 1501	24.1	31.6	41.0	0.7	2.6	0.32	0.09	0.24	0.43	15.3	36.0	16.65	—	1.40	108	17	50	24.5	8.5
Si 4	40.1	35.7	23.4	0.1	0.7	0.39	0.06	0.18	0.33	4.6	36.5	23.0	—	12.3	171	25.5	40	23	11.5
M 3127	34.0	40.6	22.1	1.4	1.9	0.27	0.24	0.06	0.39	11.0	49.25	18.15	—	7.45	156	26	42.5	16.5	15
G 3136	29.9	35.1	32.9	0.2	1.9	0.31	0.21	0.21	0.38	7.8	40.5	18.0	—	1.25	131	20.5	46.5	22	11
G 3140	24.6	30.6	41.2	0.4	3.2	0.23	0.12	0.34	0.30	12.3	39.15	11.85	2.5	—	126	16.5	47.5	25.5	10.5
P 3170	26.7	40.2	30.4	0.7	2.0	0.23	0.19	0.003	0.45	13.75	51.8	15.15	—	0.85	127	22	54.5	9.5	14
M 3104	29.8	36.5	30.7	0.7	2.3	0.19	0.14	0.13	0.39	12.3	49.5	11.35	—	4.55	141	20.5	50.5	15	14
G 26	44.4	37.8	16.9	0.3	0.6	0.15	0.42	0.36	0.35	5.0	53.3	9.65	—	17.7	235	28	27.5	24	20.5
B 3161	43.1	43.2	12.3	0.6	0.8	0.13	0.45	0.07	0.25	5.3	62.8	9.10	—	14.2	243	33	30.5	11	25.5

Cp + Ilm + Mt have been united to Acc. It is at once evident that in comparison with G_M and G_{MO} the pegmatitic or doleritic facies (G_{MP}) are on an average richer in Cp, Ilm, Mt, Or, Ab, and Wo and noticeably poorer in An. π, k and γ (see table 6) are therefore correspondingly higher and mg is lower. The ophite 3144 from the critical zone shows a similar tendency, though to a lesser degree. Or is particularly high (compare the k!) in the chilled zone (G 604) without any enrichment in Wo. The aplite (G 26) exhibits a high value of Or + Ab + Q and low ones of An and En + Hy without any enrichment of Acc. A normal differentiation would lead to an enrichment of Or + Ab accompanied by a decrease of π and mg.

The chief peculiarity of the critical zone therefore lies in the fact that an increase of Ab + Or goes hand in hand with an increase in Cp + Ilm + Mt and Wo, and this without making the disappearance of Ol necessary or of producing Q in any considerable amount.

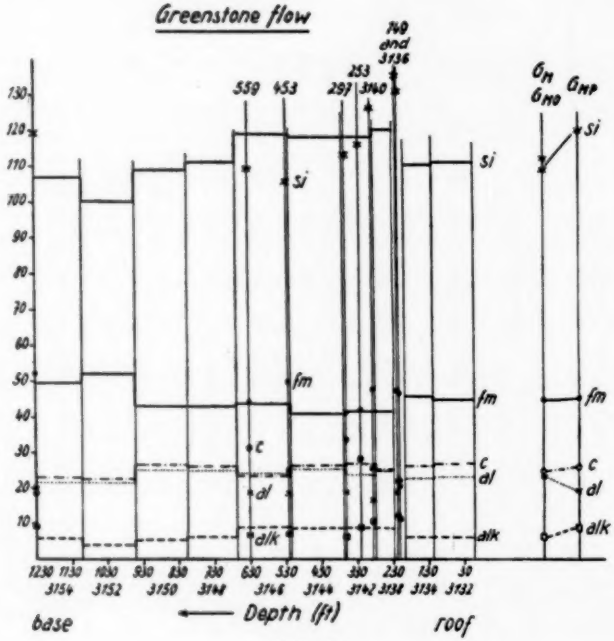

Fig. 4

TABLE 6

Greenstone Flow

	Cp	Basis									π	k	γ	mg
		Ru	Kp	Ne	Cal	Cs	Fo	Fa	Fs	Q				
G_M	0.4	1.1	1.7	14.8	20.4	4.7	14.4	9.8	3.1	29.6	0.55	0.11	0.14	0.52
G_{MO}	0.35	1.0	1.45	13.3	21.7	4.5	15.5	9.5	3.3	29.4	0.58	0.10	0.14	0.55
3144	0.6	1.4	2.6	16.8	19.6	5.1	10.3	9.3	4.2	30.1	0.50	0.14	0.18	0.43
G_{MP}	0.6	2.0	3.8	17.0	12.6	9.5	10.9	12.0	4.0	27.5	0.37	0.18	0.26	0.41
604	0.4	1.5	9.8	12.8	12.5	4.2	16.5	9.2	5.1	28.2	0.36	0.43	0.12	0.54
26	0.3	0.6	13.3	18.7	5.8	6.1	3.8	3.5	3.5	44.4	0.15	0.42	0.36	0.35

	Molecular norm										Niggli values				
	Cp	Ilm	Mt	Or	Ab	An	Wo	En+Hy	Ol	Q	si	al	fm	c	alk
G_M	0.4	2.2	3.1	2.85	24.65	34.0	6.25	22.15	4.4	——	112	23.5	45.0	25.0	6.5
G_{MO}	0.35	2.0	3.3	2.4	22.2	36.1	6.0	23.25	4.4	——	109	24.0	45.0	25.0	6.0
3144	0.6	2.8	4.2	4.35	28.0	32.65	6.8	20.55	—	0.05	118	25.0	40.5	26.0	8.5
G_{MP}	0.6	4.0	4.0	6.3	28.35	20.95	12.65	20.95	2.2	——	120	19.5	45.5	26.0	9.0
604	0.4	3.0	5.1	16.35	21.35	20.85	5.6	25.9	1.45	——	119	20.0	52.0	18.5	9.5
26	0.3	1.2	3.5	22.15	31.15	9.65	8.15	6.2	—	17.7	235	28.0	27.5	24.0	20.5

The relationships emerge clearly from the three triangles Q-L-M (fig. 8*a*),K-Ca-Na of the L components (fig. 8*b*), and Mg-Ca-Fe of the M components (Fig. 8*c*). Starting from the composition G_{MO} and G_{M} in the Q-L-M triangle (fig. 8*a*), a differentiation toward albite rocks or fm-poor keratophyres would move toward F, while a tendency toward quartzdioritic or liparitic magmas would move toward 26 and beyond. To 3144 which lies in the direction of the keratophyres, G_{MP} may be assigned the antipole in the critical zone in the general direction of M (relatively rich in ore and perhaps in c). This corresponds to the enrichment of Cp and particularly of Ilm, Mt (perhaps Hm) and Wo in the molecular norm. Figure 8*c* shows that an enrichment of Ab + Or takes place simul-

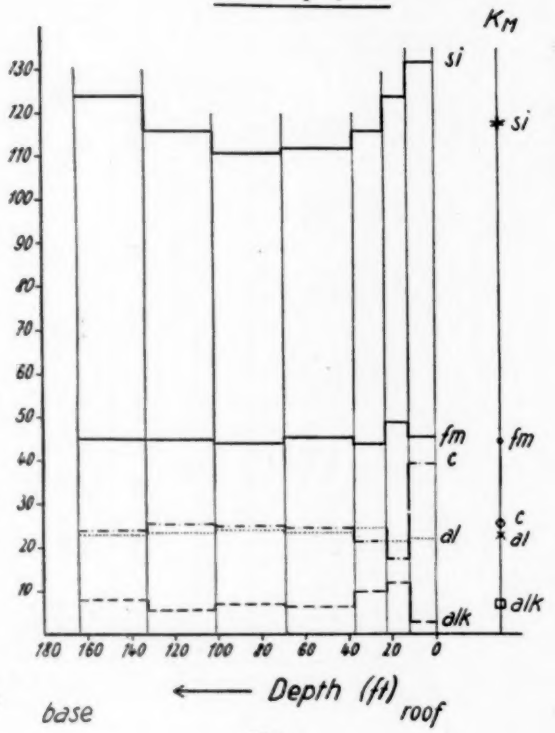

Fig. 5

taneously. The projection points of G_{MP}, 604, 3144 and 26 all lead away from the composition of the first crystallizations of basic plagioclase and differ solely in respect to the degree of K enrichment. Figure 8*c* indicates that apart from 604 (chilled zone) the differentiation products tend to become relatively richer in Ca and Fe in the M_P portion and aplite. These tendencies can be ascribed to crystallizations of olivine and augite in varying proportions.

We now turn to the actual (modal) mineral composition and note that according to Cornwall's investigations the plagioclase in all the pegmatitic facies is much poorer in An than indicated by the norm. The feldspars are albite, albite-oligoclase, or, in extreme cases, oligoclase. The main amount of Ca is contained in epidote or zoisite and besides in prehnite. The pyroxenes and olivines are partly replaced by chlorite.

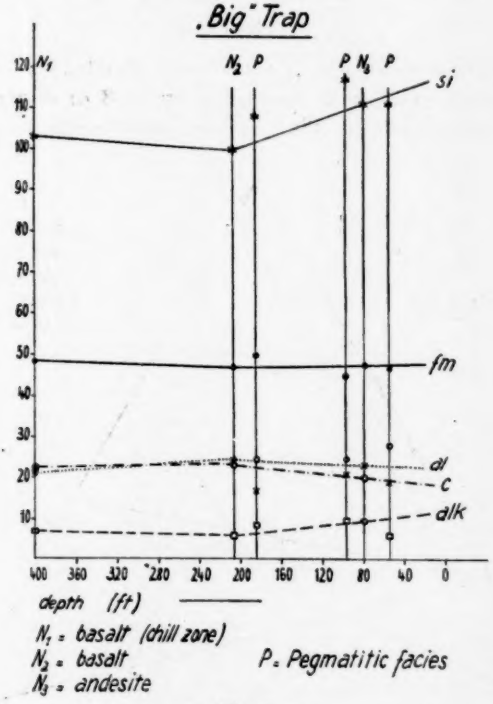

Fig. 6

Greenstone flow

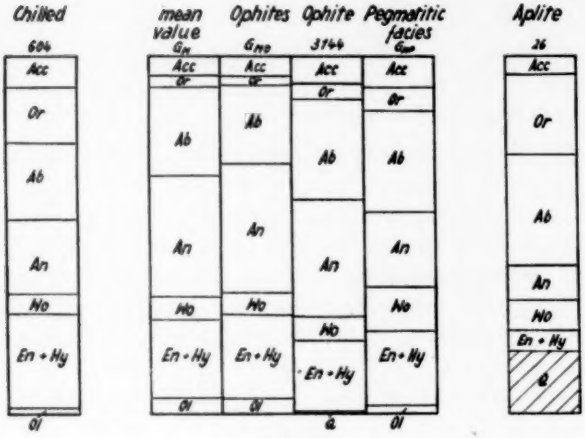

Fig. 7

This partial replacement of water-free silicates by those containing water (for rocks sometimes up to 3 or 4 per cent by weight) probably took place at an early stage (autohydro-

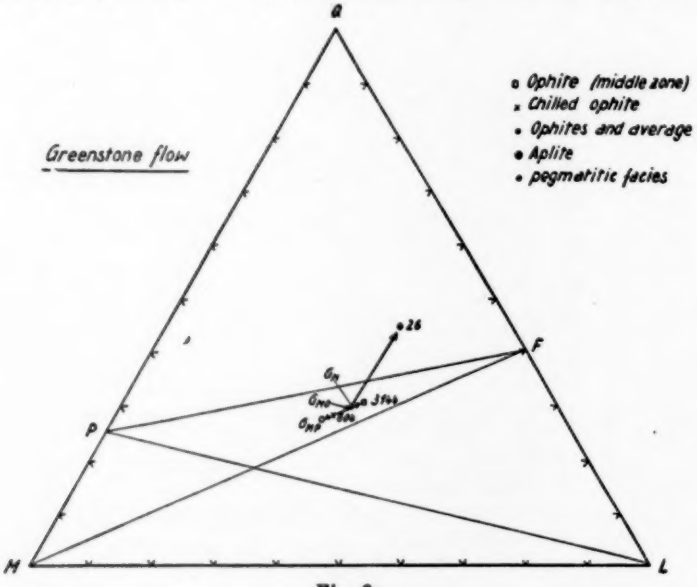

Fig. 8a

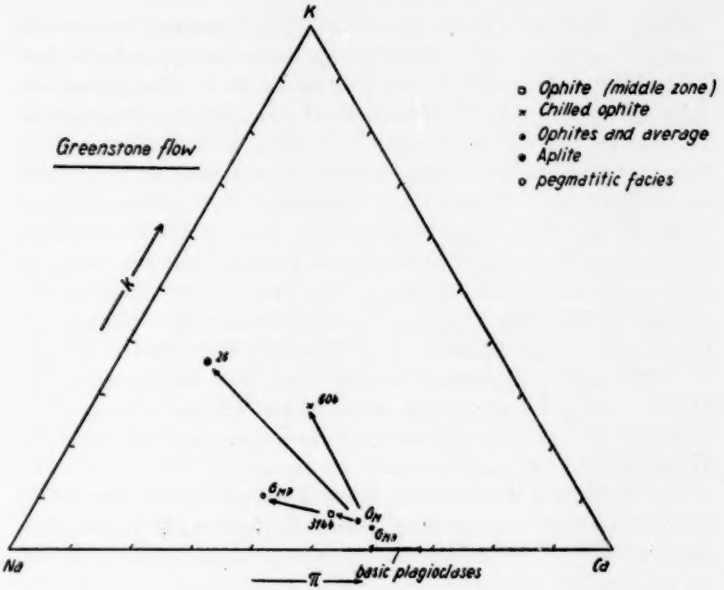
K
Greenstone flow
K
Na
Ca
π
basic plagioclases
o Ophite (middle zone)
× Chilled ophite
• Ophites and average
• Aplite
o pegmatitic facies

Fig. 8b

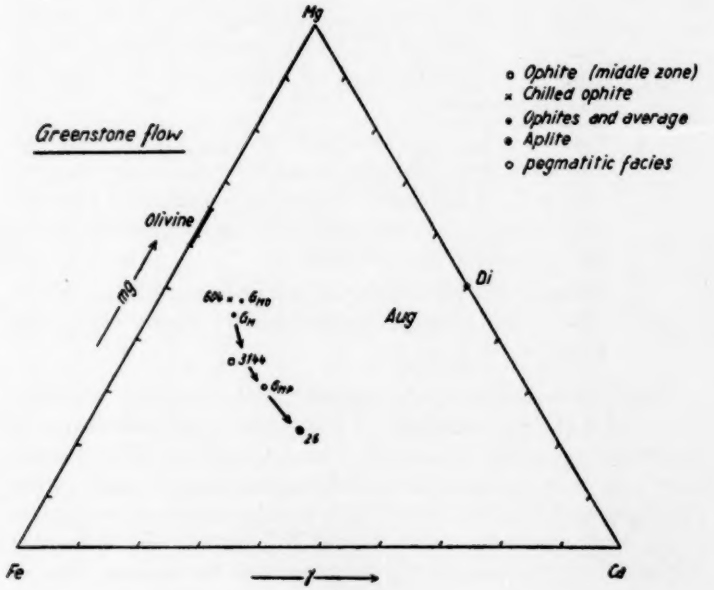
Mg
Greenstone flow
Olivine
mg
Di
Aug
Fe
Ca
f
o Ophite (middle zone)
× Chilled ophite
• Ophites and average
• Aplite
o pegmatitic facies

Fig. 8c

thermal changes, or perhaps crystallizations from water-rich residual melts). The mineral paragenesis corresponds to that of spilitic rocks, though there can be no doubt that pyroxenes and olivine actually crystallized at the outset. One has the impression that in the central critical zone a magma rich in volatile constituents, whose early crystallization proceeded on normal lines, assumed the character of a spilitic residual magma. In this stage and under the influence of H_2O, basic plagioclase could no longer crystallize and that already separated out became unstable. Prehnite, epidote, and zoisite, besides albite, take its place and simultaneously chlorite and ores are formed instead of water-free Mg-Fe silicates. This is a widespread phenomenon indeed, one that is characteristic of the spilitic keratophyre association (B and N, p. 490, *et seq.*) and often connected with the appearance of iron ores, titanium-iron ores and apatite-iron ores.

In the central parts of the thick Greenstone flow this differentiation could only develop internally and without complete separation. The essential traits however are clearly visible in the initial stages and comprise

1. Removal of Ca from compounds such as anorthite and calcic pyroxenes with strong migrational tendencies, e.g., as carbonate if CO_2 is present simultaneously; otherwise crystallization of zoisite and compounds of zeolitic character.
2. Far-reaching decomposition of iron-bearing silicates. Trivalent iron; phosphates and Ti can remain in solution and not crystallize till later; considerable amounts of originally divalent iron may undergo oxidation in the course of this process.
3. Substitution of nearly all water-free silicates except albite and perhaps orthoclase by those containing water.

These phenomena, which together with extremely variable values of c are characteristic of the typical spilite-keratophyre provinces (compare B and N), would seem to offer a most favorable starting point for studying the early stages of the development of spilitic lavas. This can be shown more impressively than with the mean values by uniting the molecular norms of all the pegmatitic facies of the Greenstone flow in

a single diagram (fig. 9). The values have been somewhat simplified for this purpose by uniting Ab + An as Alkf and noting the k value separately. Similarly Wo + En + Hy have been united as Aug and γ and mg noted for the total Aug + Ol. Numbers 453, 3136 and 149 show a decrease of An in the sequence given, and in these rocks γ is practically normal, *i.e.* no enrichment of Wo is found; mg, however, sinks and k can become relatively high. Numbers 559, 297, 253, 3140 show a progressive decrease of An and mg, while γ is relatively high. Here an enrichment of Ca in the M silicates has taken place.

In the triangle Mg-Ca-Fe (fig. 2*c*) unusual rocks like the pegmatitic-doleritic facies to the amygdaloid facies of the Greenstone flow, the Kearsage flow, and the Big Trap flow have special numbers. The other facies are only indicated by crosses or circles. It is thus easy to recognize that similar tendencies appear in all cases (ordinary Fe-enrichment or Fe-Ca-enrichment). In figure 2*b* a varied assortment of differentiation products of the Keweenawan lavas are plotted in the K-Ca-Na triangle, and the direction of their differentiation in relation to the central field of basic magmas is shown.

Cornwall has attempted to determine the weight percentage modes of the analyzed rocks by measurements on the thin sections. This meets with rather considerable difficulties, not the least of which are due to the fact that in the pegmatitic facies a single thin section can scarcely be representative of the mean composition of a rock. Inhomogeneities due to the

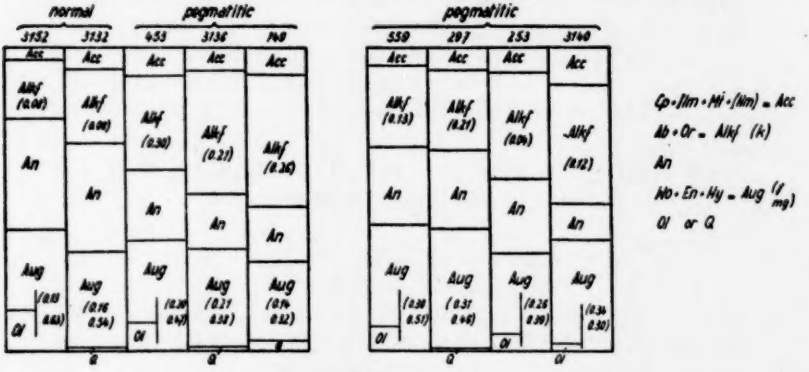

Greenstone flow

Fig. 9

migration of remaining or newly formed solutions are bound to occur. In addition the amount of relict pyroxene and olivine vary considerably. The process that would finally have effected a complete substitution of most of the water-free silicates by water-bearing ones remained incomplete. This makes it the more desirable to calculate from the chemical composition the hypothetical mineral composition that would finally have resulted.

The molecular norm makes such a calculation easy. The molecular norms hitherto used may be called kata-molecular norms. From these (or from the molecular base) epi-molecular norms containing prehnite (Preh) or epidote (Ep[l]) as chief calcic minerals can be quickly derived. The following equations can be used to obtain a preliminary insight into the relationships:

(a) From the molecular base:

$$2\ CaAl_2O_4 + Ca_2SiO_4 + 5\ SiO_2(+\ 2\ H_2O) = Ca_4Al_4Si_6O_{22}\cdot 2\ H_2O$$

$$6\ Cal + 3\ Cs + 5\ Q\ (+\ H_2O) = 14\ Preh$$

$$Fe_2SiO_5 = Fe_2O_3 + SiO_2$$

$$3\ Fs = 2\ Hm + 1\ Q$$

$$Fe_2SiO_4(+\tfrac{1}{2}O_2) = Fe_2O_3 + SiO_2$$

$$3\ Fa\ (+\ O) = 2\ Hm + 1\ Q$$

$$Ca_4Al_4Si_6O_{22}\cdot 2\ H_2O + Fe_2O_3 = Ca_4Al_4Fe_2Si_6O_{25}\cdot H_2O(+\ 1\ H_2O)$$

$$14\ Preh + 2\ Hm = 16\ Ep(l)\ (+\ 1\ H_2O)$$

$$3\ Mg_2SiO_4 + 1\ SiO_2 + 4\ H_2O = Mg_6Si_4O_{14}\cdot 4\ H_2O$$

$$9\ Fo + 1\ Q\ (+\ H_2O) = 10\ Serp$$

$$Ca_2SiO_4 + 2\ CO_2 = 2\ CaCO_3 + SiO_2$$

$$3\ Cs\ (+\ CO_2) = 2\ Cc + 1\ Q$$

3 Ne + 2 Q are used to form 5 Ab, even when some Kp is present in addition to Ne.

3(Cs + Fo + Fa) + 1 Q may leave a remainder of 4 Aug.

(b) From the kata-molecular norm (with possible formation of pennine = $Chl_{(P)}$ instead of Serp

$$15\ An + 3\ Mt + 6\ Fo + 2\ Wo(+ H_2O) = 16\ Ep(l) + 10\ Chl_{(P)}$$

$$15\ An + 3\ Mt + \underbrace{8(En+Hy) + 2\ Wo}_{10\ Aug}\ (+ H_2O) = 16\ Ep(l) + 10\ Chl_{(P)} + 2\ Q$$

$$15\ An + 2\ Wo(+ H_2O) = 16\ Zo + 1\ Q$$

$$5\ An + 2\ Wo(+ H_2O) = 7\ Preh$$

$$6\ Ol + 4\ (En + Hy) + H_2O = 10\ Serp$$

In idealized epi-molecular norms only Cp, Ru, Hm, Ab (containing potash), Serp, Preh or Ep(l), Cc and Q are assumed to be present. The results obtained for G 253 on these lines are as follows:

Preh-variant		Ep-variant		example with Preh and Ep		
Cp	0.8	Cp	0.8	Cp	0.8	
Ru	1.9	Ru	1.9	Ru	1.9	9.55
Hm	10.1	Hm	5.25	Hm	7.65	
Ab	35.15	Ab	35.15	Ab	35.15	
Preh	34.05	Ep(l)	38.9	Preh	17.0	
Serp	11.0	Serp	11.0	Ep(l)	19.5	30.5
				Serp	11.0	
Cc	1.25	Cc	1.25	Cc	1.25	
Q	5.75	Q	5.75	Q	5.75	

The mode in weight percentages given by Cornwall for this rock is contained on the first line. Our mean Preh-Ep molecular epi-norm is noted below.

Apatite	Plag(Aug)	Ore	Prehnite	Epidote+Chlorite	Pyroxene	
0.4	37.3	13.3	14.6	15.8	18.6	weight percentages (mode)
Cp	Ab	Ru+Hm	Preh	Ep+Serp	Cc+Q	
0.8	35.15	9.55	17.0	30.5	7.0	epi-molecular norm

If we take into consideration that part of the pyroxene did not react and that only Ab and Serp have been calculated in the epi-molecular norm, the agreement may be considered very satisfactory.

The analyses can, of course, be used for making calculations

with relict pyroxene and oligoclase instead of albite. We obtain, for example,

	Cp	Ru	Hm	Aug.	$Ab_{80}An_{20}$	Preh	Ep(l)	Serp	Q	
G 453	1.0	2.1	9.1	8	38.8	7.55	16.0	13.1	4.35	molecular variant
	Acc			Pyroxene	$Ab_{88}An_{12}$	Preh	Epidote + Chlorite			
observed	8.6			8.3	53.7	4.8	24.1		0.5	weight percentages

In this case it is evident that the measured thin section did not agree with the specimen analyzed. Calculation of the weight percentage norm from the analysis leads to 49.44 feldspar with An_{54}, so that after loss of An it is quite impossible to obtain 53.7 per cent of plagioclase. Discrepancies of this kind can be spotted immediately when our method of calculation is used. However, these two examples of the calculation of epi-molecular norms and transition norms are sufficient for our present purpose.

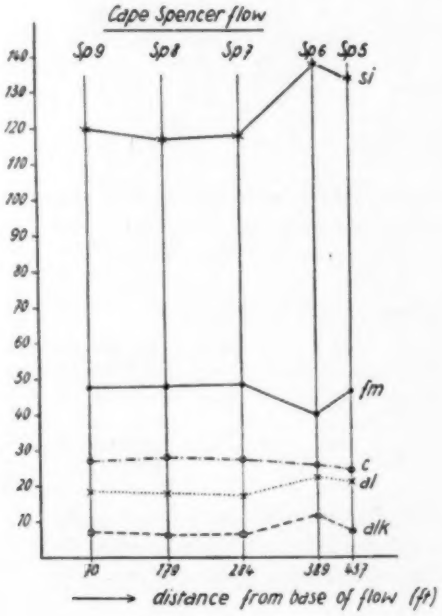

Fig. 10

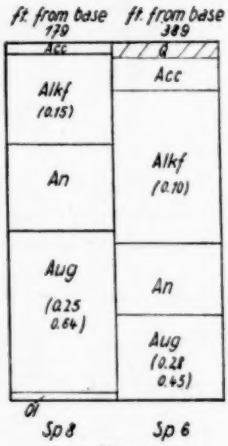

Fig. 11

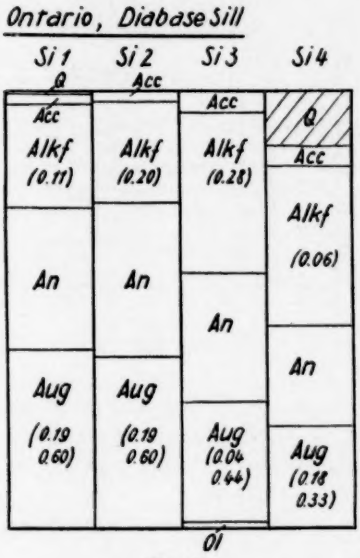

Fig. 12

In conclusion we give the si-, al-, fm-, c-, alk-diagram for the Spencer flow in connection with the depth (feet above basis) of the analyzed specimens (fig. 10). The molecular norm of Sp 8 and Sp 6 in figure 11 shows that we are dealing with a fairly normal differentiation with an upward increase of Ab

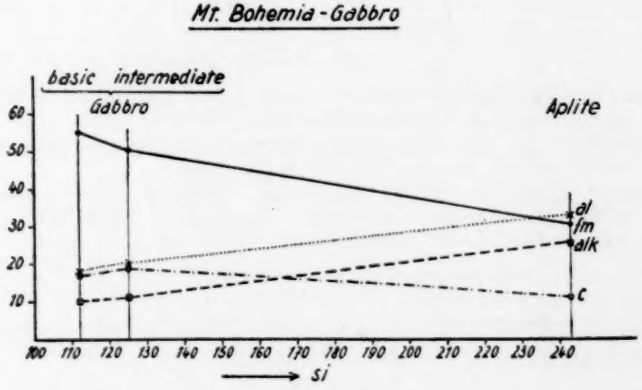

Fig. 13

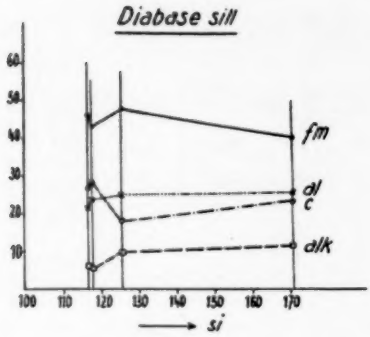

Fig. 14

+ Or and an increase of An and augite. Here, too, the accessories show a slight simultaneous increase. Figure 12 depicts the corresponding relationships in the differentiation of the diabase sill of Ontario.

Finally, ordinary differentiation diagrams (with si as abscissa) representing the gabbro from Bohemia and the associated aplite are given in figure 13 and diagrams of the diabase sill in figure 14.

Closer study of all the rocks of the Keweenawan lavas on the lines indicated would confirm the results arrived at by Broderick and Cornwall. However, a certain increase in precision is obtained, the general survey is simplified, and comparisons with other provinces are facilitated.

References

Burri, C., and Niggli, P., 1945. Die jungen Eruptivgesteine des mediterranen Orogens, I, Schweizerspiegelverlag, Zürich.

Broderick, T. M., 1935. Differentiation in lavas of the Michigan Keweenawan: Geol. Soc. America Bull., vol. 46, pp. 503-558.

Cornwall, Henry R., 1951. Differentiation in lavas of the Keweenawan series and the origin of the copper deposits of Michigan: Geol. Soc. America Bull., vol. 62, pp. 159-202.

Mineralogisch-petrographisches Institut
Technische Hochschule
Zurich, Switzerland

THE SYSTEM DIOPSIDE—FORSTERITE—ANORTHITE

E. F. OSBORN AND D. B. TAIT

ABSTRACT. The system diopside—forsterite—anorthite is an example of a system containing a pyroxene, an olivine, and a feldspar in which virtually no solid solution or reaction relation among the phases exists. This system, however, may be considered as one face of a tetrahedron representing the system diopside—forsterite—anorthite—silica which is noteworthy for crystal-liquid reaction phenomena as liquids crystallize under equilibrium conditions. Phase equilibrium data are presented and their bearing on the crystallization of spinel from basaltic liquids and on the formation of coronite is discussed.

INTRODUCTION

THE minerals diopside ($CaMgSi_2O_6$), forsterite (Mg_2SiO_4), and anorthite ($CaAl_2Si_2O_8$) are representatives of three mineral groups of common occurrence, the pyroxenes, olivines, and feldspars. These three groups play an important role in the formation of igneous rocks,[1] indeed are quantitatively the major silicate structures composing the earth's crust. Olivines are constructed of isolated SiO_4 tetrahedra bound together by divalent ions of medium size, usually Mg^{2+} and Fe^{2+}; pyroxenes are composed of chains of linked SiO_4 tetrahedra united by medium or moderately large cations such as Mg^{2+}, Fe^{2+}, and Ca^{2+}; while the feldspars are characterized by a three-dimensional linkage of SiO_4 and AlO_4 tetrahedra into which network fit the large cations Ca^{2+}, Na^{+}, K^{+}, and others of similar size and charge. Owing to the fundamental difference in type of structure among the three groups, solid solution does not occur between any two of olivines, pyroxenes, and feldspars, but extensive solid solution exists within each group.

It was primarily to learn more of the phase relationships existing among these silicate types that the system diopside—forsterite—anorthite was investigated. But this system is also part of a larger project, an investigation of phase equilibria in the quaternary system $CaO—MgO—Al_2O_3—SiO_2$. This quaternary system is sketched in figure 1 as a tetrahedron having as apices the four components, CaO, MgO, Al_2O_3, and SiO_2. The four faces of the tetrahedron are ternary systems, and other ternary or partly ternary systems exist within the tetrahedron where certain combinations of three compounds are considered.

[1] For a recent summary discussion of their role, see Osborn (1950).

The system diopside—forsterite—anorthite (triangle A-D-Fo, fig. 1) is one such combination of three compounds which as a first approximation may be treated as a ternary system. Neighboring systems which have been previously studied are the triangular joins: anorthite-forsterite-silica (Andersen, 1915), $CaSiO_3$-diopside-anorthite (Osborn, 1942), pseudowollastonite-akermanite-gehlenite (Osborn and Schairer, 1941), and diopside-anorthite-silica.[2] Owing to the existence of this group of interior triangular joins which are ternary or partly ternary systems, interior tetrahedra exist which for most purposes can be treated as quaternary systems. It can be seen in figure 1 that two such tetrahedra are present having as a common face the system diopside—anorthite—silica. With this investigation of the system diopside—forsterite—anorthite, phase equilibrium data have been obtained for all seven of the faces of the two interior tetrahedra. It is therefore possible to estimate phase relations within the tetrahedra with sufficient accuracy for many purposes. In the left tetrahedron (W-D-A-SiO_2, fig. 1), for example, two quaternary invariant points must exist at temperatures of approximately 1135° and 1150°C. In the right tetrahedron (D-A-Fo-SiO_2) no liquidus invariant points are present as three univariant lines pass continuously through the tetrahedron, one passing through a maximum and the others through a minimum temperature.

METHOD OF INVESTIGATION

In this investigation the method of quenching was used which has been described in many reports from the Geophysical Laboratory (for example, Osborn and Schairer, 1941, p. 716). Homogeneous glasses were prepared from the pure ingredients $CaCO_3$, MgO, Al_2O_3, and SiO_2. The crushed glass was completely crystallized by holding it for a minimum of one day at 1000°C. A charge of about 15 mg. of the powdered crystalline material was enclosed in a platinum envelope, held at a desired temperature for a time sufficient to attain a close approach to equilibrium among the phases, and quenched in mercury. Phases present in the quenched product were identified by means of a petrographic microscope. The platinum-platinum 90 rhodium 10 thermocouples were frequently calibrated at standard melting

[2]Approximate relations in this system are sketched in figure 7 after Greig (1949).

points defined as follows: Au, 1062.6°; $CaMgSi_2O_6$, 1391.5°; and $CaSiO_3$, 1544°.

LIMITING SYSTEMS

The system diopside—forsterite—anorthite is bounded by the three systems, diopside—forsterite, forsterite—anorthite, and diopside—anorthite, all of which have been previously investigated. The equilibrium diagram of the first of these, after Bowen (1914), is shown as figure 2. The system is binary with a eutectic at 12 per cent forsterite and 1387°. The low slope of

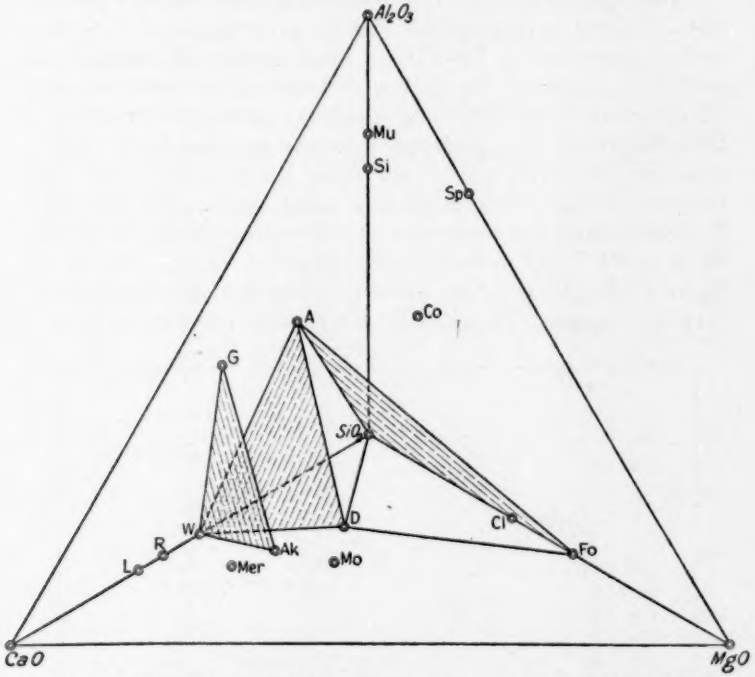

Fig. 1. Diagram representing the quaternary system CaO—MgO—Al_2O_3—SiO_2 as a tetrahedron with one component at each apex. The front face, CaO-MgO-Al_2O_3, has been removed to show the interior of the tetrahedron. Compounds are plotted in weight per cent. L = larnite (Ca_2SiO_4), Mer = merwinite ($Ca_3MgSi_2O_8$), Mo = monticellite ($CaMgSiO_4$), Fo = forsterite (Mg_2SiO_4), R = rankinite ($Ca_3Si_2O_7$), Ak = akermanite ($Ca_2MgSi_2O_7$), W = wollastonite ($CaSiO_3$), D = diopside ($CaMgSi_2O_6$), Cl = clinoenstatite ($MgSiO_3$), G = gehlenite ($Ca_2Al_2SiO_7$), A = anorthite ($CaAl_2Si_2O_8$), Co = cordierite ($Mg_2Al_4Si_5O_{18}$), Sp = spinel ($MgAl_2O_4$), Si = sillimanite (Al_2SiO_5), Mu = mullite ($Al_6Si_2O_{13}$) (after Osborn).

the diopside liquidus curve and the position of the eutectic near the diopside end are noteworthy features of the diagram.

Liquidus relations in the system forsterite—anorthite were investigated by Andersen (1915, p. 424), who found that over a certain composition range, spinel is the primary phase. Consequently, the system is not entirely binary. In the present study quenching data were obtained for six mixtures in order to extend phase data to solidus temperatures (table 1). An equilibrium diagram for the join forsterite-anorthite is shown as figure 3. Points A and B have the same compositions, and B the same temperature, as determined by Andersen (1915, p. 424). Point A is shown as $1475° \pm 5°$, as compared with Andersen's temperature of $1466° \pm 4°$. Point C may be viewed as a peritectic point for the system anorthite—forsterite—spinel. Its temperature of $1320° \pm 5°$ therefore represents a maximum temperature on the quaternary univariant line along which anorthite, forsterite, spinel and liquid are in equilibrium. The temperature must drop in passing along this line toward point K in the system forsterite—anorthite—silica (Andersen, 1915, fig. 9, p. 437) and in the opposite direction toward point D of figure 5. The temperature gradient along this line, however, is very low inasmuch as points K and D were found to be 1320°

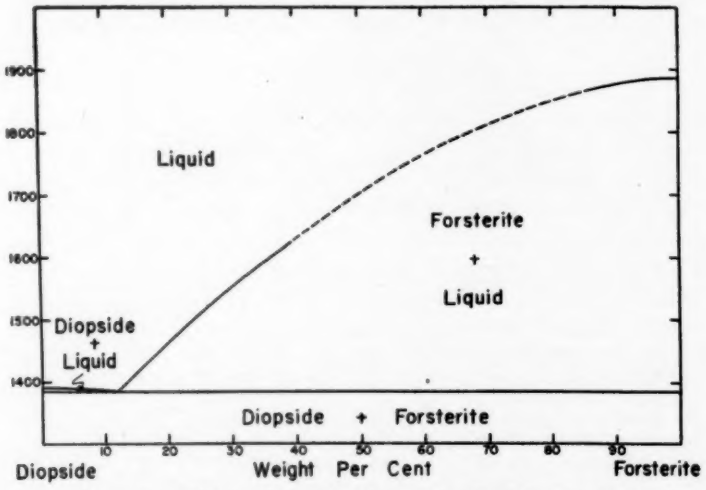

Fig. 2. Equilibrium diagram of the system diopside—forsterite (after Bowen).

(Andersen, 1915, p. 437) and 1317° respectively. Along the curves AC and BC of figure 3, spinel crystallizes from the liquid along with forsterite or anorthite as temperature drops, but at point C as the temperature remains constant and heat is withdrawn from the system, spinel dissolves as anorthite and forsterite crystallize. Below 1320°, only anorthite and forsterite are present under equilibrium conditions.

An equilibrium diagram for the system diopside—anorthite is shown as figure 4, after Osborn (1942, p. 758). The system is believed to be not completely binary, as suggested by the slight slope of the dashed line, probably because the diopside present contains a small amount of Al^{3+} occupying Mg^{2+} and Si^{4+} positions in the structure.

TABLE 1

Summary of Quench Data for the Forsterite-Anorthite Join

Composition in wt. %: Anorthite	Forsterite	Temp. (°C.)	Time (hrs.)	Phase Present*
45	55	1553	15	Fo and glass
45	55	1559	2	glass
54	46	1474	3	Fo, Sp and glass
54	46	1477	2	Fo and glass
54	46	1481	7	glass
60	40	1316	4	Fo and An
60	40	1321	10	Fo, Sp and glass
60	40	1435	1	Fo, Sp and glass
60	40	1441	1	Sp and glass
60	40	1479	2	Sp and glass
60	40	1496	10	glass
80	20	1316	4	Fo and An
80	20	1321	10	An, Sp and glass
80	20	1388	1	Sp and glass
80	20	1412	1	Sp and glass
80	20	1459	2	Sp and glass
80	20	1461	4	glass
86	14	1445	2	An and glass
86	14	1450	1	glass
95	5	1495	3	An and glass
95	5	1500	3	glass

* Fo = crystals of forsterite,
Sp = crystals of spinel,
An = crystals of anorthite.

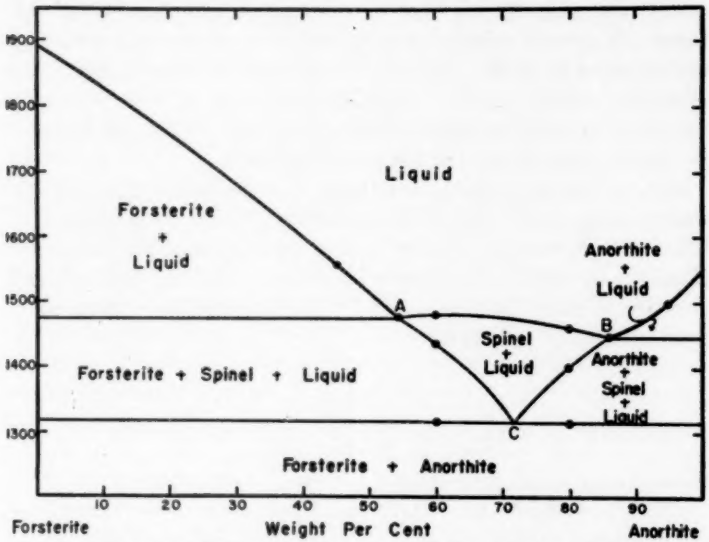

Fig. 3. Equilibrium diagram for the join forsterite-anorthite, a modification of Andersen's diagram to show sub-liquidus relationships.

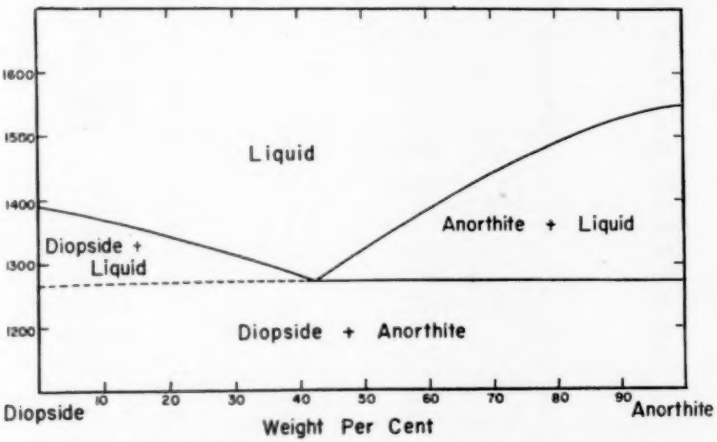

Fig. 4. Equilibrium diagram of the system diopside—anorthite (after Osborn).

QUENCHING RESULTS FOR THE SYSTEM DIOPSIDE—FORSTERITE—ANORTHITE

Data for the system diopside—forsterite—anorthite are summarized in table 2. They are the results of quenching experiments on the 40 mixtures whose compositions are shown by dots in figure 5.

The minimum liquidus temperature in the system, 1270°±5°, is that of point E (fig. 5), having the composition in weight per cent, 43.5 anorthite, 49 diopside, and 7.5 forsterite. This point resembles a eutectic, and for most purposes can be treated as such, but the diopside present in equilibrium with anorthite, forsterite, and liquid is presumed to contain a small amount of Al^{3+} on the basis of data for the system diopside—anorthite (Osborn, 1942, p. 758). Since the composition of the diopside crystals in equilibrium with liquid E cannot be represented by a point in the plane of figure 5, point E is not a ternary invari-

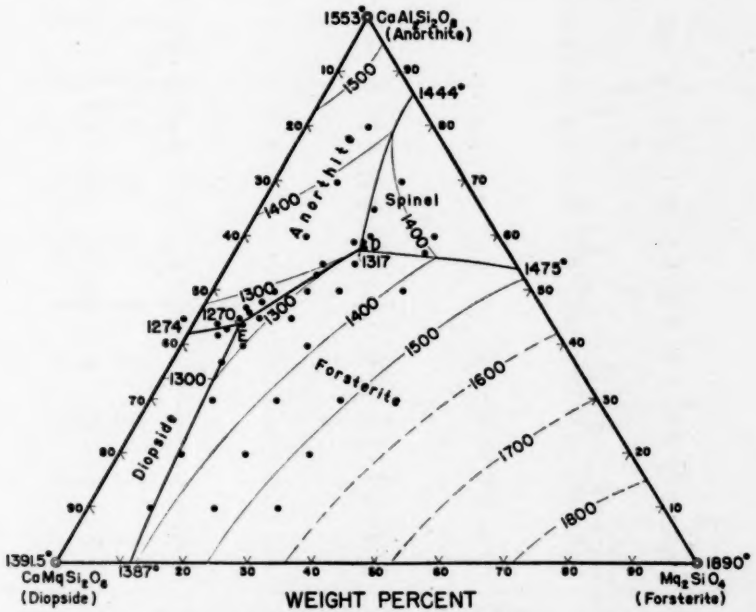

Fig. 5. Equilibrium diagram of the system diopside—forsterite—anorthite. Dots represent compositions of mixtures studied; light lines are isotherms; heavier lines are boundary curves.

TABLE 2

Summary of Quench Data for the System
Diopside—Forsterite—Anorthite

Composition in wt. %			Temp.	Time	
Anorthite	Diopside	Forsterite	(°C.)	(hrs.)	Phase Present*
44	52	4	1277	13	An and glass
44	52	4	1280	2	glass
42	53	5	1278	14	An and glass
42	53	5	1282	2	glass
43	51	6	1274	3	An, Di and glass
43	51	6	1276	13	glass
47	46	7	1285	2	An and glass
47	46	7	1288	10	glass
45	48	7	1278	3	An and glass
45	48	7	1282	5	glass
46	46	8	1291	11	An and glass
46	46	8	1285	3	glass
44	48	8	1270	4	Essentially all crystalline
44	48	8	1274	3	Fo, An and glass
44	48	8	1276	13	glass
37	55	8	1286	3	Di and glass
37	55	8	1289	2	glass
48	43	9	1288	10	An and glass
48	43	9	1293	2	glass
80	10	10	1443	2	An and glass
80	10	10	1445	2	glass
70	20	10	1389	2	An and glass
70	20	10	1395	16	glass
60	30	10	1350	3	An and glass
60	30	10	1355	2	glass
50	40	10	1294	3	An and glass
50	40	10	1297	3	glass
45	45	10	1280	2	Fo and glass
45	45	10	1283	2	glass

* An = crystals of anorthite,
Fo = crystals of forsterite,
Di = crystals of diopside,
Sp = crystals of spinel.

TABLE 2 (Cont.)

Summary of Quench Data for the System Diopside—Forsterite—Anorthite

Composition in wt. % Anorthite	Diopside	Forsterite	Temp. (°C.)	Time (hrs.)	Phase Present*
40	50	10	1299	2	Fo and glass
40	50	10	1303	2	glass
30	60	10	1340	2	Fo and glass
30	60	10	1342	3	glass
20	70	10	1345	2	Di, Fo and glass
20	70	10	1347	11	Fo and glass
20	70	10	1351	2	glass
10	80	10	1365	13	Di and glass
10	80	10	1371	2	glass
55	30	15	1303	2	An and glass
55	30	15	1306	2	glass
53	32	15	1300	3	Fo, An and glass
53	32	15	1303	4	glass
50	35	15	1303	2	Fo and glass
50	35	15	1306	4	glass
45	40	15	1309	2	Fo and glass
45	40	15	1314	2	glass
65	17	18	1355	2	Sp, An and glass
65	17	18	1362	2	Sp and glass
65	17	18	1370	2	glass
59	23	18	1322	2	An and glass
59	23	18	1327	2	glass
59	21.5	19.5	1325	2	Fo, An and Sp
59	21.5	19.5	1337	2	glass
70	10	20	1411	2	Sp and glass
70	10	20	1415	2	glass
60	20	20	1348	2	Sp and glass
60	20	20	1351	2	glass
58	22	20	1317	2	An, Fo and glass
58	22	20	1324	2	Sp and glass
58	22	20	1327	5	glass

* An = crystals of anorthite,
Fo = crystals of forsterite,
Di = crystals of diopside,
Sp = crystals of spinel.

TABLE 2 (Cont.)

Summary of Quench Data for the System
Diopside—Forsterite—Anorthite

Composition in wt. %			Temp.	Time	
Anorthite	Diopside	Forsterite	(°C.)	(hrs.)	Phase Present*
55	25	20	1324	2	Fo and glass
55	25	20	1328	2	glass
50	30	20	1350	3	Fo and glass
50	30	20	1351	2	glass
40	40	20	1365	13	Fo and glass
40	40	20	1371	2	glass
30	50	20	1415	2	Fo and glass
30	50	20	1423	5	glass
20	60	20	1423	5	Fo and glass
20	60	20	1429	3	glass
10	70	20	1445	2	Fo and glass
10	70	20	1449	2	glass
60	10	30	1422	2	Sp and glass
60	10	30	1426	2	glass
57	13	30	1380	2	Fo, Sp and glass
57	13	30	1407	2	rare Sp
50	20	30	1436	3	Fo and glass
50	20	30	1422	2	glass
30	40	30	1458	6	Fo and glass
30	40	30	1463	5	glass
20	50	30	1481	7	Fo and glass
20	50	30	1486	10	glass
10	60	30	1518	3	Fo and glass
10	60	30	1524	2	glass

* An = crystals of anorthite,
Fo = crystals of forsterite,
Di = crystals of diopside,
Sp = crystals of spinel.

ant point. Following Schairer (1942, p. 253), it may be called a piercing point.

The point D in figure 5 (1317°±5°) is also a piercing point, representing the intersection of a quaternary univariant line with the plane diopside-forsterite-anorthite. At this point, a liquid of composition D is in equilibrium with anorthite, forsterite, and spinel.

Just as the point D is not invariant, the lines bounding the field of spinel (lighter lines of fig. 5) are not univariant curves, but are the intersections with the plane diopside-forsterite-anorthite of quaternary divariant surfaces.

COURSES OF CRYSTALLIZATION

Equilibrium crystallization.—If as a first approximation point E is considered to be a ternary eutectic, courses of crystallization for mixtures within the area XDZY (fig. 6), of the system diopside—forsterite—anorthite, are of a simple ternary nature. As any liquid within this area is cooled under equilibrium conditions, the composition of the liquid changes as a consequence of the precipitation of crystals of one or more of X, Y, and Z and eventually has the composition E. As the temperature is lowered below 1270°, liquid disappears. Actually, however, diopside occurring in this system is believed not to have a composition accurately represented by the formula $CaMgSi_2O_6$, as stated above. This fact does not materially affect the nature of courses of crystallization, but has the effect of causing those liquids in equilibrium with diopside to lie slightly outside the plane of the diagram, i.e., to have compositions not accurately represented by mixtures of X, Y, and Z.

During the equilibrium crystallization of liquids within the area XDZ (fig. 6), the composition of the liquid at a certain temperature leaves the plane of the diagram (ceases to have a composition represented by mixtures of X, Y, and Z), after a temperature drop returns to the plane at point D, and with a further decrease in temperature moves to point E along the ternary boundary curve DE. This may be illustrated by noting the history of two representative points *a* and *c* (fig. 6) during their cooling from the liquidus to the solidus temperature.

Assuming that equilibrium among the phases is maintained, crystals of forsterite separate from liquid *a* as it is cooled from the liquidus temperature (1500°). The continued crystallization of forsterite from the liquid causes the composition of the latter to change along a straight line from *a* to *b*. At *b* (1400°) crystals of spinel appear. The point representing the composition of spinel (fig. 1) does not lie on an extension in the tetrahedron of the plane diopside-forsterite-anorthite, but instead lies forward (toward the CaO-Al_2O_3-MgO face) of this

plane.[3] Therefore, as the temperature is lowered below that of point *b*, the coprecipitation of spinel and forsterite causes the liquid to leave the D-Fo-A plane (fig. 1), moving behind (on the SiO_2 side of) the plane, in a direction away from forsterite and spinel. With continued decreasing temperature, the liquid therefore follows the forsterite-spinel divariant surface, with both spinel and forsterite precipitating, until the forsterite-spinel-anorthite univariant line is reached. The liquid reaches this line at a temperature between 1320° and 1317°, and at a position on this line between point C (fig. 3) and point D (fig. 6). The liquid then, with decreasing temperature, moves along this univariant line toward D as spinel dissolves and forsterite and anorthite crystallize. Just as point D is reached (1317°), the last of the spinel crystals disappear and the liquid moves down DE to E (fig. 6) as anorthite and forsterite continue to crystallize. At E, diopside, forsterite, and anorthite crystallize together as the liquid is consumed.

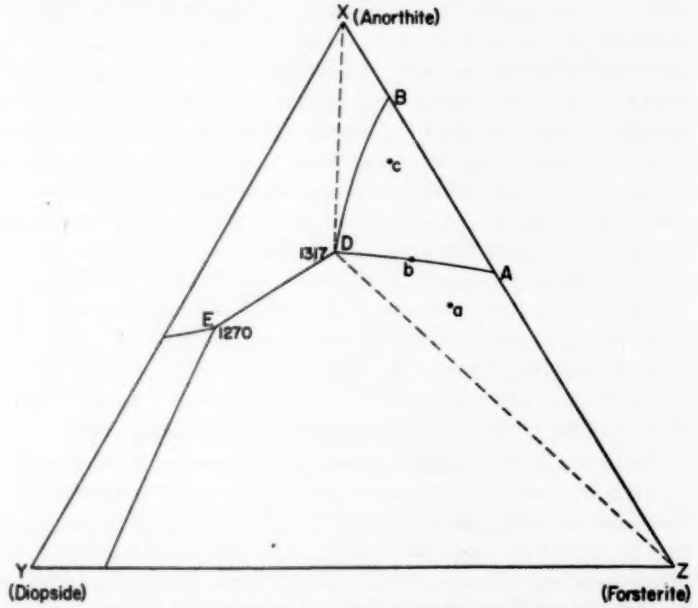

Fig. 6. Sketch of the system diopside—forsterite—anorthite to illustrate courses of crystallization.

[3] This is true also if the composition of the spinel phase lies between $MgAl_2O_4$ and Al_2O_3.

On the equilibrium cooling of liquid *c* spinel crystals appear at 1425°. The continued separation of spinel crystals with cooling causes the composition of the liquid to leave the plane XYZ (fig. 6), passing into the tetrahedral volume D-A-Fo-SiO_2 (fig. 1), where it intersects the divariant surface spinel-anorthite. These two crystalline phases then coprecipitate with decreasing temperature as the liquid moves to the diopside-forsterite-anorthite univariant line, reaching this line at a temperature between 1320° and 1317°. The subsequent history of the liquid with further cooling is similar to that of the liquid of mixture *a* in this temperature range.

Fractional crystallization.—Owing to the fact that spinel is a transient phase in the system diopside—forsterite—anorthite, and further that as a consequence of the crystallization of spinel the composition of the liquid leaves this plane to enter the tetrahedron D-A-Fo-SiO_2 (fig. 1), it is of interest to note the course of crystallization of a mixture such as *a* (fig. 6) when equilibrium is not maintained. For this purpose, let us consider the system diopside—forsterite—anorthite—silica, as sketched in figure 7.

In figure 7 the system diopside—forsterite—anorthite—silica is shown as a tetrahedron with the front face removed, reduced in size, and moved to the right. Boundary curves, invariant points, and piercing points, with their respective temperatures, are shown on each face. It can be seen that three quaternary univariant lines, depicted schematically in the lower part of figure 7, pass through this tetrahedron, and that no quaternary invariant points are present. One line, along which anorthite, forsterite, and spinel are in equilibrium with liquid, joins two piercing points, one located on the right face and one on the front face. This is a line of low temperature gradient and it possesses a temperature maximum at a point corresponding to C of figure 3. A second line, anorthite-pyroxene-forsterite, extends from the peritectic on the right face to the "eutectic" on the front face. A temperature minimum occurs on this line near the front face. A third line joins the eutectic on the right face with that on the left face. The arrows on the line indicate a temperature minimum also on this line, near the left end. Data are not available to prove this, but it is probable that such a temperature minimum exists.

As mixture *a* (fig. 6) is cooled to a temperature below that of *b*, spinel and forsterite crystallize together out of the liquid as the composition of the liquid moves from the front face (fig. 7) into the tetrahedron toward the univariant line An-Fo-Sp reaching this line at a point to the left of the maximum on the line. The liquid can remain on this univariant line with decreasing temperature only if spinel dissolves as forsterite and anorthite crystallize. If the spinel does not dissolve, as would be the case in perfect fractional crystallization where a crystal as soon as formed is effectively removed from the system, the liquid leaves the line as forsterite and anorthite continue to crystallize, and follows the forsterite-anorthite divariant surface

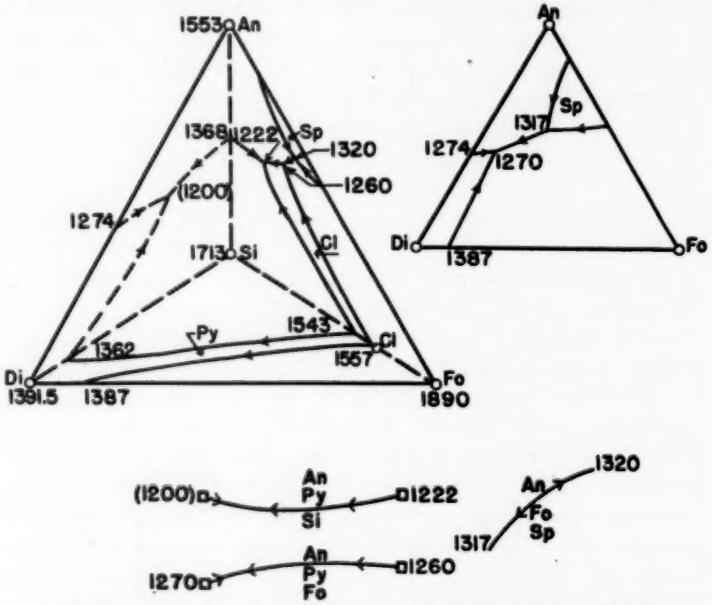

Fig. 7. Sketch to illustrate phase equilibrium relations in the system diopside—forsterite—anorthite—silica. The system is shown as a regular tetrahedron with the front face removed, reduced in size and shown at the right. The position of compounds and of boundary curves on the faces are indicated. In the lower part of the figure, the three univariant lines which pass through the tetrahedron are shown schematically, with the three crystalline phases indicated which exist in equilibrium with liquids along the line. The temperature of 1200°, shown in parentheses, is the approximate metastable eutectic of cristobolite, diopside, and anorthite, after Greig. Di = diopside, Fo = forsterite, An = anorthite, Si = silica, Cl = clinoenstatite, Py = pyroxene, and Sp = spinel.

to the second univariant line (An-Py-Fo) where a pyroxene (aluminous diopside-clinoenstatite solid solution) begins to crystallize. At this stage (about 1250°) the liquid therefore contains crystals of forsterite, pyroxene, anorthite, and spinel. If the An-Py-Fo univariant line passes inside, and not outside of the triangle whose apices are points representing the composition of forsterite, anorthite, and the pyroxene precipitating, then forsterite, pyroxene, and anorthite crystallize together as the liquid moves toward the temperature minimum and disappears. The failure of spinel to react with the liquid and disappear as anorthite and forsterite crystallize thus causes the final liquid of this crystallizing mixture to have a higher silica content than that of point E (fig. 6). Furthermore, it is possible that the pyroxene, which begins to crystallize as the liquid in mixture *a* reaches the univariant line An-Py-Fo (fig. 7), has a composition such that this univariant line passes outside the anorthite-forsterite-pyroxene composition triangle.[4] In this case part of the forsterite would react with the liquid and disappear as pyroxene and anorthite crystallize if equilibrium among anorthite, forsterite, pyroxene, and liquid were maintained as the liquid cooled. But we are considering extreme fractionation in which solution of a crystalline phase (spinel or forsterite) does not occur on cooling. Just as in the case of the failure of spinel to dissolve as anorthite and forsterite crystallize, the failure of forsterite to react with the liquid and partly disappear forces the liquid to leave a univariant line (An-Py-Fo), to move along the anorthite-pyroxene divariant surface as these two phases separate, and to reach the An-Py-Si univariant line (fig. 7) at a temperature of about 1200°. With subsequent cooling, silica

[4] Data on the composition of pyroxenes in equilibrium with anorthite, forsterite, and liquid are not available to show for what mixtures this may be true. Pyroxenes appearing during the fractional crystallization of mixture *a* (fig. 7) probably have compositions such that forsterite will crystallize along with pyroxene. But undoubtedly the pyroxene appearing during the fractional crystallization of some mixtures in the system diopside—forsterite—anorthite—silica from which spinel precipitates as the primary or secondary phase has a composition such that the forsterite structure, with equilibrium crystallization, must disappear as pyroxene crystallizes. Indeed, this is probably the general case in view of the relations in the system forsterite—anorthite—silica wherein: (a) the pyroxene present is the end member, clinoenstatite; and (b) the area in which olivine appears as the primary phase, but later must completely disappear with equilibrium crystallization, is about three times as large as the similar area in the system forsterite—diopside—silica.

crystallizes along with anorthite and pyroxene until the liquid disappears. The final aggregate is composed of spinel, forsterite, anorthite, pyroxene, and silica.

DISCUSSION

During the crystallization and differentiation of natural magmas, eutectic relations among phases must rarely if ever exist owing to the important role of solid solution and incongruent melting phenomena. In simple silicate systems, eutectics are common, but as these systems are complicated by the addition of other components, particularly if the composition is shifted toward that of natural magmas, eutectics play a less important role in the crystallization. The ternary system diopside—forsterite—silica, for example, which is sketched on the base of figure 7, is bounded by three binary systems each of which contains a eutectic, but in the ternary system no eutectic or other invariant point exists. In some other ternary systems of petrologic significance, such as the systems MgO—FeO—SiO_2 (Bowen and Schairer, 1935) and $NaAlSiO_4$—$KAlSiO_4$—SiO_2 (Schairer and Bowen, 1935), the same presence of eutectics in the bounding binary systems and absence of ternary eutectics is noteworthy. Systems approaching natural magmas in composition are thus characterized by reaction during crystallization, wherein a crystalline phase which has precipitated commonly must at a lower temperature react with the liquid and change in composition or dissolve or both. The failure of crystalline phases to react to the extent demanded by phase equilibrium relationships is the basis for the crystallization differentiation of magmas so ably expounded by Bowen (1928).

The system diopside—forsterite—anorthite has as components end members of the three minerals of most importance from a quantitative standpoint in igneous rocks of the earth's crust—pyroxenes, olivines, and feldspars. Yet in this system the three minerals crystallize together essentially as in a eutectic system, and reaction with liquid is virtually absent insofar as these phases are concerned. Similarly, the system diopside—anorthite—silica, shown as the left face in figure 7, has a ternary eutectic at which a pyroxene, a feldspar, and a silica mineral crystallize together from the liquid. But if another component is added to these systems to give the quaternary system diopside—forsterite—anorthite—silica, (fig. 7), quater-

nary invariant points are non-existent. Three univariant lines cross through the tetrahedron, any point on a univariant line representing the composition of liquid in equilibrium with three crystalline phases. As shown schematically in the lower part of figure 7, the three assemblages of crystalline phases which can exist in mixtures in this system under equilibrium conditions are: anorthite-pyroxene-silica, anorthite-pyroxene-forsterite, and anorthite-forsterite-spinel.

That three crystalline phases are in equilibrium with liquid does not however mean that they are all crystallizing from the liquid as it cools and changes composition along a quaternary univariant line. On the contrary, if equilibrium among the phases is maintained, spinel must dissolve as the liquid moves along the An-Fo-Sp line with decreasing temperature (fig. 7), and forsterite must dissolve over most of the length of the An-Py-Fo line. The composition of the liquid changes only in response to the subtraction of crystals or addition of substances, and for the liquid to change its composition along these lines, spinel and forsterite respectively must dissolve,[5] except along a short length at the left end of the An-Py-Fo line. If spinel in a liquid on the An-Fo-Sp line fails to dissolve at the required rate, as for example, because cooling is too rapid or because spinel crystals have been included in larger forsterite crystals which protect the spinel from attack by liquid, the composition of the liquid leaves the univariant line An-Fo-Sp, moves along the anorthite-forsterite divariant surface as these two phases separate, and reaches the next univariant line, An-Py-Fo. If the composition of the liquid on this line is such that with cooling forsterite should dissolve, then if it fails to do so the liquid leaves this line as anorthite and pyroxene crystallize and moves to the third univariant line. Here tridymite separates along with pyroxene and anorthite until the liquid is exhausted.

The olivine-liquid reaction is one of the well established phenomena on which the formation of igneous rock series by crystallization differentiation is based. The spinel reaction must also play a role during the crystallization of some basaltic magmas. Spinel, as pleonaste or picotite, occurs not uncommonly as primary inclusions in the olivine of basalt. Judging

[5] If one constructs a tetrahedron of the system $CaO—MgO—Al_2O_3—SiO_2$, it can be clearly seen that spinel and forsterite must dissolve as liquid moves along the An-Fo-Sp and An-Py-Fo lines, respectively, with decreasing temperature.

from the relations in the system diopside—forsterite—anorthite —silica and from the data of Schairer (1942, pp. 250-253) on the system anorthite—fayalite—silica in which hercynite appears as a transient phase just as does spinel in the former system, the pleonaste or picotite once formed in a basaltic liquid should at a lower temperature dissolve if equilibrium among the phases were realized. The failure of spinel, once formed, to dissolve during subsequent crystallization would have the same type of effect on liquid composition as the failure of olivine to dissolve, i.e., the residual liquid has a higher silica and a lower magnesia content than would be the case under equilibrium crystallization.

It will be noted from figure 7 that at temperatures above the solidus spinel cannot exist in equilibrium with a pyroxene in the system diopside—forsterite—anorthite—silica. Further, in this system diopside and clinoenstatite cannot coexist in equilibrium with liquid, but rather a solid solution of the two end members will form. On the other hand, anorthite and forsterite are compatible phases, as must also be calcic plagioclase and magnesian olivine, at least at high temperatures.

Troctolites, which are composed almost entirely of these latter two minerals, were described recently by Osborne (1949). Of special interest is the abundant growth of secondary, or reaction minerals in the troctolite, replacing the original plagioclase and olivine. The reaction minerals are dominantly a diopsidic pyroxene, enstatite, and spinel, with diopside and spinel commonly forming wormy intergrowths. The conclusions would seem to be: (1) that calcic plagioclase and magnesian olivine are not compatible within a temperature range existing below that of figure 7, (2) that in this lower temperature range spinel and diopside can coexist in equilibrium and (3) that this temperature range is also below the inversion temperature of enstatite to clinoenstatite (1145°) (Bowen and Schairer, 1935, p. 168) and is probably a few hundred degrees below this inversion temperature inasmuch as the inversion of enstatite plus diopsidic pyroxene to a diopside-clinoenstatite solid solution must occur at a lower temperature than the inversion of enstatite to clinoenstatite. Figure 7 therefore pertains to high temperature reactions such as the crystallization of plagioclase and olivine from a basaltic liquid and their settling and accumulating to form a mass of troctolite. At lower temperatures,

below a maximum of perhaps 900°C., the fields of spinel and diopside probably adjoin, as the fields of anorthite and forsterite cease to be contiguous.

In conclusion and referring to figure 5, the profound effect on the temperature of development of liquid in a forsterite body caused by small additions of lime, alumina, and silica may be noted. Liquid will appear at 1270°C. But it may also be observed that the eutectic lies close to the side line opposite the forsterite apex. At 1270° or at somewhat higher temperatures, the amount of liquid generated because of the presence of small amounts of these oxides will be small.

SUMMARY

The system forsterite—diopside—anorthite possesses a liquidus temperature minimum, which as a first approximation is a ternary eutectic, at 1270°C. where the three crystalline phases are in equilibrium with a liquid of the composition in weight per cent: 7.5 forsterite, 49 diopside, 43.5 anorthite. A field of spinel intrudes the system in view of the incompatibility of forsterite and anorthite at high temperatures. At temperatures between 1317° and 1270°C., however, spinel is not a stable phase in mixtures in this system, but instead forsterite and anorthite coexist.

The system forsterite—diopside—anorthite may be viewed as a triangular join within a tetrahedron representing the quaternary system CaO—MgO—Al_2O_3—SiO_2. As such, it is one face of an interior tetrahedron (diopside-forsterite-anorthite-silica) from whose liquids forsterite, anorthite, diopside-clinoenstatite solid solutions, spinel, and silica minerals crystallize. Although spinel crystallizes from liquids of this interior tetrahedron over a rather wide range of composition and temperature, it must at lower temperatures always react with the liquid and disappear if equilibrium is maintained. Failure of this spinel-liquid reaction to go to completion will cause the final liquid to be enriched in silica over its equilibrium composition, just as in the familiar case of the forsterite-liquid reaction. From previous work on iron silicate systems, it may be judged that this same situation obtains if ferrous ions are present in the spinel and olivine. The occurrence of spinel as inclusions in the olivine of basalt suggests that the spinel-liquid reaction is commonly deterred by the precipitation of an olivine layer about spinel crystals.

At temperatures above the solidus in the system forsterite—diopside—anorthite—silica, either forsterite, anorthite, and spinel, or forsterite, anorthite and pyroxene may coexist in equilibrium but pyroxene and spinel are not compatible. Field and laboratory studies of troctolite and associated coronite suggest, however, that at lower temperatures these relationships are reversed, i.e., spinel and diopside coexist under equilibrium conditions but not calcic plagioclase and olivine. Therefore, at some moderate temperature an accumulation of calcic plagioclase and magnesian olivine crystals becomes a metastable assemblage which will, if conditions are appropriate, transform to the low temperature stable assemblage of pyroxene, spinel, and plagioclase or pyroxene, spinel and olivine. Thus, available evidence suggests that both at high temperatures (above about 1320°) and at low temperatures (below about 900°) calcic anorthite and magnesian olivine constitute a metastable assemblage, but that at intermediate temperatures they may coexist at equilibrium.

ACKNOWLEDGMENTS

Most of the mixtures used in this study were prepared by the senior author in 1940 and 1941 while on the staff of the Geophysical Laboratory of the Carnegie Institution of Washington. The writers wish to thank Dr. L. H. Adams, Director of the Geophysical Laboratory, for releasing samples of these preparations for further study at The Pennsylvania State College.

REFERENCES

Andersen, Olaf, 1915. The system anorthite—forsterite—silica: Am. Jour. Sci., 4th ser., vol. 39, pp. 407-454.

Bowen, N. L., 1914. The ternary system: diopside—forsterite—silica: Am. Jour. Sci., 4th ser., vol. 38, pp. 207-264.

———,1928. The evolution of the igneous rocks, Princeton University Press, Princeton, New Jersey.

———, and Schairer, J. F., 1935. The system MgO—FeO—SiO_2: Am. Jour. Sci., 5th ser., vol. 29, pp. 151-217.

Greig, J. W., 1949. Personal communication.

Osborn, E.F., 1942. The system $CaSiO_3$—diopside—anorthite: Am. Jour. Sci., vol. 240, pp. 751-788.

———, 1950. Segregation of elements during the crystallization of a magma: Am. Ceramic Soc. Jour., vol. 33, pp. 219-224.

———, and Schairer, J. F., 1941. The ternary system pseudowollastonite—akermanite—gehlenite: Am. Jour. Sci., vol. 239, pp. 715-763.

Osborne, F. F., 1949. Coronite, labradorite anorthosite, and dykes of andesine anorthosite, New Glasgow, P. Q.: Royal Soc. Canada Trans., vol. 43, pp. 85-112.

Schairer, J. F., 1942. The system CaO—FeO—Al_2O_3—SiO_2: I, Results of quenching experiments on five joins: Am. Ceramic Soc. Jour., vol 25, pp. 241-274.

———, and Bowen, N. L., 1935. Preliminary report on equilibrium-relations between feldspathoids, alkali-feldspars, and silica: Am. Geophys. Union Trans., 16th Ann. Meeting, Part I, pp. 325-328.

Department of Earth Sciences
School of Mineral Industries
The Pennsylvania State College
State College, Pennsylvania

A RECONNAISSANCE OF LIQUIDUS RELATIONS IN THE SYSTEM $K_2O \cdot 2SiO_2$—FeO—SiO_2

EDWIN ROEDDER

ABSTRACT. A reconnaissance has been made of that portion of the system K_2O—FeO—SiO_2 having K_2O:SiO_2 ratios greater than 1:2. The results on 62 compositions are presented as a preliminary phase diagram for the condensed subsystem $K_2O \cdot 2SiO_2$—FeO—SiO_2 representing liquidus relationships in equilibrium with metallic iron under one atmosphere pressure of pure nitrogen. Two new compounds, $K_2O \cdot FeO \cdot 3SiO_2$ and $K_2O \cdot FeO \cdot 5SiO_2$, were found, and their relationships to equivalent compounds in the systems K_2O—Al_2O_3—SiO_2 and K_2O—MgO—SiO_2 discussed.

INTRODUCTION

IN most phase equilibrium work on silicates the major features of the phase diagram become apparent long before the work is complete. As many people who may wish to refer to the phase relationships in a given system require only the grosser aspects of the diagram, and as it will require a year or more to complete the data for this system, it was felt best to publish a preliminary account of the available information.

This system was investigated as a part of the four-component system K_2O—FeO—Al_2O_3—SiO_2, which is itself a preliminary to the addition of water as a fifth component, under pressure, to limited ranges of composition. This should yield, among other minerals, the iron analog of biotite, and, with compositions in the system K_2O—MgO—Al_2O_3—SiO_2 currently under investigation by Schairer, information of value in interpreting the stability relationships of most natural biotites and many associated anhydrous and hydrous K, Mg, Fe, Al, and Si minerals.

The author is grateful to Dr. Bowen for his pioneering work with Schairer in developing the experimental techniques so necessary for studying phase equilibria in ferrous iron bearing silicate systems (Bowen and Schairer, 1932) and for many helpful discussions with Dr. Bowen during the author's year at the Geophysical Laboratory. The author also profited considerably from discussions of technique and apparatus with Drs. M. L. Keith and J. F. Schairer. Mr. Kent Marquardson worked in the author's laboratory from January to October 1951 and presented a portion of the following data as a

Master's thesis in the Department of Mineralogy at the University of Utah.

This research was done at the University of Utah with the aid of a contract from the Office of Naval Research and assistance from the University of Utah Research Fund, for which the author is duly grateful.

EXPERIMENTAL PROCEDURE

Preparation of batches.—The procedure necessary for the study of systems including FeO as a component was first recorded by Bowen and Schairer (1932). The techniques used here are essentially theirs, with a few modifications which simplify considerably the time-consuming and laborious process of batch preparation, crystallization, and equilibrium determination. Certain of these techniques are described in the appendix to this paper for the benefit of those who may be interested. In essence, the procedure is to fuse together raw materials to give a glass of the exact K_2O:SiO_2 ratio desired with approximately the desired amount of FeO, the exact FeO per cent being determined later by analysis. The raw materials used here were as follows:

SiO_2.—Selected washed pieces of fused silica tubing were crushed in a Plattner type "diamond" mortar to pass 100 mesh, leached with hot HCl to remove metal contamination from the mortar, washed, dried, and ignited for 10-15 minutes at 600°.[1] The material then analyzed 99.98 per cent SiO_2 by HF—H_2SO_4 weight loss determinations on 5 grams. As this method of analysis will not indicate the presence of As_2O_3 or B_2O_3 (sometimes added as "promoters" during the working of silica ware) these two elements were searched for with a large spectrograph. Neither was found. The silica thus obtained is in a highly reactive state (a glass) making homogenization of the usually viscous melts obtained in this system considerably easier. High temperature ignition of the silica powder is neither necessary nor desirable, as it causes crystallization of cristobalite on the surfaces of the grains, which, although it may be insufficient

[1]Fused silica tubing cullet was obtained from the General Electric Co. Lamp Dept., Quartz Section, 1133 E 152 St., Cleveland 10, Ohio. Analysis of average material by GE showed > 99.8 per cent SiO_2. All pieces showing undissolved material were removed. From 0.01 to 0.06 per cent Fe metal was removed during the leaching. All temperatures are in degrees Centigrade.

to have an appreciable effect on the rate of solution of the silica in the melt, does have a pronounced effect on the static electrical properties of the powder, making weighing operations very difficult. Silica glass itself is very bad in this respect, requiring special techniques and care, but the ignited material, with its surface layer of cristobalite, is far worse.

K_2O.—Reagent grade $KHCO_3$[2] was converted first either to pure, completely crystalline potassium disilicate ($K_2O \cdot 2SiO_2$) or potassium tetrasilicate ($K_2O \cdot 4SiO_2$) and weighed in that form. The procedure and necessity for this step, as well as a number of other applicable items of technique are described elsewhere (Roedder, 1951*b*).

FeO.—FeO as such is very difficult to prepare, so in this work the readily formed magnetite solid solution was used. This was prepared by igniting, in air, small batches of reagent grade Fe_2O_3[3] at 1400° for 10 minutes, followed by crushing and screening thru 100 mesh. The material then analyzed 89.5 per

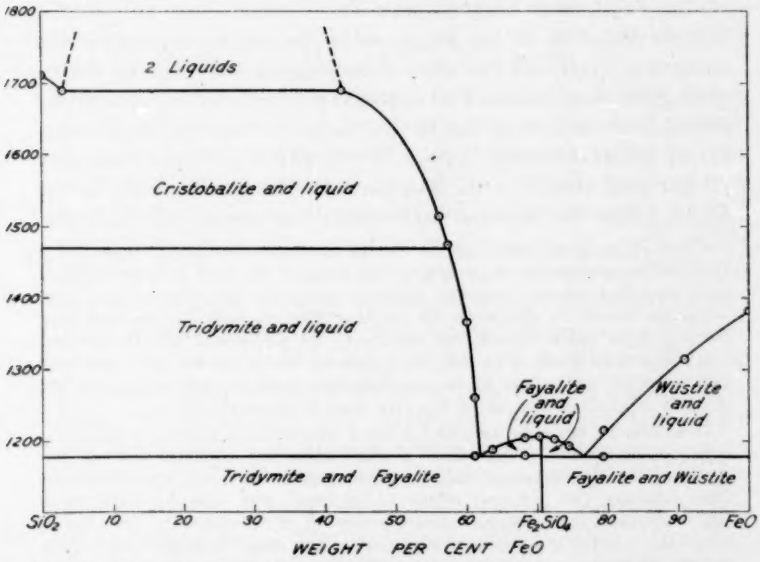

Fig. 1. Equilibrium diagram for the system FeO—SiO_2 after Bowen and Schairer (1932) and Greig (1927).

[2]J. T. Baker Company.
[3]Ibid.

cent total iron as FeO (i.e., it contained approximately 2½ per cent "excess" oxygen over the stoichiometric Fe_3O_4).

The correct amounts of silica and potassium silicate to make a 10-gram batch of the desired composition were carefully weighed out and transferred to a smooth agate mortar, and the approximately correct amount of Fe_3O_4 solid solution added (weighed to the nearest milligram).[4] The batch was mixed very completely in the mortar with care to avoid loss, approximately 3 grams of fine pure iron lathe chips added, and the mixture transferred to a 20-ml. pure iron crucible. It was then fused at approximately 1450° for ½ to 1 hour in a pure nitrogen atmosphere at room pressure and quenched in Hg. The furnace for this operation is described in the appendix. The glass and iron chips were broken out of the crucible, crushed, and the iron separated (to facilitate fine powdering of the glass), recombined, and the process repeated until the glass was homogeneous by the usual optical tests of uniformity of index of refraction of the crushed glass.[5] During the first such fusion, a part of the oxygen of the Fe_3O_4 over that in pure FeO combines with the metallic iron to add FeO to the batch, so in the batch preparation the amount of Fe_3O_4 solid solution to be weighed was found by multiplying the final desired FeO content by a factor of 0.75. About 80 per cent of the change due to this factor is from the stoichiometry of the relationship $Fe_3O_4 + Fe = 4FeO$, and approximately 20 per cent is due to the 2½ per cent "excess" oxygen in the Fe_3O_4 (over the formula requirement) as prepared, which also

[4]Loss of silica by static effects can be an important factor unless it is reduced or eliminated by weighing the silica first onto a metal balance pan, dumping off all possible material carefully into the mortar, and using the breath to discharge the sticking film of dust. The balance zero point is then redetermined and the Fe_3O_4 or potassium silicate weighed out. These effectively wipe off the remaining silica on the pan, and once the materials are mixed in the mortar, any static charge set up on the silica is dissipated and no differential loss is encountered.

[5]Preliminary crushing (minus 0.5 mm.) was done by hand in a Plattner-type hardened steel "diamond" mortar with the crushing end of the pestle of smaller diameter than the main pestle shaft and eccentric to it. Fine crushing (90 per cent minus 20 microns) was done by hand in an agate mortar. The average contamination of SiO_2 added to each batch from the mortar was determined to be less than 0.08 per cent SiO_2 on the basis of weight loss determinations on the mortar and pestle after 65 crushings. Screening greatly facilitates the preliminary crushing process but the contamination that occurs with permanent metal wire screens was avoided by using a fresh piece of fine mesh cloth (nylon curtain fabric) in a suitable holder for each batch.

combines with Fe metal to increase the FeO content of the batch. The relationship is only approximate, however, owing to several factors, not the least of which is the amount of "oxygen" that stays in the melt, tied up as the Fe_2O_3 representing equilibrium with metallic iron for that batch at that temperature. This cannot be calculated at present and hence must be determined by analysis of the completed glass, heat treated at a specific temperature (usually the liquidus), in equilibrium with metallic iron. There are thus two separate problems in such systems: first, the presence of a variable amount of Fe_2O_3 in all melts, which must be determined analytically and which makes the system really one with four components rather than three; and second, the difficulty of obtaining a batch with the desired FeO content. Obviously it is necessary to analyze all batches for total iron as well as for Fe_2O_3 because they may be either greater or less than calculated, but considerable success was had by the above technique in "placing" compositions where they were desired on the diagram.[6] In spite of the high viscosities of many of the glasses, homogenization was achieved usually in three fusions as the direct fusion in Fe at the start gives a large amount of the excellent flux FeO.

Much trouble was encountered at first in obtaining homogeneous glasses, resulting from the presence of a small amount of higher index, darker-colored glass obviously higher in iron oxide and formed by oxidation of the crucible walls at the start of the fusion by the air trapped in and over the powder and subsequent local solution of this oxide in the melt. While this resulted in only minute changes in total composition of a 10-gram batch, it was very significant in amount and particularly bothersome in the quenching determinations of equilibrium where tiny samples are used and the higher iron oxide liquid portions behave entirely differently from the remainder of the batch. This problem was eliminated by evacuating every crucible or bundle of quench charges in a miniature vacuum desiccator prior to fusion and replacing the air with exactly atmospheric pressure nitrogen, obtained by using a limp balloon as a storage tank. The tightly covered crucible or quench

[6] As has been pointed out by Bowen, only the iron content of such a batch can change, the ratios of K_2O:SiO_2 remaining fixed by synthesis, except for volatilization of K_2O which is negligible in these batches. Thus, with this ratio fixed by synthesis, and the chemical analysis for Fe_2O_3 and FeO, the total composition of the batch can be determined.

envelopes could then be taken out into the room and placed into the pure nitrogen atmosphere (also atmospheric pressure) of the furnace, with only a very minor amount of diffusion during the transfer allowing air to enter the crucible.

Precrystallization of batches.—In all compositions having liquidus temperatures less than about 1100° in this system,

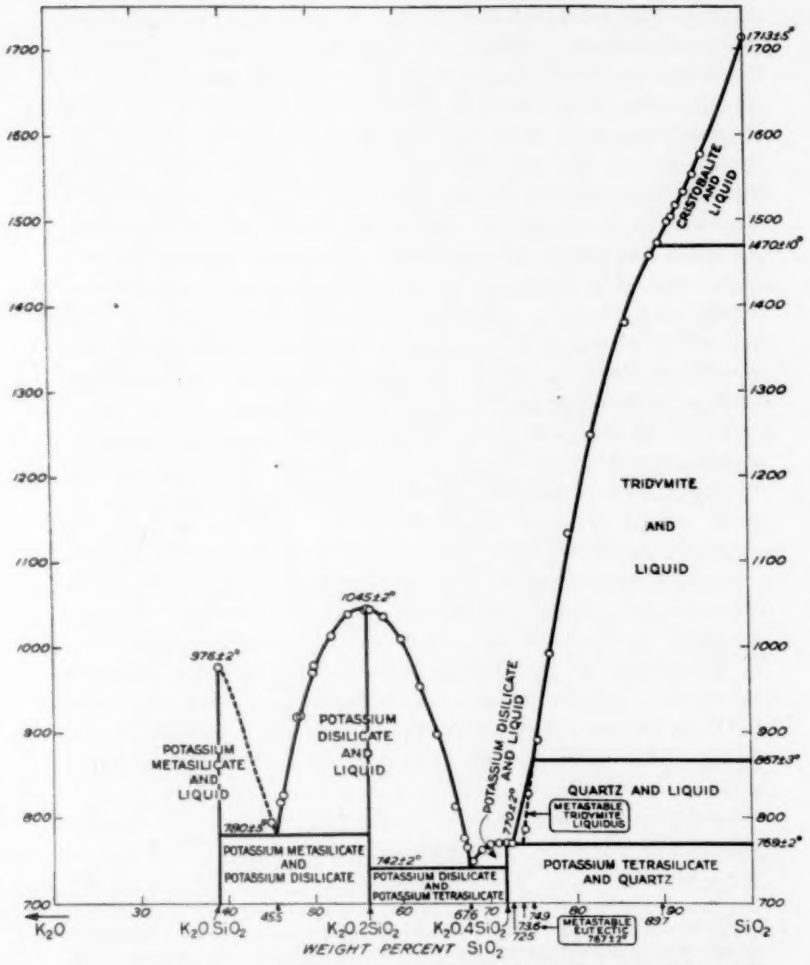

Fig. 2. Equilibrium diagram of a portion of the system K_2O—SiO_2, after Kracek, Bowen, and Morey (1937).

except those near to $K_2O \cdot 2SiO_2$ or fayalite, it was found necessary to precrystallize the glasses to avoid metastable equilibrium due to failure to nucleate the stable crystalline phases. In these cases samples of the glasses were held in pure iron containers in either a vacuum or in nitrogen at one atmosphere pressure (see appendix) at appropriate temperatures for as many hours or days as were needed to obtain a partially crystalline product which was then used in the quench runs. Certain of the batches near to $K_2O \cdot 4SiO_2$ have not yielded crystals after many days at what is believed to be optimum temperatures for crystallization of these glasses. This is in line with the visual observations of viscosity of the melts, those in that vicinity having the highest viscosities in the system (at the liquidus temperature). In general, viscosities in this system are considerably higher than in most iron-bearing silicate melts, and as a consequence, rates of crystallization are low.

Temperature measurement and control.—Temperatures were measured by a thermocouple of Pt against Pt 90 Rh 10 and a shielded potentiometer-galvanometer system reading directly in microvolts. The thermocouple was calibrated frequently in the same furnace as the quench runs, with the same technique, at the melting points of the following pure materials: NaCl (800.4°), Au (1062.6°), $Li_2O \cdot 2SiO_2$ (1201°), $CaMgSi_2O_6$ (1391.5°), and $CaSiO_3$ (1544°). Drifting between calibrations was checked by comparing the thermocouple with two other arbitrary reference thermocouples in another furnace, care being taken to make the temperatures of the three uniform by the use of a heavy platinum capsule around the three junctions among other precautions. Temperature control was obtained with photoelectric regulators, operating from a separate thermocouple 2 mm. from the furnace winding (see appendix). All thermocouple cold junctions were kept in melting ice.

Determination of equilibrium data.—The equilibrium data from which figure 4 was drawn were obtained by the quenching method, using small (1 to 10 mg.) charges of homogeneous glasses, or their crystallized products, of compositions as indicated by the circles on figure 3. These charges were held in pure iron containers (foil envelopes or tiny crucibles) in a pure nitrogen atmosphere at a given constant temperature until

equilibrium was established, and then quenched by dropping suddenly into mercury, still in a nitrogen atmosphere. The nitrogen was made sufficiently free from oxidizing substances that the envelopes come out silvery white and clean (see appendix). Where rapid quenching was necessary, a suitable sized platinum weight (1 to 10 grams) was suspended from the samples in order to make them sink beneath the mercury. Equilibrium was readily obtained in the very high temperature quench runs in 15 minutes, but the low temperature runs required 2 or more hours. In all cases where a composition fell near to a suitable boundary line and time permitted, the temperature of appearance of the second phase was determined. An approximate check was possible on the weight per cent of crystalline phase present and was used for planning of further runs whenever the composition of the original batch, the composition of the crystals, and the index of refraction of the liquid (glass) could be obtained. These data, with the isofracts shown on figure 3, permit a rough but useful evaluation of the composition of the liquid and hence the total amounts of crystals and liquid in the quenched sample. These isofracts are also useful in detecting any oxidation of the quench samples.

Chemical analysis of batches.—The compositions studied have been plotted on figure 3 by recalculating total iron oxides ($FeO + Fe_2O_3$) to FeO. This value for total iron as FeO is subtracted from 100 and the remainder divided between $K_2O \cdot 2SiO_2$ and SiO_2 in the ratio set by the original synthesis. Chemical analysis for ferrous iron was done by the modified Pratt method using CO_2 and transparent fused silica flasks (Bowen and Schairer, 1932),[7] and ferric iron was obtained by recalculating to Fe_2O_3 the difference between ferrous iron and total iron as FeO. Total iron was determined by several methods, the most rapid, which checks satisfactorily against other

[7] A one-gram sample of "pure" Fe_2O_3, treated by this technique showed <0.02 per cent FeO. All fragments of metallic iron must be carefully removed from the sample prior to analysis, and minute mercury droplets, from the quenching operation, were found to affect seriously this analysis for ferrous iron. They were subsequently removed with a mercury "magnet" (amalgamated copper wire) followed by heating the powdered sample in air to 200° for 15 minutes to vaporize all remaining mercury. Rubber stoppers were found to be unsatisfactory for closing off the flask during the solution of the sample, as accidental contact of the acid with the stopper gave high results. A loose fitting cap made of fused silica, integral with the silica inlet tube (for CO_2) was found to be satisfactory.

methods, being as follows: The titrated ferrous iron determination sample, still in the fused silica flask, is warmed to dissolve several grams of the excess boric acid crystals present[8] and cooled again at which time a new crop of boric acid crystals will form if adequate amounts have dissolved; the boric acid crystals are then filtered off and the solution passed through a Jones reductor and retitrated with permanganate. All permanganate titrations were made with a weighing burette, and the permanganate was standardized frequently against U. S. Bureau of Standards sodium oxalate according to the Bureau's recommended procedure. This method is particularly useful where small sample size precludes splitting for two separate determinations.

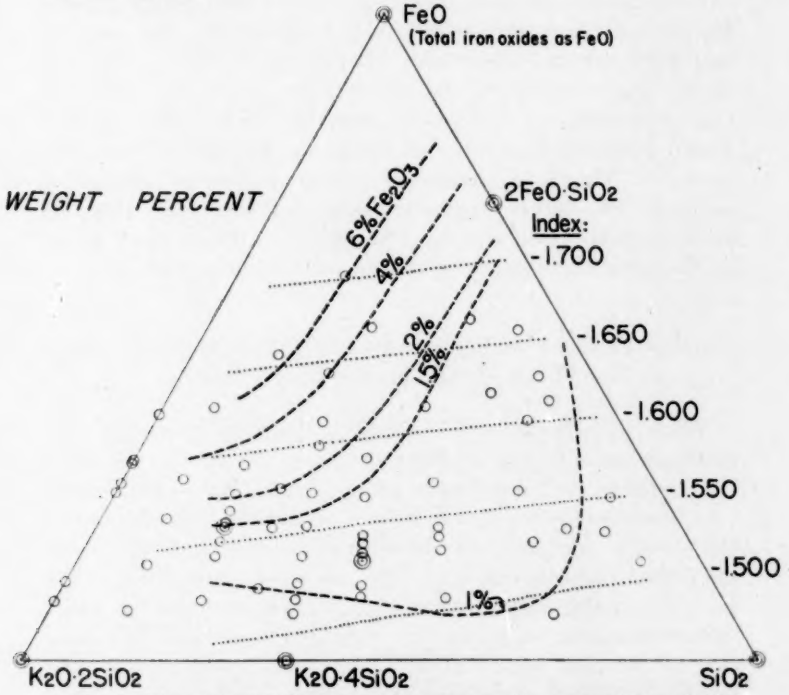

Fig. 3. The system K_2O—FeO—SiO_2, showing the compositions studied (circles), lines of equal Fe_2O_3 content in samples quenched from their individual liquidus temperatures (dashed lines), and approximate isofracts (dotted lines).

[8]This is necessary to insure complete complexing of all fluorides present; without this step considerable trouble was encountered as a result of the low solubility of boric acid.

RESULTS

Previous investigations.— Two of the three binary sidelines which limit this ternary system have been studied by Bowen and co-workers. The system FeO—SiO_2 (see figure 1) was studied by Bowen and Schairer (1932) and by Greig (1927), and the system K_2O—SiO_2 (figure 2) by Kracek, Bowen, and Morey (1937). Little is known about the possible nature of the third sideline, K_2O—FeO, and as all compositions studied here fall at less than 1:2 K_2O—SiO_2 ratios, this sideline is of little importance in this report.

General.—Figure 3 shows a series of dashed lines connecting batches having identical weight per cent Fe_2O_3 present in the glasses quenched from the liquidus temperatures for each, as best they can be drawn with available data, and a series of dotted lines connecting glasses of equal index of refraction (isofracts). Figure 4 shows the boundary lines (heavy dashed lines), isotherms (light dashed lines), and probable composition triangles. This is a preliminary diagram and is subject to revision. The ternary eutectic points indicated are only the most probable ones, and their positions are but guesses based on available data, as crystallization is exceedingly slow in these areas.

Stability Fields on the Liquidus Surface for the Various Crystalline Phases of the Limiting Binary Systems

Silica.—Tridymite and cristobalite together present a surprisingly small field of stability in view of the small area which this system covers in the more general system K_2O—FeO—SiO_2 (see figure 4a). Only tridymite and cristobalite were formed in the quench runs and crystallizations, no quartz being found up to the present, but very little work has been done in the low temperature region where quartz would be expected. High viscosities in this region and the "stuffing" and hence stabilization of the more open tridymite or cristobalite structures with K^+ would both tend to prevent the formation of quartz.

A region of liquid immiscibility, in which two silicate liquids, one rich and one poor in iron oxide, are in equilibrium with crystals of cristobalite, occurs adjacent to the FeO—SiO_2 sideline, and represents the effect of addition of alkali (as K_2O

$\cdot 2SiO_2$) to the immiscibility previously discovered by Greig in the system FeO—SiO_2 (Greig, 1927).

Low temperature silicate liquid immiscibility was discovered recently in the system leucite—fayalite—silica (Roedder, 1951*a*). If the tetrahedron representing the more general system K_2O—FeO—Al_2O_3—SiO_2 is considered it will be seen that the region of low temperature immiscibility in the plane leucite—fayalite—silica is rather close to the K_2O—FeO—SiO_2 side of the tetrahedron. The intersection of the projection of the boundaries of this region of immiscibility, on the K_2O—FeO—SiO_2 face, when projected parallel to the K_2O—Al_2O_3 edge of

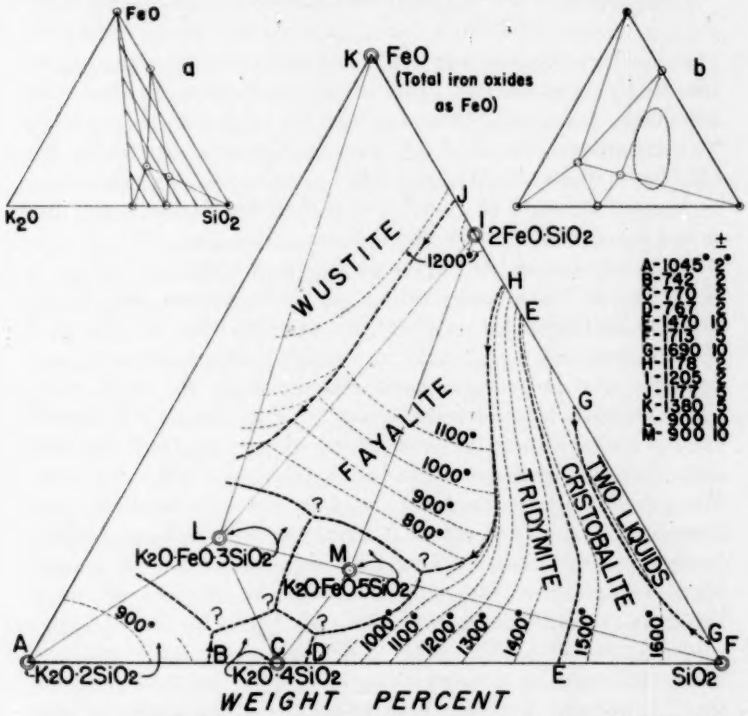

Fig. 4. Preliminary equilibrium diagram for the system $K_2O \cdot 2SiO_2$—FeO—SiO_2, subject to later revision, showing liquidus relationships in equilibrium with metallic iron. Fe_2O_3 is present in all liquids. Figure 4a shows the position of this system (shaded area) in the more general system K_2O—FeO—SiO_2, and figure 4b shows the intersection of the field of low temperature liquid immiscibility in the system leucite—fayalite—silica projected onto this system. See text.

the tetrahedron is indicated by a dashed curve in figure 4b. It is unfortunate that comparatively little data is available on compositions falling within this area, but a perfectly "normal" liquidus behavior was found for the five compositions in the area whose quenching results are complete, and no evidence of liquid immiscibility was found in any batch in the area. Thus it is seen that, although the immiscible liquids in the system leucite—fayalite—silica consist of K_2O, FeO, and SiO_2, and with only 2-9 per cent Al_2O_3, there is no evidence of similar low-temperature immiscibility in the liquidus relations in the pure system K_2O—FeO—SiO_2.

Comparatively low temperature immiscibility *was* found, however, in three compositions falling between this projected region and the high-temperature region of immiscibility adjacent to the FeO—SiO_2 sideline. The behavior of these batches was definitely anomalous, however, and an explanation can only be surmised at present. Each gave, at temperatures above the liquidus in the range 1450°-1500°, quench samples containing very small amounts of globules of high index dark brown glass embedded in the normal, much lower index glass. In no case was the amount of high index glass over a small fraction of 1 per cent. At lower temperatures the globules were not found, and the melting point of pure iron prevents the use of higher temperatures. If a region of immiscibility exists between these compositions and compositions equivalent to the high index glass globules, then batches richer in FeO than these should show a greater amount of the high index phase, but they did not. The only possible explanation that has been found for this paradox lies in the fact that this is not a simple ternary system; Fe_2O_3 is present in all batches, although admittedly in very small amounts in the region concerned. From the system leucite—fayalite—silica we know that the addition of small amounts, as little as 2 per cent, of Al_2O_3 to certain compositions in the system K_2O—FeO—SiO_2 can cause immiscibility. It might be possible that, at certain temperatures, the Fe^{+++} present in these three batches (to the extent of approximately 1 per cent "Fe_2O_3"), may act in lieu of Al^{+++} in causing an immiscibility region, above the liquidus, in the quaternary system K_2O—FeO—Fe_2O_3—SiO_2 to which these compositions really belong.

Fayalite and wüstite.—The fields of fayalite ($2FeO \cdot SiO_2$) and wüstite (FeO solid solution) on the liquidus surface are

approximately as might be expected from analogy with the system K_2O—MgO—SiO_2, as Fe^{++} may substitute readily for Mg^{++}. The analogy between the two systems is remarkably close, except that the temperatures are considerably lower in the iron system, and ferrosilite, the iron analog of the metasilicate compound $MgO \cdot SiO_2$, has not been found in any of the experimental work.

Potassium silicates.—The portion of the diagram near to the $K_2O \cdot 2SiO_2$—SiO_2 side has not been studied closely. The field of $K_2O \cdot 2SiO_2$ has been established as indicated with only a few points, but high viscosities have prevented obtaining any information on the nature of the $K_2O \cdot 4SiO_2$ field.

New ternary compounds.—Two new ternary compounds, $K_2O \cdot FeO \cdot 3SiO_2$ and $K_2O \cdot FeO \cdot 5SiO_2$, have been found in this system, and preliminary results indicate the presence of at least one more.[9] As might be expected, these compounds are closely related to those occurring in the system K_2O—MgO—SiO_2, by the substituting Fe^{++} for Mg^{++}.

One of these new compounds, $K_2O \cdot FeO \cdot 3SiO_2$ melts congruently, probably at about 900° ± 10°, as some batches in the immediate vicinity of its composition point have liquidus temperatures of 889°. It usually forms rounded crystals, although occasionally elongate, or even diamond-shaped crystals are formed, colorless under the microscope, with an average index of approximately 1.575 and birefringence approximately 0.01. Elongated crystals are usually length slow and approximately parallel in extinction. Some are definitely uniaxial negative, like the $K_2O \cdot MgO \cdot 3SiO_2$ analog, but a few are biaxial positive. Powder X-ray diffraction photographs show patterns almost identical with the equivalent magnesia compound except for line intensities and so presumably this compound is isostructural with $K_2O \cdot Mgo \cdot 3SiO_2$ and hence with the mineral kalsilite, $K_2O \cdot Al_2O_3 \cdot 2SiO_2$ (Roedder, 1951*b*). The field of the compound on the liquidus is very flat, as is that of the equivalent magnesia analog.

The other new compound $K_2O \cdot FeO \cdot 5SiO_2$ presents as close

[9] Compositions consisting of $K_2O \cdot 2SiO_2$ with approximately 25-30 per cent FeO apparently fall in the primary phase area of still another compound, crystallizing as round isotropic "fish-eggs" of index approximately 1.590. Presumably this would be the iron analog of either the isotropic compound $K_2O \cdot MgO \cdot SiO_2$ or possibly $K_2O \cdot MgO \cdot 2SiO_2$ (see Roedder, 1951b, *n.* 49).

a parallel to the equivalent magnesia compound $K_2O \cdot MgO \cdot 5SiO_2$ as the preceeding example. It forms large tetrahexahedra which at first are isotropic, but with further heating become anisotropic with usually very low birefringence. Both the isotropic and birefringent forms have an index of about 1.535. In a few cases bright anomalous blue to red interference colors were seen. The compound melts congruently, also probably at $900° \pm 10°$, as several batches in the immediate vicinity of its composition point have liquidus temperatures of 889°, and the liquidus surface is also very flat-topped. The glass surrounding the large crystals is under strain exactly as with $K_2O \cdot MgO \cdot 5SiO_2$, and the X-ray powder patterns are practically identical with those of $K_2O \cdot MgO \cdot 5SiO_2$, except for line intensities and a slightly smaller unit cell in the iron compound. Thus this compound is isostructural with leucite, $K_2O \cdot Al_2O_3 \cdot 4SiO_2$. Details of the X-ray data will be reported in a later paper. It is interesting to note that since Al^{+++} probably occurs in tetrahedral coordination (proxying for Si^{++++}) in the two compounds $K_2O \cdot Al_2O_3 \cdot 2SiO_2$(kalsilite) and $K_2O \cdot Al_2O_3 \cdot 4SiO_2$ (leucite), and since the two new compounds found here, $K_2O \cdot FeO \cdot 3SiO_2$ and $K_2O \cdot FeO \cdot 5SiO_2$, are apparently isostructural with them, the Fe^{++} in these new compounds must occur in tetrahedral coordination.

References

Bowen, N. L., and Schairer, J. F., 1932. The system FeO—SiO_2: Am. Jour. Sci., 5th ser., vol. 24, pp. 177-213.

Greig, J. W., 1927. Immiscibility in silicate melts: Am. Jour. Sci., 5th ser., vol. 13, pp. 1-44, 133-154.

Kracek, F. C., Bowen, N. L., and Morey, G. W., 1937. Equilibrium relations and factors influencing their determination in the system K_2SiO_3—SiO_2: Jour. Phys. Chem., vol. 41, pp. 1183-1193.

Roedder, Edwin, 1951*a*. Low temperature liquid immiscibility in the system K_2O—FeO—Al_2O_3—SiO_2: Am. Mineralogist, vol. 36, pp. 282-286.

———, 1951*b*. The system K_2O—MgO—SiO_2: Am. Jour. Sci., vol. 249, pp. 81-130, 224-248.

Department of Mineralogy
University of Utah
Salt Lake City, Utah

APPENDIX ON TECHNIQUE

Pure nitrogen.—Considerable difficulty was experienced at first in obtaining a sufficiently pure nitrogen atmosphere. Heated steel wool was used as the final step in the purification, after passage through a flowmeter, sulfuric acid bubbler,

and tubes of activated alumina and of magnesium perchlorate to minimize the amount of oxgyen (in the form of water) that must be removed by the steel wool. Any CO_2, CO, H_2O, or O_2 present in the nitrogen is effectively removed by the steel wool down to the partial pressure of oxygen in equilibrium with iron oxide at the temperature of the steel wool (700°). "Prepurified" tank nitrogen was used, but this always contains a prohibitive amount of oxygen or oxygen-bearing materials to be used without the above purification train. An Inconel tube, 1¼ inches in diameter and sufficiently long to permit the use of rubber stoppers, was found to be far superior to porcelain for this operation, and was filled with a roll of degalvanized screen wire (iron) separating layers of degreased 000 grade steel wool. The screen wire was found necessary to avoid the shrinking and channeling of the fine steel wool that occurs otherwise. Between the steel wool furnace and the "quenching" or "making" furnaces a long piece of transparent fused silica tubing was inserted with a Bunsen burner on a slide under it. This tube was filled with clean steel wool and acts as a visual check on the purity of the nitrogen before it is distributed to the quenching furnaces or other uses. To verify the flow, small traps filled with oil through which the nitrogen must bubble are inserted in all lines immediately before the furnace where the gas is to be used. In order to avoid the necessity of refilling the steel wool furnace frequently, hydrogen is run through it each night, reducing the iron oxide that has formed to a highly reactive sponge of iron metal. A sporatic, serious oxidation of the quench charges during the early part of the work was finally traced to the condensation of the water formed by this reduction on the walls of the tubing leading from the steel wool furnace and its subsequent slow evaporation into the pure nitrogen, contaminating it. This was eliminated by placing a two-way stopcock on the exit end of the steel wool furnace, and moving the Inconel tube in the furnace so that this exit end was kept rather warm. When hydrogen was being put through the furnace, it was expelled at this point, and the tube was warm enough to prevent any condensation between the furnace and the stopcock. This stopcock was not turned to the other position until after the hydrogen was flushed out. The more obvious procedure of placing a drying tower or tube at the exit end of the steel wool furnace would be unsatisfactory as the usual desiccants do not lower sufficiently the effective

vapor pressure of oxygen in the nitrogen. One charge of iron in the Inconel tube has been in constant use for nearly a year with no sign of exhaustion. The quenching or batch preparation runs (mainly at 700° to 1450°) come out of the furnaces as clean and bright as platinum with this procedure. Theoretically this nitrogen should be very slightly reducing toward any iron oxide at temperatures higher than that of the steel wool furnace owing to the difference in the vapor pressures of iron oxide at the two temperatures, but no effect of this kind has been observed.

Furnace for batch preparation.—Much difficulty was encountered in trying to set up a furnace in which the 10-gram batches could be fused in nitrogen in iron crucibles at 1450° and quenched, the quenching being necessary to verify batch homogeneity. For convenience, the smallest commercially available pure iron crucibles were used (20 ml.) although these were much too large except for foaming batches. A number of attempts were made before the following design evolved.

The operation of this furnace is as follows (letters refer to figure 5): The iron crucible with its charge, and non-gas-tight lid crimped into three notches filed near the edge of the crucible, is placed in the miniature vacuum desiccator (not shown) and the air in it replaced with atmospheric pressure nitrogen. The crucible hanger assembly consists of a hook *a* made of 5 mm. diameter Puron[1] iron rod supported by a porcelain ring *b* (3/16″ wide, cut from a 7/16″ x 11/16″ thermocouple protection tube), in turn supported from a heavy platinum hook (3 mm. diameter wire) and wire *c* (0.3 grams per cm.) which connects to a ¼″ iron rod *d* hung from a chain which goes through the top of the hood in which the furnace is kept to eliminate mercury vapors. It is lowered and the bottom of the furnace is then opened by pulling lever *e*, thus lowering yoke *f* supporting the Pyrex quencher *g* from two pins *h* mounted on a metal band clamped around the quencher. This breaks the flat ground surface seal *i* between *g* and the flat ground end of the 2″ x 2¼″ x 16″ porcelain tube *j*. This seal is made gas tight with silicone stopcock lubricant, which is kept from baking hard by water-cooling pipes soldered to the outside of 1″ wide copper band *k*, in close contact with

[1]Obtained from Westinghouse Electric Corporation.

the tube. The platinum support wire is sufficiently long so that the iron rod *d* does not enter the furnace. The lever *e* is fastened in the down position, the crucible transferred from the vacuum desiccator to the Puron hook, and the quencher replaced around it. After flushing with nitrogen the crucible is pulled into the hottest part of the furnace with the chain. The

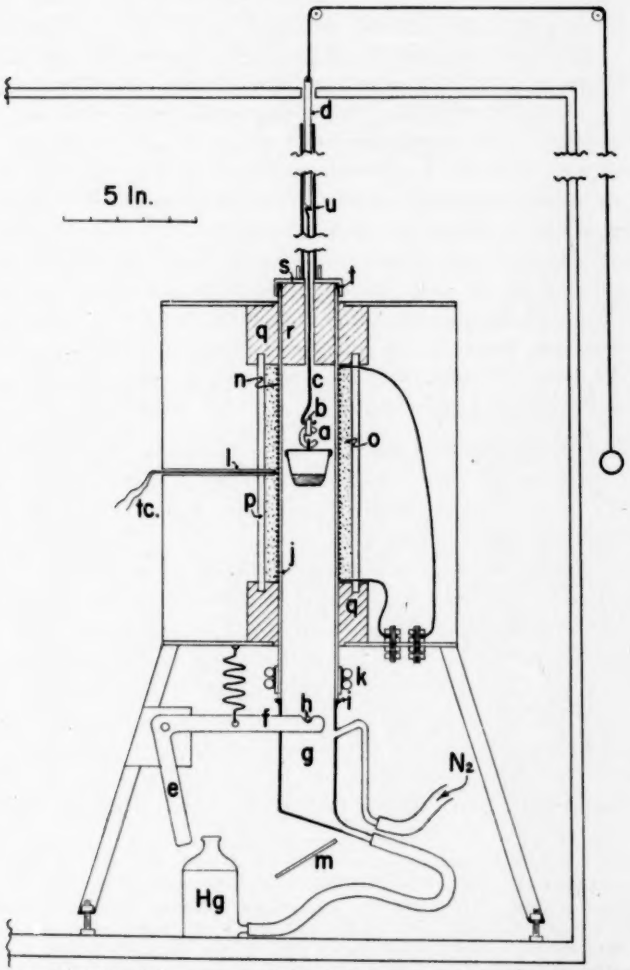

Fig. 5. Sketch of furnace used for batch preparation. Letters refer to description in text.

temperature is read with the shielded thermocouple *l*, near the winding, which had been compared with another thermocouple at the sample location within the tube. The bottom of the quencher is made of a sloping sheet of Pyrex plate so that the crucible in the furnace can be examined with the aid of mirror *m*. During the run a layer of clean mercury is kept in the quencher over this plate to aid in heat reflection.[2]

The platinum winding *n* is wrapped and cemented directly to the porcelain tube and is surrounded by granular insulating Alundum grain *o*[3] held in by alundum tube *p* and K30 insulating bricks *q*. Surrounding this is the usual can filled with extra-light MgO. The insulating brick plug *r* is cemented to the metal cap *s* which is effectively sealed to the porcelain tube by an asbestos gasket *t* soaked in silicone grease. The pipe *u*, ground flat on the lower end, is slightly larger in bore than the iron rod *d*, and these two effectively eliminate convective circulation of air into the furnace. Nitrogen is fed into the bottom and exits around this rod at the top. For quenching the mercury level in the quencher is raised and the crucible quickly lowered until its bottom sits on the mercury, with the N_2 still flowing.

Precrystallization of batches.—The technique used by Bowen and Schairer for precrystallization of batches involved sealing the charges in an evacuated fused silica tube. This method is still far superior for long term crystallizations, but for shorter term crystallizations, particularly at higher temperatures where the fused silica tube may collapse, a different method was used here. The individual charges (up to 20 or more), in iron foil capsules, were put in the bottom of a closed-end Vycor or fused silica tube approximately 20 mm. diameter by 18 cm. long. A standard taper 24/40 male joint was ground on the open end and lugs fused on for attaching tension springs. The female portion of this joint, of Pyrex, had a side arm with stopcock and a vertical tube on top which was rounded off and

[2]In the small bore (17 mm.) quenching furnace used for equilibrium determinations a somewhat similar quencher is used, but with a standard taper 24/40 male joint ground on the bottom of the porcelain tube and a matching female fitting at the top of the Pyrex quencher. As this porcelain tube is small bore and sticks out 5 cm. below the bottom of the furnace, no water-cooling ring is needed for the silicone grease seal even with the furnace at 1500°.

[3]Norton Company, No. E-163.

almost sealed. An ordinary rubber balloon was fastened over this, and the whole evacuated through the side arm, the hole in the vertical tube being too small to permit sucking in the balloon. Atmospheric pressure nitrogen was admitted, the stopcock closed, and the lower end of the tube with the samples placed into a furnace through a hole in an insulating brick. On heating, a small positive pressure is set up in the balloon, providing a continuous check on the seal. With this procedure the tube can be opened up at any time and part of the samples examined. A variable-voltage transformer, using current from a constant-voltage transformer, was found to give adequate temperature control for the crystallizations.

Iron foil for quench charges.—The comparatively long times necessary to reach equilibrium in many of the compositions in this system made it imperative to run more than one quench charge at a time. Through the use of pure iron foil, with techniques similar to those used with Pt foil (Roedder, 1951*b*) it was found possible to make up a bundle of 20 envelopes, each a different charge and approximately 4 x 5 x 0.5 mm. in size, containing 2-5 mg. of sample, that measured overall 4 x 5 x 10 mm. This is well within the size of the effectively uniform temperature region in the furnace and requires only about 10 grams of Pt weights to cause it to sink in the mercury during quenching. The individual envelopes can be easily labeled with a scriber, and are held together with iron foil strips or wire. No separators were used below a time-temperature combination of 1380° and 30 minutes, but above this trouble was encountered from coarse recrystallization of the iron foil causing serious welding together of the envelopes. A thin layer of MgO in xylol painted on the envelopes satisfactorily cured this trouble at temperatures up to 1500° for 15 minutes. At the conclusion of the run three sides of each envelope are snipped off for easy opening. Although these envelopes are not sufficiently air-tight to prevent the evacuation of the air inside of them and replacement with nitrogen prior to the run, in those cases where oxygen got into the quench furnace and the outside of the envelopes was covered with magnetite crystals, the inside surfaces were still bright and shiny. For the very fluid high iron batches it was found that capillarity would empty the melt out of the envelope through the folds. For

these batches tiny iron crucibles of 0.1 ml. capacity were formed from iron sheet or foil, but of course these quench runs could only be made singly.

As pure iron foil sufficiently thin for use in these envelopes (approximately 0.0015″) was not found to be available commercially,[4] pure iron sheet, available in 0.018″ thickness, was rolled on a Noble and Hunt 2-high, 6″ rolls powered by a 2 h.p. motor. The material as supplied (work-hardened) was taken to 0.006″ by 12 passes through the rolls, followed by pack rolling of 2 layers down to a total of 0.006″ and then of four layers down to 0.006," making individual sheets 0.0015." A large amount of the material was ruined by pinholing during the last passes. This could probably have been avoided by intermediate anneals, but a low yield was taken in preference to the trouble of bright annealing. The foil was finally bright annealed in nitrogen to facilitate folding the envelopes. Small crucibles for the chemical analysis runs where 0.5 grams must be fused were formed by folding 0.002-0.003″ foil around the round end of a 0.410″ diameter hard steel mandrel and hammering this into a hard steel die of 0.440″ I.D.

Temperature measurement and control.—Except for the crystallizations, a standard Geophysical Laboratory type platinum-wound electrical resistance furnace was used throughout. These furnaces have their winding wrapped on an alundum tube which surrounds the porcelain tube in which the nitrogen atmosphere is maintained. Outside of the winding is another alundum tube, providing an annular space of approximately 3 mm. radius around the winding which is filled with insulating grain alundum,[5] and outside of this is a layer of approximately 4 inches of extra-light magnesia. At first temperature control was attempted from a Pt-Pt 90 Rh 10 thermocouple embedded in the inside of the wall of the outermost alundum tube, approximately 3 mm. from the platinum heating element and parallel to the tube axis. This was found to be completely unsatisfactory as a result of a combination of conduction and induction of the heating current into the thermocouple circuit, particularly the surge of current from making or breaking the relays in

[4] Later a supply of .002″ sheet was obtained through the courtesy of the Allegheny Ludlum Steel Corporation, but it is not a commercial product.

[5] Norton Company, No. E-163.

the heating element control system. A thermocouple was then inserted through the wall of the furnace perpendicular to its axis, with the junction approximately 2 mm. from the winding near the center of the furnace. One wire of this couple was enclosed in a fine single bore porcelain capillary, and in turn the whole couple was enclosed in a larger thin-walled porcelain tube of which one end had been sealed off with an oxy-gas flame. Around this was wrapped a 0.01 mm. grounded platinum foil shield, separated from the winding of the furnace by approximately 2 mm. of alundum cement.

The e.m.f. from this thermocouple was fed through cold junctions with copper kept in an ice bath into a non-proportioning photoelectric controller.[6] This controller does not perform on-off control, but throws in and out of the line a variable resisance in series with the furnace winding, set to cut the total amperage in the system approximately 20 per cent below the high position. Also in the line is a variable voltage autotransformer connected so that the neutral side of the 110 V.A.C. is on the "through" side of the transformer to decrease leakage into the thermocouple circuits. This transformer is set at a voltage sufficient to cause an amperage approximately 10 per cent too large for the desired temperature to flow through the furnace, and the controller cuts in the variable resistance to reduce this to 10 per cent too little when the control thermocouple reaches the controlling temperature.

Temperature measurement, for equilibrium determination, is performed with a thermocouple which is entirely independent of the temperature control circuit. The controlling circuit described merely maintains the temperature at whatever value is desired, this being measured right at the exact sample location, by another thermocouple, adequately shielded and carefully calibrated. The small number of turns on the main slidewire in the controllers as sold precludes setting them accurately to a given temperature, so fine adjustment of the control point was obtained by throwing the instrument "off balance" against the standard cell, a single turn on the variable resistance in the battery-balancing circuit having a much smaller effect on the control point temperature than a single turn on the main

[6]Tagliabue "Celectray" photoelectric indicating controllers equipped with a manganin slidewire, a more sensitive galvanometer, and with the automatic temperature compensator removed were used.

balancing slidewire. With this arrangement, the oscillation in temperature due to regulator action at the sample location amounts to only ± 0.5 to 5 microvolts, depending on the temperature range involved and occurs through a 10- to 60-second cycle. This surprisingly small range of oscillation is not a function of the photoelectric regulators in that they are far less sensitive than this, but it is a result of the greater distance the heat has to flow from the winding to the sample location than from the winding to the control thermocouple.

The instruments used have manual comparison of the batteries against standard cell, making runs of several hours' duration subject to fluctuations of several degrees unless checked every hour. As the technique of determining equilibrium on iron-bearing silicates necessarily precludes the presence of the thermocouple in the furnace during the run (Bowen and Schairer, 1932), temperatures must be measured before and after the run. The above controlling circuit was found to be completely satisfactory, provided the controlling relays did not malfunction. A multichannel waxed-paper tape recorder, designed to record the action of these relays, helped considerably not only by verifying constancy of relay action (and hence of temperature), but also by aiding the correct positioning of the variable voltage transformer whenever the furnace was set to a new temperature.

LEUCITE, POTASH NEPHELINE, AND CLINOPYROXENE FROM VOLCANIC LAVAS FROM SOUTHWESTERN UGANDA AND ADJOINING BELGIAN CONGO

TH. G. SAHAMA

Chemical analyses by H. B. Wiik

ABSTRACT. Four specimens of rocks from the young volcanic belt of southwestern Uganda and adjoining Belgian Congo have been investigated. Leucite, nepheline, and clinopyroxene (diopside), extracted from the rocks by means of heavy liquids, have been analyzed chemically. Optical properties are also given. Chemical compositions of the analyzed minerals are discussed.

INTRODUCTION

A feature in the geology of the Western Rift of Equatorial East Africa is the occurrence of a series of young volcanic lavas and near-surface plugs and sheets accompanied by tuffs and other ejectamenta along a belt extending from the Fort Portal area northeast of Mt. Ruwenzori in southwestern Uganda to Lake Kivu in Belgian Congo. The petrology of these lavas and pyroclasts has been described in a series of papers by Holmes and Harwood (1932, 1937), Holmes (1942), Combe and Holmes (1945), Friedlaender (1949), Holmes (1950), and others. These volcanics exhibit a rather unique series of undersaturated alkaline rocks from extremely potassic to comparatively sodic. As has been specially emphasized by Friedlaender (1949), the soda-to-potash ratio shows certain regional variations. On the other hand, Holmes (1950) has produced evidence indicating that this ratio varies considerably also within a single flow, the nose of a flow sometimes being richer in potash then the lava nearer its source.

The general undersaturated character and the relatively high potash content are reflected in the mineralogical composition of the rocks for which new rock names are introduced. The potash-rich rock suite of the area has been classified by Holmes according to a triangular scheme in which the following rock species with their critical minerals serve as end members:

Ugandite: leucite, augite, olivine.
Mafurite: kalsilite, augite, olivine.
Katungite: melilite, olivine, potash-rich glass.

Between these rocks, all intermediate types occur. Olivine is mostly very abundant. Potash ankaratrites, conspicuously rich in augite and relatively poor in olivine, represent a parallel with the ugandite-mafurite series. The potash ankaratrites vary from typical leucite-ankaratrite with predominantly leucite among the leucocratic constituents to kalsilite-ankaratrite in which kalsilite preponderates over leucite. The intermediate types of potash ankaratrites contain very potash-rich nepheline in association with leucite. Feldspars and amphiboles are not essential constituents of these rocks.

Most of the lavas in question are very fine grained, only larger phenocrysts of olivine, augite, and occasional melilite being commonly detectable with the naked eye. In rarer instances, phenocrysts of leucite, and, exceptionally, nepheline aggregates and phenocrysts are of sufficient size to be identified in hand specimen. The leucocratic minerals usually occur only in the ground mass. It is therefore understood that the variation of the chemical composition of leucite and nepheline in these rocks has been very little investigated. Not only large phenocrysts should be studied but also nephelines and leucites of the fine-grained ground mass. The ground mass nepheline and leucite certainly are not easily extracted from the rocks for chemical analysis. However, the authors had the privilege of receiving five specimens specially selected for the purpose by Professor Arthur Holmes of Edinburgh from his excellent collection of the Uganda volcanic rocks. Four of these rocks have been subjected to mineral separation and subsequent chemical analysis, the results of which are presented below.

SPECIMENS INVESTIGATED

The rock specimens were crushed and ground down to a grain size of 10-20 microns. The powdered material was centrifuged several times in Clerici's solution using relatively high speed on the centrifuge. In this way, leucite and nepheline could be separated out of the fairly fine-grained rock material. The purity of the final material to be analyzed was tested under the microscope by counting a large number of grains. On doing the grain counting, it is important to immerse the material in a liquid that shows approximately the same index of refraction as the mineral. The mineral to be tested thus almost disappears and the impurities, usually having different

index, become easily detectable. The analyzed materials of leucite and nepheline were sent to Dr. F. A. Bannister, of the British Museum, London, for powder pattern test. According to a personal communication received from him, no foreign lines in any of the separated fractions of leucite and nepheline were detected. The specimens investigated are described below.

Specimen C. 9956. Aggregates of phenocrysts of potash nepheline and leucite in a dark gray ground mass. Southern slope of Mt. Ninagongo at a height of *ca.* 2900 meters, Lake Kivu National Park Area, Belgian Congo.

The aggregates of phenocrysts are fairly large, up to 5 mm. or more in diameter. They consist of well developed idiomorphic crystals of potash nepheline and leucite with some additional augite. Separate phenocrysts of these minerals and melilite are scattered in the ground mass between the large aggregates. Some few phenocrysts of opaque ore also occur. The vesicular ground mass, partly glassy, contains the same minerals as tiny crystals. No sign of any flow structure was detectable in the specimen. For mineral separation, 113 g. of the rock were available.

The potash nepheline of the aggregates is clear and shows no zoning $\epsilon = 1.539$, $\omega = 1.543$. The product of separation, amounting to 5.5 g., was analyzed chemically. The analysis is given in table 1. Grain counting of the analyzed material gave the following result:

1952	water clear nepheline grains	91.4 per cent
182	nepheline grains with some inclusions	8.5
2	leucite grains	0.1

Assuming that the grains with inclusions contain 5 per cent impurities on the average, the total amount of impurities in the analyzed fraction will be *ca.* 0.6 per cent. This figure is considered a maximum value.

The very high purity of the analyzed material suggests that the content of ferric and ferrous iron and of lime is not caused by impurities but belongs to the nepheline itself. The analysis shows a slight deficiency in alkalis with respect to silica.

The very high potash content of the nepheline C. 9956 from Mt. Ninagongo is specially noteworthy. The weight per cent of potash is even higher than that of soda, yet the mineral is

TABLE 1

Chemical Composition of Potash Nepheline from Specimen C. 9956. Mt. Ninagongo, Belgian Congo

	Weight per cent found	Molecular ratio multiplied by 1000	Number of atoms in the unit cell assuming oxygen = 32	
SiO_2	40.20	669	Si	8.01
TiO_2	0.05	1	Ti	0.01
Al_2O_3	32.51	319	Al	7.64
Fe_2O_3	1.82	11	Fe^{3+}	0.26
FeO	0.57	8	Fe^{2+}	0.10
MgO	0.10	2	Mg	0.02
CaO	1.44	26	Ca	0.31
Na_2O	10.86	175	Na	4.19
K_2O	12.22	130	K	3.11
H_2O+	0.00	—		
H_2O-	0.00			
Total	99.77			

nepheline, and not kalsilite (X-ray test; personal communication from Dr. Bannister). The molecular soda-to-potash ratio amounts to Na: K=57.4: 42.6. Thus, the nepheline from Mt. Ninagongo represents the most potash-rich nepheline analyzed so far. As compared with the data given by Bannister and Hey (1931), the refractive indices of this nepheline are relatively low. Evidently the refractive indices of nephelines cannot be simply predicted on the basis of the soda-to-potash ratio and vice versa.

The leucite of the aggregates is almost free from inclusions, beautifully twinned, and shows no rims around the crystals. n = 1.510. The amount of the mineral in the specimen is considerably smaller than that of nepheline. Accordingly, the fraction extracted out of the rock was too small (0.49) to allow a complete chemical analysis to be made. No grains of foreign minerals were detected in the analyzed material. An alkali determination on leucite gave:

Na_2O 0.98 per cent
K_2O 19.44

As might be expected from the chemical composition of the nepheline (table 1) coexistent with this leucite, the soda content of the leucite is relatively low, as compared with leucites from other petrographic provinces.

Specimen C. 2912 (=*C. 2911*). Mikenite (leucitite of Mikeno

type). Flow from Mt. Mikeno, 1 mile S. of Rulenga Mission, Lake Kivu National Park Area, Belgian Congo.

The specimen (C. 2911) has been fully described by Holmes and Harwood (1937). They also give a bulk analysis of the rock. The rock contains numerous phenocrysts of leucite, titanian augite, and opaque ore. The leucite crystals are very fresh, containing only tiny prisms of augite and apatite as inclusions. They are beautifully twinned and show outer rims of pseudoleucite. About 219 g. of rock was crushed, ground, and subjected to mineral separation. The leucite fraction, tested under the microscope by grain counting, shows the following purity:

1790	completely clear leucite grains	92.6 per cent
142	leucite grains with very little pigment	7.3
2	foreign grains	0.1

No grains having refractive indices lower than that of leucite were detected. The amount of impurities in the grains with pigment is estimated to be less than 5 per cent (probably much less). Thus, the total amount of impurities would be less than 0.5 per cent. An analysis of the bulk rock reproduced from Holmes and Harwood (1937) and of leucite is given in table 2. The index of refraction of leucite was determined to $n = 1.509$. The material available for chemical analysis amounted to 5 g.

As is shown by the analysis, the leucite from specimen C. 2912 is unusually pure and very low in soda. The norm of the corresponding rock (C. 2911) given by Holmes and Harwood (1937) is, for the main salic constituents, as follows: orthoclase 36.56, anorthite 4.23, leucite 1.22, nepheline 23.86 or, if priority is given to leucite: leucite 29.87, nepheline 14.52, anorthite 4.23, albite 17.21. The occurrence of the rims of pseudoleucite around the leucite phenocrysts indicate instability of leucite in its present environment. The composition of mikenite is interpreted by Holmes and Harwood as a result of assimilation of highly silicic material by niligongite magma. If this interpretation is correct, the leucite phenocrysts may have originally crystallized in an environment chemically different from the present ground mass of the rock. The discrepancy between the modal and normative composition would thus become understandable. An example of the occurrence of

TABLE 2

Chemical Composition of Leucite from Mikenite C. 2912 and of Mikenite C. 2911. Rulenga Mission, Belgian Congo

	Leucite from specimen C. 2912		Mikenite (bulk rock) specimen C. 2911	
	Weight per cent found	Molecular ratio multiplied by 1000	Weight per cent found	Molecular ratio multiplied by 1000
SiO_2	54.62	909	47.68	794
TiO_2	0.00	—	2.54	32
Al_2O_3	22.93	225	17.08	168
Fe_2O_3	0.26	2	3.45	22
FeO	0.26	4	5.26	73
MnO	0.00	—	0.14	2
MgO	0.00	—	2.90	72
CaO	0.08	1	7.17	128
Na_2O	0.66	11	5.33	86
K_2O	21.02	223	6.45	68
H_2O+	0.12	7	0.37	21
H_2O-	0.00		0.24	
Total	99.95		99.92*	

* The sum includes: Co_2 0.02, ZrO_2 none, P_2O_5 0.77, Cl 0.14, F 0.08, S 0.01, Cr_2O_3 none, V_2O_3 0.03, NiO none, BaO 0.22, SrO 0.10, Li_2O trace, —O. 0.06.

leucite in a rock in which it is chemically not anticipated, has been given by Wade and Prider (1940) from the leucite-bearing rocks of the West Kimberley area, Western Australia. These rocks are not undersaturated, yet the most striking feature in their mineralogy is the abundant occurrence of leucite, mostly completely altered.

Specimens C. 5549 and C. 5550. Potash ankaratrite. Ejected blocks from the W. side of crater slope near top, Nyamunuka Crater, Katwe-Kikorongo field, southwestern Uganda.

These two specimens are virtually identical with each other and with the specimen C. 1000 fully described by Holmes and Harwood (1932). Therefore, they are given here together. The constituents are: clinopyroxene, olivine (with brown reaction rims), nepheline, leucite, biotite, opaque ore, apatite, perovskite. In addition, analcite and sodalite have been mentioned by Holmes and Harwood (1932). Clinopyroxene forms most of the rock and shows numerous tiny crystals of perovskite as inclusions along the margins. Nepheline is more abundant than leucite. Both occur in the space between large pyroxene crystals. Nepheline is rarely idiomorphic, very clear, free from turbidity and without sign of zoning. The grains measure up to

0.2 mm. Leucite occurs as clear rounded grains, up to 0.05 mm. in size. Alkali determinations carried out on the bulk rocks gave:

	Specimen C. 5549	Specimen C. 5550
Na_2O	1.43 per cent	1.65 per cent
K_2O	2.28	2.40

Of specimen C. 5549, *ca.* 500 g. were available for mineral separation. Nepheline and leucite were extracted from the rock. Of specimen C. 5550, *ca.* 760 g. were available. In addition to nepheline and leucite, clinopyroxene was also extracted for analysis. The following amounts of nepheline and leucite were obtained: specimen C. 5549, 2.6 g. leucite and 1.7 g. nepheline; specimen C. 5550, 1.4 g. leucite and 2.9 g. nepheline. The optical properties are:

	Specimen C. 5549	Specimen C. 5550
Leucite	$n = 1.511$	$n = 1.511$
Nepheline	$\epsilon = 1.542$	$\epsilon = 1.543$
	$\omega = 1.548$	$\omega = 1.548$

Of nepheline C. 5549 and of leucite C. 5550 only alkali determinations were made with following results:

	Specimen C. 5549 Nepheline	Specimen C. 5550 Leucite
Na_2O	13.23 per cent	0.60 per cent
K_2O_3	8.78	18.50

Complete analyses of leucite from specimen C. 5549 and of nepheline from specimen C. 5550 are given in table 3. A bulk analysis of specimen C. 1000, reproduced from Holmes and Harwood (1932), is added to the table.

According to microscopic estimation, the analyzed samples of leucite C. 5549 and of nepheline C. 5550 are slightly more impure than leucite C. 2912 and nepheline C. 9956. The amount of impurities in the sample of leucite C. 5549 and nepheline C. 5550 is about 1 per cent. The contents of minor oxides in these two samples apparently are only in small part caused by foreign contamination.

TABLE 3

Chemical Composition of Leucite from Specimen C. 5549, of Nepheline from Specimen C. 5550, and of Potash Ankaratrite C. 1000. Nyamunuka Crater, Katwe-Kikorongo Field, Southwestern Uganda

	Leucite Specimen C. 5549		Nepheline Specimen C. 5550			Potash ankaratrite Specimen C. 1000	
	Weight per cent found	Molecular ratio multiplied by 1000	Weight per cent found	Molecular ratio multiplied by 1000	Number of atoms in the unit cell assuming oxygen = 32	Weight per cent found	Molecular ratio multiplied by 1000
SiO_2	54.30	904	40.78	679	8.08	40.53	675
TiO_2	0.26	3	0.07	1	0.01	4.47	56
Al_2O_3	20.08	197	30.95	304	7.24	6.80	67
Fe_2O_3	1.44	9	2.41	15	0.36	6.05	38
FeO	0.22	3	0.57	8	0.10	8.11	113
MnO	n.d.	—	n.d.	—	—	0.15	2
MgO	0.00	—	0.07	2	0.02	10.98	272
CaO	1.84	33	0.78	14	0.17	17.25	308
Na_2O	1.88	30	13.93	225	5.36	1.27	20
K_2O	19.02	202	9.78	104	2.48	1.71	18
H_2O+	0.75	42	0.32	18	—	1.31	73
H_2O-	0.00		0.00			0.54	
Total	99.79		99.66			100.04*	

*The sum includes: CO_2 0.06, ZrO_2 0.04, P_2O_5 0.53, Cl,F trace, S none, Cr_2O_3 0.02, V_2O_3 0.02, NiO trace, BaO 0.10, SrO 0.10, Li_2O none.

The analyses of leucite and nepheline and of the bulk rock of table 3 are all made on different specimens. These three specimens are, however, very similar and evidently justify a comparison of the corresponding analyses with each other as if they were made on materials derived from the same specimen. In addition to general microscopic evidence, the similarity of specimens C. 5549 and C. 5550 is shown by the alkali determinations on nepheline extracted out of these specimens. The alkali determinations on the bulk rocks given above yield values not far from the corresponding figures of the seventh column of table 3.

A comparison of the analyses of the leucites C. 2912 and C. 5549 with each other shows that the latter corresponds less closely to the ideal leucite composition. The soda-to-potash ratio of nepheline C. 5550 amounts to Na: K = 68.4: 31.6. The norms for specimen C. 1000 calculated by Holmes and Harwood (op. cit.) show *ca.* 8 per cent leucite and *ca.* 6 per cent soda nepheline. The high potash content of the modal nepheline is thus a consequence of the composition of the bulk rock.

The clinopyroxene of specimen C. 5550 was also extracted out of the rock and analyzed. The optical properties of this pyroxene are:

$$a = 1.695^1$$
$$\beta = 1.701$$
$$\gamma = 1.721$$
$$2V_\gamma = 60^\circ \pm 2^\circ$$
$$c \wedge \gamma = 46^\circ$$

Frequent twinning on (100).

The chemical composition of this pyroxene is shown in table 4. Grain counting made on the analyzed sample gave:

1117 clear pyroxene grains	56.5 per cent
817 pyroxene grains with some inclusions	41.3
42 pyroxene grains with many inclusions	2.1

The inclusions are mostly perovskite. Assuming that the grains with some inclusions contain 5 per cent impurities on the average, and the grains with many inclusions *ca.* 30 per cent, the total amount of impurities will be 3 per cent.

[1] Owing to slight zoning, the indices of refraction vary up to ± 0.002.

TABLE 4

Chemical Composition of Clinopyroxene from Potash Ankaratrite C. 5550. Nyamunuka Crater, Katwe-Kikorongo Field, Southwestern Uganda

	Weight per cent found	Atomic ratios —multiplied by 1000—	
SiO_2	49.23	Si	820
TiO_2	2.25	Ti	28
Al_2O_3	2.01	Al	39
Fe_2O_3	2.87	Fe^{3+}	36
FeO	3.53	Fe^{2+}	49
MnO	0.09	Mn	1
MgO	14.69	Mg	364
CaO	24.23	Ca	432
Na_2O	0.46	Na	15
K_2O	0.15	K	3
H_2O+	0.38	OH	42
H_2O-	0.00		
Total	99.89		

A part of the titania shown by the analysis of table 4 is probably contained in the perovskite inclusions. Adding titania and alumina to silica, ferric iron, ferrous iron, and manganese to magnesia, and the alkalis to lime, the analysis corresponds closely to a metasilicate composition. The molecular ratio $(Fe^{3+} + Fe^{2+}) : Mg : Ca = 9.7 : 41.3 : 49.0$. Thus, according to the nomenclature presented by Hess (1941), the clinopyroxene from specimen C. 5550 is no augite proper but has to be classified as a diopside close to salite. The refractive indices are, however, somewhat higher than those indicated by the diagrams of Tomita (1934), Deer and Wager (1938), and Hess (1949). The reason for this discrepancy might be the relatively high ferric iron and titania content of the mineral. Although a part of the titania content apparently is caused by the perovskite inclusions, some part of it very probably belongs to the pyroxene.

DISCUSSION

The data given above are too scattered to allow any more general conclusions about the mineralogy of the potash rich rock suite of southwestern Uganda and adjoining Belgian Congo. The results of this preliminary investigation are given only to show that, in addition to considerable petrological interest, the rocks in question offer excellent material for

studying the general mineralogy of leucite, nepheline, etc. On a later occasion, the authors hope to study these rocks in more detail. Therefore, only a few remarks are added in the following.

The diopside from specimen C. 5550 so far being the only analyzed pyroxene from the rock suite in question, no further comments are possible at present.

In connection with the study of the formation of pseudoleucite, Bowen and Ellestad (1937) published an analysis of leucite occurring as phenocrysts in leucite theralite on Mt. Nyamlagira. This leucite, like those given in this paper, is relatively poor in soda. The average molecular soda-to-potash ratio for the leucites from Mt. Nyamlagira and from the specimens C. 9956, C. 2912, C. 5549, and C. 5550 amounts to Na: K = 8.5: 91.5. An average of fourteen analyses of leucites from Vesuvius calculated by Chirwinsky (1931) amounts to Na: K = 15.4: 84.6. No indication of the existence of the compound $K_2O \cdot MgO \cdot 5SiO_2$ in the rocks in question has been found so far. According to Roedder (1951), this compound forms a complete series of solid solutions with leucite and might well be expected to occur in nature.

As to nepheline, the occurrence of a more or less continuous rock series from ugandite to mafurite and of the corresponding potash ankaratrites and, on the other hand, the variation of the soda-to-potash ratio in these rocks, offer a rather unique opportunity for studying the mineralogy of the nepheline-kalsilite series. The extremely potassic character of the nephelines in these rocks, very rare elsewhere, was noted by Bowen and Ellestad (1936). Their analysis of a nepheline occurring in a relatively coarse-grained, melilite-leucite nephelinite from Ngoma Crater on Lake Kivu shows it to be the most potash-rich nepheline analyzed up to that time. The molecular soda-to-potash ratio of the Ngoma Crater nepheline amounts to Na : K = 63.1: 36.9. Later, the mineral kalsilite ($KAlSiO_4$) was discovered by Bannister and Hey (1942) from a certain type of mafurite in which the mineral occurs as pegmatoidal aggregates associated with diopside, calcite, zeolite, etc. The existence of a relatively pure potash analogue to nepheline in these rocks was suggested by Holmes (1942). According to Bannister and Hey (1942), kalsilite represents a polymorph of kaliophilite with a smaller unit cell and forms an incomplete

series of solid solutions with nepheline proper. Another analysis of nepheline from a phonolite on the Nairobi-Nyeri road in Kenya in the Eastern Rift of Equatorial East Africa, also published by Bowen and Ellestad (1936), shows a molecular soda-to-potash ratio of Na: K = 86.3: 13.7, in accordance with the generally sodic character of the volcanics of the Eastern Rift. However, on the basis of microscopic observations, the occurrence of comparatively potash-rich nephelines in the Eastern Rift lavas was suggested by Ödman (1930) and by King (1948). An analysis of a very potash-rich nepheline from ijolite from Homa Bay, Kenya, has been given by Pulfrey (1949), showing Na: K = 67.0: 33.0.

In this connection, Buerger, Klein, and Hamburger (1946, 1947) concluded that two of the eight alkali atoms in the unit cell occupy positions structurally different from those of the remaining six. On the basis of the chemical composition of natural nepheline, they suggest that these two positions, representing larger holes produced by collapse of voids in the tridymite structure, are occupied by larger potassium atoms. Thus, the ideal formula of nepheline would be $KNa_3Al_4Si_4O_{16}$. The data referred to above for nephelines from the East African volcanics may suffice to show that, as was emphasized already by Bowen and Ellestad (1936), the composition of nepheline largely depends on the composition of the bulk rock. Potash-rich rocks show more potassic nephelines, provided, of course, that the silica content is low enough for the formation of nepheline. That the common range of variation of the soda-to-potash ratio appears to be comparatively narrow and that only a few examples of very potash-rich nephelines are known, may be attributed to the relative rarity of rocks in which the more potassic nephelines may be anticipated. Therefore, even if the two alkali sites of the nepheline unit cell are preferred by the potassium atoms, the nepheline formula suggested by Buerger, Klein, and Hamburger (1946, 1947) represents an idealization of the actual nepheline composition that neglects the existence of the nepheline-kalsilite solid solution series. In this series, the nepheline C. 9956 from Mt. Ninagongo, given above, represents the most potash-rich member known so far that still shows the nepheline structure. On the other hand, the only analysis of natural kalsilite, derived from Uganda mafurite, has been published by Bannister and

Hey (1942). Accordingly, the width of the probable gap in the solid solution series between natural nepheline and kalsilite cannot be considered known. It is entirely possible that more potash-rich nephelines and more soda-rich kalsilites will be found. High temperature synthetic studies made by Bowen (1917) and Schairer and Bowen (1935) have revealed a complete mutual solid solubility between $NaAlSiO_4$ and $KAlSiO_4$. Recently, a review of the existing data for the composition of natural nephelines has been given by Miyashiro (1951). He argues that the physical conditions under which a nepheline crystallizes are largely responsible for its composition.

ACKNOWLEDGMENTS

The authors wish to express their gratitude to Professor Arthur Holmes for selecting and delivering the specimens investigated, to Dr. F. A. Bannister for making the X-ray tests of the leucite and nepheline samples extracted from the rocks, and to Mr. Kai Hytönen, of this Institute, for making the optical determinations.

REFERENCES

Bannister, F. A., and Hey, M. H., 1931. A chemical, optical, and X-ray study of nepheline and kaliophilite: Mineralog. Mag., vol. 22, pp. 569-608.

———, ———, 1942. Kalsilite, a polymorph of $KAlSiO_4$, from Uganda: Mineralog. Mag., vol. 26, pp. 218-224.

Bowen, N. L., 1917. The sodium-potassium nephelites: Am. Jour. Sci., 4th ser., vol. 43, pp. 115-132.

———, and Ellestad, R. B., 1936. Nepheline contrasts: Am. Mineralogist, vol. 21, pp. 363-368.

———, ———, 1937. Leucite and pseudoleucite: Am. Mineralogist, vol. 22, pp. 409-415.

Buerger, M. J., Klein, G. E., and Hamburger, Gabrielle, 1946. The structure of nepheline. Complete structure determination (abst.): Geol. Soc. America Bull., vol. 57, pp. 1182-1183.

———, ———, ———, 1947. The structure of nepheline (abst.): Am. Mineralogist, vol. 32, p. 197.

Chirwinsky (Tschirwinsky), Peter, 1931. Durchschnittliche chemische Zusammensetzung der wichtigen Mineralien der Eruptivgesteine und der Meteorite (summary by the author): Neues Jahrb., Referate, II, pp. 160-170.

Combe, A. D., and Holmes, Arthur, 1945. The kalsilite-bearing lavas of Kabirenge and Lyakauli, southwest Uganda: Royal Soc. Edinburgh Trans., vol. 61, part 2, pp. 359-379.

Deer, W. A., and Wager, L. R., 1938. Two new pyroxenes included in the system clinoenstatite, clinoferrosilite, diopside, and hedenbergite: Mineralog. Mag., vol. 25, pp. 15-22.

Friedlaender, C., 1949. Beitrag zur Petrographie des Kivusee-Gebietes: Schweizer. min. pet. Mitt., Band 29, pp. 156-192.

Hess, H. H., 1941. Pyroxenes of common mafic magmas: Am. Mineralogist, vol. 26, pp. 515-535.

———, 1949. Chemical composition and optical properties of common clinopyroxenes. Part I: Am. Mineralogist, vol. 34, pp. 621-666.

Holmes, Arthur, 1942. A suite of volcanic rocks from southwest Uganda containing kalsilite (a polymorph of $KAlSiO_4$): Mineralog. Mag., vol. 26, pp. 197-217.

———, 1950. Petrogenesis of katungite and its associates: Am. Mineralogist, vol. 35, pp. 772-792.

———, and Harwood, H. F., 1932. Petrology of the volcanic fields east and south-east of Ruwenzori, Uganda: Geol. Soc. London Quart. Jour., vol. 88, pp. 370-439.

———, ———, 1937. The volcanic area of Bufumbira; Part II, The petrology of the volcanic field of Bufumbira, southwest Uganda, and of other parts of the Birunga field: Uganda Geol. Survey Mem. 3.

King, B. C., 1948. The Napak area of southern Karamoja, Uganda: Uganda Geol. Survey Mem. 5.

Miyashiro, Akiho, 1951. The ranges of chemical composition in nepheline and their petrogenetic significance: Geochim. Cosmochim. Acta, vol. 1, pp. 278 ff.

Ödman, O., 1930. Volcanic rocks of Mt. Elgon in British East Africa: Geol. fören. Stockholm Förh., Band 52, pp. 455-537.

Pulfrey, William, 1949. Ijolitic rocks near Homa Bay, Western Kenya: Geol. Soc. London Quart. Jour., vol. 105, pp. 425-454.

Roedder, E. W., 1951. The system K_2O—MgO—SiO_2: Am. Jour. Sci., vol. 249, pp. 81-130, 224-248.

Schairer, J. F., and Bowen, N. L., 1935. Preliminary report on equilibrium-relations between feldspathoids, alkali-feldspars, and silica: Am. Geophys. Union Trans., 16th Ann. Meeting, pp. 325-328.

Tomita, T., 1934. Variations in optical properties, according to chemical composition, in the pyroxenes of the clinoenstatite-clinohypersthene-diopside-hedenbergite system: Shanghai Sci. Inst. Jour., sec. 2, vol. 1, pp. 41-58.

Wade, Arthur, and Prider, R. T., 1940. The leucite-bearing rocks of the west Kimberley area, Western Australia: Geo. Soc. London Quart. Jour., vol. 96, pp. 39-98.

Institute of Geology
Helsinki, Finland

THE SYSTEM $FeO—Al_2O_3—SiO_2$

J. F. SCHAIRER AND KENZO YAGI*

ABSTRACT. Phase-equilibrium studies of this system, at and just below temperatures where a liquid phase is present, show one ternary compound, the iron analog of cordierite ($2FeO·2Al_2O_3·5SiO_2$), which decomposes at 1210° ± 10° C. to mullite, tridymite, and liquid. The fields of stability of corundum, mullite, hercynite, iron cordierite, cristobalite, tridymite, fayalite, and wüstite have been delineated. The following invariant points (the first two eutectics and the remainder reaction points) were located:

Fayalite + wüstite + hercynite + liquid 1148° ± 5°
Fayalite + iron cordierite + tridymite + liquid 1083° ± 5°
Fayalite + iron cordierite + hercynite + liquid 1088° ± 5°
Hercynite + iron cordierite + mullite + liquid 1205° ± 10°
Iron cordierite + mullite + tridymite + liquid 1210° ± 10°
Corundum + mullite + hercynite + liquid 1380° ± 5°
Cristobalite + tridymite + mullite + liquid 1470° ± 10°

Iron cordierite crystallizes with some reluctance, and the metastable invariant points fayalite + tridymite + spinel + liquid at 1073° ± 5°, and mullite + hercynite + tridymite + liquid at 1205° ± 10° can be realized. No ferrosilite or almandine garnet could be crystallized from the melts at any temperature even when melts were seeded with these crystalline phases. Natural almandine from Botallack, England (91.3 per cent almandine), when heated begins to decompose at an appreciable rate as low as 900° C. and yields a mixture of hercynite, iron cordierite, and fayalite. The bearing of these results on petrology and slags is discussed.

INTRODUCTION

WHEN we examine the average composition of igneous rocks as given by Clarke and Washington (1922, p. 112) we see that the principal rock-forming oxides, in the order of their abundance, are SiO_2, Al_2O_3, iron oxides, CaO, Na_2O, MgO, K_2O, H_2O, TiO_2, P_2O_5, and MnO. The first three total more than 81 per cent of the composition; the last two are small in amount (0.30 and 0.12 per cent, respectively); and all other substances not listed but present in igneous rocks total only one half of 1 per cent. The first ternary system of rock-forming oxides, $CaO—Al_2O_3—SiO_2$, was completed at the Geophysical Laboratory and published by Rankin and Wright (1915). Since that time phase-equilibrium data on the three additional systems of SiO_2 and Al_2O_3 plus one other of the principal rock-forming oxides have been published from this Laboratory—$MgO—Al_2O_3—SiO_2$ by Rankin and Merwin (1918), $Na_2O—Al_2O_3—SiO_2$ and $K_2O—Al_2O_3—SiO_2$ by Schairer and Bowen (1947). One ter-

*Professor of Geology, Tohoku University, Sendai, Japan; visiting investigator at Geophysical Laboratory for the year 1950-1951 under a Carnegie Institution of Washington Fellowship.

nary system, $MnO—Al_2O_3—SiO_2$, was studied by Snow (1943) at the Research Laboratory of the United States Steel Corporation.

The results of a study of the system $FeO—Al_2O_3—SiO_2$ are presented in this paper. While there are but few minerals that consist solely of FeO, Al_2O_3, and SiO_2, a knowledge of this system is essential to studies of rock-forming olivines, pyroxenes, pyroxenoids, melilites, and cordierites in one or both of the quaternary systems $CaO—FeO—Al_2O_3—SiO_2$ (Schairer) and $MgO—FeO—Al_2O_3—SiO_2$ (Keith) and as basic data for the interpretation of metamorphic mineral assemblages.

The system $FeO—Al_2O_3—SiO_2$ was studied by Hay, White, and Caulfield (1937) who used heating curves and molybdenum crucibles *in vacuo* below 1458° and in nitrogen above this temperature. They took no cognizance of the equilibrium between ferrous silicates and metallic iron or of the presence of Fe_2O_3 in the liquid phase. They presented phase assemblages which are incompatible according to the studies we present in this paper. Some good work on this system was published by Snow (1937) and Snow and McCaughey (1942) who used large iron crucibles in a Méker muffle-type gas furnace. In preparing the compositions Snow used analyzed Florida kaolin and Missouri burley clay as a source of Al_2O_3. The phase assemblages agree with the preliminary results obtained by one of us (Schairer, 1942, fig. 4, p. 245). The ternary compound iron cordierite did not crystallize from the viscous melts, and some of the ternary invariant points are, therefore, metastable. Snow's temperatures are all about 100° C. low, partly because of impurities in the kaolin and burley clay as shown by his analyses, but largely owing to difficulties in determining the temperature of the charge in a large crucible in a muffle furnace. The compositions of his ternary invariant points (two of them metastable) are in good agreement with our preliminary results.

Schairer (1942, table 1, p. 244, and fig. 4, p. 245) in his report on a portion of the system $CaO—FeO—Al_2O_3—SiO_2$ gave a preliminary diagram for $FeO—Al_2O_3—SiO_2$ and a table of ternary invariant points. He stated that experiments at subliquidus temperatures and chemical and optical data on the solid phases were not yet complete at that time. Most of the melts were viscous except those near the FeO apex where liquids were so fluid that they could not be quenched rapidly enough to give

undevitrified glass. No crystals of iron cordierite, almandine, or ferrosilite were encountered in the preliminary studies, and publication of the quenching data was delayed until there should be opportunity to crystallize melts at temperatures considerably below the liquidus to ascertain whether ferrous iron garnet (almandine) or iron cordierite ($2FeO \cdot 2Al_2O_3 \cdot 5SiO_2$), the ferrous iron analog of cordierite ($2MgO \cdot 2Al_2O_3 \cdot 5SiO_2$), could be crystallized and whether it might be possible to crystallize the pure metasilicate of ferrous iron ($FeO \cdot SiO_2$), which has been found in nature and described (Bowen, 1935) as the mineral clinoferrosilite, but which, although sought, was not encountered by Bowen and Schairer (1932 and 1935) in their studies of the systems $FeO—SiO_2$ and $MgO—FeO—SiO_2$ and by Bowen, Schairer, and Posnjak (1933*b*) in their study of the system $CaO—FeO—SiO_2$.

In the preliminary work Schairer prepared 125 separate compositions and studied them by the method of quenching in iron crucibles in purified nitrogen and made chemical analyses for FeO and total iron to locate the exact composition of each melt. Recently we were able to continue the investigation of this interesting system.

LIMITING SYSTEMS

Bowen and Schairer (1932) showed that ferrous silicates are in equilibrium with metallic iron and that Fe_2O_3 is always present in the liquid phase, the equilibrium amount being usually small except for compositions low in silica. Their equilibrium diagram for $FeO—SiO_2$ is reproduced here as figure 1. They found only one binary compound, fayalite ($2FeO \cdot SiO_2$), an end member of the olivine group of minerals. This compound has a congruent melting point. The delineation of the region of two immiscible liquids on the high silica side of the diagram was made by Greig (1927, p. 479).

Bowen and Greig (1924) determined the relations in the binary system $Al_2O_3—SiO_2$. They found only one binary compound, mullite ($3Al_2O_3 \cdot 2SiO_2$), which has an incongruent melting point. Their equilibrium diagram is reproduced here as figure 2. The temperature of the binary eutectic has been corrected (Schairer, 1942, footnote 57, p. 274) on the basis of additional studies by Schairer and Bowen.

The system $FeO—Al_2O_3$ was studied by Herty (1934) and

by McIntosh, Rait, and Hay (1937) who published data on a portion of this system. These investigators had no cognizance of the equilibrium between ferrous oxide melts and metallic iron and they used cooling curves instead of the method of quenching. No reliable data on this system are available and none have been obtained in this investigation for the following reasons: (a) the temperatures are high and above the melting point of pure iron crucibles, except for a narrow range of compositions near the FeO side; (b) the melts are very fluid and probably cannot be cooled rapidly enough to prevent complete or nearly complete crystallization during cooling; (c) these compositions are not of sufficient geological interest to warrant a study of this difficult system on our part.

METHOD OF INVESTIGATION

The methods used for the investigation of mixtures containing iron in the ferrous condition have been described in detail in previous papers on iron silicate systems from this Laboratory (Bowen and Schairer, 1932, pp. 178-186, 193-196; 1938, pp. 399-403). Only a brief summary is given here with emphasis on particular difficulties encountered in this system.

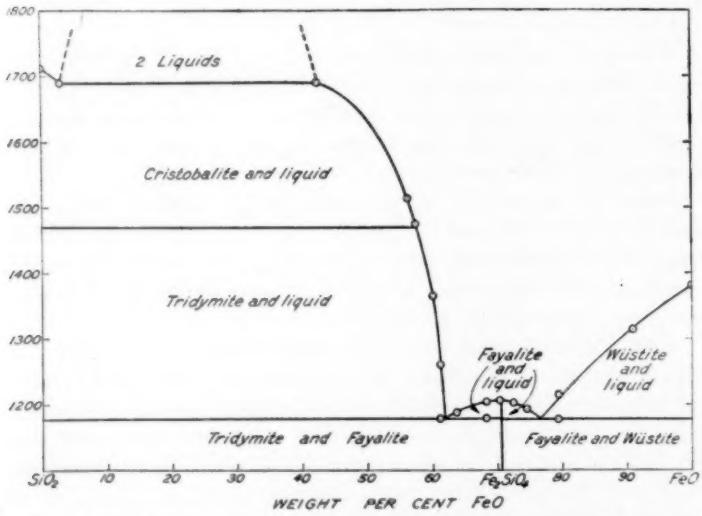

Fig. 1. Equilibrium diagram of the system FeO—SiO_2 after Bowen and Schairer (1932) and Greig (1927).

Preparation of mixtures.—Mixtures in the system FeO—Al_2O_3—SiO_2 were prepared by taking pure silica (quartz which gives only 0.03 per cent residue on treatment with hydrofluoric acid and sulfuric acid and subsequent ignition of the residue), C. P. Fe_2O_3 (Baker and Adamson), and pure alumina (tabular alumina T-61, free from iron, from the Aluminum Company of America) in the proportions calculated to give the desired product and melting them together three times in air in a platinum crucible and then three times in a Méker gas furnace with intermediate crushing of the charges between the several fusions and quenchings. Thus was obtained a product deviating somewhat from the desired composition by reason of a small deficiency of iron (removed by the platinum crucible by alloying) and also the existence of some of the iron in the ferric state.

Heating in iron crucibles in nitrogen.—Small samples of the mixtures were then heated in an iron crucible [1] in a stream of nitrogen in a quenching furnace. The nitrogen was freed from

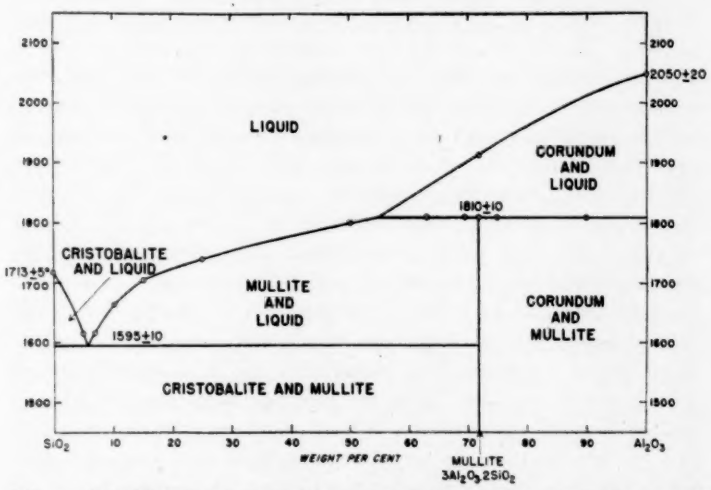

Fig. 2. Equilibrium diagram of the system Al_2O_3—SiO_2 after Bowen and Greig (1924) and Schairer (1942, footnote 57, page 274).

[1]The small iron crucibles used in this investigation were made from pure iron sheet obtained through the courtesy of the research staff of the American Rolling Mill Company (now the Armco Steel Corporation), Middletown, Ohio, whose generosity is gratefully acknowledged. A typical analysis of the sheet gave C under 0.02, P 0.006, S 0.027, Mn 0.015, Si 0.003.

oxygen and moisture by passing over heated iron wire at 700° C. and drying over P_2O_5. The surface of the iron wire was regenerated periodically between runs by heating in hydrogen.

Temperatures at which phase changes took place were determined by the method of quenching, combined with microscopic or X-ray powder pattern determination of the crystalline phases in the quenched product. The upper temperature limit at which the investigations could be made was set by the melting point of the iron crucible at about 1523° C.

Upon heating in an iron crucible, a small change in composition of the charge occurs which is principally due to reduction of the excess of Fe_2O_3 over an equilibrium amount by the iron crucible and a consequent increase in the total iron content of the charge. For viscous compositions small pieces of pure iron were admixed with the charge to insure an intimate contact with metallic iron. The increase in total iron content of the charge may partly balance, or it may more than balance, the deficiency produced by the original melting in platinum. In all cases it was, therefore, necessary to make a chemical analysis of each mixture after a run in an iron crucible at the temperature at which a change of phase was found to occur. Ordinarily the temperature of the run made for this purpose was that at which completion of melting had been found to occur and the analysis gave the composition of the liquid at the liquidus point for the particular mixture. Compositions containing more than about 75 per cent iron oxides were difficult to quench rapidly enough to yield glass but gave a devitrified glass in which primary crystals could be distinguished with certainty under the petrographic microscope from fine-grained crystalline material formed on quenching. For these, the liquidus was determined by using only a small pinch of material in the iron crucible, which quenched very rapidly. After the liquidus temperature had been located, a small iron crucible full of the material was run at the liquidus temperature to obtain the sample for analysis. This procedure is necessary in mixtures high in iron oxide, but is not so accurate as the procedure usually employed.

By repeating the procedures outlined above for a series of mixtures and plotting the determined liquidus temperatures and analyzed compositions, the liquidus surfaces of the primary crystalline phases recognized by petrographic examination can be constructed. In a similar manner the solidus relations may

be determined for those compositions which crystallize readily and completely.

Crystallization of glasses.—In the present investigation, before proceeding with quenching runs, it was necessary to crystallize portions of the glasses which had been prepared in iron crucibles by holding them in iron foil in sealed evacuated silica-glass tubes for several days or weeks at temperatures (850° to 1050° C.) well below the solidus. Unless this precaution was taken, iron cordierite failed to crystallize in its stability range from the viscous melts and only metastable equilibrium was realized. In some mixtures far removed from the iron cordierite composition, crystals of this compound failed to crystallize even after several weeks in the sealed tubes. When these mixtures were seeded with only a very small amount of iron cordierite crystals, crystallization of this phase proceeded promptly. The seed crystals were prepared from mixtures near iron cordierite in composition and the quantity of the seed added was so small that there could be only an insignificant change in the total composition of the mixture which had been seeded.

Measurements of temperatures.—As described in a previous paper (Bowen and Schairer, 1932, pp. 181-182), temperatures were measured before and after each run with a thermocouple but never in the presence of the iron crucible, which causes a rapid change in the thermocouple readings. The readings of the Pt-Pt 90 Rh 10 thermocouples used to measure temperatures were checked by frequent calibration at standard melting points defined in degrees centigrade as follows: NaCl 800.4°, Au 1062.6°, diopside ($CaO \cdot MgO \cdot 2SiO_2$) 1391.5° and Pd 1549.5°.

Methods of chemical analysis.—Ferrous oxide was determined by the Pratt method modified as described in detail in a previous paper (Bowen, Schairer and Posnjak, 1933*a*, pp. 274-275) and total iron was determined by titration with $KMnO_4$ solution after reduction of the ferric iron with a Jones reductor as described in detail in a previous paper (Bowen and Schairer, 1938, p. 400). The amounts of Al_2O_3 and SiO_2 are, of course, fixed by synthesis and require no analytical determination.

EXPERIMENTAL RESULTS

The results of the determination of liquidus temperatures by the method of quenching, data on the chemical composition of

the mixtures from chemical analyses and synthesis, and data on the indices of refraction of the glasses are given in table 1.

TABLE 1

Results of Quenching Experiments

(All compositions expressed in weight per cent)

(Duration of runs—one hour)

Experiment No. FAS	Planned Composition			Final Composition by analysis			Temp. of completion of melting ± 5°	Refractive index of glass ± 0.003
	FeO	Al_2O_3	SiO_2	FeO	Fe_2O_3	Total Fe as FeO		
	(a) Mixtures Having Tridymite as Primary Phase							
6	50	5	45	51.6	0.0	51.6	1324	1.714
7	35	15	50	38.8	0.2	39.0	1288	1.638
10	45	10	45	49.0	0.0	49.0	1183	1.698
14	25	20	55	30.3	0.1	30.4	1325	1.598
18	40	10	50	42.7	0.1	42.8	1375	1.657
19	44	13	43	46.2	0.0	46.2	1133	1.684
20	33	19	48	37.3	0.0	37.3	1181	1.634
21	25	15	60	31.7	0.1	31.8	1425	1.603
24	15	20	65	30.5	0.1	30.6	1382	1.589
31	36	17	47	38.2	0.2	38.4	1200	1.644
35	32	20	48	34.4	0.0	34.4	1201	1.621
40	18	21	61	29.6	0.2	29.8	1369	1.594
44	39	16	45	41.7	0.0	41.7	1165	1.655
66	8	21	71	35.0	0.2	35.2	1345	1.612
68	8	23	69	24.5	0.1	24.6	1400	1.577
78	31	10	59	43.5	0.0	43.5	1420	1.656
79	54	2	44	58.8	0.6	59.4	1240	....
94	5	18	77	28.0	0.0	28.0	1460	1.576
	(b) Mixtures Having Fayalite as Primary Phase							
1	60	5	35	60.0	0.9	60.9	1177	....
2	55	5	40	55.2	0.6	55.8	1154	1.736
9	55	10	35	57.7	1.3	59.0	1148	....
17	61	9	30	60.4	2.0	62.4	1148	....
32	46	12	42	48.4	0.2	48.6	1093	1.701
36	67	7	26	66.1	1.8	67.9	1156	....
45	59	2	39	61.1	0.7	61.8	1181	....
56	55	3	42	59.5	0.9	60.4	1170	....
63	73	3	24	71.4	2.4	73.8	1168	....
96a	73	5	22	72.2	3.6	75.8	1153	....
102	75	3	22	71.6	4.8	76.4	1168	....
105	77	2	21	72.6	4.1	76.7	1175	....
112	70	2	28	66.9	2.4	69.3	1198	....
113	65	3	32	66.0	2.3	68.3	1193	....
114	53	9	38	53.5	0.5	54.0	1130	1.733
955	67	5	28	63.9	2.1	66.0	1180	....

TABLE 1 (*Cont.*)

Results of Quenching Experiments
(All compositions expressed in weight per cent)
(Duration of runs—one hour)

Experiment No. FAS	Planned Composition			Final Composition by analysis			Temp. of completion of melting ± 5°	Refractive index of glass ± 0.003
	FeO	Al_2O_3	SiO_2	FeO	Fe_2O_3	Total Fe as FeO		
				(c) Mixtures Having Mullite as Primary Phase				
8	30	25	45	34.2	0.3	34.5	1314	1.635
11	30	30	40	35.8	0.5	36.3	1390	1.648
27	32	27	41	37.1	0.4	37.5	1338	1.651
41	27	22	51	32.1	0.3	32.4	1239	1.618
47	33	25	42	35.9	0.1	36.0	1318	1.638
51	24	25	51	31.0	0.3	31.3	1348	1.610
52	24	27	49	33.4	0.4	33.8	1368	1.622
53	25	29	46	33.2	0.3	33.5	1399	1.628
71a	17	26	57	30.6	0.2	30.8	1320	1.608
71b	17	26	57	28.0	0.3	28.3	1365	1.596
72a	19	28	53	32.6	0.2	32.8	1353	1.619
72b	19	28	53	27.6	0.2	27.8	1406	1.603
81	18	38	44	31.6	0.5	32.1	1480	1.635
84	26	35	39	33.4	0.5	33.9	1475	1.645
85	13	25	62	21.9	0.0	21.9	1444	1.571
87	15	28	57	28.7	0.1	28.8	1370	1.603
88	22	31	47	29.9	0.1	30.0	1460	1.619
92	10	24	66	22.7	0.1	22.8	1400	1.567
				(d) Mixtures Having Hercynite as Primary Phase				
3	45	15	40	46.0	0.4	46.4	1144	1.696
4	40	25	35	41.6	0.7	42.3	1364	1.688
5	50	20	30	52.0	1.8	53.8	1357	....
12	35	20	45	38.1	0.4	38.5	1211	1.648
13	50	15	35	49.2	0.7	49.9	1208	1.718
16	55	15	30	53.1	1.2	54.3	1276	....
22	32	23	45	36.6	0.0	36.6	1246	1.643
26	31	21	48	36.8	0.0	36.8	1205	1.628
29	48	13	39	47.7	0.5	48.2	1108	1.697
30	57	11	32	56.1	1.1	57.2	1158	....
34	31	22	47	35.1	0.3	35.4	1223	1.633
39	34	31	35	41.0	0.8	41.8	1415	1.682
43	35	19	46	36.9	0.0	36.9	1183	1.632

TABLE 1 (*Cont.*)

Results of Quenching Experiments
(All compositions expressed in weight per cent)
(Duration of runs—one hour)

Experiment No. FAS	Planned Composition			Final Composition by analysis			Temp. of completion of melting ± 5°	Refractive index of glass ± 0.003
	FeO	Al_2O_3	SiO_2	FeO	Fe_2O_3	Total Fe as FeO		
46	39	21	40	39.8	0.5	40.3	1258	1.664
49	60	10	30	65.5	2.0	67.5	1160	....
50	45	25	30	53.2	2.0	55.2	1415	1.742
55	33	28	39	39.5	1.0	40.5	1358	1.663
57a	32	34	34	44.6	2.0	46.6	1455	1.702
57b	32	34	34	38.6	1.3	39.9	1440	1.682
58	46	27	27	51.2	2.4	53.6	1468	....
59	35	33	32	47.1	2.6	49.7	1460	1.719
60	72	10	18	68.0	4.3	72.3	1310	....
61	70	13	17	65.5	4.3	69.8	1380	....
62	68	16	16	66.9	4.7	71.6	1450	....
64	43	21	36	48.0	1.0	49.0	1303	1.707
65	33	26	41	38.2	0.6	38.8	1320	1.653
69	41	26	33	47.8	1.2	49.0	1397	1.717
70	57	13	30	58.8	1.9	60.7	1230	....
73	38	31	31	45.4	2.4	47.8	1454	1.711
74a	33	29	38	38.8	0.8	39.6	1367	1.662
74b	33	29	38	37.4	0.8	38.2	1370	1.658
75	28	36	36	39.6	1.0	40.6	1440	1.680
76	52	24	24	54.5	2.4	56.9	1460	....
83	30	37	33	42.3	1.8	44.1	1475	1.706
86	57	17	26	56.4	2.0	58.4	1356	....
90	47	28	25	50.2	2.5	52.7	1490	....
91	40	16	44	43.0	0.2	43.2	1138	1.664
95	39	22	39	40.6	0.7	41.3	1283	1.667
97	72	8	20	70.9	3.1	74.0	1250	....
98	76	10	14	71.2	6.9	78.1	1360	....
99	72	14	14	68.0	5.2	73.2	1443	....
100	64	19	17	61.0	4.2	65.2	1475	....
101	76	7	17	73.2	4.0	77.2	1230	....
104	80	7	13	73.6	5.8	79.4	1275	....
107	78	11	11	71.9	8.6	80.5	1420	....
108	65	12	23	63.8	3.0	66.8	1295	....
115	84	6	10	74.8	8.2	83.0	1265	....
116	86	7	7	75.0	8.6	83.6	1355	....
117	86	9	5	78.5	9.5	88.0	1450	....
118	76	14	10	71.2	7.0	78.2	1463	....

TABLE 1 (*Cont.*)

Results of Quenching Experiments
(All compositions expressed in weight per cent)
(Duration of runs—one hour)

Experiment No. FAS	Planned Composition			Final Composition by analysis			Temp. of completion of melting ± 5°	Refractive index of glass ± 0.003
	FeO	Al_2O_3	SiO_2	FeO	Fe_2O_3	Total Fe as FeO		
119	90	5	5	80.0	11.7	91.7	1315	....
901	63.5	10	26.5	67.7	2.2	69.9	1180	....
855	59.9	15	25.1	62.5	3.0	65.5	1330	....
802	56.4	20	23.6	57.0	2.7	59.7	1430	....
755	52.9	25	22.1	54.0	2.1	56.1	1500	....
				(e) Mixtures Having Corundum as Primary Phase				
28x	29.5	32.7	37.8	37.8	0.8	38.6	1407	1.661
28	31	32	37	37.1	0.6	37.7	1398	1.663
37	33	30	37	37.7	0.5	38.2	1385	1.663
38	30	34	36	36.3	0.8	37.1	1451	1.660
80a	24	38	38	36.8	0.5	37.3	1469	1.660
80b	24	38	38	34.1	0.7	34.8	1495	1.653
82x	23	38.5	38.5	33.5	0.6	34.1	1505	1.648
				(f) Mixture Having Iron Cordierite as Primary Phase				
15	40	15	45	47.7	0.1	44.8	1103	1.678

(g) Mixtures Having Wüstite as Primary Phase

Experiment No. FAS	Planned Composition			Final Composition by analysis			Temp. of completion of melting ± 10°
	FeO	Al_2O_3	SiO_2	FeO	Fe_2O_3	Total Fe	
96b	73	5	22	72.1	5.2	77.3	1160
103	77	5	18	72.7	5.8	78.5	1180
109	80	2	18	72.6	7.0	79.6	1180
110	81	3	16	75.7	6.5	82.2	1210

TABLE 1 (*Cont.*)

Experiment No. FAS	Planned Composition FeO	Al_2O_3	SiO_2	Final Composition by analysis FeO	Fe_2O_3	Total Fe as FeO	Temp. ± 5° C.	Results of microscopic examination	Refractive index of glass ± 0.003
(h) Quenching experiments on Mixtures with more than One Solid Phase									
2	55	5	40	55.2	0.6	55.8	1154 1149	Very rare olivine in glass. Small amount of olivine and very rare tridymite in glass.	1.736
15	40	15	45	44.7	0.1	44.8	1105 1102 1098	All glass. Very rare iron cordierite in glass. Rare iron cordierite and very rare tridymite in glass.	1.678
19x	44	13	43	47.7	0.1	47.8	1085 1080	All glass. Rare tridymite and rare fayalite in glass.	1.686
20	33	19	48	37.3	0.0	37.3	1181 1165	Very rare tridymite in glass. Small amount tridymite and very rare iron cordierite in glass.	1.634
23	23	22	55	27.2	0.0	27.2	1315 1310	All glass. Very rare tridymite and very rare mullite in glass.	1.594
25	46	11	43	49.8	0.0	49.8	1105 1100	All glass. Very rare tridymite and rare fayalite in glass.	1.706

TABLE 1 (*Cont.*)

Experiment No. FAS	Planned Composition FeO	Al_2O_3	SiO_2	Final Composition by analysis FeO	Fe_2O_3	Total Fe as FeO	Temp. ± 5° C.	Results of microscopic examination	Refractive index of glass ± 0.003
30	57	11	32	56.1	1.1	57.2	1160 1155 1140	All glass. Rare hercynite in glass. Small amount hercynite and very rare fayalite in glass.	....
33	49	8	43	52.2	0.4	52.6	1130	Very rare tridymite and very rare fayalite in glass.	1.718
37	33	30	37	37.7	0.5	38.2	1385 1380 1375	Very rare corundum in glass. Rare corundum, rare hercynite and very rare mullite in glass. Small amount hercynite and rare mullite in glass.	1.663
41	27	22	51	32.1	0.3	32.4	1240 1235 1230	All glass. Rare mullite in glass. Small amount mullite and very rare tridymite in glass.	1.618
42	50	12	38	55.3	0.0	55.3	1120	Very rare hercynite and rare fayalite in glass.	1.739
43	35	19	46	36.9	0.0	36.9	1185 1180 1160	All glass. Rare hercynite in glass. Small amount hercynite and very rare iron cordierite in glass.	1.632

TABLE 1 (*Cont.*)

Experiment No. FAS	Planned Composition FeO	Al_2O_3	SiO_2	Final composition by analysis FeO	Fe_2O_3	Total Fe as FeO	Temp. ± 5° C.	Results of microscopic examination	Refractive index of glass ± 0.003
44	39	16	45	41.7	0.0	41.7	1165 1150	Very rare tridymite in glass. Rare tridymite and very rare iron cordierite in glass.	1.655
48	71	7	22	72.4	3.4	75.8	1150 1145	Very rare hercynite and very rare wüstite in glass. Rare fayalite, rare wüstite and rare hercynite in glass.	....
49	60	10	30	65.5	2.0	67.5	1160 1155 1150	Very rare hercynite in glass. Rare hercynite in glass. Rare hercynite and rare fayalite in glass.	....
54	25	31	44	37.2	0.5	37.7	1345 1340	All glass. Rare mullite and rare hercynite in glass.	1.653
56	55	3	42	59.5	0.9	60.4	1170 1165 1160	Very rare fayalite in glass. Rare fayalite in glass. Rare fayalite and rare tridymite in glass.	....
67	28	23	49	34.0	0.1	34.1	1225	Very rare mullite and very rare hercynite in glass.	1.629

TABLE 1 (*Cont.*)

Experiment No. FAS	Planned Composition FeO	Al_2O_3	SiO_2	Final Composition by analysis FeO	Fe_2O_3	Total Fe as FeO	Temp. ± 5° C.	Results of microscopic examination	Refractive index of glass ± 0.003
82	22	39	39	31.4	0.4	31.8	1520	Rare corundum and rare mullite in glass.	1.640
83	30	37	33	39.3	0.4	39.7	1470	Very rare corundum and very rare hercynite in glass.	1.677
84	26	35	39	34.1	0.4	34.5	1465	Very rare corundum and very rare mullite in glass.	1.652
89	22	35	43	36.5	0.3	36.8	1400	Very rare corundum and very rare mullite in glass.	1.654
102	75	3	22	71.6	4.8	76.4	1170 1165 1160	All glass. Rare fayalite in glass. Rare fayalite and rare wüstite in glass.	....
105	77	2	21	72.6	4.1	76.7	1175 1170 1165	Very rare fayalite in glass. Rare fayalite in glass. Small amount fayalite and rare wüstite in glass.	....
111	83	5	12	79.0	9.3	88.3	1225 1215	All devitrified glass. Rare spinel and rare wüstite in devitrified glass.	....

In a previous paper (Bowen and Schairer, 1932, pp. 188-193) it was shown that even after melting in an iron crucible in an evacuated, sealed, silica-glass tube, there is still persistence of some ferric iron in silicate liquids and reasons were there given for the belief that the amounts of ferric iron persisting in the nitrogen runs represents equilibrium with metallic iron. The same is true of mixtures in $FeO—Al_2O_3—SiO_2$. Iron is incapable of further reducing the Fe_2O_3 content of these silicate melts. Any attempt at reduction with the aid of a reducing agent would result only in separation of metallic iron from the liquid without decrease of its Fe_2O_3 content.

For a full and accurate presentation of the experimental results it would, in light of the above facts, be necessary to refer them to quaternary equilibrium in the system $Fe—Fe_2O_3—Al_2O_3—SiO_2$. The results are much more conveniently and lucidly presented by neglecting the amount of Fe_2O_3 in the liquid, calculating total iron as FeO and plotting the data on a ternary diagram. We have adopted this course here. Throughout the paper,

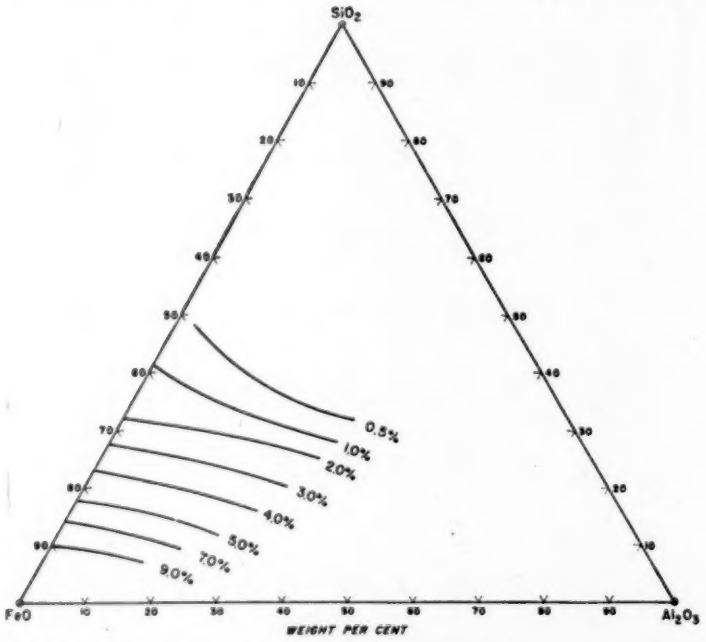

Fig. 3. Diagram showing the approximate Fe_2O_3 content of liquids in equilibrium with metallic iron.

whenever we speak of a binary or ternary invariant point it is to be borne in mind that it can be treated as binary or ternary, respectively, only when the small content of Fe_2O_3 is arbitrarily regarded as FeO.

Figure 3 shows the manner in which the equilibrium content of Fe_2O_3 in the liquids varies with composition. The data are remarkably consistent when the small size (0.1 to 0.2 g.) of the samples used in the analyses is considered. For SiO_2 contents greater than 60 per cent, the Fe_2O_3 content falls off rapidly to an amount so small that the error of determination is a large proportion of its total.

The melting point of an iron crucible limited the range of compositions studied. Most of the mixtures could be cooled rapidly enough (quenched) to a glass and the refractive index of the glass was determined under the petrographic microscope by comparison with immersion liquids of known index of refraction at 25° C. The values are given in table 1 and plotted in figure 4. After the isofracts shown in this figure were determined, we found that the measurement of the refractive index of the

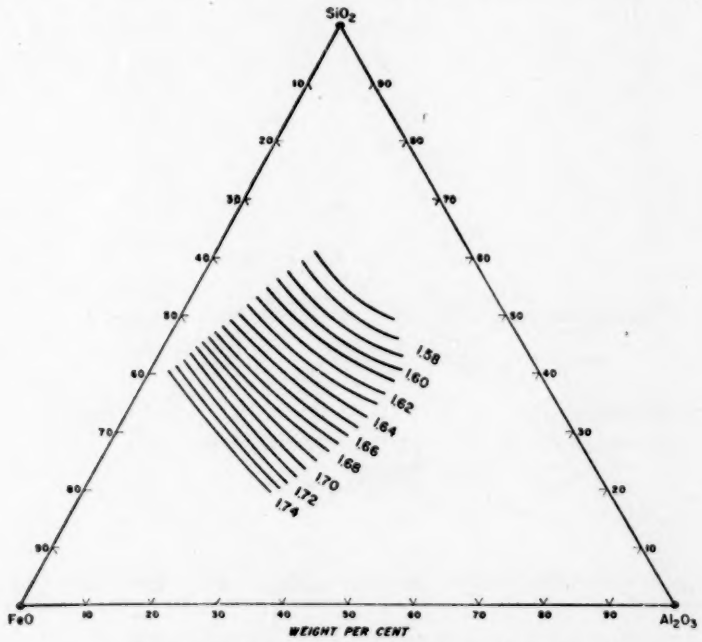

Fig. 4. Refractive indices of glasses at 25° C.

glass present in quenched charges was a very useful method of determining the composition of the liquid phase present in such a charge. This was particularly helpful in delineating the boundaries of the narrow field of iron cordierite. Those glasses with an index above 1.740 were not measured. Most of the compositions with a glass index above this value could not be quenched rapidly enough to give a clear glass free from fine-grained devitrification products formed during the cooling. Under the microscope it was easy to identify primary crystals, when present in the liquid, from these fine-grained, feathery, devitrification products.

THE EQUILIBRIUM DIAGRAM

Figure 5, the equilibrium diagram for the system $FeO—Al_2O_3—SiO_2$, is based on the results of quenching experiments and the results of chemical analyses given in table 1. It shows the fields of the primary crystalline phases with their boundary curves, the seven ternary invariant points (two of them eutectics *O*

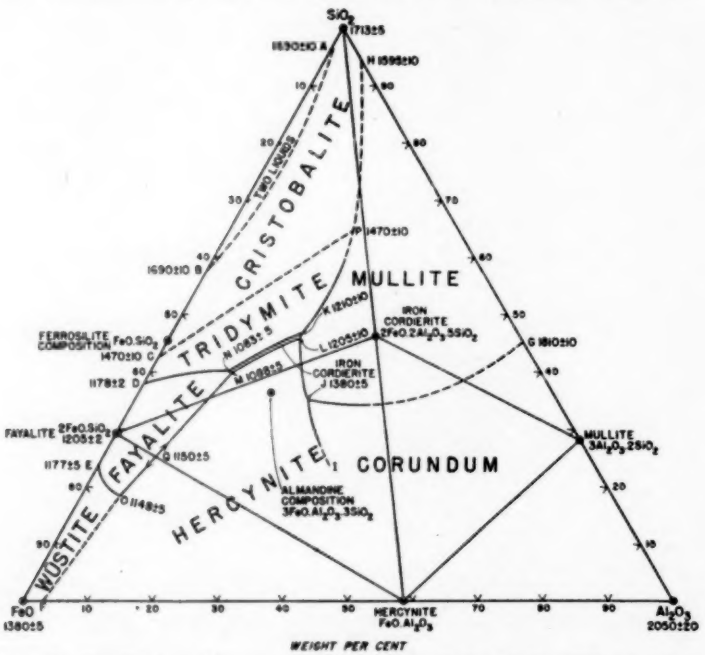

Fig. 5. Equilibrium diagram of the system $FeO—Al_2O_3—SiO_2$ showing fields of primary crystalline phases, tie lines, and invariant points.

and *N*, four reaction points *J*, *L*, *K*, and *M*, and the inversion point *P*), and the tie lines which divide the system into triangular areas. The compositions of the compounds are shown as open double circles. Only one ternary compound, iron cordierite $2FeO \cdot 2Al_2O_3 \cdot 5SiO_2$, appears on the liquidus surface. The stability relations of almandine garnet, $3FeO \cdot Al_2O_3 \cdot 3SiO_2$, will be discussed later.

The isotherms are shown on figure 6. In this figure the tie lines have been omitted and the compositions studied are shown as small black dots. Because of the limitation imposed by the melting of an iron crucible at about 1523° C., compositions studied are confined to temperatures below 1520°. Arrows on the boundary curves indicate the direction of falling temperature.

Attention is called to the narrow field (*NKLM*, fig. 5) of iron cordierite. All of the crystalline solid phases which appear on the liquidus surface in this system crystallize readily except

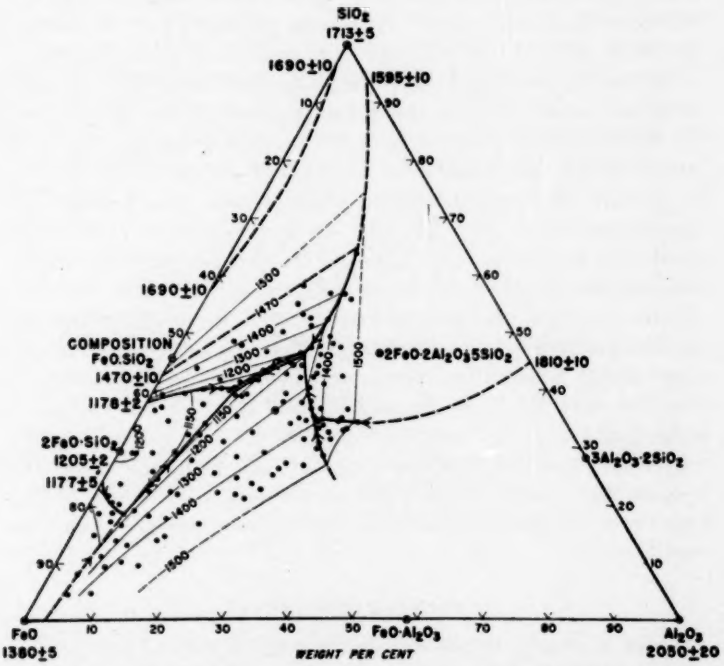

Fig. 6. Equilibrium diagram of the system FeO—Al_2O_3—SiO_2 showing compositions studied and the isotherms.

iron cordierite. In all of the melts except those near the field of this ternary compound, the stable solid phases crystallize so readily that when a glass is heated in an iron crucible it crystallizes during the short interval of time required to bring the temperature of this small crucible up to furnace temperature. Using this procedure in the region of the iron cordierite field, only tridymite in nice pseudohexagonal plates and small sharp octahedrons of hercynite crystallize with equant fayalite crystals or mullite needles at appropriate temperatures in appropriate compositions, and no iron cordierite forms near liquidus temperatures even with runs of several hours' duration. In fact, one always obtains metastable equilibrium unless iron cordierite crystals, developed by crystallization of the glasses in sealed tubes at temperatures between 850° and 1000° C., are present in the charges used for the quenching runs. In the preliminary experiments we determined the metastable eutectic fayalite + tridymite + hercynite + liquid (FeO 47.2 Al_2O_3 12.5 SiO_2 40.3) at 1073° ± 5° and the metastable reaction point mullite + tridymite + hercynite + liquid (FeO 33.5 Al_2O_3 20.0 SiO_2 46.5) at 1205° ± 5°.

As may be seen by inspection of figures 5 and 6, iron cordierite has a narrow field along the temperature trough between the fields of tridymite and hercynite and is delineated by four boundary curves. Experimentally it was difficult to determine the nature of these boundaries. However, it was possible to demonstrate that: (1) *KL* (fig. 4) is a reaction curve along which iron cordierite crystallizes at the expense of mullite upon lowering the temperature, because tangents to *KL* always intersect the conjugation line mullite-iron cordierite produced beyond the iron cordierite composition; (2) similarly, *LM* is a reaction curve along which iron cordierite crystallizes while hercynite dissolves; (3) *KN* is a subtraction curve along which iron cordierite and tridymite crystallize simultaneously, since tangents to *KN* always intersect the conjugation line SiO_2-iron cordierite between these two compositions; (4) similarly, *MN* is a subtraction curve along which fayalite and iron cordierite crystallize simultaneously.

INVARIANT POINTS

There is a temperature maximum at *Q* (fig. 5) on the boundary curve *MQO*. The system fayalite—hercynite is a binary system within the ternary system FeO—Al_2O_3—SiO_2 and *Q*

is the binary eutectic between fayalite and hercynite at the composition fayalite 89.3 per cent, hercynite 10.7 per cent at 1150° ± 5°.

One binary and seven ternary invariant points within the system FeO—Al_2O_3—SiO_2 are listed in table 2 and the quenching data on which four of them are based are given in table 3. At *J* the reaction corundum + liquid *J* ⇌ mullite + hercynite occurs at 1380° ± 5°. At *K* the reaction tridymite + mullite + liquid *K* ⇌ iron cordierite occurs at 1210° ± 10°. The highest temperature in the field of iron cordierite is at *K* and above this temperature iron cordierite is not stable. This temperature is, therefore, the incongruent melting temperature of iron cordierite at which this ternary compound dissociates into tridymite, hercynite, and a liquid of composition *K*. At *L* the reaction mullite + liquid *L* ⇌ hercynite + iron cordierite occurs at 1205° ± 10°. At *M* the reaction fayalite + iron cordierite ⇌ hercynite + liquid *M* occurs at 1088° ± 5°. The point *P* is the ternary inversion point where two forms of crystalline silica, tridymite and cristobalite are in equilibrium in the presence of mullite and the liquid *P*. The point *O* is the ternary eutectic between wüstite, fayalite, hercynite and liquid at 1148° ± 5°. The point *N* is the lowest temperature on the liquidus surface in the system and at this eutectic point fayalite, tridymite, and iron cordierite are in equilibrium with the liquid *N* at 1083° ± 5°.

SEARCH FOR FERROSILITE

Special effort was made to crystallize the metasilicate of ferrous iron $FeO \cdot SiO_2$, the monoclinic form of which, as noted previously, has been described as the mineral clinoferrosilite. No lines of this compound were found in any of the X-ray powder patterns of crystallized glasses of compositions from which this might be expected to crystallize. There is the possibility that ferrosilite might be a stable crystalline solid phase at some subsolidus temperature. We see little hope of obtaining equilibrium in solid phase reactions at such temperatures in the ternary system FeO—Al_2O_3—SiO_2.

ALMANDINE GARNET

Preliminary experiments showed that the composition $3FeO \cdot Al_2O_3 \cdot 3SiO_2$ lies in the field of hercynite and that a melt of this composition has a liquidus of about 1300°. Many experi-

ments were made to explore the possibility that almandine might be stable in some temperature range below the liquidus. No almandine crystallized from any of our glasses even when they were seeded with natural almandine from Botallack, England. Glasses near almandine in composition when crystallized at temperatures between 750° and 1050° in sealed tubes for three weeks showed only fayalite, hercynite and iron cordierite. A liquid of almandine composition becomes completely crystalline at the temperatures of *M* (fig. 5) 1088° ± 5° and consists only of fayalite, hercynite and iron cordierite.

Attempts were made to crystallize almandine by heating glass near almandine in composition and seeded with natural almandine, in iron foil with a small amount of perlite from Superior, Arizona (3.70 per cent H_2O+ and 3.70 per cent H_2O-), in a platinum envelope in an evacuated sealed silica-glass tube for two months at 800° C. No new almandine was formed, nor was there any decomposition of the almandine used as seed. When a glass near almandine in composition was heated in a hydrothermal pressure vessel at 600° for 83 hours at 15,000 pounds per square inch water vapor pressure, only iron cordie-

TABLE 2

Invariant Points within the System $FeO—Al_2O_3—SiO_2$

Letter (Fig. 5)	Temp. ° C.	Solid and liquid phases phesent
Q	1150 ± 5	Fayalite + hercynite + liquid (Fayalite 89.3 Hercynite 10.7)
N	1148 ± 5	Fayalite + hercynite + wüstite + liquid (FeO 75.8 Al_2O_3 5.9 SiO_2 18.3)
J	1380 ± 5	Corundum + mullite + hercynite + liquid (FeO 38 Al_2O_3 27 SiO_2 35)
K	1210 ± 10	Iron cordierite + tridymite + mullite + liquid (FeO 33.3 Al_2O_3 20.0 SiO_2 46.7)
L	1205 ± 10	Iron cordierite + hercynite + mullite + liquid (FeO 33.9 Al_2O_3 20.1 SiO_2 46.0)
M	1088 ± 5	Iron cordierite + hercynite + fayalite + liquid (FeO 47.7 Al_2O_3 12.6 SiO_2 39.7)
N	1083 ± 5	Iron cordierite + fayalite + tridymite + liquid (FeO 47.5 Al_2O_3 12.0 SiO_2 40.5)

TABLE 3

Quenching Experiments to Determine Four Invariant Points Which Limit Field of Iron Cordierite

Experiment No. FAS	Planned Composition			Final Composition by analysis			Temp. ± 5° C.	Results of microscopic examination	Index refraction of glass ± 0.003
	FeO	Al_2O_3	SiO_2	FeO	Fe_2O_3	Total Fe as FeO			
(1) Reaction Point *K* (Figure 5) 1210° ± 10°									
14	25	20	55	30.3	0.1	30.4	1205	Tridymite and iron cordierite in glass.	1.623
							1210	Tridymite, iron cordierite and mullite in glass.	1.621
							1215	Tridymite and mullite in glass.	1.619
51	24	25	51	31.0	0.3	31.3	1205	Iron cordierite and mullite in glass.	1.624
							1210	Iron cordierite, mullite and tridymite in glass.	1.619
68	8	23	69	24.5	0.1	24.6	1210	Tridymite, iron cordierite, and mullite in glass.	1.623
							1215	Tridymite and mullite in glass.	1.623
71	17	26	57	30.6	0.2	30.8	1210	Iron cordierite and mullite in glass.	1.623
72	19	28	53	32.6	0.2	32.8	1205	Mullite, iron cordierite and tridymite in glass.	1.625
							1210	Mullite, iron cordierite and tridymite in glass.	1.618
							1215	Mullite and tridymite in glass.	1.622
92	10	24	66	22.7	0.1	22.8	1210	Tridymite, mullite, and iron cordierite in glass.	1.625

TABLE 3 (*Cont.*)

Quenching Experiments to Determine Four Invariant Points Which Limit Field of Iron Cordierite

Experiment No. FAS	Planned Composition			Final Composition by analysis			Temp. ± 5° C.	Results of microscopic examination	Index refraction of glass ± 0.003
	FeO	Al_2O_3	SiO_2	FeO	Fe_2O_3	Total Fe as FeO			
94	5	18	77	28.0	0.0	28.0	1205	Tridymite, iron cordierite and mullite in glass.	1.624
							1210	Tridymite, mullite and iron cordierite in glass.	1.623
							1215	Tridymite and mullite in glass.	1.623
				(2) Reaction Point L (Figure 5) 1205° ± 10°					
47	33	25	42	35.9	0.1	36.0	1205	Iron cordierite and hercynite in glass.	....
							1210	Iron cordierite, hercynite and mullite in glass.	1.623
							1215	Hercynite and mullite in glass.	....
53	25	29	46	33.2	0.3	33.5	1205	Mullite, hercynite, and iron cordierite in glass.	1.628
							1210	Mullite and hercynite in glass.	1.620
67	28	23	49	34.0	0.1	34.1	1205	Iron cordierite, hercynite and mullite in glass.	....
							1210	Hercynite, iron cordierite and mullite in glass.	....

TABLE 3 (*Cont.*)

Quenching Experiments to Determine Four Invariant Points Which Limit Field of Iron Cordierite

Experiment No. FAS	Planned Composition FeO	Al_2O_3	SiO_2	Final Composition by analysis FeO	Fe_2O_3	Total Fe as FeO	Temp. ± 5° C.	Results of microscopic examination	Index refraction of glass ± 0.003
88	22	31	47	29.9	0.1	30.0	1200	Iron cordierite and hercynite in glass.	1.630
							1205	Iron cordierite, hercynite and mullite in glass.	1.628
							1210	Iron cordierite, mullite and hercynite in glass.	1.628
							1215	Mullite and hercynite in glass.	1.622
89	22	35	43	36.5	0.3	36.8	1200	Iron cordierite and hercynite in glass.	1.626
							1205	Iron cordierite, hercynite and mullite in glass.	1.628
							1210	Mullite and hercynite in glass.	1.626
				(8) Reaction Point M (Figure 5) 1088° ± 5°					
13	50	15	35	49.2	0.7	49.9	1085	Fayalite, hercynite and iron cordierite with rare glass.	1.690
							1090	Fayalite and hercynite in glass.	1.700
16	55	15	30	53.1	1.2	54.3	1085	Fayalite, hercynite and iron cordierite with rare glass.	1.692
							1090	Fayalite and hercynite in glass.	1.695
29	48	13	39	47.7	0.5	48.2	1085	Fayalite, hercynite and iron cordierite with rare glass.	1.700
							1090	Fayalite and hercynite in glass.	1.700

TABLE 3 (*Cont.*)

Quenching Experiments to Determine Four Invariant Points Which Limit Field of Iron Cordierite

Experiment No. FAS	Planned Composition FeO	Al_2O_3	SiO_2	Final Composition by analysis FeO	Fe_2O_3	Total Fe as FeO	Temp. ± 5° C.	Results of microscopic examination	Index refraction of glass ± 0.003
64	43	21	36	48.0	1.0	49.0	1085	Hercynite, fayalite and iron cordierite with rare glass and very rare tridymite.	1.689
							1090	Hercynite and iron cordierite in glass.	1.689
95	39	22	39	40.6	0.7	41.3	1085	Hercynite, iron cordierite and fayalite with rare glass.	1.690
							1090	Hercynite and iron cordierite in glass.	1.692
				(4) Eutectic Point N (Figure 5) 1083° ± 5°					
7	35	15	50	38.8	0.2	39.0	1085	Iron cordierite and tridymite in glass.	1.688
15	40	15	45	44.7	0.1	44.8	1080	Iron cordierite, fayalite and tridymite in glass.	....
							1085	Iron cordierite and tridymite in glass.	1.690
25	46	11	43	49.8	0.0	49.8	1080	Fayalite, iron cordierite and tridymite with rare glass.	1.685
							1085	Fayalite and tridymite in glass.	1.690
44	39	16	45	41.7	0.0	41.7	1080	Iron cordierite, tridymite and fayalite in glass.	1.690
							1085	Iron cordierite and tridymite in glass.	1.687

rite and magnetite were obtained. No almandine was produced in any of the hydrothermal experiments. All our efforts to prepare almandine crystals from synthetic glasses failed. Almandine has not been synthesized from artificial melts, although it has been reported from time to time as occurring in slags, always, however, without confirmatory evidence.

Several natural garnet samples were used in our experiments. The garnet highest in the almandine molecule was one described by Alderman (1935, pp. 42-48) from Botallack, Cornwall, England. His analysis showed almandine 91.3, spessartite 1.7, pyrope 2.4, grossularite 4.6. Through the courtesy of Professor C. E. Tilley we obtained a sample of this analyzed garnet. Even when samples were heated for 80 days at 800° and at 850° there was no sign of any dissociation. However, after heating at 900° C. for two weeks in evacuated tubes some dissociation was observed. Minute amounts of small octahedra of hercynite and tiny birefringent crystals too small to recognize were observed in the garnet. After heating at 1000° for 72 hours, these birefringent crystals were sufficiently large to identify as cordierite and fayalite. Therefore the dissociation temperature of this almandine-rich garnet is at least as low as 900°, and the dissociation is very sluggish. Some liquid (a small amount of glass in the quenched product) was observed as low as 1050° C. in a sample heated at this temperature in N_2 for 10 hours, and its amount increases rapidly with temperature. At 1090° (10 hours) cordierite and fayalite had disappeared and only crystals of hercynite were present in the quenched glass. The thermal behavior of the Botallack garnet at elevated temperatures was quite similar to that of the artificial glasses except for the presence of liquid below 1088° ± 5°, the temperature of *M* (fig. 5). The presence of liquid in this garnet as low as 1050° is not surprising for a sample with 91.3 per cent almandine and 8.7 per cent of other garnet molecules. When the Botallack garnet is subjected to a hydrothermal environment it appears to decompose with very long runs as low as 500°. Some grains become clouded with magnetite and show low birefringence. Other grains are surrounded with a thin shell of highly birefringent material which was not identified.

A sample of garnet from Shurezkay, Kariffan, A.S.S.R., Russia, was obtained through the courtesy of Dr. William F. Foshag. No analysis was available but determination of FeO

34.0 per cent and Fe_2O_3 1.6 per cent showed that it was high in the almandine molecule. No decomposition was observed in 3 weeks at 850° and incipient decomposition was in progress after 2 weeks at 900°. At 1020° after 72 hours, spinel, fayalite, and cordierite were easily recognized. A garnet from Fort Wrangell, Alaska, was also obtained from Dr. Foshag. Its composition was almandine 69.6, spessartite 3.5, pyrope 21.2, grossularite 5.7. It also yielded olivine, cordierite, and spinel on dissociation.

When a sample of garnet from Gore Mountain, New York (almandine 40, pyrope 43, grossularite 1.4, spessartite 1, andradite 2 [Levin, 1950, p. 534]), was heated it yielded Mg-rich cordierite (lower indices than iron cordierite), rhombic pyroxene and a spinel. This garnet was too far removed from almandine composition to be useful in our studies.

CRYSTALLINE PHASES

Corundum crystallized in small equant facetted hexagonal crystals. β-Al_2O_3 did not appear in any of the melts. Mullite appeared as needles, occasionally with small terminal faces; the spinel hercynite always crystallized as perfect octahedrons; fayalite was present in the glasses as stout prismatic facetted crystals, somewhat elongated in the siliceous compositions; wüstite always appeared as small rounded opaque masses except when it formed during the quenching period when it appeared as strings of tiny octahedrons.

As mentioned previously, iron cordierite could be obtained only by crystallization experiments in sealed tubes after several days or weeks of heating in the temperature range between 800° and 1050°. In the fine-grained crystallization product of these experiments iron cordierite could be recognized positively only by its X-ray powder diagram. It was present as fibrous aggregates radially disposed and showing undulatory extinction under the microscope. The best crystals obtained were not large and were admixed with other crystalline phases. Because of the fibrous nature of the aggregates it was impossible to determine either the optic angle or the optic sign. The crystals showed negative elongation and indices were approximately $\alpha = 1.551$, $\beta = 1.564$, $\lambda = 1.574$. Twinned crystals were common and sometimes showed the interpenetration trillings commonly found in natural cordierites in metamorphic or volcanic rocks. Pleochroism was absent. Sometimes the small cordierite crystals

contained minute inclusions of hercynite, cristobalite, or glass which disappeared as the glasses containing these iron cordierite crystals were heated at higher temperatures. X-ray diagrams of iron cordierite, crystallized from melts widely different in composition, showed identical patterns and there must be little or no variation in its composition in this system through solid solution. An X-ray powder pattern of iron cordierite is compared with a similar pattern for synthetic magnesium cordierite in figure 7. The close similarity of the interplanar spacing, d, in both is apparent.

In many silicate systems cristobalite forms and persists metastably in the temperature range of stability of tridymite. In the system FeO—Al_2O_3—SiO_2, tridymite crystallized readily in appropriate compositions at temperatures just below the liquidus temperatures and small tridymite crystals formed during the short interval of time necessary to heat up to furnace temperature a small crucible containing glass. It appears as thin pseudohexagonal plates with perfect hexagonal outline. In figures 5 and 6, the isotherm for 1470° separates the fields of tridymite and crystobalite. In the crystallization experiments in sealed evacuated silica-glass tubes in the temperature range between 800° and 950° quartz often appeared. Some of our X-ray powder patterns showed the presence of quartz even when the crystallization temperature was above 867° ± 3°, the

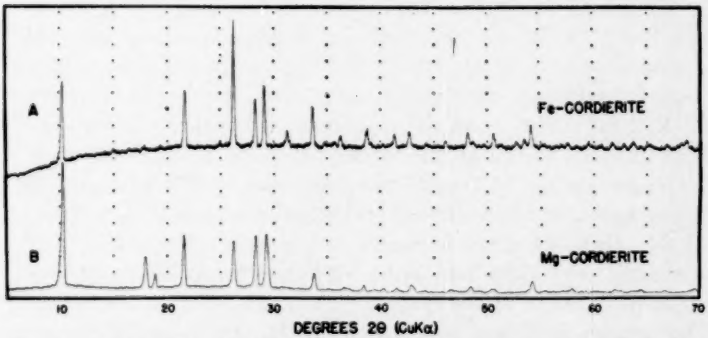

Fig. 7. Photograph of powder X-ray diffraction patterns of synthetic iron cordierite and synthetic magnesium cordierite.

(A) Prepared from glass near iron cordierite in composition held at 850° C. for three weeks in an evacuated sealed tube.

(B) Prepared from a glass of cordierite ($2MgO \cdot 2Al_2O_3 \cdot 5SiO_2$) composition held at 1400° C. for two hours in air.

inversion temperature of quartz to tridymite (Kracek, 1939, pp. 2874-2875). Quartz may have crystallized while the glasses in the sealed tubes were heating up to the furnace temperature, and once formed it persisted metastably. When this quartz was heated at or above 1050° it always inverted to cristobalite, not tridymite. At 1000° both quartz and cristobalite persisted. Thus, a metastable transformation of quartz to cristobalite occurred approximately at 1000° C.

CRYSTALLIZATION

Crystallization in the system $FeO—Al_2O_3—SiO_2$ is quite simple because all of the crystalline phases are of fixed composition. Tie lines divide the system into six triangular areas. With perfect equilibrium between crystals and liquid, all compositions in each of these areas complete their crystallization on cooling (or conversely begin to melt on heating) at the particular temperature of one of the ternary invariant points, and the last bit of liquid on cooling (or the first bit of liquid on heating) has the composition of the particular ternary invariant point.

On cooling with perfect equilibrium all compositions in the area hercynite—mullite—Al_2O_3 (corundum) of figure 5 become completely solid at the temperature of *J*, 1380° ± 5°; those in the area iron cordierite—mullite—hercynite at *L*, 1205° ± 10°; those in the area iron cordierite—mullite—SiO_2 (tridymite) at *K*, 1210° ± 10°; those in the area fayalite—hercynite—iron cordierite at *M*, 1088° ± 5°; those in the area fayalite—iron cordierite—SiO_2 (tridymite) only at the ternary eutectic *N*, 1083° ± 5°; and those in the area fayalite—hercynite—FeO (wüstite) only at the ternary eutectic *O* at 1148° ± 5°.

Crystallization of typical mixtures may be followed with the aid of figure 8, where the central portion of the system $FeO—Al_2O_3—SiO_2$, as given in figure 5, has been enlarged in order to clarify crystallization paths. In figure 8 the SiO_2 apex and the lower portion of the system have been cut off to save space. The ternary invariant points *J*, *K*, *L*, *M*, and *N* and the binary invariant points *C*, *D*, and *G* are similarly labelled in figures 5 and 8. The compositions of iron cordierite, mullite and fayalite are labelled *X*, *Y*, and *Z*, respectively, in figure 8. Arrows on boundary curves show the direction of falling temperature.

The crystallization of liquids of the compositions *b* and *a* is

typical of compositions in the triangular area mullite (*Y*)—iron cordierite (*X*)—SiO_2 except for the small range of compositions near the SiO_2 apex where cristobalite crystallizes first. Crystallization of liquid *b* begins with the separation of corundum (the temperature can be interpolated from the isotherms of figure 6) and proceeds along the straight line Al_2O_3—*b*—4 from *b* to 4 where mullite crystals appear; the liquid follows *GJ* from 4 to 5 with corundum reacting with liquid to form mullite. At 5 corundum has disappeared and the liquid follows the straight line *Y*—5—*a*—*g*—1 from 5 to 1 with separation of mullite crystals. At 1, mullite is joined by tridymite crystals and the liquid follows the boundary curve 1*K* with both mullite and tridymite crystallizing until *K* is reached. At this point a reaction takes place between the crystals and liquid producing iron cordierite crystals until the liquid is entirely consumed by reaction at constant temperature. The wholly crystalline product consists of mullite, tridymite, and iron cordierite. The crystallization path of *a* is similar to *b* except that the complication of corundum crystallizing first and then disappearing by reaction is lacking in the case of *a*.

The crystallization of liquids of the compositions *d*, *c*, and *e* (fig. 8) is typical of compositions in the triangular area iron cor-

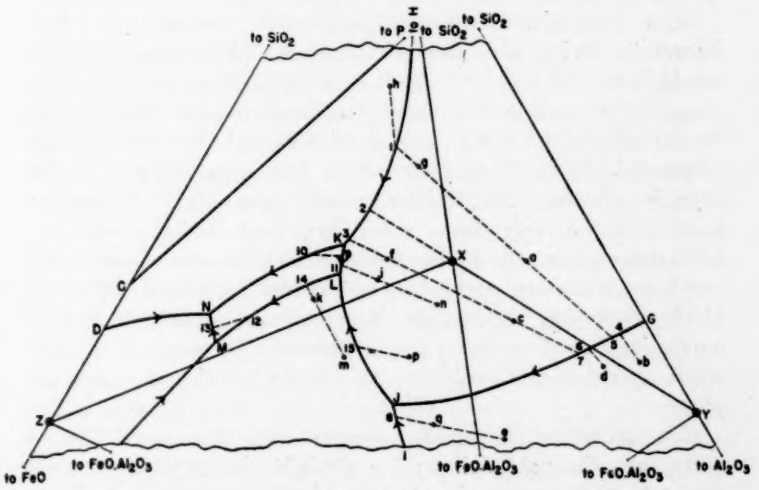

Fig. 8. Central portion of system FeO—Al_2O_3—SiO_2 truncated to save space and enlarged to depict crystallization paths clearly.

dierite (X)—mullite (Y)—hercynite. In a manner similar to the early crystallization of b, crystallization of liquid d begins with the separation of corundum, proceeds along the straight line Al_2O_3d6 from d to 6, where mullite crystals appear, the liquids follow GJ from 6 to 7 with corundum dissolving by reaction with liquid to give mullite. At 7 corundum has disappeared and the liquid follows the straight line Y—d—7—c—f—3 from 7 to 3 with separation of mullite crystals. At 3, mullite is joined by tridymite crystals and the liquid follows the boundary curve from 3 to K with both mullite and tridymite crystallizing until K is reached. At this point a reaction takes place between crystals and liquid producing iron cordierite crystals, the tridymite being completely dissolved while some liquid still remains. As soon as tridymite has disappeared by reaction at constant temperature (that of K, 1210° ± 10°) the liquid follows the boundary curve KL with iron cordierite increasing and mullite decreasing in amount. At L hercynite as well as iron cordierite is produced by the reaction of mullite and liquid of composition L until the liquid disappears by reaction at constant temperature (1205° ± 10°). The resultant aggregate consists of mullite, iron cordierite, and hercynite. The crystallization path of c is similar to b except that the complication of corundum crystallizing first and then disappearing by reaction is lacking in the case of c.

If a composition had been selected in the area X—Y—hercynite, which also lies in the area YKL, crystallization would have been similar to d or c in the early stages, but after crossing the mullite field the crystallization path would reach the boundary curve KL instead of HK and it would proceed along KL to L. If a composition had been selected in the area X—Y—hercynite which also lies in the area YJL, crystallization in the early stages would have been similar to d or c, but after crossing the mullite field the crystallization path would reach the boundary curve JL and proceed towards L with hercynite increasing and mullite decreasing in amount. At L iron cordierite as well as hercynite is produced by reaction at constant temperature (1205° ± 10°) and crystallization is complete.

Crystallization of liquid e begins with the separation of corundum, the path follows the straight line Al_2O_3—e—q—8 from e to 8 where corundum is joined by hercynite and the liquid follows the boundary curve 8J to J, where corundum disappears

by reaction at constant temperature (1380° ± 5°) to form mullite. When all corundum has disappeared by reaction the liquid leaves *J* and follows *JL* to *L* where crystallization is completed at the constant temperature of *L* (1205° ± 10°). Thus, we have seen that all compositions in the area *X*—*Y*—hercynite complete their crystallization at *L*(1205° ± 10°) and consist of iron cordierite, mullite, and hercynite, but may reach this goal by somewhat different paths.

The crystallization of liquids of the compositions *n*, *p*, *q*, and *m* (fig. 8) is typical of compositions in the triangular area *Z*—*X*—hercynite. Compositions in this triangular area which also lie in the field of mullite first crystallize mullite and proceed in a straight line (for examples *nj*—11 or *p*—15 to reach, depending on their initial compositions: (1) the boundary curve *HK* between 2 and *K* and from there along *KL* to *L* and from there along *LM* to *M;* or (2) the boundary curve *KL* between *K* and *L* and from there to *L* and from there along the boundary curve *LM* to *M;* or (3) the boundary curve *JL* between *J* and *L* and from there to *L*, and from there along *LM* to *M*.

Compositions in the triangular area *Z*—*X*—hercynite which also lie in the field of corundum first crystallize corundum and proceed in a straight line (for example Al_2O_3—*e*—*q*—8 from *q* to 8) to reach either the boundary curve *GJ* or *IJ* depending on their initial composition. Those that reach *GJ* follow it for a short distance until corundum has all dissolved and then cross the mullite field to *JL*. Those that reach *IJ* follow it to *J* where all of the corundum disappears by reaction at constant temperature (1380° ± 5°) and then follow *JL* to *L* where all mullite disappears by reaction at 1205° ± 5° and iron cordierite crystals appear, and from there along *LM* to *M* where fayalite appears.

Compositions in the triangular area *Z*—*X*—hercynite which lie in the field of hercynite and also lie in the area hercynite—*L*—*M*, first crystallize hercynite and proceed in a straight line (for example, *hercynite*—*m*—*k*—14 from *m* to 14) to reach the boundary curve *LM* between *L* and *M* and follow along it to *M* where fayalite appears and crystallization is complete at 1088° ± 5°. Those compositions in the triangular area *Z*—*X*—hercynite—which lie in the field of hercynite and also lie in the area hercynite—*M*—*Z* first crystallize hercynite, follow a straight line until they reach the boundary curve between the fields of

fayalite and hercynite where crystals of fayalite first appear, thence along this boundary curve to *M* where iron cordierite appears and crystallization is completed.

Compositions in the triangular area *Z*—*X*—hercynite which lie in the field of fayalite first crystallize fayalite, then proceed in a straight line to the boundary curve between the fields of fayalite and hercynite, and then follow this boundary curve to *M* where iron cordierite first appears and crystallization is completed. Thus, we have seen that all compositions in the area *Z*—*X*—hercynite complete their crystallization at *M* (1088° ± 5°) and consist of fayalite, iron cordierite, and hercynite, but may reach this goal by somewhat different paths.

All compositions in the area *Z*—*X*—SiO_2 complete their crystallization at the ternary eutectic *N* at 1083° ± 5° and consist of fayalite, tridymite, and iron cordierite. For most of them the crystallization path is very simple. For example *h* and *g* first crystallize tridymite or mullite, respectively, follow the straight line path, *h*—1 or *g*—1, respectively, to the boundary curve *HK*, follow it to *K* where iron cordierite appears and mullite disappears at constant temperature by reaction and thence along *KN* to *N* where crystallization is completed.

Only two areas in the triangle *Z*—*X*—SiO_2 are of particular interest and we shall discuss these. The first is the area *XKL*. At some point during crystallization the liquid reaches *KL*, follows it for a short distance, leaves it, and crosses the field of iron cordierite to reach *KN* at some point and then follows it to *N*. For example *f* first crystallizes mullite, follows the straight line *Y*—*f*—3 from *f* to 3 where mullite is joined by tridymite, follows this boundary curve *HK* from 3 to *K* where tridymite disappears by reaction, thence along *KL* to 9 (this point is located by the straight line *X*—*f*—9) where mullite has disappeared and only iron cordierite crystals remain; from 9 the straight line 9-10 is followed to the boundary curve *KN*. At 10 tridymite appears again and the liquid proceeds along *KN* from 10 to *N* where fayalite appears and crystallization is completed.

The second area of particular interest is the area *MXL*. At some point during crystallization the liquid reaches *LM*, follows it for some distance, leaves it and crosses the field of iron cordierite to reach *MN* or *KN* and from there to *N*. Two points in this area will be discussed. The liquid *j* first crystallizes mullite, follows the straight line *Y*—*n*—*J*—11 from *j* to 11 where mullite

is joined by iron cordierite, from there along *KL* from 11 to *L* where mullite disappears by reaction with liquid, from there along *LM* to 12 where hercynite has disappeared by the reaction taking place along the curve *LM*, thence with only iron cordierite present across the iron cordierite field along the straight line *X—j—k—*12—13 from 12 to 13 where iron cordierite is joined by fayalite, then along *MN* from 13 to *N* where tridymite appears and crystallization is completed. The liquid *k* first crystallizes hercynite, follows the straight line hercynite—*m—k—*14 from *k* to 14, where hercynite is joined by iron cordierite, thence along *LM* from 14 to 12 with hercynite disappearing by reaction with liquid. At 12 all hercynite has disappeared and the liquid follows the straight line *X—j—k—*12—13 from 12 to 13 across the iron cordierite field to reach the boundary curve *MN* at 13 where fayalite joins iron cordierite, along *MN* from 13 to *N* where tridymite appears and crystallization is completed.

So far we have discussed crystallization with perfect equilibrium between crystals and liquid. Fractional crystallization always pushes the course of crystallization toward the ternary eutectic *N* regardless of the original composition of the liquid (unless it is in the ternary system wüstite—fayalite—hercynite whose crystallization is not of sufficient interest to discuss here). With lack of equilibrium between crystals and liquid during fractionation more than three crystalline phases may coexist metastably and the end product of crystallization might have either or both corundum and mullite in addition to iron cordierite, fayalite and tridymite.

OCCURRENCES OF IRON-BEARING CORDIERITES

Bücking (1900) found cordierite crystals with augite or sillimanite in obsidian-like, black fragments associated with andesite from the volcano Seputan, north Celebes. Analysis of these crystals which he called lime iron cordierite showed 11.49 per cent FeO. Fermor (1924) applied the name iron cordierite to a violet-colored cordierite very rich in FeO from a shale fused by a burning coal seam. Ramdohr (1927) found an iron-rich cordierite (12.87 $FeO + Fe_2O_3$) in the iron ore thermally metamorphosed by granite in the Harz. It occurred with fayalite, iron spinel and almandine. Shibata (1936) described the occurrence of iron cordierite from pegmatites intrusive into

and contaminated by sandstone and amphibolite at Sasago and Dosi, Japan. Two analyses showed 15.31 and 13.17 per cent FeO in the cordierites. The Sasago cordierite is richest in ferrous iron among natural cordierites. Pure iron cordierite ($2FeO \cdot 2Al_2O_3 \cdot 5SiO_2$) contains 22.18 per cent FeO. Because of its intimate graphic intergrowth with quartz, Shibata concluded that the iron cordierite probably crystallized from a melt. Morimoto (1947) found beautiful cordierites in the drusy cavities and porous groundmass in the biotite-bearing hypersthene-plagioliparite at Sakurajima volcano. This cordierite showed 9.97 per cent FeO and was associated with olivine (Fa 84 Fo 16) and tridymite or quartz. He postulated that the cordierite crystallized at a very late stage when the iron content of the magma was high, presumably during the assimilation of xenoliths in the liparitic magma.

Richardson and Rigby (1949) obtained iron cordierite in blast furnace linings and showed that these crystals are nearly pure iron cordierite with a very low MgO content. The lining itself contained only 0.68 per cent MgO. Their interplanar spacings show close agreement with those of our synthetic iron cordierite, the pattern of which is shown in figure 7. The association iron cordierite—hercynite—mullite found in the furnace lining corresponds with the assemblage expected from the equilibrium diagram (figs. 5 and 6).

Stability of almandine.—The common garnet of regionally metamorphosed argillaceous sediments is essentially of almadine composition with small amounts of MgO. Almandine is also found in contact zones if it contains notable amounts of MnO (Tilley, 1926). In addition, the almandine-spessartite garnet is recorded in granite pegmatites and vesicles of rhyolites. The almandine-pyrope garnets are characteristic of eclogites. It is apparent that almandine, when containing quantities of pyrope and spessartite, can occur over a large range of conditions. However, almandine free from appreciable amounts of MnO is known to break down in some contact aureoles to cordierite and magnetite or to biotite (Bailey and Maufe, 1916). Alteration to hypersthene and pleonaste are of less common occurrence. The field observations indicate, therefore, that there are limits to the stability of almandine.

Natural almandine was found to decompose at least as low as 900° in a nitrogen atmosphere. It is believed to be stable to a temperature at least as high as 850° in such an atmosphere.

For this reason it should not be surprising to find pure almandine stable at some granite contacts where, according to Bowen and Tuttle (personal communication, 1952), the initial temperature of an extremely "wet" magma may have been as low as 640°. On the other hand, when subjected to the oxidizing conditions of a hydrothermal environment almandine appeared to decompose as low as 500°. On the basis of these data and on data obtained on pyrope, Yoder (personal communication, 1952) was of the opinion that almandine as well as pyrope was unstable at all temperatures in the presence of an excess of water vapor. The production of iron cordierite and magnetite from a glass near the almandine composition under hydrothermal conditions supports this view.

It is concluded that the occurrence of almandine in contact aureoles is dependent on the MnO content, on the amount of water present, and on the temperature. These variables may be determined when work on the systems almandine—spessartite and almandine—water is undertaken.

Mineral assemblages.—The concept of mineral facies is helpful in the discussion of mineral assemblages in rocks. Laboratory conditions of moderate temperatures at atmospheric pressure correspond approximately to the relations in the sanidinite or pyroxene hornfels facies as defined by Eskola (1939). Figure 9 shows the assemblages in FeO—Al_2O_3—SiO_2 at temperatures above 900° C. In rocks andalusite or sillimanite is found instead of mullite, and silica is present as quartz. This facies includes xenoliths pyrometamorphosed in volcanic rocks. In the xenoliths in volcanic or hyperbyssal rocks the assemblage of spinel with sillimanite or with andalusite is very common. Brauns (1911) described ejecta from the Laachersee district with spinel along with sillimanite, andalusite and staurolite. Thomas (1922) mentioned that the buchite from Mull contains spinel and cordierite and gave an analysis of the spinel which is a solid solution of hercynite and magnesia spinel. Bowen, Greig and Zies (1924) first described mullite from this rock. Sugi (1931) described a xenolith in the quartz porphyry at Nikko with corundum fringed by and replacing spinel. Watanabe (1943) described a similar association in a xenolith in porphyritic granite from the Suian district. Teall observed the association spinel—sillimanite—corundum in the hornfels from Ben Cruachan.

Sillimanite porhyroblasts in cordierite—anthophyllite horn-

fels surrounded by a reaction rim of cordierite were described by Eskola (1939) and called armored relics. The association cordierite—fayalite—hercynite is not common but was found in the Harz iron ores metamorphosed by Brocken granite (Ramdohr, 1927). In these ores magnetite and quartz occur together but under some conditions fayalite was formed. In aluminous portions of the ore fayalite is joined by hercynite and iron-rich cordierite. In the pegmatites from Sasago and Dosi (Shibata, 1936) a graphic intergrowth of iron cordierite and quartz is associated with andalusite. Iron-rich cordierite is associated with fayalite and tridymite in the drusy cavities or groundmass of liparites from Sakurajima volcano (Morimoto, 1947).

From the thermal behavior of Botallack almandine we might expect that at temperatures somewhat below 900° C. this mineral might be present in assemblages in rocks. Ferrosilite may also occur, especially if some magnesia is present. Figure 10 shows some of the mineral assemblages that might be found.

According to Eskola the assemblage cordierite—corundum

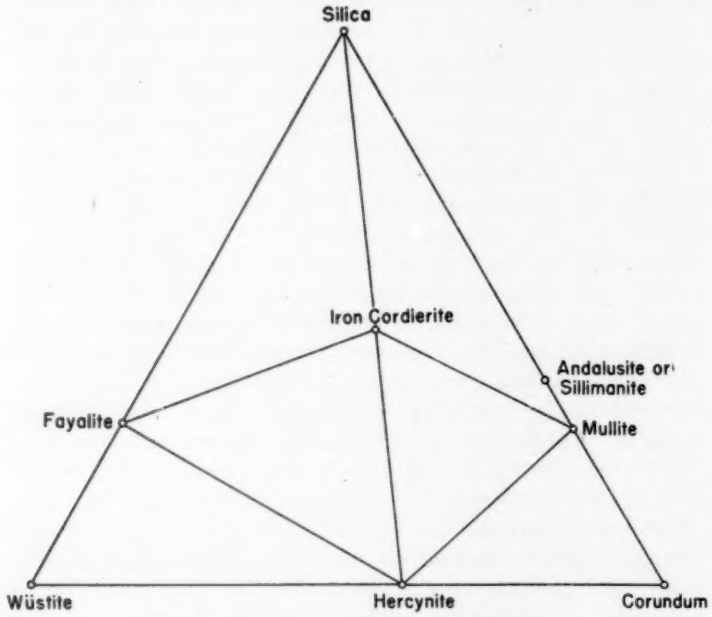

Fig. 9. Mineral assemblages above 900° C.

occurs in the pyroxene hornfels facies of MgO—Al_2O_3—SiO_2, instead of the assemblage spinel—andalusite which occurs in the sanidinite facies. Tilley (1923) suggested that both assemblages may occur in hornfels. What happens to these assemblages when most of the MgO is replaced by FeO is not known.

With the appearance of almandine in figure 10 the assemblage fayalite—iron cordierite—hercynite is replaced by assemblages with almandine as one of the minerals. The association almandine—fayalite—ferrosilite is represented in the eulysites. Tilley (1936) described an eulysite from Loch Duich with fayalite, iron hypersthene with hedenbergite, spessartite-almandine and magnetite in order of abundance. Similar rocks are known from Tunaberg (Palmgren, 1917) and Mansjo (von Eckermann, 1922). When the bulk composition of these rocks is plotted on the FeO—Al_2O_3—SiO_2 diagram, they fall within the triangle almandine—fayalite—ferrosilite. In the siliceous iron ore from the Harz (Ramdohr, 1927), the association fayalite—almandine—pleonaste with a small amount of iron cordierite is found. In xenoliths in andesitic rocks of the Setouchi

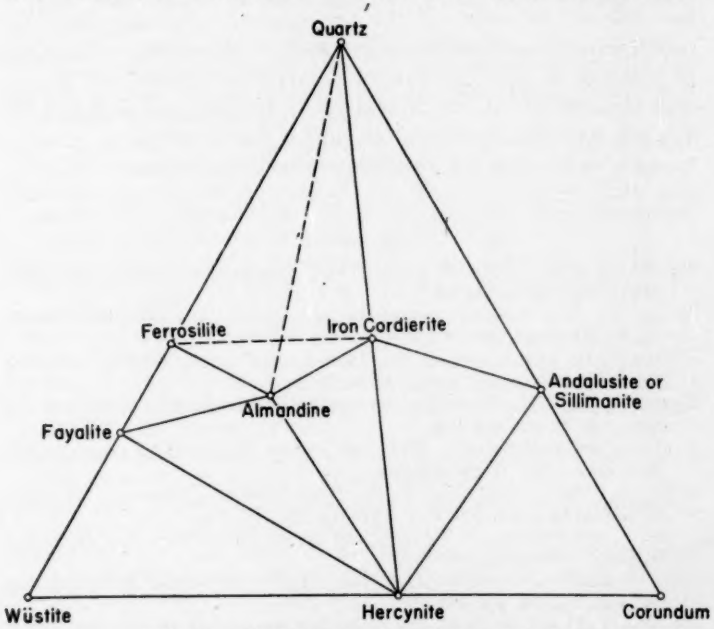

Fig. 10. Mineral assemblages below 900° C.

region such as Amataki volcano (Takeuchi, 1941; Kozu and Yagi, 1941) and Nijo volcano (Omori, 1942) the assemblage almandine—iron cordierite—spinel is commonly observed. The garnets in these rocks are high in almandine with a variable content of the pyrope and spessartite molecules.

Some eulysites from Manchuria contain almandine (with a small amount of the grossularite molecule), ferrosilite (a high iron orthopyroxene), magnetite and quartz (Asano, 1942) corresponding closely to the assemblage ferrosilite—almandine —quartz, and when they are plotted in FeO—Al_2O_3—SiO_2 they fall in this triangle.

The association almandine—cordierite—quartz is not common but may be represented in some granulites where garnet (pyrope—almandine) is associated with cordierite which, however, is not a typical mineral of granulite and often is replaced by almandine (Eskola, 1939). The association quartz—hypersthene—cordierite is quite common in ordinary hornfels of classes 4 and 5 of Goldschmidt (1911). The corresponding iron-rich combination ferrosilite—iron cordierite—quartz may be expected in some of the ferruginous hornfels. Since the combination iron cordierite—ferrosilite—almandine is unknown or uncommon, the lines ferrosilite—iron cordierite and almandine—quartz are shown tentatively as broken lines in figure 10. We still have much to learn about mineral associations in metamorphic rocks and the conditions which limit them.

References

Alderman, A. R., 1935. Almandine from Botallack, Cornwall: Mineralog. Mag., vol. 24, pp. 42-48.

Asano, G., 1942. Studies of eulysite or eulysitic iron ore: Manchoukuo Geol. Inst. Mem. 17.

Bailey, E. B., and Maufe, H. B., 1916. Geology of Ben Nevis and Glen Coe: Scotland Geol. Survey Mem. 53.

Bowen, N. L., 1935. Ferrosilite as a natural mineral: Am. Jour. Sci., 5th ser., vol. 30, pp. 481-494.

———, and Greig, J. W., 1924. The system Al_2O_3—SiO_2: Am. Ceramic Soc. Jour., vol. 7, pp. 238-254.

———, ———, and Zies, E. G., 1924. Mullite, a silicate of alumina: Washington Acad. Sci. Jour., vol. 14, pp. 183-191.

———, and Schairer, J. F., 1932. The system FeO—SiO_2: Am. Jour. Sci. 5th ser., vol. 24, pp. 177-213.

———, and ———, 1935. The system MgO—FeO—SiO_2: Am. Jour. Sci. 5th ser., vol. 29, pp. 151-217.

———, and ———, 1938. Crystallization equilibrium in nepheline-albite-silica mixtures with fayalite: Jour. Geology, vol. 46, pp. 397-411.

———, ———, and Posnjak, E., 1933*a*. The system Ca_2SiO_4—Fe_2SiO_4: Am. Jour. Sci., 5th ser., vol. 25, pp. 273-297.

———, ———, and ———, 1933*b*. The system CaO—FeO—SiO_2: Am. Jour. Sci., 5th ser., vol. 26, pp. 193-284.

Brauns, R., 1911. Die Kristallinen Schiefer des Laachersee Gebietes und ihre Umbildung zu Sanadinite, Stuttgart.

Bücking, H., 1900. Cordierit von Nord-Celebes und aus den sog. verglasten Sandsteinen Mitteldeutschlands: Ber. Senck. Naturfor. Gesell. Frankfurt, Wiss. Abh., vol. 31, pp. 3-20.

Clarke, F. W., and Washington, H. S., 1922. The average chemical composition of igneous rocks: Nat. Acad. Sci. Proc., vol. 8, pp. 108-115.

Eskola, P., 1939. Die Enstehung der Gesteine. Die metamorphen Gesteine, Berlin.

Fermor, L. L., 1924. In discussion on paper by C. E. Tilley entitled "Contact-metamorphism in the Combrie Area of the Perthshire Highlands": Geol. Soc. London Quart. Jour., vol. 80, pp. 22-71; discussion pp. 70-71.

Goldschmidt, V. M., 1911. Die Kontacktmetamorphose im Kristianiagebiet: Vidensk. Skr. I, Mat.-naturv. Kl. no. 11.

Greig, J. W., 1927. On liquid immiscibility in the system FeO—Fe_2O_3—Al_2O_3—SiO_2: Am. Jour. Sci., 5th ser., vol. 14, pp. 473-484.

Hay, R., White, James, and Caulfield, T. H., 1937. The ternary system FeO—Al_2O_3—SiO_2: Glass Technology Soc. Jour., vol. 21, pp. 270-280.

Herty, C. H., 1934. Physical chemistry of steel making: Carnegie Inst. Tech., Mining and Met. Inv., Coop. Bull. 69, p. 17.

Kozu, S., and Yagi, K., 1941. Chemical studies of garnet and its mother rock from Amtaki: Japanese Assoc. Min. Pet. Econ. Geology Jour., vol. 26, pp. 73-93.

Kracek, F. C., 1939. Phase equilibrium relations in the system Na_2SiO_3—Li_2SiO_3—SiO_2: Am. Chemical Soc. Jour., vol. 61, pp. 2863-2877.

Levin, S. B., 1950. Genesis of some Adirondack garnet deposits: Geol. Soc. America Bull., vol. 61, pp. 519-565.

McIntosh, A. B., Rait, J. R., and Hay, R. 1937. The binary system FeO—Al_2O_3: Royal Tech. College Glasgow Jour., vol. 4, pp. 72-76.

Morimoto, R., 1947. On the mode of occurrence of cordierite from Sakkabira, Town Tarumizu, Kimotsuki Province, Kagoshima Prefecture, Japan: Earthquake Res. Inst. Bull., vol. 25. 33-35.

Omori, K., 1942. Studies of garnets in the andesites forming the volcano Nijo-san.: Japanese Assoc. Min. Pet. Econ. Geology Jour., vol. 27, pp. 27-55, 69-87.

Palmgren, J., 1917. Die Eulysite von Sondermannland: Upsala Univ., Geol. Inst. Bull. 14.

Ramdohr, P., 1927. Die Eisenerzlager des Oberharzer Diabaszuge und ihre Verhalten im Bereich des Brockenkontakts: Neues Jahrb., Beilage-Band 55, pp. 333-392.

Rankin, G. A., and Merwin, H. E., 1918. The system MgO—Al_2O_3—SiO_2: Am. Jour. Sci., 4th ser., vol. 45, pp. 301-325.

———, and Wright, F. E., 1915. The system CaO—Al_2O_3—SiO_2: Am. Jour. Sci., 4th ser., vol. 39, pp. 1-79.

Richardson, H. M., and Rigby, G. R., 1949. The occurrence of iron cordierite in blast furnace linings: Mineralog. Mag., vol. 28, pp. 547-556.

Schairer, J. F., 1942. The system CaO—FeO—Al_2O_3—SiO_2: I. Results of quenching experiments on five joins: Am. Ceramic Soc. Jour., vol. 25, pp. 241-274.

———, and Bowen, N. L., 1947. Melting relations in the systems Na_2O—Al_2O_3—SiO_2 and K_2O—Al_2O_3—SiO_2: Am. Jour. Sci., vol. 245, pp. 193-204.

Shibata, H., 1936. Graphic intergrowth of cordierite and quartz in pegmatites from Sasago and Dosi, Province of Kai, Japan: Japanese Jour. Geol. Geog., vol. 13, pp. 205-227.

Snow, R. B., 1937. Equilibrium studies in the system FeO—Al_2O_3—SiO_2: Abstracts of Doctors' Dissertations, Ohio State University Press, No. 21, pp. 327-338.

———, 1943. Equilibrium relationships on the liquidus surface in part of the MnO—Al_2O_3—SiO_2 system: Am. Ceramic Soc. Jour., vol. 26, pp. 11-20.

———, and McCaughey, W. J., 1942. Equilibrium studies in the system FeO—Al_2O_3—SiO_2: Am. Ceramic Soc. Jour., vol. 25, pp. 151-160.

Sugi, K., 1931. Contact metamorphism, Iwani Koza Geol. Min., Tokyo.

Takeuchi, T. 1941. Studies of garnet and of its country rock from Amataki: Japanese Assoc.. Min. Pet. Econ. Geology Jour., vol. 26, pp. 33-60.

Thomas, H. H., 1922. On certain xenolithic tertiary minor intrusions in the island of Mull (Argyllshire): Geol. Soc. London Quart. Jour., vol. 78, pp. 229-260.

Tilley, C. E., 1923. Paragenesis of the minerals of the three-component system MgO—Al_2O_3—SiO_2 in thermal metamorphism: Geol. Mag., vol. 60, pp. 101-107.

———, 1926. On garnet in pelitic contact-zones: Mineralog. Mag., vol. 21, pp. 47-50.

———, 1936. Eulysites and related rock types: Mineralog. Mag., vol. 24, pp. 331-342.

von Eckermann, H., 1922. The rocks and contact minerals of the Mansjö Mountain: Geol. fören Stockholm Förh., vol. 44, pp. 203-410; especially pp. 253-293.

Watanabe, T., 1943. Geology and mineralization of the Suian District, Korea—the geology of the Suian gold mining district: Fac. Sci. Hokkaido Univ. Jour., 4th ser., vol. 6, pp. 205-303.

J. F. Schairer
Geophysical Laboratory, Carnegie Institution of Washington
Washington, D. C.

Kenzo Yagi
Department of Geology
Tohoku University
Sendai, Japan

SINGLE-CRYSTAL MEASUREMENTS ON PARACELSIAN

J. V. SMITH

ABSTRACT. The cell dimensions and space group of paracelsian have been determined and these have been compared with those of topaz and danburite. There is a close similarity between paracelsian and danburite.

PARACELSIAN, $BaO \cdot Al_2O_3 \cdot 2SiO_2$, was first described in detail by Spencer (1942). His goniometric measurements showed that the crystals have orthorhombic morphology but his optical measurements could be rationalized only if the crystals were assumed to have lower symmetry. Twinning and striations, indicating lower symmetry, were observed.

X-ray measurements have now been made on several crystals obtained from Spencer's original material. All of these were found to be single crystals with the following crystal properties:

From precession photographs (not assumed to be orthorhombic)	From Geiger-counter spectrometer (assumed to be orthorhombic)
$a \sin \beta = 9.02 \pm 0.09$Å	$a' = 9.076 \pm 0.005$Å
$b = 9.50 \pm 0.09$Å	$b = 9.583 \pm 0.005$Å
$c \sin \beta = 8.47 \pm 0.09$Å	$c' = 8.578 \pm 0.005$Å
$\beta = 90° \pm 0.5°$	using CuK_{a1}, $\lambda = 1.54050$Å
using MoK_a, $\lambda = 0.7107$Å	CuK_{a2}, $\lambda = 1.54434$Å

Using the density found by Spencer, 3.31, there are 4(calc. 3.95) units of $BaO \cdot Al_2O_3 \cdot 2SiO_2$ in the unit cell. The more accurate measurements give $a' : b : c' = 0.9471 : 1 : 0.8952$ which compare well with Spencer's goniometric axial ratios $a : b : c = 0.9470 : 1 : 0.8956$.

Comparison of intensities on single-crystal photographs showed that the crystals are monoclinic. There are pseudo-mirror planes of symmetry parallel to (100) and (001), and the mismatch of intensities over these planes is very small. The crystals therefore are very markedly pseudo-orthorhombic. Systematic absences were found only for reflections with h odd in ($h00$), k odd in ($0k0$), l odd in ($00l$), h odd in ($h0l$). In addition systematic absences for reflections with $(k + l)$ odd in ($0kl$) were at first found. However, long-exposure photographs revealed a few very weak reflections with $(k + l)$ odd in ($0kl$). The space group is therefore $P2_1/a$, assuming that reflections with k odd in ($0k0$) are truly absent; if not, the

space group is P2/a or Pa. The crystals are in pseudo space groups Pna or Pnam.

Optical measurements, kindly carried out by W. S. MacKenzie of this Laboratory, showed that a ≅ X, b = Z, c ≅ Y, $2V = 52.7° + 0.5°$ (sodium light), optically negative. Spencer found that $\alpha = 1.5702$, $\beta = 1.5824$, $\gamma = 1.5869$, optically negative, $2V = 50°\ 35'$ (sodium light). MacKenzie found that the isogyres in convergent polarized light were single, and no peculiar effects (as described by Spencer) occurred upon rotation of the crystal in convergent polarized light.

Spencer pointed out the "very remarkable agreement between the (goniometric) angles of paracelsian and those of topaz and danburite." Comparison of the X-ray properties of the crystals further extends this agreement.

By interchanging the x and y axes of paracelsian, we have the following comparison:

	Paracelsian	Topaz	Danburite
Axial ratios..	1.056 : 1 : 0.9456	1.0570/2 : 1 : 0.9540	1.0888 : 1 : 0.9614
a	9.58Å	4.64Å	8.75Å
b	9.08Å	8.78Å	8.01Å
c	8.58Å	8.38Å	7.72Å
Space group..	Pbnm (pseudo)	Pbnm	Pbnm
Composition..	$BaAl_2Si_2O_8$	$Al_4F_4Si_2O_8$	$CaB_2Si_2O_8$
No. of units in unit cell ..	4	2	4

The structures of topaz (Pauling, 1928; Alston and West, 1928) and danburite (Dunbar and Machatschki, 1930) are known, whereas the structure of paracelsian is unknown. Comparison of the properties given above suggests that the structure of paracelsian may be similar to that of topaz or that of danburite (there is no obvious relation between the structures of topaz and danburite). It appears more likely that the structure of paracelsian is similar to that of danburite, with the calcium replacing the barium and the aluminium replacing the boron. If this were true, then the increased axial lengths[1] of paracelsian would be expected because the ionic radii of barium and aluminium atoms are respectively larger than the radii

[1] Note added in proof. The structure of paracelsian has now been determined and it is indeed similar to that of danburite. Full details will be published elsewhere.

of calcium and boron atoms. The increase in the axial lengths is approximately that to be expected from the theoretical ionic radii.

The structure of celsian, which has the same chemical composition as paracelsian, is similar to that of orthoclase (Taylor, Darbyshire and Strunz, 1934). There is no obvious relation between the axial lengths and space groups of paracelsian and celsian.

Weissenberg and precession photographs have been taken in preparation for a structure determination.

ACKNOWLEDGMENTS

I am grateful for the assistance given by G. L. Davis, W. S. MacKenzie, and O. F. Tuttle.

REFERENCES

Alston, N. A., and West, J., 1928. The structure of topaz $[Al(F,OH)]_2SiO_4$: Zeitschr. Kristallographie, vol. 69, pp. 149-167.

Dunbar, C., and Machatschki, F., 1930. The structure of danburite, $CaB_2Si_2O_8$: Zeitschr. Kristallographie, vol. 76, pp. 133-146.

Pauling, L., 1928. The crystal structure of topaz: Nat. Acad. Sci. Proc., vol. 14, pp. 603-606.

Taylor, W. H., Darbyshire, J. A., and Strunz, H., 1934. An X-ray investigation of the feldspars: Zeitschr. Kristallographie, vol. 87, pp. 464-498.

Spencer, L. J., 1942. Barium-feldspars (celsian and paracelsian) from Wales: Mineralog. Mag., vol. 26, pp. 231-245.

GEOPHYSICAL LABORATORY
CARNEGIE INSTITUTION OF WASHINGTON
WASHINGTON, D. C.

TEMPERATURE SCALES AND SILICATE RESEARCH

ROBERT B. SOSMAN*

ABSTRACT. The temperature scale for the range 300° to the melting-point of platinum, used by the Geophysical Laboratory from 1912 to the present, was based on the nitrogen thermometer work of Day and Sosman. The first International Temperature Scale (1927) was a thermodynamic scale, with fixed points a little higher than those of Day and Sosman. The revision of the I.T.S., adopted in 1948, by raising the value of the constant in the Wien-Planck Law of radiation, brings the high-temperature scale nearer to the Geophysical Scale. Curves show the difference between the Geophysical and the I.T.S. of 1927 and 1948.

INTRODUCTION

ONE of the first problems that faced the growing group of students of high-temperature silicates in the early 1900's was the problem of the temperature scale. Precise measurements were beginning to replace the crude melting points of earlier years, but there was no accepted scale to which they could be referred.

Arthur Louis Day had received his Ph.D. at Yale University in 1894 and, after serving there as instructor in physics for a few years, had taken up work on high-temperature gas thermometry at the Physikalisch-Technische Reichsanstalt in Germany. When he became the first Director of the Geophysical Laboratory of the Carnegie Institution of Washington in 1907, it was natural that the first large piece of apparatus installed in the new laboratory should be a gas thermometer, designed for improved accuracy of measurement of the most essential variable in high-temperature research on silicate systems.

In 1908 I had the good fortune to become associated with Day and Allen in the Laboratory's work on high-temperature thermometry, and I assisted in the development of a temperature scale that met the needs of the Laboratory in the range between the melting point of zinc (419° C.) and the melting point of palladium (1549° C.).

This work was completed in 1912, and we turned back to our natural field of work, the mineral oxides, sulfides, and silicates. In the years 1928-1947 I found myself deep in

* Visiting Professor of Ceramics, Rutgers University (State University of New Jersey), New Brunswick, New Jersey.

pyrometry again, in the Research Laboratory and the plants of the United States Steel Corporation; hence I have never lost interest in the problem of temperature scales.

In what follows I shall have little to say about the instruments of high-temperature thermometry used in silicate research—the thermocouple, the electrical resistance thermometer, and the optical pyrometer—but will concentrate on the vicissitudes of the temperature scale itself during the period 1907-1948.

TEMPERATURE SCALES

Before 1848, science had no universal temperature scale. It had a lot of competing scales, differing one from another at every point except at the freezing and boiling points of water, and there was no good ground for choosing one in preference to another except the convenience of the experimenter. The scale went with the thermometer.

In 1848, William Thomson (later Baron Kelvin) pointed out that a temperature scale independent of the properties of any substance can be defined in terms of the convertibility of heat into other forms of energy. It is only necessary to select two reproducible temperatures, such as the temperature of equilibrium of ice and water in air at one atmosphere (the "ice point"), and the temperature of equilibrium of water and its vapor at a pressure of one atmosphere (the "steam point"), and give an arbitrary quantitative value, say 100°, to the difference between them, just as we do when we say that the distance between two marks on a certain platinum bar shall be called 1 meter; we must then adopt, arbitrarily, some mathematical relationship between temperature and quantity of energy, and the scale is set. Kelvin adopted the relationship $Q_1/Q_2 = \theta_1/\theta_2$, in which Q_1-Q_2 is the amount of heat reversibly converted by a thermodynamic engine into other forms of energy when its temperature falls from θ_1 to θ_2. The absolute value of any temperature could then be experimentally measured; the temperature of the ice point, for example, turns out to be 273.16°. The steam point, consequently, is 373.16°. These are temperatures on the *absolute thermodynamic scale* or the *Kelvin thermodynamic scale.*

By subtracting the experimentally determined value of

273.16° from all temperatures of the Kelvin scale, we create the more familiar *Celsius thermodynamic scale*[1] with its ice point of 0°.

PRECISE THERMOMETRY

It is one thing to define an independent scale such as the Kelvin. It is quite another to realize it experimentally in a form that permits high precision of measurement. In principle, any scale whatever can be evaluated in terms of either the Kelvin or the Celsius thermodynamic scale, provided the necessary energy data are available. Actually, only two varieties of temperature scale have met the requirements, which have to do, first, with the precision of the measurement, second, with the definiteness of the thermodynamic relations. They are: the gas thermometer scales, up to temperatures near 1600° C. where materials of construction begin to fail; and the optical pyrometer scale, from about 1000° C. up into indefinitely high temperatures.

Now to return to the matter of precision. Precise thermometry need not wait upon the realization of a thermodynamic scale any more than precise measurements of mass needed to wait upon the determination of the density of water. Precise weighing became possible as soon as a sensitive balance was constructed and a reproducible standard kilogram was accepted, no matter whether it represented accurately the mass of a cubic decimeter of water or not. So precise thermometry in the range −30° to +200° C. followed upon the development of special glasses for the mercury-in-glass thermometer; it spread out to cover the range −180° to +600° C. with the development of the hydrogen and nitrogen gas thermometers employing vitreous silica; reached on up past 1100° C. with the invention of the platinum resistance thermometer; and attained over 1700° C. with the construction by Carl Barus and Henri Le Chatelier of thermocouples made from the platinum-group metals. All these thermometers were capable of precise measurement in varying degree; none gave directly the temperature on the independent thermodynamic scale.

[1]This is the scale commonly known as the *centigrade scale*, which is a misnomer, because the Kelvin scale is also centigrade; both are based on an arbitrary difference of 100° between ice and steam points.

CALIBRATING A SCALE

Heat is such an imaginary and imponderable thing that temperature standards comparable to the standard meter and kilogram are out of the question. The standard scale has to be defined in terms of a series of fixed and reproducible temperatures combined quantitatively with reproducible phenomena. A million fixed temperatures are readily available, each determined by Gibbs' Phase Rule, which says that in a chemical system in which the number of phases in equilibrium exceeds by 2 the number of components, the temperature and the pressure can have but a single value. If the pressure be arbitrarily set, say at 1 atmosphere, the number of phases needs to exceed the number of components only by 1, in order to fix the temperature. The ice point and the steam point are fixed temperatures of this kind; whether they were the best fixed temperatures to take in defining the fundamental interval is open to question, but the matter is now academic, as they are very unlikely to be abandoned in favor of some other pair. Two points much farther apart in temperature would have been a better choice, from the standpoint of precision.

For fixed points above the fundamental interval, the freezing points of pure metals have been preferred, with boiling points of pure liquids at 1 atmosphere as next most popular choice. For interpolation between fixed points, either the electrical resistance thermometer or the thermoelectric couple is accepted, while at temperatures above the highest fixed point, as well as between the higher points, dependence is placed on the Wien-Planck Law of monochromatic radiation.

THE GAS THERMOMETERS

It was early perceived that the perfect thermometer for the realization of a thermodynamic scale is one that measures either the change of volume or the change of pressure of an ideal gas. The ideal gas is defined as one which (1) obeys Boyle's Law, $(pv)_t$ = constant, and (2) neither absorbs nor evolves heat when expanding into a vaccum.

Helium comes nearest to meeting these specifications, but helium had not even been discovered in the early decades of temperature standardization. Air, hydrogen, and nitrogen became the preferred thermometric gases.

Private initiative had already made considerable progress with gas thermometry when the national (and international) standardizing institutions began to appear in the field. The first of these was the Bureau International des Poids et Mesures at Sèvres, France, where Chappuis did his pioneering work on the hydrogen thermometer. Next followed the Physikalisch-Technische Reichsanstalt in Germany, where gas thermometry was ultimately carried to 1680° C. The National Physical Laboratory in England worked with air and nitrogen, mainly in the intermediate range of 100°-900° C. At the National Bureau of Standards of the United States, Buckingham in 1906 made the best analysis of the derivation of the thermodynamic scales from the gas scales that had been made up to that date, but the Bureau attempted no experimental gas thermometry at all, confining its interest to the optical pyrometer above 1000° C., so far as high-temperature standardization was concerned.

STATUS OF TEMPERATURE SCALES IN 1907

In 1907, then, the year in which the Geophysical Laboratory was established, there was no international temperature scale possessing the official sanction of the governments which had cooperated in establishing the international meter and kilogram. There was general satisfaction with the hydrogen thermometer scale for temperatures up to about 200° C. For higher temperatures the platinum resistance thermometer with Callendar's formula was accepted by many, while others preferred the platinum-platinrhodium thermocouple using a quadratic formula through 3 calibration points. Standard calibration points had not been agreed upon. The boiling points of water and sulfur and the melting points of ice, zinc, antimony, silver, gold, and copper were the most commonly used standard points.

Above the gold point the platinum alloy thermocouple was being extrapolated to about 1600° C., with some support from gas thermometer measurements in Germany and England. At still higher temperatures every investigator was on his own.

STATUS OF TEMPERATURE SCALES IN 1912

In 1911 the Carnegie Institution of Washington issued Publication 157, "High Temperature Gas Thermometry," by

Day and Sosman, and this was followed in 1912 by their paper on "The Nitrogen Thermometer Scale from 300° to 630°, with a Direct Determination of the Boiling Point of Sulphur," which supplied more accurate data for the lower part of the scale. These papers became the basis for the Geophysical Laboratory's scale of temperature for the range 300° C. to 1755° C.

The original temperatures were on the *constant-volume nitrogen scale with initial pressure* 200-500 *mm. of mercury.* Buckingham's calculations, made from a variety of experimental data on thermometric gases, had shown that the corrections to convert the Day and Sosman nitrogen scale to true thermodynamic temperatures are positive, and do not exceed 1° at any temperature up to 1500° C. The corrections increase with the initial pressure of nitrogen and with the temperature, and become more uncertain as the temperature rises. Thermodynamic corrections of 0.1° to 0.2° were applied to the Day and Sosman scale below 650° C., but the higher temperatures were at first left unchanged.

In 1914 L. H. Adams, following up a preliminary note by Johnston and Adams in 1912, reviewed the status of the Geophysical Scale and published comprehensive tables for typical copper-constantan and platinum-platinrhodium thermocouples from 0° to 1755° C., converting all the Day and Sosman fixed calibration points to thermodynamic, and expressing the relation of e.m.f. and temperature by means of formulas having e.m.f. as argument in place of temperature. The principal fixed points were:

Naphthalene	b. p.	217.95°
Benzophenone	b. p.	305.9
Zinc	m. p.	419.4
Sulfur	b. p.	444.55
Antimony	m. p.	630.0
Silver	m. p.	960.2
Gold	m. p.	1062.6
Copper	m. p.	1082.8
Diopside	m. p.	1391.5
Palladium	m. p.	1549.5
Platinum	m. p.	1755.

This scale is still used by the Geophysical Laboratory.

The nitrogen-thermometer calibration by Day and Sosman had ended at the palladium melting point, 1549.2°. Extension to

the platinum point, taken as 1755°, was based on optical pyrometer measurements at the Bureau of Standards and the Reichsanstalt, which gave the *difference* between the palladium and platinum points. The platinum point thus derived was appreciably lower than the value obtained by extrapolating the thermocouple curve, or the value that had been recently obtained in Germany with a small and consequently less precise nitrogen thermometer with an iridium bulb. The value 1755° was, however, acceptable to the Bureau of Standards and was used there in the calibration of pyrometers for a number of years.

THE INTERNATIONAL SCALE OF 1927

After World War I the international conference finally got around to the matter of a temperature scale. Scheduled to meet every six years, the General Conference on Weights and Measures, representing 33 nations, elects 18 scientists to an International Committee on Weights and Measures, which thereupon meets every two years. Their recommendations as to a temperature scale were adopted by the Seventh General Conference in 1927, and were widely accepted under the designation *International Temperature Scale of 1927*.

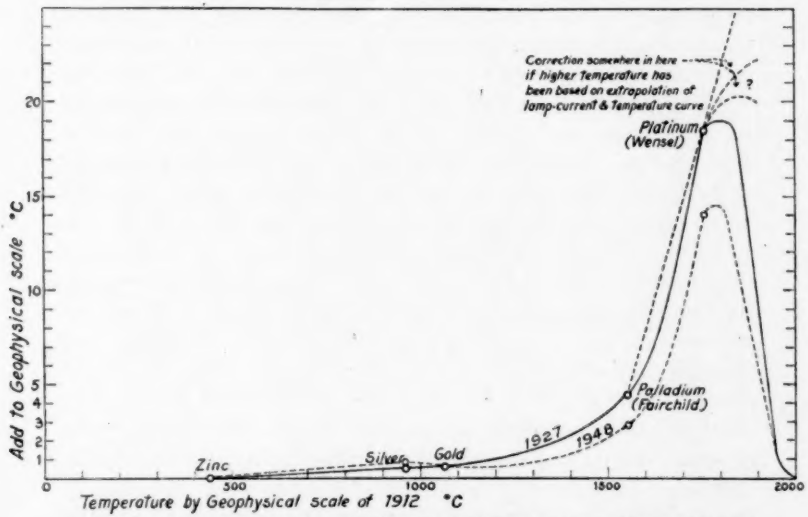

Fig. 1. Corrections to the Geophysical Laboratory temperature scale of 1912, to convert to International Temperature Scale of 1927 and of 1948.

The fixed points of this scale, in addition to ice and steam, were: oxygen and sulfur boiling points, — 182.97° and 444.60°; silver and gold freezing points, 960.5° and 1063°. Above the gold point the scale was based on this point and on the Wien formula for the intensity, $J_{\lambda T}$, of monochromatic radiation:

$$J_{\lambda T} = c_1 \lambda^{-5} e^{-c_2/\lambda T}$$

in which T is Kelvin temperature, λ is wave-length, c_1 and c_2 are constants, and e is the base of natural logarithms. Since all temperatures are related to the gold point as a standard, the value of c_1 does not have to be specified, but c_2 has to be known; its value was set at 1.432 cm. degrees.

The International Scale of 1927 made some significant departures from the Geophysical Scale based on the work of Day and Sosman. The silver point was set 0.3° higher, gold 0.4° higher, and palladium 5.5° higher than their value. The most important effect in the high-temperature region was on the freezing point of platinum, which was presently shown by the optical pyrometer measurements of Wensel and Roeser to be unquestionably higher than the extrapolated value previously quoted; the new datum was 1773.

The atlas of four large-scale ternary phase equilibrium diagrams of silica, alumina, lime, and magnesia, prepared by Sosman and Andersen from Geophysical Laboratory data and published by the Research Laboratory of the United States Steel Corporation in 1933, was probably the first publication on silicates to use the I.T.S. of 1927. Investigators at the Geophysical Laboratory continued to use the scale adopted in 1914, so that their temperatures remained consistent. The difference between the Geophysical Scale and the 1927 I.T.S. is shown in figure 1. The rather odd shape of this curve emphasizes the fact that most recorded temperatures up to the freezing point of platinum could be referred to a reliable standard, either the melting point of a silicate or the freezing point of palladium or platinum, and that the really important changes were in the interval 1550° to 1773°. Above 1773° the basis of calibration of the silicate and oxide points was, in many cases, too uncertain to make a definite correction feasible, although in most of the Geophysical Laboratory measurements a stated melting point of platinum had been used, so that it became possible to make an approximate cor-

rection of temperatures between 1750° and 2050° C. There was no good reason for making any change in the very high and somewhat uncertain melting points of the pure basic oxides: MgO, 2800°, and CaO, 2570°.

EVIDENCE FROM AN UNANTICIPATED SOURCE

During the 1930's a new line of evidence, to which the International Committee of 1927 had given little if any attention, began to influence physicists concerned with the high-temperature scale. Since physical measurements can all be reduced to five elementary concepts—length, mass, time, electric charge, and temperature (or entropy)—the fundamental constants of physicochemical science must bear certain necessary relations to one another. Consistency among the constants gives independent evidence as to the reliability of any one of them.

In 1926 R. T. Birge began a thorough-going intercomparison among 11 fundamental constants, including the speed of light, Faraday's electrochemical constant, Rydberg's spectroscopic constant, Avogadro's number, the volume of a mole of the ideal gas, the pressure of the standard atmosphere, and the ice point on the Kelvin scale. Among constants derived from the foregoing 7 are: the charge of the electron e, the constants c_1 and c_2 of the Wien-Planck law of monochromatic radiation, and the constant σ of the Stefan-Boltzmann law of total radiation.

In 1929 the consistency was satisfactory throughout, except for a disagreement between two methods for determining e. This was cleared up in 1935. In the meantime a new discrepancy turned up, between Millikan's value for e by the oil drop method and the value derived from the grating measurement of X-ray wave lengths. New data correcting Millikan's viscosity of air resolved this difference, but immediately introduced several new discrepancies, of which the worst were in c_2 and σ.

THE INTERNATIONAL SCALE OF 1948

The conviction spread, among physicists interested in the subject, that c_2 would have to be raised, for it was evident that the others would then fall into line. A correction could and should have been made in 1939, for the newly created (1937) Advisory Committee on Thermometry was ready with

a report to the International Committee, but World War II interrupted everything international. A new scale (Stimson, 1949) was finally adopted by the Ninth General Conference in October, 1948, and became the *International Temperature Scale of 1948.*

The two most important changes from the 1927 scale are: (1) the melting point of silver is raised from 960.5° to 960.8°; (2) the value of c_2 is raised to 1.438. In effect, this latter change nearly restores the Geophysical Scale in the vicinity of 1550° C., for the Day and Sosman gold and palladium points corresponded to $c_2 = 1.439$. (Note: an *increase* of 0.010 in c_2 at 1550° is equivalent to a *decrease* of 4.0° in the temperature.) The change from the Wien to the Wien-Planck radiation formula

$$J_{\lambda T} = c_1 \lambda^{-5} (e^{c_2/\lambda T} - 1)^{-1}$$

does not appreciably change any temperature below about 3500° C.

On the basis of the 1948 scale, the corrections made by Sosman and Andersen in 1933 at 1550° C. and lower, none of which exceeded + 5° C., are reduced to about 2/3 their former magnitude, and the original Geophysical temperatures can usually be left unchanged without error beyond the experimental uncertainty. Temperatures above 1550°, however, will still have to be proportionately increased, as in figure 1, to bring them into line with the International Scale. The melting point of pure silica as cristobalite, for example, originally 1713°, becomes 1723° C.

It should be emphasized again that the standard calibration points recommended for the International Scales of both 1927 and 1948 are temperatures on the Celsius thermodynamic scale. The two methods recommended for interpolation between these temperatures in the range −183° to 1063° C., however, are strictly methods of interpolation, and their accuracy is not involved in the choice between the gas thermometer scales (hydrogen, helium, nitrogen), and the thermodynamic scale. Enough intermediate points have been checked with the hydrogen, helium, or nitrogen thermometer to assure that the interpolated temperature is not off the Celsius thermodynamic scale by more than a fraction of a degree. The International Committee does, in fact, give certain secondary fixed points

for calibration purposes; these include the freezing points of lead, 327.3°; zinc, 419.5°; antimony, 630.5°; and aluminum, 660.1°.

Above 1063° the temperatures are *per se* thermodynamic, because the Wien-Planck law, originally proved by reference to gas-thermometer temperatures, corrected to thermodynamic, between 1000° and 1600°, is now so thoroughly grounded in theory and in measurement as to be virtually a definition.

Calibration points recommended in this region, points between which the platinum-platinrhodium couple with quadratic formula will doubtless continue to be used for interpolation, though not included as a part of the I.T.S., are the freezing points of copper, 1083°; nickel, 1453°; cobalt, 1492°; palladium, 1552°; and platinum, 1769°. In silicate research, particularly when the quenching method is to be used, melting points such as those of diopside ($CaMgSi_2O_6$) at 1392° C. and anorthite ($CaAl_2Si_2O_8$) at 1552° C. (both I.T.S., 1948) are more convenient.

THE KELVIN SCALE

An international Kelvin or absolute thermodynamic scale, not yet adopted, except in principle, by the General Conference, would involve an entirely distinct international agreement, such as the proposal made by the Advisory Committee on Thermometry in 1939, that the best value of the ice point is 273.15° K. American scientists have usually used the value 273.16°. Addition of either of these values to a temperature measured on the Celsius thermodynamic scale gives the Kelvin temperature with any desired accuracy to ± 0.01°.

THE FAHRENHEIT SCALE

Nothing has been said in foregoing pages concerning the Fahrenheit scales because they are never used in silicate research. It is unfortunate that two scales with different fundamental intervals have come into general use, when either one would have served the purpose. The only advantage possessed by the Celsius scale is that its zero is at the lower end of the fundamental interval. There is nothing decimal about it, and nothing that has any relation to the meter and kilogram.

If we call the interval between ice and steam points 180° instead of 100°, we will have the *Rankine thermodynamic scale*

on which the ice point is 491.67°. If now we subtract the figure 459.67 from all temperatures on this scale, we will have a *Fahrenheit thermodynamic scale*, parallel to the Celsius, but with a zero 32° below the ice point and not defined by any naturally reproducible fixed temperature.[2]

The persistence of the Fahrenheit scale after the scientific world had adopted the Celsius is, I suspect, the result of economic inertia, first of the British, then of the American instrument manufacturers. Sixty years ago either scale could have been discontinued without much monetary loss, but so many millions of dollars are now invested in thermometers, pyrometers, and temperature control mechanisms that the replacement of either scale by the other is now hopeless, except by the methods used by Genghis Khan and Tamerlane.

Reference

Stimson, H. F., 1949, The international temperature scale of 1948: Bur. Standards Jour. Research, vol. 42, pp. 209-217. Research Paper RP 1962.

Rutgers University
New Brunswick, New Jersey

[2]Logically, the International Celsius is now no longer different from the Fahrenheit in this respect, for the new definition of the Celsius zero is "the temperature 0.0100 degree below that of the triple point of pure water." This definition was adopted because the invariant point of equilibrium between ice, water, and water vapor is more precisely reproducible than the old ice point.

SOME TRENDS OF BASALTIC MAGMA IN LIMESTONE SYNTEXIS

C. E. TILLEY

ABSTRACT. The trend of basaltic magma consequent on limestone reaction is considered in the light of new data from the contact zones of Camas Mòr, Muck, and Scawt Hill, County Antrim in the British Tertiary igneous province. The chain of reaction products—melilitic theralites, melilitic nepheline dolerites and the derivative nepheline dolerites—expresses the trend of a residual liquid in which the concentration of iron relative to magnesia is strongly emphasized. In this and other features these assemblages present a contrast to the more common mafic alkali rocks of the type of nepheline basalt, nephelinite, and their melilitic and monticellite-bearing varieties. Some reference is made to the genetic features of these latter rocks and to the problem of the desilication of granitic liquid by limestone syntexis.

THE British Tertiary igneous province has now provided a number of examples demonstrating the production on a small scale of basic feldspathoidal rocks by reaction of basic igneous magma with carbonate sediments. Since the original detailed account of such rock types at Scawt Hill, County Antrim (Tilley and Harwood, 1931), a preliminary description has been given of a somewhat similar development at Camas Mòr, Muck, in the Inner Hebrides (Tilley, 1947), while more recently still, a third example has been very briefly recorded from Ardnamurchan (Agrell, 1950). At each of the localities named the participating liquid was basaltic in character, the carbonate rocks at Scawt Hill being pure limestone (chalk), those at Camas Mòr, more variable, in part dolomitic as revealed in contact metamorphic assemblages bearing melilite, monticellite and periclase.

In the light of accumulating chemical data I propose to supplement the preliminary statement on the Camas Mòr assemblages and to take stock of the position now reached by reviewing the trend of the contamination processes which have operated both there and at Scawt Hill and to compare the products with normal mafic alkali rocks. It may be recalled that at Camas Mòr, Muck, a great vertical dike of olivine gabbro about 30 yards broad intersecting Jurassic limestones is bordered by narrow zones of pyroxenite with theralite and nepheline gabbro carrying titanaugite, melilite, analcime and zoned iron-wollastonite solid solutions, the last partly in intimate intergrowth with nepheline. Monzonitic and shonkinitic

lenses carrying abundant sanidine and a fayalitic olivine also appear in the border zones. These rocks are associated with clinopyroxene, wollastonite, sanidine, analcime assemblages which have resulted from the soaking of the limestones by solutions emanating from the modified gabbro. The reaction processes in the endogenous zone were held to resemble those responsible for the development of the hybrid zones at Scawt Hill, though some of the products exhibit distinctive characters.

As some additional analyses of Scawt Hill assemblages have later become available, these have been tabulated along with some relevant analyses already published (table 1, nos. 1-6; nos. 4, 5 and 6 are new analyses). Comment on these new analytical data from Scawt Hill will be made in the sequel.

In table 2 are given the analyses of some of the chief rock types of the Camas Mòr occurrence. They include that of the olivine gabbro, its hybrid reaction products, and a typical skarn and hornfels, and succeeding tables present the compositions (with optical data for which I am indebted to Dr. I. D. Muir) of the clinopyroxene and olivine of the main gabbro and its mode (tables 3 and 4).

The texture of the gabbro indicates that the olivine and clinopyroxene overlapped in their crystallization ranges and the analyses reveal that the olivine (Fa_{62}) is less magnesian than the associated clinopyroxene ($Wo_{42}\,En_{33}\,Fs_{25}$) in correspondence with the experimental results for the magnesia-iron clinopyroxenes and olivines of the system MgO—FeO—SiO_2 (Bowen and Schairer, 1935). Basic igneous rocks of comparable iron enrichment are uncommon among analyzed types in the British Tertiary province, the nearest example being an olivine-tholeiite of Salen type from Mull.

A closer comparison is afforded by the average of two "middle gabbros" of the Skaergaard instrusion of East Greenland as shown in table 2, no. 12. The Skaergaard "middle gabbros" show the presence of two pyroxenes and contain only very subordinate olivine as a rim mineral though the norms of their analyses show substantial amounts of this mineral. In figure 1 further comparison is made with the East Greenland assemblages. The position of the Camas Mòr gabbro clinopyroxene is shown in relation to the trend of the clinopyroxene succession in the Skaergaard layered intrusion (Muir, 1951, pp. 701, 710), and also the relation of the clinopyroxene-

TABLE 1

	1	2	3	4	5	6
SiO_2	47.55	46.77	42.24	44.61	45.93	45.26
Al_2O_3	16.18	14.93	13.16	12.44	12.18	18.48
Fe_2O_3	2.46	2.20	4.48	3.71	4.06	1.62
FeO	8.35	5.65	12.61	11.69	13.32	7.62
MgO	8.62	7.87	1.66	3.00	3.21	9.23
CaO	11.86	17.87	13.66	15.42	10.08	11.41
Na_2O	2.19	1.50	3.84	3.04	3.51	1.98
K_2O	0.35	0.29	0.78	0.52	1.30	0.10
H_2O+	0.80	1.72	4.48	2.10	2.07	2.40
H_2O-	0.42	0.24	0.48	0.24	0.63	0.93
CO_2	0.03	0.16	0.12	0.18	.....	.....
TiO_2	1.11	1.06	1.81	2.65	3.00	0.83
P_2O_5	0.14	0.28	0.60	0.31	0.63	0.10
MnO	0.16	0.09	0.30	0.26	0.32	0.16
BaO	0.02	tr.	0.06	.....	.....	.....
S	.....	0.02	0.21	.....	.....	.....
	100.24	100.65	100.49	100.17	100.24	100.12

Norms

		4		5		6	
Or		2.78		7.78		0.56	
Ab		12.84		24.76		16.77	
Ne		6.96		2.49		.....	
An		18.90		13.90		41.14	
Di	Wo	21.46	43.48	13.69	27.79	6.15	11.93
	En	7.50		4.60		3.80	
	Fs	14.52		9.50		1.98	
Wo		1.28		.....		.....	
Hyp	En	.....		.....		3.10	4.55
	Fs	.....		.....		1.45	
Ol	Fo	.....		2.38	7.89	11.34	17.66
	Fa	.....		5.51		6.32	
Mt		5.34		5.80		2.32	
Il		5.02		5.78		1.52	
Ap		0.67		1.34		0.34	
Ct		0.51		.....		.....	
H_2O		2.34		2.70		3.33	
		100.12		100.23		100.12	

1. Olivine dolerite .....
2. Pyroxene-rich dolerite ..... } Scawt Hill (Tilley and Harwood, 1931, p. 448)
3. Nepheline (hydronephelite) dolerite .....

4. Titanaugite dolerite with analcime, vein on vertical face, Scawt Hill .....
5. Anorthoclase-fayalite-dolerite segregation vein on vertical face, Scawt Hill ..... } Analyst, J. H. Scoon
6. Olivine dolerite bounding vein (5) .....

TABLE 2

	9	10	11	12	13	14
SiO_2	46.24	41.38	38.63	46.90	55.20	34.18
Al_2O_3	17.21	9.81	10.16	16.55	12.17	9.51
Fe_2O_3	2.89	4.17	4.10	2.96	0.48	0.03
FeO	12.19	15.88	13.18	12.18	6.88	4.08
MnO	0.22	0.30	0.31	0.14	0.05	0.19
MgO	5.01	5.29	1.79	5.80	4.37	2.88
CaO	9.60	13.67	19.36	9.67	10.17	42.84
Na_2O	3.18	1.79	1.35	2.97	0.96	0.22
K_2O	0.28	0.93	1.96	0.21	7.17	1.25
H_2O+	0.42	1.38	1.82	0.21	0.58	0.51
H_2O-	0.56	0.34	0.33	0.05	0.35	0.06
TiO_2	2.08	4.06	3.12	2.61	0.78	0.54
P_2O_5	0.28	0.34	0.93	0.06	0.66	.....
CO_2	0.17	1.02	2.62	.....	0.44	3.40
S	.....	.....	0.35	.....	.....	0.08
	100.33	100.36	100.01	100.31	100.26	99.77
Less O = S	.....	.....	0.17	.....	.....	0.04
			99.84			99.73

Norms

	9	10	11	12	13
Orthoclase	1.67	5.56	8.34	1.25	42.81
Leucite	.....	.....	2.62	.....	.....
Albite	27.25	10.61	.....	25.15	8.38
Nepheline	.....	2.49	6.25	.....	.....
Anorthite	31.69	15.85	15.57	31.06	7.51
Diopside	10.92	36.79	38.73	13.67	29.65
Wollastonite	.....	.....	5.80	.....	.....
Hypersthene	3.71	.....	.....	8.13	4.21
Olivine	15.00	10.62	.....	11.22	2.17
Magnetite	4.18	6.03	6.03	4.29	0.70
Ilmenite	3.95	7.75	5.93	5.02	1.52
Apatite	0.67	0.70	2.02	0.20	1.51
Calcite	0.39	2.32	5.95	.....	1.00
Water ±	0.98	1.72	2.15	0.26	0.93
Pyrites	.....	.....	0.65	.....	.....
	100.41	100.44	100.04	100.25	100.39

9. Olivine gabbro, Camas Mòr, Muck .....
10. Pyroxenite, W. contact of gabbro, Camas Mòr ..... } Analyst, J. H. Scoon
11. Wollastonite-nepheline gabbro, Camas Mòr .....
12. Average of 2 "middle gabbros" Skaergaard intrusion E. Greenland (Wager and Deer, 1939, p. 97).
13. Clinopyroxene sanidine skarn, contact of gabbro, Camas Mòr ..... } Analyst, J. H. Scoon
14. Melilite-rankinite-tilleyite rock, near contact of gabbro, Camas Mòr .....

TABLE 3

	1	2	metal atoms to 6(O) in (2)			3		mol. ratios	
SiO_2	46.24	49.60	1.888	1.970		34.04	567	1.00	
Al_2O_3	17.21	1.77	0.082			0.91			
Fe_2O_3	2.89	1.56	0.041			1.46			
FeO	12.19	13.00	0.412			40.37			
MnO	0.22	0.42	0.014	1.229		0.68			
MgO	5.01	12.58	0.717		2.04	20.32	1084*	1.91	
TiO_2	2.08	1.62	0.045			0.43			
CaO	9.60	19.36	0.790	0.817		0.81			
Na_2O	3.18	0.34	0.027			.....			
K_2O	0.28	0.05	.....			.....			
H_2O+	0.42	0.07	wt %			0.09	wt % $(Fe, Mn)_2SiO_4$		61.0
H_2O-	0.56	0.02	.....			.....	Mg_2SiO_4		37.3
P_2O_5	0.28	.....	$Wo_{42}En_{33}Fs_{25}$			.....	Ca_2SiO_4		1.7
CO_2	0.17	.....	γ 1.732, $2V_\gamma$ 51°			.....			
			Sp. Gr. 3.41				α 1.742, $2V_\alpha$ 76° - 78°		
	100.33	100.39				99.11			

* RO after subtracting FeO with equivalent Fe_2O_3 and TiO_2 for magnetite and ilmenite.

1. Olivine gabbro, Camas Mòr, Muck.

2 and 3. Clinopyroxene (2) and olivine (3) of olivine gabbro (1). Analyst, J. H. Scoon.

olivine tie lines of rock types in parts of that succession to that of the Camas Mòr gabbro.

The most conspicuous reaction products in the endogenous zone of the contact are, as in the case of Scawt Hill, dense pyroxenites. In some examples the cores of the dominant clinopyroxenes are almost colorless indicating that a magnesian-rich diopsidic member was early precipitated. Assemblages of this character pass out into coarser varieties built of titanaugite, labradorite, iron ores and analcime with some sanidine. In these coarser parts the titanaugite may be fringed with alkali-amphibole of hastingsite type but this is scarce. Compared to the average olivine gabbro, the great increase in pyroxene and virtual disappearance of olivine are the chief

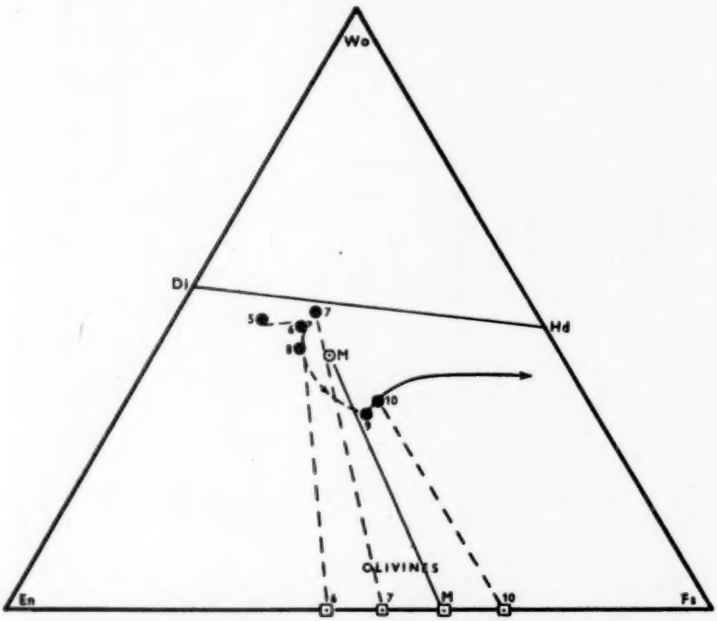

Fig. 1. Plot of the composition (weight per cent) of the clinopyroxene (M) of the Camas Mòr olivine gabbro showing its position in relation to the clinopyroxene succession of the Skaergaard intrusion of East Greenland (numbered points refer to analyses in Muir, 1951, pp. 695-696).

The tie lines join the compositions of clinopyroxenes to their associated olivines. Analyses 8 and 9 are of clinopyroxenes of the Skaergaard "middle gabbros" in which olivine is absent or present only as a rim reaction mineral.

distinguishing features. The analyses of a finer grained pyroxenite, in which the clinopyroxenes however do not exhibit the lighter colored more diopsidic cores noted above, is set down in table 2, no. 10, and an analysis of the contained clinopyroxene in table 5, no. 2. The higher FeO/MgO ratio of both rock and pyroxene compared with that of the gabbro and its pyroxene is evident from these analyses. In the rock this feature is emphasized by the greater amount of iron ore. In these characters this pyroxenite differs from the analyzed Scawt Hill pyroxene-enriched dolerite though there such iron enriched pyroxenites are also to be recognized. This point will be commented upon at a later stage in this discussion.

Wollastonite-nepheline-gabbro.—The description of this assemblage given in the earlier account may be supplemented by the analyses set down in table 2, no. 11. Particularly characteristic of this phase is the iron wollastonite solid solution in large crystals or in finger-like intergrowths with nepheline or its analcite representative.

It will be convenient to add here the analyses of a prevalent skarn at the immediate contact of the gabbro and a melilite-bearing hornfels more remote from the contact. The analysis in table 2, no. 13, gives the composition of a clinopyroxene-sanidine skarn, the composition of the contained clinopyroxene in table 6. The principal interest of the skarn analysis is the evidence it provides of a strong potash metasomatism and the similarity in composition of the clinopyroxene to that of the analysed pyroxenite.

The lime-rich hornfels (table 2, no. 14) is built of melilite (68 per cent), rankinite (12 per cent) and tilleyite (19 per cent), the last mineral a retrograde product of spurrite.

REVIEW OF THE REACTION PROCESSES

Broadly, as has been noted, the trend of the reaction processes at Camas Mòr is similar to that revealed at Scawt Hill. One variation that is distinctive is the role of potash, significant both in the contaminated products and in the skarn assemblages. At Scawt Hill, on the other hand, potash becomes significant only in the anorthoclase fayalite-bearing vein rock. The differences are brought out in figure 3 where the salic constituents (less *an*) of the norms of the rocks of the two series are

TABLE 4

	Ap	Ct	Mt	Il	Pyr	Ol	An	Ab	Or	Qz	Total	Calculated mode	
SiO_2	....	....	.....	.....	6.86	5.65	13.53	18.17	1.08	0.95	46 24		
Al_2O_3	....	....	.....	.....	0.26	.....	11.50	5.15	0.30	.....	17.21	Plagioclase (An_{54})	57.8
Fe_2O_3	....	....	2.68	.....	0.21	.....	.....	.....	.....	.....	2.89		
FeO	....	....	1.20	1.67	1.80	7.52	.....	.....	.....	.....	12.19	Clino-pyroxene	13.9
MnO	....	....	.....	.....	0.06	0.16	.....	.....	.....	.....	0.22	Olivine	16.6
TiO_2	....	....	.....	1.86	0.22	.....	.....	.....	.....	.....	2.08	Ores	7.4
MgO	....	....	.....	.....	1.74	3.27	.....	.....	.....	.....	5.01	Or, Qz	2.6
CaO	0.39	0.22	.....	.....	2.68	.....	6.31	.....	.....	.....	9.60	Ap, Ct	1.1
Na_2O	....	....	.....	.....	0.05	.....	.....	3.13	.....	.....	3.18		—
K_2O	....	....	.....	.....	.....	.....	.....	.....	0.28	.....	0.28		99.4
P_2O_5	0.28	....	.....	.....	.....	.....	.....	.....	.....	.....	0.28		
CO_2	....	0.17	.....	.....	.....	.....	.....	.....	.....	.....	0.17		
	0.67	0.39	3.88	3.53	13.88	16.60	31.34	26.45	1.66	0.95	99.35		

TABLE 5

	1	2	metals to 6(0) in (2)
SiO_2	41.38	47.33	1.843 } 1.99
Al_2O_3	9.81	3.20	0.147 }
Fe_2O_3	4.17	1.61	0.047 }
FeO	15.88	14.25	0.463
MnO	0.30	0.67	0.021
TiO_2	4.06	1.82	0.053 } 2.04
MgO	5.29	9.18	0.535
CaO	13.67	21.06	0.879
Na_2O	1.79	0.44	0.033
K_2O	0.93	0.19	0.010 }
H_2O+	1.38	0.34	.....
H_2O-	0.34	0.09	wt %
P_2O_5	0.34	....	$Wo_{47.1}$ $En_{24.7}$ $Fs_{28.2}$
CO_2	1.02	....	.....
	100.36	100.18	

1. Pyroxenite, west contact of gabbro, Camas Mòr, Muck.
2. Clinopyroxene in (1).

TABLE 6

	1	2	3	metal atoms to 6(0)
SiO_2	50.90	7.99	48.90	1.900
				0.100 } 2.00
Al_2O_3	4.73	2.26	2.81	0.126
				0.026 }
Fe_2O_3	0.34	....	0.39	0.014
FeO	13.21	....	15.06	0.487
MnO	0.11	....	0.12	0.004
TiO_2	1.09	....	1.24	0.035 } 2.01
MgO	8.51	....	9.70	0.564
CaO	17.92	....	20.42	0.849
Na_2O	0.35	....	0.40	0.028
K_2O	2.09	2.09	nil	.....
H_2O+	0.27	....	0.30	.....
H_2O-	0.05	....	0.06	.....
	99.57	12.34	99.40	.....

1. Clinopyroxene concentrate from clinopyroxene-sanidine skarn, contact zone, Camas Mòr, Muck. Analyst, J. H. Scoon.

2 and 3. Removal of potash feldspar from 1 (column 2) to give composition of clinopyroxene ($Wo_{44.6}En_{25.9}Fs_{29.5}$) wt % (column 3).

plotted in the diagram $NaAlSiO_4$-$KAlSiO_4$-SiO_2. These differences are doubtless to be ascribed in the first instance to the fact that at Camas Mòr the carbonate sediment, unlike that at Scawt Hill, was not pure limestone but a variable unit carrying magnesia and possibly potash in an aluminous impurity.

The most striking characteristic of the assemblages at both localities is the storing up of iron relative to magnesia in the residual liquids. This feature may be illustrated by the tabulation of the Fe/Mg ratios of the analyzed types both from Scawt Hill and Camas Mòr noted below.

Scawt Hill	Fe/Mg		Camas Mòr
Pyroxenite (pyroxene)	0.7		
Pyroxene-rich dolerite	1.2		
Olivine dolerite	1.6		
		3.8	*Olivine gabbro*
		4.8	Pyroxenite (titaniferous)
Titanaugite analcime dolerite ..	6.5		
Anorthoclase fayalite dolerite ..	6.8		
Melilite nepheline dolerite	8.3		
		12.2	Nepheline gabbro with wollastonite
Nepheline dolerite	13.0		
Melilite rock	19.0		

The precipitation of a diopsidic clinopyroxene as the first stage of assimilation is accompanied by the disappearance of olivine from which indeed the clinopyroxene in part derives[1]

$$3NaAlSi_3O_8 + 2Mg_2SiO_4 + 4CaO \rightarrow 4CaMgSi_2O_6 + 3NaAlSiO_4 \nearrow .$$

Only at the latest stages does olivine reappear, and then in the form of a fayalite-rich variety, as in the nepheline dolerite and anorthoclase-bearing vein rock of the contaminated zone.

The increasingly titaniferous character of the clinopyroxene of the alkali hybrids and the eventual incorporation of alumina in it at the expense of the anorthite component of the plagioclase has already been discussed in the original Scawt Hill

[1] From a saturated (olivine-free) basaltic magma, an early precipitation of wollastonite along with diopside would be facilitated.

paper. Similarly it was shown that the ultimate appearance of melilite was at the expense both of plagioclase and titanaugite, perovskite eventually appearing as a released mineral on resorption of the titanaugite. The analysed melilite from Scawt Hill (Tilley, 1929) came from the melilite rocks. Distinguished by its high soda content, it shows its derivation in its composition which can be expressed in terms of akermanite (46 per cent), gehlenite (19 per cent) and the hypothetical compound $CaNaAlSi_2O_7$ (35 per cent). In these assemblages it accumulated principally at the expense of clinopyroxene and nepheline.

The chain of reaction products at both localities may be expressed in the attached sequence where it is noted that localized concentrations of titanaugite may appear at various stages, the analyzed pyroxenite of Camas Mòr (table 2, no. 10) belonging to an intermediate point of the reaction process.

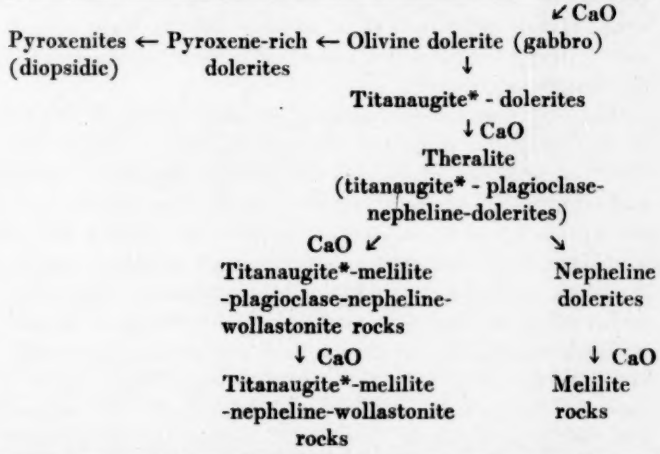

* Localized concentrations of titanaugite at these stages may give rise to pyroxenite assemblages distinct from the diopsidic pyroxenites and characterized by relatively high alumina content where they are derived in part at the expense of the anorthite content of the plagioclase.

COMPARISON OF THE SYNTECTIC ASSEMBLAGES WITH MAFIC ALKALI ROCKS

When we compare the assemblages of Scawt Hill and Camas Mòr with normal mafic alkali rocks, we note that the former include types designated: nepheline dolerite, melilite nepheline

dolerite, theralite and melilite theralite. Conspicuous is the absence of olivine, except as accessory fayalite in the nepheline-dolerite; further, the association in intermediate types of melilite and basic plagioclase is distinctive, for it is a paragenesis which is almost unknown among mafic igneous rocks bearing melilite. Among lavas the mineralogically comparable rocks are nephelinites, melilite nephelinites and nepheline tephrites which have as characteristic associates their olivine-rich relatives: nepheline basalt, nepheline basanite and melilite basalt.

The chemical contrast with the syntectics is revealed especially in the iron-magnesia ratios, well illustrated in figure 2 which plots the FMA ratios ($F = FeO + Fe_2O_3$, $M = MgO$, A = alkalis) of the hybrid sequences and presents the variation curves of two typical alkali igneous series (basalt-mugearite-trachyte). In this diagram the field of the basic alkali rocks carrying nepheline and the related assemblages with melilite is plotted for the Hawaiian province and indicated by the ringed area. If the general field of melilite basalts were added, this would partly overlap this area and extend in the direction of the magnesian corner.

These chemical and mineralogical comparisons do not present in a favourable light the conception held in some quarters that the presence of lime-rich minerals—melilite, monticellite, wollastonite—in mafic alkali rocks is attributable to limestone absorption by basaltic magma, a reaction whereby the alkalic character of the containing rock has itself resulted. Fortunately the work of Bowen has provided an alternative derivation for such rock assemblages, particularly in his study of the alnoites of Quebec and the accompanying experimental investigation of the system diopside—nepheline (Bowen, 1922, 1923). From these and later studies it becomes clear that minerals like melilite and monticellite can be interpreted dominantly as products of normal reaction processes in the consolidation of basic alkali magmas of the nature of nepheline basalts[2] and nephelinites. The reaction processes now referred to and those associated with the earlier stages of basalt-limestone syntexis provide indeed a striking contrast. In the latter, lime assimilation is accompanied by desilication of the feldspathic constituents of

[2] Among the more remarkable nepheline basalts rich in reactional monticellite deserving closer study are those of Shannon Tier, Tasmania, and those, more appropriately described as melilite basalts and even richer in monticellite, found among the Sutherland volcanic pipes of South Africa.

the magma, and magnesian olivine is silicated to form diopsidic pyroxene, while in the former nepheline in effect desilicates clinopyroxene to give olivines and melilites with the attendant formation of analcite or its equivalent.

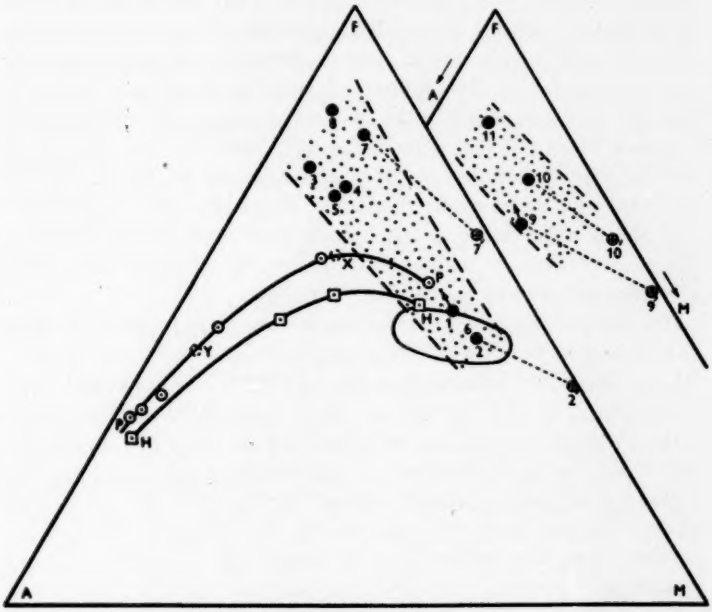

Fig. 2. Plot of the oxides FeO + Fe_2O_3 (F), MgO (M) and alkalis (A) for the rocks of Scawt Hill, County Antrim and Camas Mòr, Muck.

Scawt Hill series 1-8: 1-6 table 1, 7 melilite-bearing nepheline dolerite, 8 melilite rock (hybrid), 2′ pyroxene of pyroxenite 2, 7′ pyroxene of 7 (Tilley and Harwood, 1931, pp. 448, 451 and 454).

Camas Mòr series 9-11 : 9-11 table 2, 9′ pyroxene of olivine gabbro 9, 10′ pyroxene of pyroxenite 10. Tables 3 and 4.

In the same diagram are plotted the trends of the basalt-mugearite-trachyte alkali magma series of the Hebrides (PP) (Bailey and Thomas, 1924, p. 26) and of the corresponding alkali series of the Hawaiian magmatic province (HH) (Macdonald, 1949, p. 1371). The basic member of this series plotted is the average of the basalts of Hualalai (Hawaii). The ringed area at the basic end of this series is the composition field of the late stage basic and ultrabasic nepheline-bearing rock group of this province. The points X and Y which fall on the trend of the Hebridean alkali magma series represent plots of new analyses of a mugearitic basalt of the River Rha, Skye (X) and of a mugearite-trachyte of Totardor, Bracadale, Skye (Y).

FURTHER DIFFERENTIATION OF THE SYNTECTIC MELT

On possible further stages of fractionation of the syntectic melt Scawt Hill and Camas Mòr give limited information. It is clear that continued lime absorption results in exhaustion of the liquid with the formation of the melilite rocks (Tilley and Harwood, 1931, pp. 459, 464). But it is possible that fractionation at the theralite or nepheline dolerite stage—lime reaction now being inhibited—might lead on towards a nepheline syenite (phonolite) facies. The anorthoclase fayalite dolerite (table 1, no. 5) is approximately at the same stage of relative iron enrichment as the theralitic titanaugite dolerite, but bears now a soda-potash feldspar in place of nepheline. It is nevertheless essentially a basic rock. Similarly at Camas Mòr monzonitic and shonkinitic lenses in the hybrid zone point to the building up of soda-potash feldspars in parts of the melt, but these assemblages are not particularly alkaline.

Bowen (1945) in an interesting review of experimental work carried out in portions of the quaternary system Na_2O—CaO—Al_2O_3—SiO_2 has deduced that fractionation of a simplified melilite nephelinite of that system (nepheline-melilite-wollastonite) leads through assemblages of what may be described as simplified tephrites and phonolites, a possibility conditioned by the property of incongruent melting of mixtures of congruent phases. On this particular possibility, the syntectics provide no further clue, for melilite is seen there only in the process of synthesis.

DESILICATION OF GRANITIC LIQUID BY LIMESTONE SYNTEXIS

The preferred method of derivation of phonolite or nepheline syenite by the chief proponents of limestone syntexis is however not via basaltic liquid but through granitic melt (Daly, 1933, p. 502; Shand, 1930). It is not within the scope of the present article to follow the larger problems of limestone-granite syntexis, but the field occurrences of nepheline syenites marshalled in evidence of the operation of this particular mechanism can seldom be claimed as providing an unequivocal demonstration. Nevertheless, that at the contact of granite and limestone mildly alkali assemblages may be produced, and even a process of desilication accomplished, is clear from the accounts of limestone contacts in Skye (Tilley, 1949) and Carlingford, Eire (Nockolds, 1950). In these examples the alkalinity and the desilication (particularly at Carlingford) are to be attributed to a more or less one-way transfer of alumina and silica

to the limestone, leaving the magma locally deficient in alumina insufficient to form feldspar with all the alkalis so that part of the soda with ferric oxide goes to form an acmite-bearing pyroxene. The alkali facies of syenites (sviatonossites) described by Eskola (1921) illustrate the same operation though at the Transbaikalian locality the removed alumina is locked in a grossular andradite from resorbed skarn, precipitated anew in the syenitic rock itself. The plots of analyses of alkali syenites, the desilication products of granitic magma, are indicated in the accompanying diagram (fig. 3). It remains to

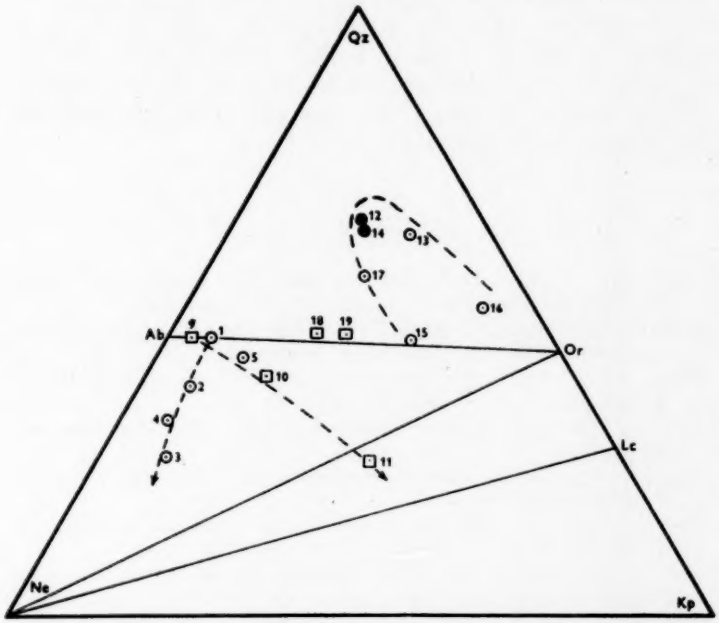

Fig. 3. Trend of the composition of the normative salic constituents (less *an*) of the rocks of the Scawt Hill and Camas Mòr, Muck, series. The numbers refer to analyses in tables 1 and 2 (Scawt Hill succession 1, 2, 4, 3 (also 5); Camas Mòr succession 9, 10, 11.) In the upper portion of the figure are plotted the positions of the alkali facies of syenites and granites which appear at limestone contacts in the vicinity of normal type granites. Skye: 12, normal granite, 13 alkali facies (Tilley, 1949, p. 84).

Carlingford, Eire: 14 normal granite, 15 and 16 syenite and quartz syenite (Nockolds, 1950, p. 31).

Port Shepstone: 17 alkali granite (Tilley, 1949, p. 87) 18 and 19 represent the porphyritic and aplitic sviatonossites of Transbaikalia (Eskola, 1921, p. 80). Ne = $NaAlSiO_4$, Kp = $KAlSiO_4$, Qz = SiO_2, Ab = albite, Or = orthoclase, Lc = leucite.

emphasize that convincing examples of an overstep of the Or-Ab line in this region of the diagram with the appearance of nepheline are still to seek.

More recent conceptions which attribute the development of nepheline in some alkali provinces to a process of metasomatism, styled nephelinization, whether by replacement of granite or granitic gneiss as envisaged and discussed with a great wealth of detail by Eckermann (1948) for the Alnö carbonatite complex, or by the mechanism urged by Gummer and Burr (1946) for the classical Bancroft area of Ontario, show the diversity of problems linked with the genesis of nepheline.

Assuredly the evolution of ideas on the origin of the feldspathoidal rocks has reached a most interesting stage calling urgently for still more field facts, and not less, the development of experimental lines of attack to test and sift the accumulating inferences from field observations.

References

Agrell, S. O., 1950. A gabbro-limestone contact near Camphouse, Ardnamurchan: Am. Mineralogist, vol. 35, p. 1080 (in abstract).

Bailey, E. B., Thomas, H. H., *et al.*, 1924. The Tertiary and post-Tertiary geology of Mull, etc.: Geol. Survey Scotland Mem., pp. 1-445.

Bowen, N. L., 1922. Genetic features of alnoitic rocks at Isle Cadieux, Quebec: Am. Jour. Sci., 5th ser., vol. 3, pp. 1-34.

———, 1923. The genesis of melilite: Washington Acad. Sci. Jour., vol. 13, no. 1, pp. 1-4.

———, 1928. The evolution of the igneous rocks, Princeton University Press, Princeton, New Jersey.

———, 1945. Phase equilibria bearing on the origin and differentiation of alkaline rocks: Am. Jour. Sci., vol. 243-A, pp. 75-89.

———, and Schairer, J. F., 1935. The system MgO-FeO-SiO_2: Am. Jour. Sci., 5th ser., vol. 29, p. 213.

Daly, R. A., 1933. Igneous rocks and the depths of the earth, McGraw-Hill Book Co., New York.

Eckermann, H. von, 1948. The alkaline district of Alnö Island: Sveriges geol. undersökning, ser. Ca, no. 36, pp. 1-176.

Eskola, P., 1921. On the igneous rocks of Sviatoy Noss in Transbaikalia: Översikt av Finska vetensk.-soc. Förhandlingar, vol. 62, pp. 1-99.

Gummer, W. K., and Burr, S. V., 1946. Nephelinized paragneisses in the Bancroft area, Ontario: Jour. Geology, vol. 54, pp. 137-168.

Macdonald, G. A., 1949. Hawaiian petrographic province: Geol. Soc. America Bull., vol. 60, pp. 1567-1574.

Muir, I. D., 1951. The clinopyroxenes of the Skaergaard intrusion Eastern Greenland: Mineralog. Mag., vol. 29, pp. 690-714.

Nockolds, S. R., 1950. On the occurrence of neptunite and eudialyte in quartz-bearing syenites from Barnavave, Carlingford, Ireland: Mineralog. Mag., vol. 29, pp. 27-38.

Shand, S. J., 1930. Limestone and the origin of feldspathoidal rocks: Geol. Mag., vol. 67, pp. 415-427.

Tilley, C. E., 1929. On melilite as a product of interaction of limestone and basaltic liquid: Geol. Mag., vol. 66, pp. 347-353.

———, 1947. The gabbro-limestone contact zone of Camas Mòr, Muck, Inverness-shire: Soc. géol. Finlande Comptes Rendus, no. 20, pp. 97-105.

———, 1949. An alkali facies of granite at granite-dolomite contacts in Skye: Geol. Mag., vol. 86, pp. 81-93.

———, and Harwood, H. F., 1931. The dolerite-chalk contact of Scawt Hill, County Antrim: Mineralog. Mag., vol. 22, pp. 439-468.

Wager, L. R., and Deer, W. A., 1939. Geological investigations in East Greenland, Part III, Petrology of the Skaergaard intrusion: Meddelelser om Grönland, vol. 105, no. 4, pp. 1-352.

CAMBRIDGE, ENGLAND

THE ANGLE BETWEEN THE *a*-AXIS AND THE TRACE OF THE RHOMBIC SECTION ON THE {010}-PINACOID IN THE PLAGIOCLASES

GEORGE TUNELL

ABSTRACT. The angle σ between the a-axis and the trace of the rhombic section on the {010}-pinacoid is given in terms of γ, the angle between the a-axis and the b-axis, and the angle between the {001}-pinacoid and the {010}-pinacoid by the formula

$$\cot \sigma = \frac{\cos (001 \wedge 010)}{\cot \gamma} .$$

Values of σ for a number of plagioclases from pure albite to pure anorthite were calculated from the interaxial angles of Wülfing by means of this formula. The values of σ for these plagioclases calculated from the interaxial angles of Wülfing previously by Rosenbusch and Mügge were computed by means of an incorrect formula.

THE position of the rhombic section of any plagioclase can readily be calculated from the crystallographic interaxial angles, α, β, γ. Rosenbusch and Mügge (1927, p. 744) calculated the values of the angle σ (the angle between the a-axis and the trace of the rhombic section on the {010}-pinacoid) for plagioclases of the following compositions: $Ab_{100}An_0$, $Ab_{96}An_4$, $Ab_{85}An_{15}$, $Ab_{76}An_{24}$, $Ab_{63}An_{37}$, $Ab_{48}An_{52}$, $Ab_{36}An_{64}$, $Ab_{25}An_{75}$, Ab_3An_{97}, Ab_0An_{100}, making use of the crystallographic axial angles of Wülfing. Unfortunately, however, their calculated values were obtained by the use of an incorrect formula.[1]

The rhombic section is defined as the plane through the b-axis that intersects the {010}-pinacoid in a line perpendicu-

[1] The incorrect formula of Rosenbusch and Mügge (1927, p. 744) is

$$\cot \sigma = \cot \beta - \frac{c}{a} \frac{\cos \alpha}{\cos \gamma \sin \beta} .$$

If one solves the oblique spherical triangle formed by the poles of the pinacoids 100, 010, and 001, for the value of the angle between 010 and 001 as a function of the interaxial angles α, β, and γ, and substitutes this value in equation 1 of the present paper, one obtains

$$\cot \sigma = \cot \beta - \frac{\cos \alpha}{\cos \gamma \sin \beta} .$$

The latter formula is in accord with the statement of Rosenbusch and Mügge that "massgebend für die Lage des rhombischen Schnittes ist lediglich die Lage von (010) zu [010]" (op. cit., p. 747), whereas the formula of Rosenbusch and Mügge is not.

lar to the *b*-axis.[2] The position of the rhombic section can be found by the following construction. In figure 1 *aca'* is the great circle through the poles of 100, and 001, and $\bar{1}00$, and *xx'* is the trace of a plane through the center of the reference sphere parallel to 010. The intersection *u* of *aca'* and *xx'* is a point lying in a plane parallel to the rhombic section through the center of the sphere, since the radius of the sphere *ou* lies in the plane parallel to 010 through the center of the sphere and also lies in a plane through the center of the sphere perpendicular to the *b*-axis (the plane of the zone-circle containing the poles of 001 and 100 being perpendicular to the *b*-axis). The pole *r* of the rhombic section must then lie on the zone-circle containing the poles of 001 and 100 and at a

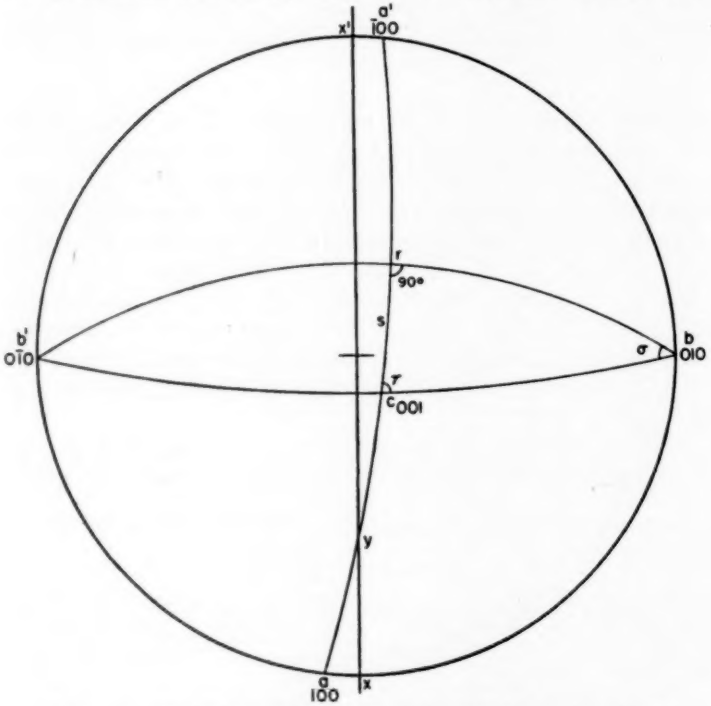

Fig. 1. Construction of the pole of the rhombic section from the poles of the faces 100, 010, and 001.

[2] If the crystal were ideally developed so that the faces, 110, $\bar{1}10$, $1\bar{1}0$, $\bar{1}10$ had equal intercepts on the *a*-axis, then the intersection of the plane of the rhombic section with these faces would be a rhombus, one diagonal of which would be the *b*-axis.

distance of 90° from *u*. The spherical triangle *crb* is a right spherical triangle: $\angle\, crb = 90°$ since the axis of the zone-circle *brb'* is the trace of the rhombic section on the plane 010 and the axis of the zone-circle *arcua'* is the *b*-axis. The angle σ between the *a*-axis and the trace of the rhombic section on 010 can be obtained by solving the right spherical triangle *crb*. In the triangle *crb*, the side *cb* is the angle between the {001}-pinacoid and the {010}-pinacoid, and the angle *rcb* is the interaxial angle γ. Hence, applying Napier's rules, we obtain

$$\cot \sigma = \frac{\cos(cb)}{\cot \gamma},$$

and

$$\cot \sigma = \frac{\cos(001 \wedge 010)}{\cot \gamma}.^{3} \qquad (1)$$

According to the convention used by Schmidt (1919), by Wülfing (1915), and by Rosenbusch and Mügge (1927), the sign of σ is positive when the pole of *r* lies between the pole of $\bar{1}00$ and the pole of 001, and is negative when the pole of *r* lies between the pole of 100 and the pole of 001.

Recalculated values of σ computed by means of this formula are given in table 1 together with the incorrect values calculated by Rosenbusch and Mügge.

The angle *s* between the rhombic section and the plane 001 differs only slightly from the angle σ, as is readily proved. By applying Napier's rules to the right spherical triangle *crb*, we obtain

$$\cot s = \frac{\cot(001 \wedge 010)}{\cos \gamma}. \qquad (2)$$

The values of *s* computed by the use of this formula are also given in table 1 for comparison with the values of σ.

[3] This equation leads to the same absolute values of σ as does the equation of E. Schmidt (1919, p. 401). According to Schmidt

"cot $\gamma = \pm$ tg σ cos *MP*

wo das obere Vorzeichen für die Verhältnisse in Fig. 7, das untere für die in Fig. 8 gilt." Schmidt's figure 7 represents the angular relations of albite and his figure 8 represents those of anorthite (1919, pp. 392-93). Moreover in Schmidt's table 27 (1919, p. 400) he gives for albite ($Ab_{100}An_0$) $MP = 86°26.0'$, $\sigma = +40°$, $\gamma = 87°0.7'$, and for anorthite (Ab_0An_{100}) $MP = 85°48.0'$, $\sigma = -20\frac{1}{2}°$, $\gamma = 91°34.1'$. Schmidt's statement that the negative sign in his equation is to be applied in the case of anorthite thus conflicts with his own figures and with his statement "Bei Albit haben wir also einen positiven, bei Anorthit einen negativen σ -Wert" (1919, p. 392).

TABLE 1

The Position of the Rhombic Section in the Plagioclase Feldspars Calculated from the Interaxial Angles *

% An	0	4	15	24	37	52	64	75	97	100
α	94°36′	94°15′	93°36′	93°29′	93°27′	93°27′	93°26′	93°24′	93°10′	93°06′
β	116°38′	116°36′	116°29′	116°24′	116°17′	116°10′	116°05′	115°58′	115°53′	115°52′
γ	87°00′	87°46′	89°19′	89°38′	89°55′	90°08′	90°19′	90°31′	91°16′	91°28′
σ ..... (Calc. by R.-M.)	44°49′	36°09′	12°06′	6°29′	1°26′	–2°14′	–5°12′	–8°18½′	–19°04′	–21°40′
σ ..... (Calc. by G. T.)	39°31′	31°35′	10°31′	5°39′	1°15′	–1°57′	–4°33′	–7°18′	–17°02′	–19°27′
s ..... (Calc. by G. T.)	39°25′	31°31′	10°30′	5°38′	1°15′	–1°57′	–4°33′	–7°17′	–17°00′	–19°23′

*The values of α, β, and γ in this table are those used by Rosenbusch and Mügge (1927, table 2, p. 744); they were based on the axial angle values of Wülfing.

The importance of the rhombic section in petrography arises from the fact that in ideal pericline twins it is the composition plane. That the composition plane of pericline twins in the plagioclases in many cases does not coincide with the rhombic section is, however, indicated by observations of Reinhard (1931, p. 87), of Mügge and of Barth (1928). Thus Reinhard stated that "Wir haben an sehr albitreichen Plagioklasen an Hand der Spaltrisse (001) feststellen können, dass die Periklinverwachsungsfläche bei demselben Anorthitgehalt sehr vershiedene Lagen einnehmen kann. Es scheinen alle Übergänge vorzukommen, zwischen (001) = Aklin und dem von Wülfing angegebenen Wert des rhombischen Schnittes von Albit + 37°. Mügge hat kürzlich ähnliches vom Anorthit mitgeteilt, wo wir es übrigens ebenfalls festgestellt haben."

References

Barth, Tom. F. W., 1928. Die Lage des rhombischen Schnittes bei sauren Plagioklasen: Zeitschr. Kristallographie, Band 68A, pp. 616-618.

Reinhard, M., 1931. Universaldrehtischmethoden, Wepf & Cie., Basel.

Rosenbusch, H., 1927. Mikroskopische Physiographie der petrographisch wichtigen Mineralien, 5th ed., Vol. I, 2d half by O. Mügge, Schweizerbart'sche Verlagsbuchlandlung, Stuttgart.

Schmidt, E., 1919. Die Winkel der kristallographischen Achsen der Plagioklase: Chemie der Erde, vol. 1, pp. 351-406.

Wülfing, E. A., 1915. Sitzungsberichte der Heidelberger Akademie der Wissenschaften, Mathematisch-naturwissenschaftliche Klasse, Band 6A, 13. Abhandlung.

Department of Geology
University of California
Los Angeles, California

OPTICAL STUDIES ON ALKALI FELDSPARS

O. F. TUTTLE

ABSTRACT. Optical properties of alkali feldspar phenocrysts from extrusive rocks place these feldspars, sanidines, and anorthoclases, in a series with high-temperature albite as the soda end member. This information, together with the results of Spencer (1937), permits classifying the alkali feldspars into four series.

INTRODUCTION

THE discovery of high-temperature albite (Tuttle and Bowen, 1950) prompted a study of the feldspar phenocrysts of rhyolitic rocks in an effort to find examples of similar high-temperature feldspars and to determine the effects of potash and lime on the optical properties of high albite. Many examples were found showing that high albite is an end member of a series of alkali feldspars that includes sanidines and anorthoclases. This report will describe these feldspars and show their relation to the alkali feldspars described by Spencer (1937).

Spencer (1930, 1937, 1938) demonstrated that there is an unbroken series of alkali feldspars extending from orthoclase ($KAlSi_3O_8$) to compositions containing up to 60 per cent albite ($NaAlSi_3O_8$), and that this series probably continues to albite (low-temperature albite). Most representatives of this "orthoclase-microperthite" series were shown to be perthitic. Most specimens could be homogenized by heating at 850° C. with little effect on the optic axial angle, but with measureable changes in refractive index and specific gravity.

Microcline was observed to show similar relations, but analyzed samples extend only to 22 per cent albite.

It was also demonstrated that orthoclase-microperthite, microcline-microperthite and adularia were changed to a high temperature modification by heating at 1075° C. for long periods. Spencer (1937, p. 492) called this high temperature form an "abnormal type of feldspar" and termed the process of changing to this form "sanidinization."

COMPOSITION OF THE FELDSPARS STUDIED

Optical measurements have been made on 14 specimens of which 9 are chemically analyzed; the orthoclase content of 5

samples was determined by the X-ray method described by Bowen and Tuttle (1950, p. 491). The compositions of the analyzed specimens are set down in table 1. In addition, optical properties of 83 analyzed alkali feldspars of all types were collected from the literature (table 2). In most cases only the optic axial angle was reported.

Twelve of the 14 feldspars studied are perthitic, some microperthitic, but others are sub-microscopically unmixed and the inhomogeneity can be discovered only by X-ray studies. Two of the specimens (sanidine, Eifel, Germany, and adularia, St. Gothard, Switzerland) are essentially homogeneous.

OPTIC AXIAL ANGLE STUDIES

The optic axial angle is one of the most useful properties for classifying the alkali feldspars. If the values for $2V_\alpha$ given by Spencer (1937, pp. 458, 461) are plotted against orthoclase content of the specimens, the unheated samples fall into two series (fig. 1), orthoclase cryptoperthite and microcline-cryptoperthite,[1] the axial angles changing toward the $2V_\alpha$ of low-temperature albite with increasing albite content. Also, those specimens heated at 1075° C. until no further change occurred fall into a third series when plotted in this manner. Spencer called this group "abnormal" feldspars, presumably because the optic plane lies in the symmetry plane for the potash-rich members and such an optical orientation is rare in natural feldspars. (Three unheated natural feldspars shown in figure 1 have axial angles that place them near this series.) $2V_\alpha$ for this third series changes with increasing albite content toward the $2V_\alpha$ of high-temperature albite (fig. 1). It is proposed that the potash-rich members of this series be called high sanidine to distinguish them from the "normal" sanidine which has a low 2V and has the optic plane perpendicular to the symmetry plane.

The optic axial angles, then, permit a classification of the alkali feldspars into three series on the basis of the results given by Spencer: (1) microcline-low albite, (2) orthoclase-low albite, and (3) high sanidine-high albite.

The first two series are normally perthitic, and, as demonstrated by Spencer, most of them can be homogenized by heat-

[1]Structural evidence for the series from microcline to low albite has recently been discovered by Laves (1951).

TABLE 1

Composition and Optical Properties of Alkali Feldspars.

	Sanidine* Eifel, Germany	Sanidine* Kokomo, Colorado	Sanidine* Grant Co., New Mexico	Sanidine† Mitchell Mesa Rhyolite, Texas	Anorthoclase† Grande Caldeira, Azores	Anorthoclase* Victoria, Australia	High Albite‡ No Aqua Volcano, New Mexico	Adularia* St. Gothard, Switzerland	Moonstone* Island of Ceylon
SiO_2	63.52	63.58	65.44	67.27	66.97	66.24	65.81	63.95	65.15
TiO_2	tr.	0.00	tr.	n.d.	0.04	0.00	n.d.	0.00	0.00
Al_2O_3	19.00	19.07	18.73	18.35	18.75	19.89	20.86	19.66	19.44
Fe_2O_3	0.11	0.18	0.04	0.92	0.88	0.08	0.65	0.00	0.00
FeO	0.00	0.07	0.07			0.07		0.05	0.10
MgO	0.00	n.d.	0.00	0.00	0.00	0.00	0.00	0.04	0.00
CaO	0.18	0.69	0.06	0.15	0.36	0.25	2.19	0.04	0.16
Na_2O	2.60	2.77	4.82	6.45	7.88	8.93	8.98	1.17	4.56
K_2O	13.58	11.96	10.01	7.05	5.39	3.95	1.12	14.43	10.10
H_2O+	0.60	0.57	0.68	0.08	0.01	0.44	0.15	0.56	0.50
H_2O-	0.54	0.22	0.33	0.08	0.03	0.09	n.d.	0.16	0.18
BaO	—	—	—	—	—	—	—	0.08	—
Total	100.13	99.11	100.18	100.35	100.31	99.94	99.76	100.14	100.20
Or	78	73	59	43	32	23	7	89	60
Ab	21	24	41	56	66	76	81	11	39
An	1	3	—	1	2	1	12	—	1
$2V_\alpha$	17	29	26-35	33	46	47	59	64	74
$\eta\alpha$	1.5201	1.5212	1.5220	1.5232	1.5239	1.5253	—	—	—
$\eta\beta$	1.5248	1.5261	1.5266	1.5289	1.5299	1.5311	—	—	—
$\eta\gamma$	1.5252	1.5268	1.5272	1.5296	1.5308	1.5321	—	—	—

* These feldspars made available by Th. G. Sahama, F. C. Kracek, and K. J. Neuvonen who used these specimens in their calorimetric studies. See Kracek and Neuvonen, "Thermochemistry of plagioclase and alkali feldspars" in the present volume. Analyst for all but St. Gothard, V. Knorring; St. Gothard analyst, F. A. Gonyer.

† Analyses kindly made available by C. E. Tilley, Cambridge, England. Analyst, J. H. Scoon.

‡ This specimen was supplied by E. S. Larsen (Larsen, E. S. *et al.*, 1938, Am. Mineralogist, vol. 23, p. 235). Analyst, F. A. Gonyer. This specimen has two different plagioclase feldspars, *ca.* 95 per cent albite and 5 per cent An_{30}.

ing for a short time at 850° C. without changing the axial angle appreciably. Examples of the high sanidine-high albite series are now being studied, but it is not yet known whether these high temperature natural feldspars are perthitic or not. However, synthetic alkali feldspars unmix readily (Bowen and Tuttle, 1950) and they probably belong to the high sanidine-high albite series (the synthetic material is too fine-grained to permit optical studies).

Method of measurement.—In the present study optic axial angles were determined on cleavage fragments using the interference figure method with the universal stage. The use of this conoscopic method permits more accurate determination of the axial angle and is considerably less time-consuming than extinction methods. The alkali feldspars give sharp interference figures suitable for use on the universal stage if cleavage fragments having a thickness of approximately 0.4 mm. are used. Satisfactory results have been obtained on fragments as thin as 0.1 mm.

Results.—Optic axial angles of the 9 feldspars studied are set out in table 1, and in figure 1 together with the optic axial angles of 75 analyzed feldspars taken from the literature and 5 specimens analyzed by the X-ray. Twelve of the 14 new feldspar specimens are from rhyolitic rocks and would be classified as either sanidine or anorthoclase by most petrographers. The values for the axial angles of these 12 specimens fall on a line extending from high-temperature albite (crystallized at 800° C. and 1000 kg/cm$_2$ water pressure) to a theoretical potash feldspar with a $2V_\alpha$ of approximately 17°. Axial angles of representatives of this series lie between the values for the orthoclase-low albite and the high sanidine-high albite series, and represent a fourth series of alkali feldspars which includes sanidines and anorthoclases. It is proposed that this series be called the sanidine-anorthoclase cryptoperthite series.

It is not known whether the potash end member of this series is structurally different from orthoclase or not. The optical results indicate that it is different from the end member of the orthoclase-microperthite series of Spencer (1937), but the evidence is not conclusive. If further thermal and X-ray studies establish a difference, then the end member should be called low-temperature sanidine to distinguish it from high-temperature

sanidine which can be formed by heating any of the other types of potash-rich feldspars (i.e., microcline, adularia, orthoclase, "low" sanidine).

Synthetic potash feldspar crystallized at 800° C. and 1000 kg/cm$_2$ water pressure has an optic axial angle of 63° and the optic plane lies in the symmetry plane. This value coincides with the extrapolated value of 2V for the potash end member of the heated potash-rich alkali feldspars studied by Spencer (see fig. 1).

The values for the optic axial angles at the albite end of the high sanidine-high albite series are not entirely satisfactory because of the fine twinning present in most heated and synthetic specimens. Single crystal X-ray studies of fragments

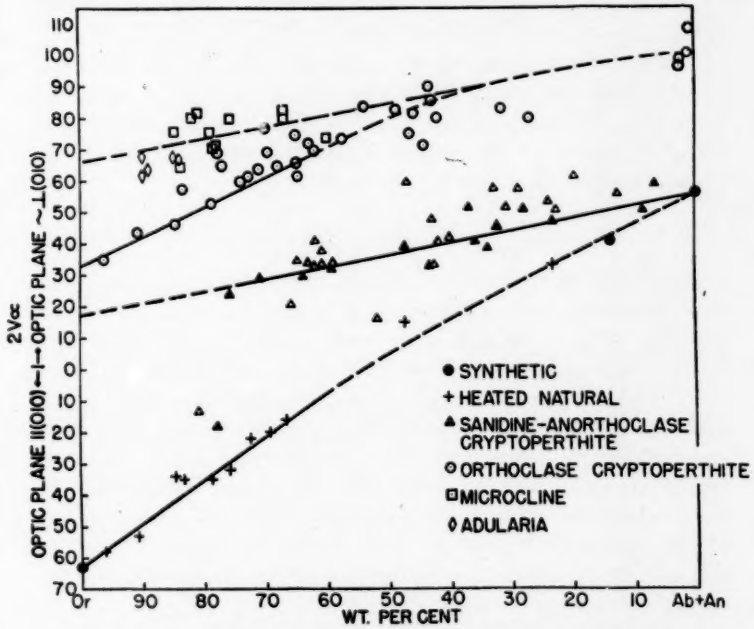

Fig. 1. Graph showing the relation between optic axial angles and composition of alkali feldspars listed in table 2. The solid triangles show the 2V$_\alpha$ of sanidine and anortholase specimens measured by the writer. The range of values for 2V$_\alpha$ of natural feldspars precludes using this graph for determination of compositions. The graph will serve, however, to place a feldspar into one of the four series if the composition is known approximately, from chemical analyses, from the ($\bar{2}$01) spacing measured on heated material, or from other optical properties such as refractive indices.

that appeared untwinned optically showed that twinning may or may not be present. The presence of such twinning may alter the axial angle results somewhat.

Resumé.—Alkali feldspars can be grouped into four series on the basis of optic axial angle and orientation of the optic plane. The four series are:

1. High sanidine-high albite (cryptoperthite ?)
2. Sanidine-anorthoclase cryptoperthite
3. Orthoclase cryptoperthite
4. Microcline cryptoperthite

The optic axial angle of these perthitic feldspars is changed only a small amount or none at all upon homogenization by heating for a short time (see Spencer, 1937, p. 462).

The scatter of values for the optic axial angle of the sanidine-anorthoclase cryptoperthites (fig. 1) is in part a result of variations in lime content. Lime raises the value of 2V and therefore many of the values above the line in figure 2 represent lime-bearing feldspars (see table 2).

INDICES OF REFRACTION STUDIES

Method of measurement.—Indices of refraction of 6 analyzed specimens have been determined on fragments by the immersion method, using a variable wave length light source. Immersion liquids having known refractive indices and dispersion were used. The immersion liquids were calibrated for each determination by mixing fragments of a glass of known dispersion and refractive index with the crystal fragments, the wave length at which the glass and the immersion liquid have the same refractive index being one point on the dispersion curve of the immersion medium. This point, in effect, served to measure the temperature of the immersion liquid. Results are reproducible to $\pm$ 0.0003.

Results.—Refractive indices of 7 analyzed specimens are listed in table 1 and shown in figure 2 together with results of Spencer (1937) on the orthoclase-cryptoperthites and high sanidine-high albite series (two values for sanidine, specimens G and P, are from Spencer, 1937, p. 458, and two are from Heald, 1950, p. 78). The solid lines show the most probable

values for the orthoclase-low albite series. The three values that lie above the line at 45-50 per cent orthoclase have over 4 per cent anorthite in solid solution.

Dashed lines have been drawn for α and γ of the sanidine-anorthoclase series. The β index is essentially the same in both groups. The greatest difference between the refractive index of members of the two series is shown by the γ index.

The differences in refractive indices between the orthoclase-low albite and the sanidine-anorthoclase high albite series are not great, but there is little doubt that the two groups are different and that the soda end of the latter series has refractive

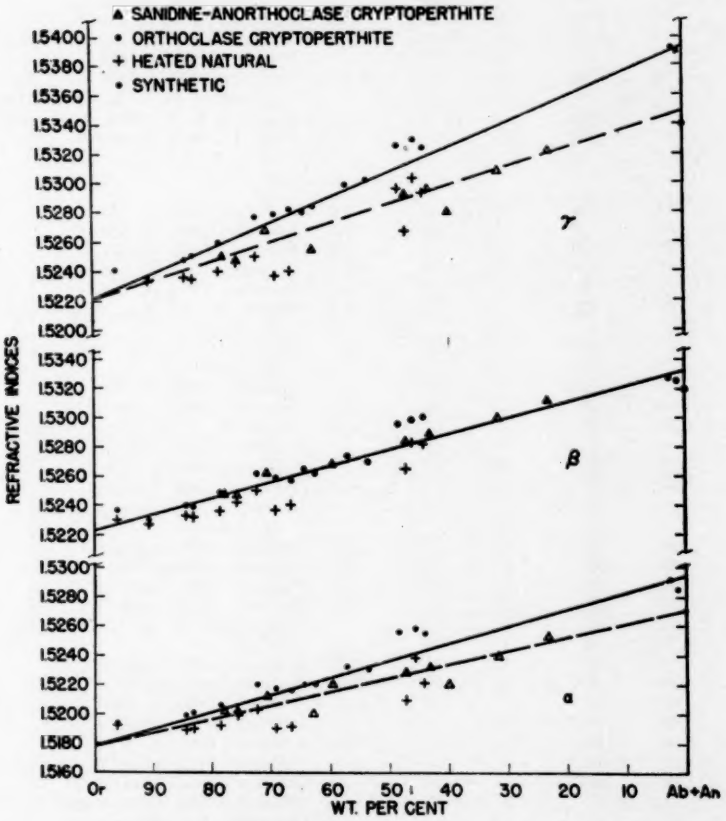

Fig. 2. Refractive indices of alkali feldspars.

TABLE 2

Composition and Optical Properties of Analyzed Alkali Feldspars

Composition (Wt. %) Or	Ab	An	2Va	Extinction (010)	Reference*
			Microcline and Adularia		
90	10	0	62		Spencer, 1930, p. 344
90	8	1	68	5.3	Spencer, 1937, p. 455
89	11	0	64		Table 1
85	13	2	76	7.5	Spencer, 1937, p. 456
85	14	1	68		Byelyankin, D. S., M.A.† 1, p. 89
84	15	1	64	6.0	Spencer, 1937, p. 456
84	13	1 (Ce=2)	69		Spencer, 1937, p. 474
82	18	0	81		Keith, M. L., 1939, Bull. G.S.A., 50, p. 1810
81	18	1	82	7.5	Spencer, 1937, p. 456
79	19	2	76	7.5	Spencer, 1937, p. 456
79	21	0	68-86		Byelyankin, D. S., M.A. 3, p. 80
78	20	2	72		Spencer, 1937, p. 456
76	22	2	80	7.5	Spencer, 1937, p. 456
67	31	2	80		Byelyankin, D. S., M.A. 1, p. 89
67	29	4	79-87		Soloviev, S. P., M.A. 10, p. 67
60	40	0	74		Grip, E., M.A. 8, p. 104
			Orthoclase		
96	4	0	35	5.0	Spencer, 1930, p. 344
91	7	2	44	5.3	Spencer, 1930, p. 331
85	14	1	46	6.2	Spencer, 1930, p. 331
83	15	2	58	7.5	Spencer, 1937, p. 455
79	19	2	53	7.0	Spencer, 1930, p. 331
78	22	0	70		Heald, M. T., Am. Min. 35, p. 78, 1950
77	23	0	65		Heald, M. T., Am. Min. 35, p. 78, 1950
74	24	2	60		Spencer, 1938, p. 109
73	26	1	61	7.7	Spencer, 1930, p. 331
71	25	4	63		Barth, T. F. W., 1931, Norske Geol. Tidssk. 12, pp. 57-72
70	27	3	77		Spencer, 1938, p. 113
69	29	2	69	9.5	Spencer, 1937, table 2
68	32	0	65		Heald, M. T., Am. Min. 35, p. 78, 1950
65	32	1	75	10.5	Spencer, 1937, table 2
65	33	2	66	8.8	Spencer, 1930, p. 330
64	34	2	61	8.5	Spencer, 1937, table 2
63	36	1	72	10.5	Spencer, 1937, table 2
62	36	2	70		Byelyankin, D. S., M.A. 1, p. 89
61	38	1	74		Table 1
57	40	3	74	10.5	Spencer, 1937, table 2
54	45	1	84	11.0	Spencer, 1937, table 2
48	47	5	83	11.7	Spencer, 1930, p. 344
46	53	1	75		Oftedahl, Chr., 1948, p. 26
46	50	4	82	11.6	Spencer, 1930, p. 344
44	52	4	71	11.7	Spencer, 1937, table 2
43	54	3	86		Oftedahl, Chr., 1948, p. 26
43	55	2	90		Oftedahl, Chr., 1948, p. 26
42	54	4	80		Oftedahl, Chr., 1948, p. 26
31	67	2	83		Oftedahl, Chr., 1948, p. 29

Composition (Wt. %) Or	Ab	An	2V$_\alpha$	Extinction (010)	Reference*
			Sanidine and Anorthoclase		
81	16	3	13	‖(010)	Spencer, 1937, p. 476
78	21	1	11-18	‖(010)	Table 1
76	21	Ce = 3	24	5.8	Spencer, 1937, p. 455
72	24	4	29		Table 1
66	31	3	21		Larsen, E. S. *et al.*, Am. Min., 23, p. 421, 1938
66	31	3	30	8.3	Spencer, 1930, p. 336
65	35	0	30-40		Gerasimov, A. P., M.A. 7, p. 179
64	composition by X-ray		30		(Jemez Mountains, New Mexico)
63	37	0	34		Heald, M. T., Am. Min., 35, p. 78, 1950
62	35	3	41		Larsen, E. S. *et al.*, Am. Min., 23, p. 421, 1938
62	35	3	33		Spencer, 1937, p. 482
61	34	5	38		Kozu, S., M.A. 1, p. 280
59	41	0	26-35		Table 1
59	35	6	34		Spencer, 1937, p. 482
52	43	5	15-18		Tućan, F., M.A. 10, p. 67
49	47	4	40	9.5-10.5	Spencer, 1930, p. 338
47	51	2	60	5.2-7	Ho, T. L., M. A. 5, p. 439
44	composition by X-ray		34		(San Juan Mountains, Colorado)
43	57	1	33		Table 1
43	52	5	48	6.0	Weigel, O. and Krüger, E., M.A. 7, p. 331
42	52	3	41		Larsen, E. S. *et al.*, Am. Min., 23, p. 421, 1938
40	60	0	42		Heald, M. T., Am. Min., 35, p. 78, 1950
37	composition by X-ray		52		Bowen, N. L., 1937, Am. Jour.
36	composition by X-ray		41		Sci., 33, locality same as No. 303, p. 15
34	composition by X-ray		39		Bowen, N. L., 1937, Am. Jour. Sci., 33, p. 15, No. 303
33	61	6	58		Spencer, 1937, p. 489
32	66	2	46		Table 1
31	66	3	52		Byelyankin, D. S., M.A. 1, p. 89
29	68	3	58		Barth, T. F. W., 1931, Norske Geol. Tidssk., 12, p. 61
28	62	10	51		Spencer, 1937, p. 489
27	62	11	80		Spencer, 1937, p. 489
24	66	10	54		Spencer, 1937, p. 489
23	76	1	47		Table 1
23	73	4	51	8.0	Montalto, M., M.A. 7, p. 294
20	61	19	62		Spencer, 1937, p. 489
13	78	9	46-66		Gerasimov, A. P., M.A. 7, p. 179
			Albite		
9	88	3	51	18.5	Spencer, 1930, p. 336
7	82	11	59		Table 1
3	93	4	99	18.5	Spencer, 1930, p. 340
3	96	1	98	18.8	Spencer, 1930, p. 340
1	98	1	100		Keith, M. L., 1939, p. 1810
1	98	1	102	19.5	Spencer, 1937, table 2

* References for which only the year is given will be found in the list of references at the end of paper.

† M.A. = Mineralogical Abstracts.

indices close to those found for high albite (Tuttle and Bowen, 1950).

Refractive indices for the microcline-low albite series are not shown, but they show appreciable differences from the above two series (Spencer, 1937, p. 481).

Indices of the high sanidine-high albite (heated natural) specimens are in general below the values for the orthoclase-low albite or the sanidine-anorthoclase series and if these values are extrapolated to albite composition they fall below those found for high albite crystallized hydrothermally at 800° C. and 1000 kg/cm_2 water pressure. In view of the results of X-ray studies on high albite by MacKenzie (1952) it will be interesting to check the refractive indices of high albite grown above 950° C. to see if they are lower than the values obtained on high albite grown at 800° C. Unfortunately the material now available is too fine-grained to permit accurate refractive index measurements.

EXTINCTION ON (010)

Extinction angles on (010), against (001), have been measured on 9 samples of sanidine and anorthoclase and are shown in figure 3 together the results of Spencer (1937) on orthoclase-microperthites. As with the other optical properties, the differences in extinction on (010) between the two series are greatest in the soda-rich specimens.

OPTICAL ORIENTATION OF SODA-RICH SPECIMENS

Universal stage studies of natural soda-rich alkali feldspars give highly variable results for the orientation of the indicatrix from one specimen to another and in some instances from one grain to another of the same sample. The results were puzzling until it was discovered by the X-ray that the specimens were submicroscopically perthitic and that consistent results could be obtained after heating the specimens until the X-ray indicated that they were homogeneous.

Natural soda-rich alkali feldspars that have compositions within the triclinic range ($Or_{65}Ab_{35}$, Or_0Ab_{100}) discovered by Donnay and Donnay (1952) from X-ray studies of synthetic materials are commonly monoclinic optically. The explanation of this optical character of cryptoperthitic crystals appears to be that proposed by Oftedahl (1948) for the orthoclase

cryptoperthites. He demonstrated by single crystal X-ray studies that crystals which were optically monoclinic may consist of an intergrowth of monoclinic potash feldspar and triclinic soda feldspar which is twinned in such a manner that the crystals appear monoclinic by optical tests.

An example of the effect of homogenization on optical orientation of anorthoclase from Victoria, Australia, is illustrated in figure 4. Most cleavage fragments studied were essentially monoclinic as shown; however, a few grains departed slightly from this monoclinic character but the departure was about the order of magnitude of the error of measurement. After heating there is no doubt of the triclinic character of this specimen as the acute bisectrix moves out of the (010) cleavage as shown in figure 4.

Progressive changes in the optical orientation of the high-temperature albite with increasing orthoclase content are illustrated in figure 5. High temperature albite was synthesized from albite glass at 800° C. and 1000 kg/cm$_2$ water pressure.

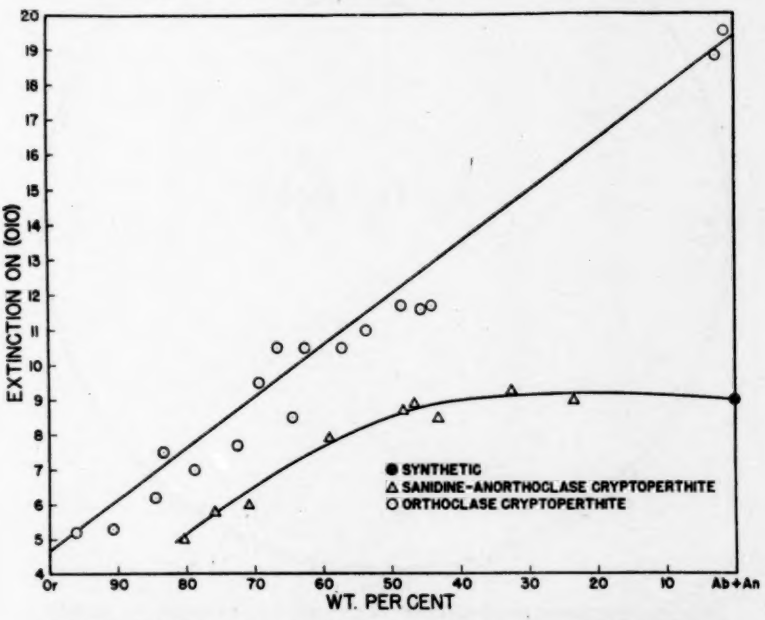

Fig. 3. Relation between extinction on (010) and composition of some alkali feldspars.

All other specimens illustrated were heated at 900° C. for 20 hours to homogenize any perthitic structure that may have been present. This heat treatment alters the optic axial angle only a few degrees or none at all and may increase or decrease the axial angle.

Evidence for gradational optics.—The orthoclase-low albite and microcline-low albite series appear, from optic axial angle values (fig. 2) and index of refraction data (Spencer, 1937, pp. 457, 461), to be gradational. It is not known whether this gradational relation in optics is a reflection of continuous structural changes between the two series or not. Further X-ray studies of analyzed specimens will be necessary to decide whether the structural changes are gradational or discontinuous.

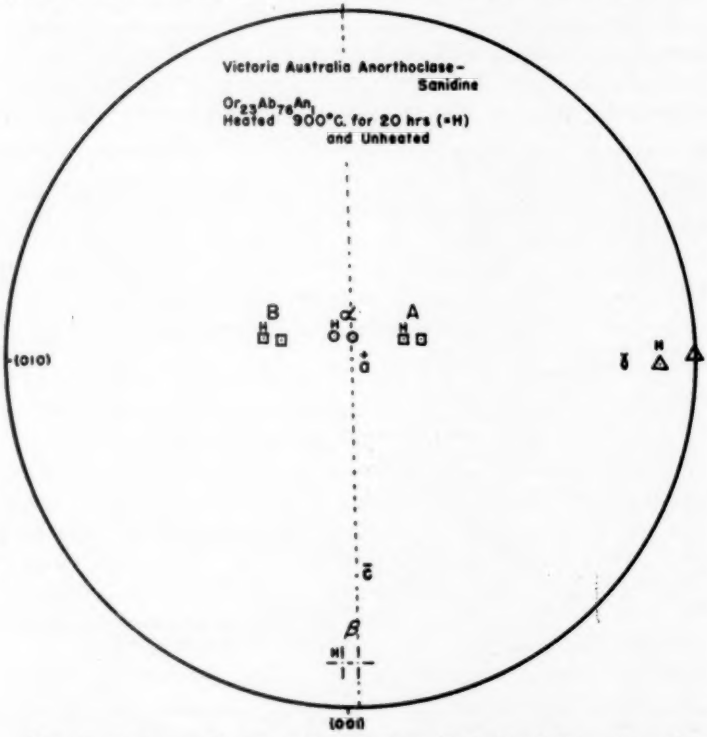

Fig. 4. Stereographic projection of the optical orientation of anorthoclase from Victoria, Australia, before and after homogenizing by heating at 900° C. for 20 hours.

Heating experiments on specimens belonging to the sanidine-anorthoclase series show a gradual change in optic axial angle as the time of heating is increased (Spencer, 1937, fig. 13). Also, slow cooling of representatives of the high sanidine-high albite series results in a slight lowering of the optic axial angle (Spencer, 1937, p. 477). These results suggest that gradational relations between these two series may exist.

Stability relations.—Synthetic and natural alkali feldspars heated at elevated temperatures for long periods belong to the high sanidine-high albite series and represent the high-temperature modifications of this feldspar group. The sanidines and anorthoclases are also high temperature forms in that they commonly occur in glassy extrusive rocks. The temperature

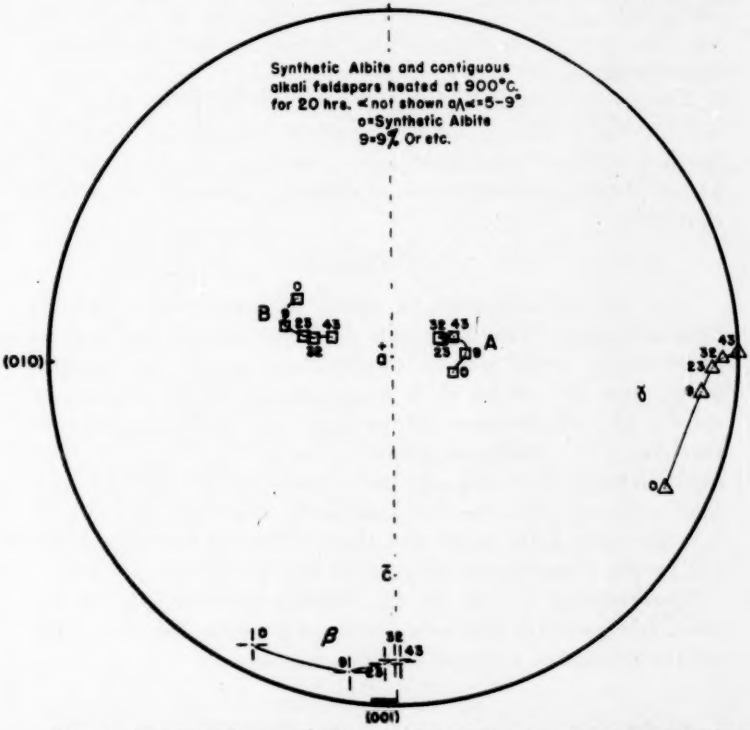

Fig. 5. Stereographic projection of the optical orientation of soda-rich sanidine and anorthoclase after heating at 900° C. for 20 hours. 0 = synthetic albite, 9 = 9 per cent orthoclase, etc.

range of stability of these two series is not known; indeed it is not certain that the sanidine-anorthoclase series has a stable range of existence. On cooling, the high sanidine-high albite series becomes unstable at 660° C. for compositions near $Ab_{55}Or_{45}$, and unmixing into two phases takes place (Bowen and Tuttle, 1950). On the other hand, natural sanidines of the same composition unmix (Adams, 1951, p. 35) at about 590° C. (Temperature varies somewhat with lime content.) The solvus for the natural sanidines and anorthoclases has approximately the same shape and position with respect to composition as the solvus determined for synthetic materials, but as just noted it is displaced downward about 70° C. at the maximum and somewhat less on the flanks of the curve.

It is obvious that one or the other of these solvuses is metastable. It is believed that the solvus determined for the natural materials is metastable, but this has not been proven experimentally.

Temperature ranges of stability of the other two series are not known. Most of the homogeneous crystals produced by heating perthitic microcline and orthoclase for short periods at moderate temperatures probably represent metastable equilibria.

CONCLUSIONS

The optical properties of alkali feldspars determined by Spencer together with the results presented here on phenocrysts of extrusive rocks permit a classification of this feldspar group into four series. It is proposed that the four series be called: (1) microcline-cryptoperthite, (2) orthoclase-cryptoperthite, (3) sanidine-anorthoclase cryptoperthite, (4) high sanidine-high albite series. If the composition of an alkali feldspar is known from chemical analysis or from the $(\bar{2}01)$ spacing, the optic axial angle and the position of the optic plane will permit classification into one of the four series.

The stability ranges of the various modifications of the alkali feldspars are unknown, but some progress has been made toward a solution of these complex relations.

ACKNOWLEDGMENTS

The writer is indebted to Drs. Edmondson Spencer, E. S. Larsen, N. L. Bowen, Chr. Oftedahl, C. S. Ross, and J. W. Greig for specimens studied during this investigation.

References

Adams, L. H., 1951. Annual Report of the Director: Carnegie Inst. Washington Year Book 50.

Bowen, N. L., and Tuttle, O. F., 1950. The system $NaAlSi_3O_8$—$KAlSi_3O_8$—H_2O: Jour. Geology, vol. 58, pp. 489-511.

Donnay, G., and J. D. H., 1952. The symmetry change in the high-temperature alkali-feldspar series: Am. Jour. Sci., present vol.

Heald, M. T., 1950. Thermal study of the potash-soda feldspars: Am. Mineralogist, vol. 35, pp. 77-89.

Laves, F., 1951. Artificial preparation of microcline: Jour. Geology, vol. 59, pp. 511-512.

MacKenzie, W. S., 1952. The effect of temperature on the symmetry of high-temperature soda-rich feldspars: Am. Jour. Sci., present vol.

Oftedahl, Chr., 1948. Studies on the igneous rock complex of the Oslo region. IX. The feldspars: Norske vidensk.-akad. Oslo Skr., I Math.-naturv. Kl. no. 3, pp. 1-71.

Spencer, Edmondson, 1930. A contribution to the study of moonstone from Ceylon and other areas and of the stability relations of the alkali feldspars: Mineralog. Mag., vol. 22, pp. 291-367.

———, 1937. The potash-soda-feldspars. I. Thermal stability: Mineralog. Mag., vol. 24, pp. 453-494.

———, 1938. The potash-soda-feldspars. II. Some applications to petrogenesis: Mineralog. Mag., vol. 25, pp. 87-118.

Tuttle, O. F., and Bowen, N. L., 1950. High-temperature albite and contiguous feldspars: Jour. Geology, vol. 58, pp. 572-583.

Geophysical Laboratory
Carnegie Institution of Washington
Washington, D. C.

THE $MgO—Al_2O_3—SiO_2—H_2O$ SYSTEM AND THE RELATED METAMORPHIC FACIES

HATTEN S. YODER, JR.

ABSTRACT. Equilibria in a portion of the system $MgO—Al_2O_3—SiO_2—H_2O$ have been determined at temperatures from 430° to 990° C. at pressures of water vapor up to 30,000 psi (pounds per square inch). The univariant pressure—temperature curves have been bracketed for the following reactions:

Brucite + clinochlore ⇌ forsterite + spinel + vapor,
Talc + clinochlore ⇌ forsterite + cordierite + vapor,
Clinochlore ⇌ forsterite + cordierite + spinel + vapor,

and some of the previously investigated reactions in the $MgO—SiO_2—H_2O$ system are confirmed.

A new low-temperature form having the clinochlore composition was prepared, but its stability has not been fixed with certainty. It is suspected that this form may be isostructural with one form of serpentine. Pyrope was not synthesized and natural pyrope was not found to be stable in the presence of an excess of water vapor in the pressure and temperature range investigated. Amesite and magnesian chamosite were not produced. Metastable growth of many of the phases occurring in the system is common and they survive long periods of time.

The phase assemblages obtained in equilibrium with vapor are summarized at significant temperature intervals at 15,000 psi. These assemblages outline compositions in the system for which water is prohibited as a stable phase. The conclusion is reached that the presence of an "excess" or "deficiency" of water vapor greatly influences the mineralogy of a metamorphic rock. On this basis, it is demonstrated that all the now accepted critical assemblages which define the metamorphic facies *may* have formed under the same pressure and temperature conditions, the different facies being primarily a function of the bulk composition. A new set of critical assemblages indicative of significant pressure and temperature conditions is required for the various stages in progressive metamorphism. In addition, it is shown that a common hydrothermal alteration which has been interpreted as retrograde metamorphism need not mean a change in pressure or temperature conditions, but may mean access of water vapor.

INTRODUCTION

THE largest group of rocks with which the metamorphic petrologist must deal is that developed during the metamorphism of the argillaceous sediments. The composition of the bulk of these sediments can be closely approached by mixtures in the magnesia—alumina—silica—water system. Therefore a study of that system is pertinent to the understanding of the origin of many metamorphic rocks.

Most of the important minerals which occur in the system are plotted in figure 1. The four-component system is repre-

sented by means of a one-point projection: All points within the tetrahedron are projected from the apex H_2O to the plane $MgO—Al_2O_3—SiO_2$.

All four of the planes bounding the tetrahedron have been investigated. The system $MgO—Al_2O_3—SiO_2$ has been studied by Rankin and Merwin (1918) and corrected by Bowen and Greig (1924) and recently by Foster (1950, 1951). The phase assemblages stable at the solidus are given in figure 2. The system $MgO—SiO_2—H_2O$ has been investigated by Bowen and Tuttle (1949). The two remaining planes $Al_2O_3—SiO_2—H_2O$ and $MgO—Al_2O_3—H_2O$ were determined by R. Roy and Osborn (1950) and D. M. Roy and Osborn (1951) respectively. It is the phase assemblages *within* a portion of the tetrahedron which are now to be presented.

METHOD OF INVESTIGATION

Equipment.—The equilibrium relations for selected compositions in the system were investigated by means of apparatus

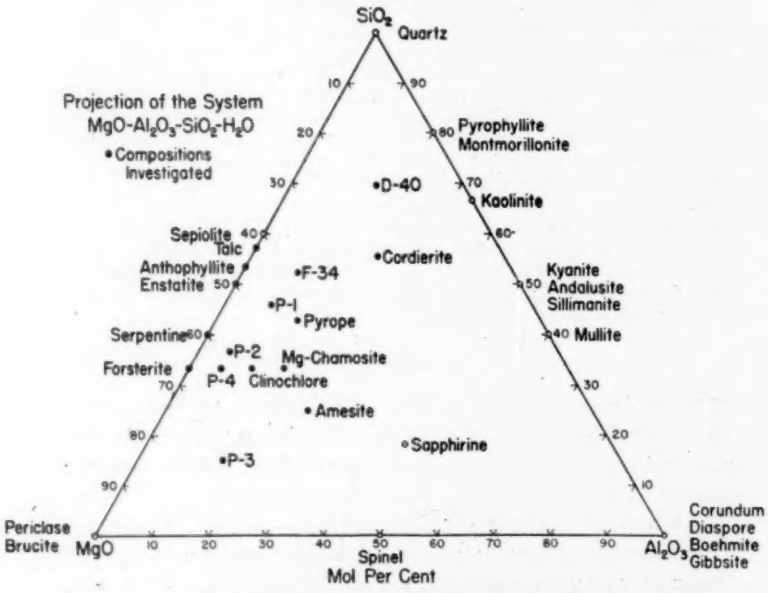

Fig. 1. A one-point projection of the $MgO—Al_2O_3—SiO_2—H_2O$ system showing some of the naturally occurring compounds and all of the compositions investigated.

similar to that designed by Tuttle (1948, 1949) and improved by Van den Heurk (1952, unpublished). The desired water pressure was maintained in a vessel by a pump actuated by a regulator connected to a Bourdon pressure gauge. The pressures, read from the Bourdon gauge, are believed to be accurate to about ± 400 psi. The pressure vessels were heated externally by means of tubular resistance furnaces controlled by suitable temperature regulators. The temperature was measured with chromel-alumel or iron-constantan thermocouples inserted in a well in the pressure vessel 3 mm. from the charge. The error of the temperature measurement is considered to be less than ± 5° C.

Materials.—The compositions investigated were prepared in several ways. For some compositions the dry oxides of magnesium, aluminum, and silicon were mixed in the desired proportion and ground together to obtain an intimate mixture. Materials prepared in this way will be referred to as a powdered "mix." Where it was possible to quench the com-

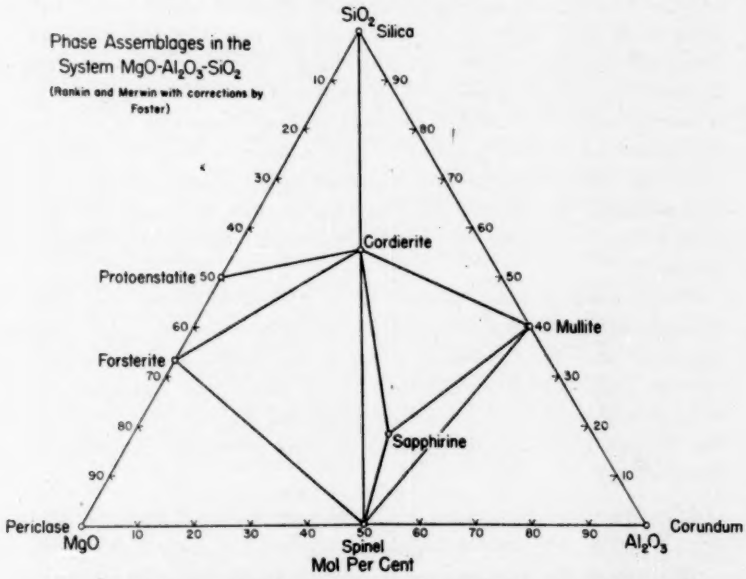

Fig. 2. Phase assemblages stable at the solidus in the system MgO—Al_2O_3—SiO_2 (after Rankin and Merwin with corrections by Bowen and Greig and by Foster).

position to a glass, or where the melting temperature was low enough for the available equipment, some of the powdered mix was converted to a glass. If glass was not so obtained, some of the powdered mix was sintered at a temperature which would yield the desired crystalline product or products. In addition, natural minerals, or natural minerals mixed with synthetic products, were used as initial materials. Frequently the same experiment was repeated, differing only in the initial material.

The raw materials used were MgO (Baker's analyzed) ignited to constant weight; cristobalite, precipated SiO_2, or silica glass; corundum, or γ-alumina; and distilled water.[1] In the Tuttle apparatus as conventionally used it is not possible to regulate the water content. All experiments were performed in the presence of an excess of water.

Procedure.—The initial materials were ground in acetone in a power-driven grinder (agate) for at least 1 hour in order to reduce the grain size and thereby facilitate reaction. The charge was placed in a platinum-foil crucible about 0.15 inch long and 0.06 inch in diameter which was covered with an inverted crucible similar in shape and of such size as to give a close fit. These telescoped crucibles were in turn placed in a similar set of crucibles about 0.25 inch long and 0.10 inch in diameter and were packed in such a manner that the smaller crucibles were completely surrounded with material of identical composition, i.e., a buffer. The charge was thus always surrounded with a vapor saturated with respect to the constituents present.

The crucibles were placed in a pressure vessel and first brought up to the desired temperature. The water at the desired pressure was then released from a reservoir into the vessel. At the end of the experiment the charge was quenched by swinging the furnace aside and directing an air blast against the pressure vessel. The pressure was released immediately thereafter.

Identification of phases.—The phases obtained hydrothermally, usually very fine-grained, were identified mainly by their

[1] The cristobalite was prepared by heating quartz from Lisbon, Maryland, at 1500° for 3 hours. The γ-alumina was prepared by heating $AlCl_3 \cdot 6H_2O$ at 750° C. for 1 hour. This method of preparation of very fine-grained alumina was suggested by Dr. J. W. Greig.

powder X-ray diffraction patterns. When the products were coarse-grained, or when the initial stages of a reaction were being investigated, identification of phases was made by means of their optical properties.

The compositions which were investigated were selected so that none of the possible phases when completely crystallized would be present in amounts less than that detectable by X-rays. For routine identification the Norelco Geiger-Counter X-ray Spectrometer was used. For greater precision and resolution the improved Norelco instrument, capable of recording the back-reflection region, was employed. Standard X-ray diffraction patterns were prepared for all the compounds occurring in the system. These were compared with the composite patterns obtained from the products as aids in deciphering the several phases present. Since the powder X-ray diffraction patterns are not unique in every detail, particularly for compounds consisting of the same kinds of atoms, considerable judgment is involved in the identification.

PROPERTIES OF COMPOUNDS

Talc.—The compound $Mg_3(Si_4O_{10})\ (OH)_2$ crystallizes rapidly and is usually the first mineral to form in compositions in which it is a stable phase. Talc also readily forms metastably below its decomposition temperature in some compositions in which it is not a stable phase, and only slowly reacts to yield the stable products. The compound usually forms in very fine fibrous aggregates, but when well developed it occurs as plates or blades. The indices of refraction for the pure synthetic material are approximately $\gamma = 1.575$ and $\alpha = 1.540$. Although the crystals were not suitable for accurate measurements, there appeared to be no difference in indices of refraction of talc obtained from compositions in which alumina was also a constituent. The powder X-ray diffraction patterns reflected the poor quality of the crystals produced. The peaks were usually broad and of low intensity, indicative of very fine-grained and poorly crystallized material. For runs of short duration or low temperature the X-ray pattern is similar to that shown in figure 3A. Under more favorable conditions for crystallization the X-ray pattern for synthetic talc is similar to that in figure 3B. For the most part, the X-ray pattern for synthetic talc agrees with that of natural talc. It was not found possible

to prepare a powder X-ray diffraction mount which would yield reflections of reliable relative intensities. Preferred orientation of the cleavage plates of natural talc in most mounts yielded strong 001 reflections. The synthetic talc usually gave weak 001 reflections. Attention is called to the peak at approximately $2\theta = 19°$ (Cu Kα), the reflection corresponding to the spacing of the 020, $11\bar{1}$, 004 planes (Gruner, 1934). The slope of the peak on the high angle side is interpreted as due to irregular shifts in the stacking of the primary structural layers (Hendricks, 1938, p. 271). This appears to be a common phenomenon in compounds in the MgO—Al_2O_3—SiO_2—H_2O system having layered structures (see pyrophyllite, clinochlore, Al-serpentine). In compositions in which alumina is present, the unit cell of talc shrinks measurably in the c dimension (compare figures 3A and 3B). The unit cell dimensions then appear to approach those of pyrophyllite and their X-ray patterns can be easily confused in mixtures of several phases. On this evidence, there is a basis for concluding that talc does take limited amounts of aluminum into its structure. The alumina content of some natural talc is as high as 3.75 per cent (Wells, 1937), and in one specimen analyzed in 1851 the alumina was 4.7 per cent (Scheerer). Bowen and Tuttle

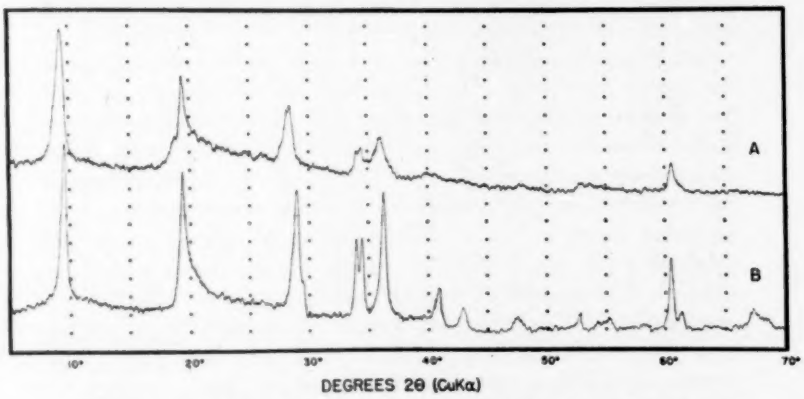

Fig. 3. A. Powder X-ray diffraction pattern of a synthetic talc prepared at 425°, 70 hours, 15,000 psi, from a mix of the appropriate composition.

B. Powder X-ray diffraction pattern of a synthetic talc prepared at 680°, 1 hour, 15,000 psi, from a glass of the F-34 composition. Peaks due to cordierite are deleted.

(1949, p. 443) have demonstrated that talc does not take up MgO or SiO_2 in excess of that of the accepted formula. The water content of the pure synthetic talc is in accord with the theoretical value of 4.75 per cent. Recent chemical analyses suggest, however, that natural talc may have a variable water content.

Pyrophyllite.—Although no compositions were investigated in which pyrophyllite, $Al_2(Si_4O_{10})(OH)_2$, crystallizes as a stable phase, it appeared metastably in the cordierite composition and in a mixture on the cordierite—quartz join below 525° C. at 15,000 psi. The X-ray pattern was similar to that obtained from a natural pyrophyllite from Hawthorne, Nevada.

Serpentine.—Subjecting powders of the composition $3MgO \cdot 2SiO_2$ to hydrothermal treatment resulted in a dense fibrous mass of minute crystals. The index of refraction of the mass was approximately 1.54. The crystals were isotropic or had very low birefringence. The water content was found to be about 13.7 per cent. Usually the mass contained crystals of forsterite, presumably the result of a change of bulk composition effected by the loss of silica. Longer runs yielded more forsterite and the buffer contained more forsterite than the charge.

The compound $Mg_6(Si_4O_{11})(OH)_6 \cdot H_2O$ has been thought in the past to exist in at least two forms, chrysotile (fibrous) and antigorite (platy). On the basis of morphological, optical, and differential thermal data, Bowen and Tuttle (1949, p. 443) have shown that the compound formed at any temperature below 500° ± 10° and at pressures from 2000 to 40,000 psi is chrysotile. However, the X-ray powder diffraction pattern of the material produced by the writer, as well as that of the material produced by Bowen and Tuttle, is too diffuse to determine with certainty whether the synthetic product is either antigorite or chrysotile on the basis of criteria set up by Selfridge (1936, pp. 466-471). From a study of natural serpentines by the writer the X-ray pattern of material thought to be chrysotile on other evidence is diffuse compared to the more distinct pattern given by material identified as antigorite. The poor quality of the X-ray pattern, in addition to the similarity of some interplanar spacings, suggests that the syn-

thetic product is chrysotile. The X-ray pattern of a synthetic serpentine produced at 450° for 1 day at 15,000 psi, that of a natural chrysotile, and that of a natural antigorite are given in figure 4.

Recently Bates and Mink (1951, p. 310) have presented morphological data which suggest that chrysotile is the pure compound and that antigorite may require the presence of trivalent ions replacing magnesium in the structure. Although the chemical analyses of minerals now classified as antigorite and chrysotile do not fully support this view, new supporting data will be presented in a following section.

Clinochlore.—The compound $Mg_5Al_2Si_3O_{10}(OH)_8$, having properties identical with those of the natural mineral clinochlore, can be prepared with long runs between approximately 520° and 680° and at pressures from 2000 to 30,000 psi. The compound crystallizes slowly and forms in minute plates having an average index of refraction of 1.580 and low birefringence. The powder X-ray diffraction pattern agrees with that of a

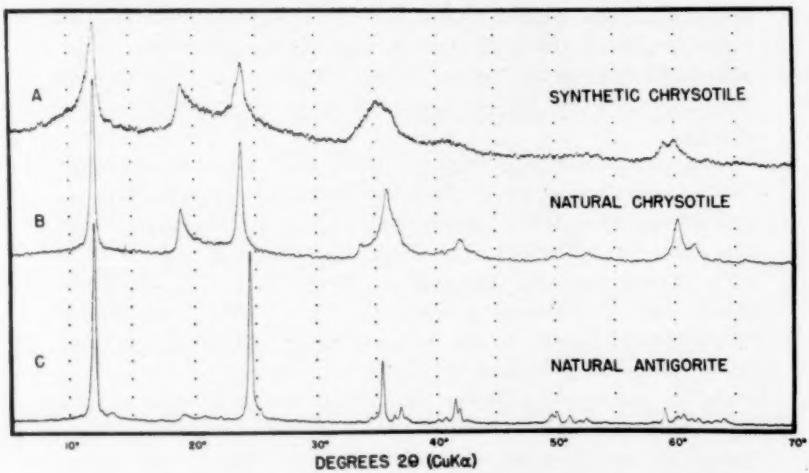

Fig. 4. A. Powder X-ray diffraction pattern of synthetic chrysotile prepared at 400°, 72 hours, 15,000 psi, from a mix of the appropriate composition.

B. Powder X-ray diffraction pattern of a natural chrysotile from Hoboken, New Jersey.

C. Powder X-ray diffraction pattern of a natural antigorite from Caracas, Venezuela (Hess, Smith and Dengo, 1952).

natural leuchtenbergite from New Gabbs, Nevada (Wells, 1937, p. 106). The interplanar spacings of the synthetic clinochlore are given in table 1.

The growth of synthetic clinochlore takes place in roughly three stages (see fig. 5). A new form, having the composition of clinochlore, grows rapidly from a mixture of periclase, γ-alumina, and silica glass in the formula proportions under all pressures of water vapor. This serpentine-like form, figure 5D, will be described fully in the next section. Slowly a clinochlore-like pattern appears, similar to that in figures 5B and 5C. This in turn slowly resolves into the clinochlore pattern given in figure 5A. Although the synthesis of clinochlore has

TABLE 1

Powder X-ray Diffraction Measurements of Synthetic Cordierite, Synthetic Aluminous Serpentine, and Synthetic Clinochlore

Syn. Cordierite		Syn. Al-Serpentine		Syn. Clinochlore	
d (Å)	I	d (Å)	I	d (Å)	I
8.52	100	7.12	100	14.42	32
4.92	26	4.61	38	7.20	100
4.67	13	3.56	80	4.78	52
4.11	50	2.87	5	4.61	13
3.39	60	2.64	36	3.58	75
3.15	60	2.61	18	2.87	10
3.04	54	2.58	20	2.67	1
2.65	14	2.49	29	2.59	5
2.52	1	2.442	18	2.55	10
2.45	3	2.380	48	2.45	12
2.433	1	2.321	6	2.391	4
2.419	1	2.263	8	2.277	3
2.336	9	2.126	2	2.075	1
2.282	2	2.024	9	2.049	4
2.237	3	2.005	20	2.014	8
2.172	3	1.962	4	1.892	3
2.109	6	1.942	8	1.836	3
2.103	6	1.879	2	1.722	1
2.048	1	1.662	9	1.664	2
1.944	3	1.563	8	1.583	4
1.933	2	1.550	6	1.539	8
1.878	7	1.535	34	1.501	2
1.851	2	1.500	10	1.480	2
1.813	3	1.477	2	1.405	4
1.807	4	1.470	2	.....	..
1.693	13	1.429	6	.....	..

d = spacing I = intensity Cu Kα; λ = 1.5418 Å

Intensity based on arbitrary scale; highest peak defined as 100 units.

been previously demonstrated by Tu (1950, unpublished) using various alkali salts as catalysts, only "serpentine or boehmite and a little of an unknown compound" were obtained in experiments in which no "motivator" was present. The

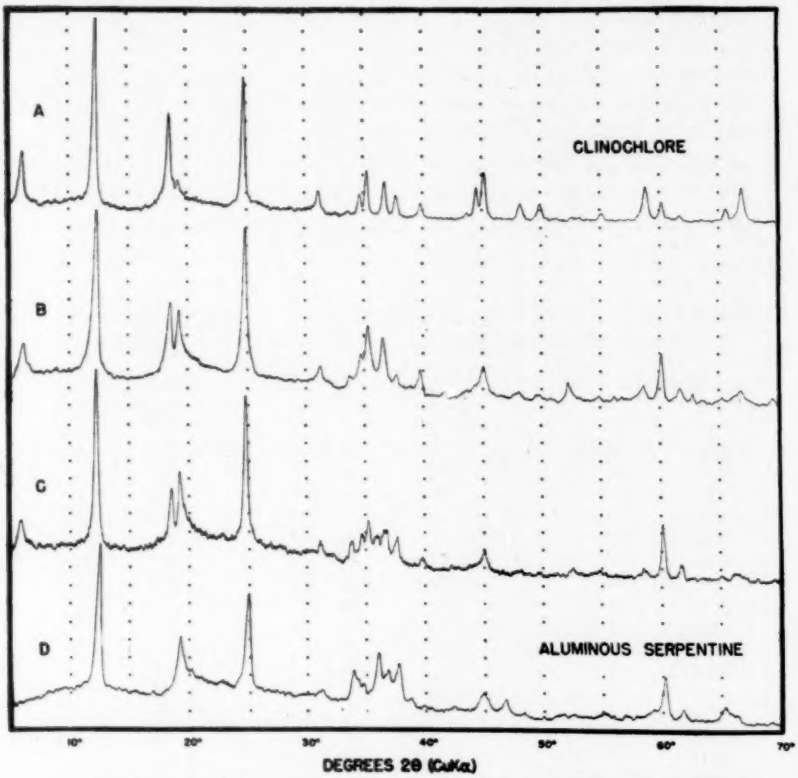

Fig. 5. Photograph of a series of powder X-ray diffraction patterns showing the progressive transformation of aluminous serpentine (D) to clinochlore (A).

A. Synthetic clinochlore prepared at 670°, 167 hours, 15,000 psi, from a glass of the pyrope composition (see table 1).

B. Mixture of synthetic clinochlore and aluminous serpentine prepared at 650°, 239 hours, 15,000 psi, from a mix of the clinochlore composition.

C. Mixture of synthetic clinochlore and aluminous serpentine prepared at 650°, 172 hours, 15,000 psi, from a glass of the pyrope composition.

D. Aluminous serpentine prepared at 480°, 163 hours, 15,000 psi, from a mix of the amesite composition.

The peaks due to other phases have been deleted from some of the patterns.

"phases" mentioned by Tu are probably the equivalent of the new form.

Aluminous-Serpentine.—Below approximately 520° C. at pressures of water vapor from 2000 to 30,000 psi, a mixture of powders in the proportions of $5MgO{\cdot}Al_2O_3{\cdot}3SiO_2$ yields a product similar in structure to that of a serpentine. As in the case of serpentine proper, the powders react completely within a day. The aggregates consist of minute plates having an average index of refraction of 1.57. The birefringence is nil or very low. One measurement of the water content gave 13.4 per cent. Tentatively the material will be referred to as aluminous serpentine.

The powder X-ray diffraction pattern is given in figure 5D and the interplanar spacings are given in table 1. The characteristic clinochlore peak at approximately $2\theta = 6°$ (CuKα) is absent. Of particular interest is the observation that the greater distance between the peaks at $2\theta = 19°$ and 25° is, according to Selfridge (1936, p. 470), characteristic of antigorite rather than of chrysotile. The X-ray pattern is sufficiently unique to warrant the conclusion that the product is a new form having the clinochlore composition and a kaolinite-like structure.

The differential thermal analysis pattern, obtained by Dr. George Faust of the U. S. Geological Survey, is given in figure 6B. According to Dr. Faust, the pattern is distinct from patterns obtained from purified natural materials commonly called chrysotile, antigorite, and clinochlore. And by comparison with figure 6A, it is seen that the pattern is distinct from that of a material approaching synthetic clinochlore in structure (see X-ray pattern in fig. 5B). The pattern in figure 6A is obviously that of a mixture. It cannot be determined from the differential thermal data whether or not the pattern for Al-serpentine (fig. 6B) may also be that of a mixture.

The electron photomicrograph shown in figure 7 was prepared by Dr. T. F. Bates of the Mineral Industries School, Pennsylvania State College. The platy nature of the aluminous serpentine suggests that it is more closely related to antigorite than to chrysotile. It is likely, therefore, that in the past aluminous serpentine has been identified as antigorite and in some instances as clinochlore. The platy habit of aluminous serpentine supports the contention of Bates and Mink that

antigorite may require the presence of trivalent ions in its structure.

In view of the fact that the new form slowly changes to clinochlore above 520°, an alternative interpretation of the data is possible. If the new form is metastable, it could be converted to clinochlore at every temperature below 680° C. presumably given sufficient time or the presence of a suitable catalyst. Since it was not possible to convert clinochlore to the new form, reversibility has not been demonstrated, and

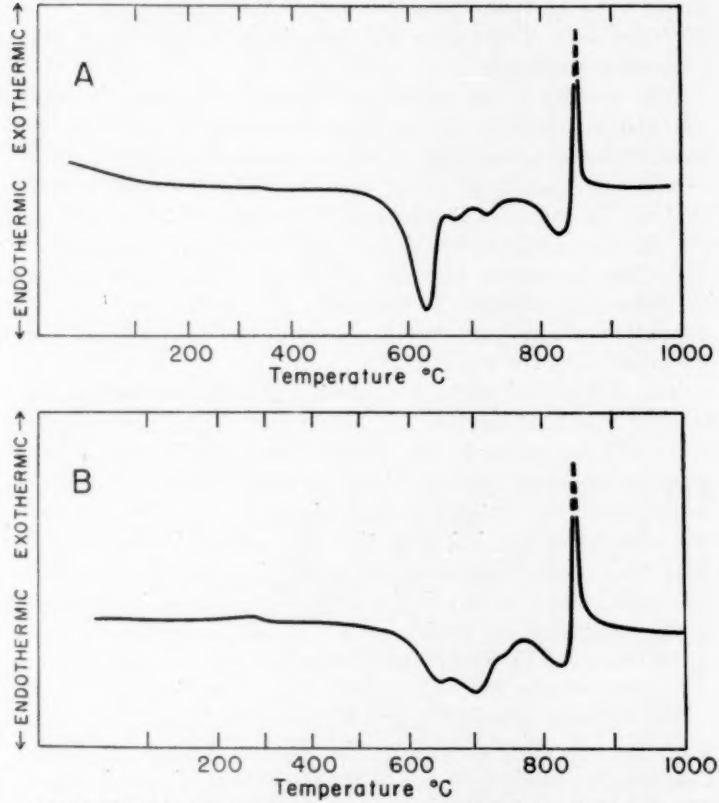

Fig. 6. Tracing of the differential thermal patterns taken by Dr. George Faust, U. S. Geological Survey.

A. Mixture of synthetic clinochlore and aluminous serpentine (see X-ray pattern in figure 5B).

B. Synthetic aluminous serpentine prepared at 500°, 16 hours, 15,000 psi, from mix A of the clinochlore composition.

therefore it cannot be stated with certainty that the new form has a stable range. However, in future discussion the new form will be assumed to have a stable range up to approximately 520° C., where it would transform into clinochlore under equilibrium conditions.

There is no natural mineral of the requisite composition known to the writer which gives an X-ray pattern similar to that of the new form. Some specimens of serpentine identified solely on optical properties give similar X-ray patterns, but without corroborative evidence they cannot be described as Al-serpentine. It would seem reasonable to assume that if the new form is a stable mineral it would be found in "chlorite" schists or in spotted slates having "chlorite" porphyroblasts.

Experiments involving a composition of equal molecular portions of the serpentine and clinochlore mixtures yielded a single phase also having a kaolinite-like structure. On the basis of these experiments and the similarity of the resulting structures, it is believed that there is a complete series of solid solutions between one form of serpentine and the new form of clinochlore composition. Since the synthetic serpentine decomposes at a temperature lower than that at which clinochlore was produced, it is not possible to judge if there are solid solutions between one form of serpentine and clinochlore. Structurally there is some reservation regarding complete solid

Fig. 7. Electron photomicrograph of aluminous serpentine prepared at 500°, 16 hours, 15,000 psi, from mix A of the clinochlore composition. Courtesy of Dr. T. F. Bates, Mineral Industries School, The Pennsylvania State College.

solution between a kaolinite-like structure and a mica-like structure. However, a possible structure which was rejected by McMurchy (1934, p. 25) in his study of chlorites does permit the stacking of mica, brucite, and kaolinite sheets. Therefore, the possibility of solid solution between a kaolinite-like and a mica-like structure is not completely ruled out, at least not on structural grounds.

The composition equivalent to amesite, $2MgO \cdot Al_2O_3 \cdot SiO_2$, was investigated hydrothermally. No amesite was produced. Instead, the equilibrium products established with other compositions were obtained. It is concluded that there is insufficient experimental evidence for a complete series of solid solutions from serpentine to amesite as suggested by Winchell (1951, p. 381). The composition equivalent to magnesian chamosite, $3MgO \cdot Al_2O_3 \cdot 2SiO_2$, was also investigated hydrothermally. No magnesian chamosite was produced.

Cordierite.—The compound $2MgO \cdot 2Al_2O_3 \cdot 5SiO_2$, which melts incongruently, will form from glass of the requisite composition below 1470° ± 5° C. in runs as short as thirty minutes performed in the dry way (unpublished data, Schairer, 1951) and above 950° C. (Rankin and Merwin, 1918, p. 325). Below about 950° C., Rankin and Merwin obtained a form (μ) which they considered to be unstable because there "appears to be no true inversion point" and reversibility could not be demonstrated. They also believed that both the stable and unstable forms form extensive solid solutions. The indices of refraction of the high-temperature, or α form, are given as $\alpha = 1.519$ and $\beta = \gamma = 1.522$ from melts containing 66 per cent SiO_2 and $\alpha = 1.524$ and $\beta = \gamma = 1.528$ from melts containing 50 per cent SiO_2. The crystals were stout, hexagonal prisms with negative elongation. An average index of refraction of the μ form is given on aggregates of fine radiating fibers as 1.535 at 68 per cent SiO_2 and 1.560 at 40 per cent SiO_2. The aggregates may have contained glass which would tend to raise the average index of refraction.

Dittler and Köhler (1938) synthesized crystals similar to the α form described by Rankin and Merwin. The material crystallized as pseudo-hexagonal prisms with $2V_a = 50° — 57°$ and $\alpha' = 1.524$. From melts having slightly more silica they obtained crystals with $2V = 65° — 78°$ and $\alpha' — 1.526$. The

silica content appears to have had the opposite effect on the indices of refraction from that obtained by Rankin and Merwin. All the cordierites produced by Rankin and Merwin and by Dittler and Köhler were optically negative.

Shand (1943, p. 393) gives the following optical properties of an analyzed synthetic cordierite which had formed on the wall of a glass manufacturing tank: $\alpha = 1.5223$, $\gamma = 1.5270 \pm 0.0003$; $2V = 82° - 83°$; optically negative. The crystals contained, in addition to the required constituents, 1.24 per cent CaO and 0.25 per cent H_2O.

Crystals of the α form prepared by Dr. J. F. Schairer were examined and found to be short, hexagonal prisms with negative elongation. The indices of refraction were $\alpha = 1.521$ and $\gamma = 1.526$; they were optically negative with a 2V of approximately 30°. The powder X-ray diffraction pattern of this material is identical with that of a natural cordierite from Guilford, Connecticut.

The compound $Mg_2Al_4Si_5O_{18}$ was prepared hydrothermally as low as 490° from a glass of the requisite composition. The interplanar spacings of a synthetic cordierite prepared in this way are given in table 1. It is believed that the compound will form in the presence of an excess of water vapor as low as *ca.* 400°. Between 400° and about 530° cordierite does not form directly but as the result of reaction between what are believed to be metastable products. For example, Al-serpentine or clinochlore and pyrophyllite usually form first and then react slowly with the remaining material to produce cordierite. Tabular crystals or short hexagonal prisms are formed directly at higher temperatures. Multiple sector twinning and wavy extinction are common. The crystals usually are skeletal and contain inclusions if other phases are present. When formed in a composition poor in cordierite, the crystals are characteristically large and few. Their growth in the laboratory is apparently similar to that in nature where cordierite also forms large crystals from few nuclei in some low-grade metamorphic rocks.

The indices of refraction of the crystals formed hydrothermally below approximately 830° are $\alpha = 1.537$, $\gamma = 1.541$ with $2V < 45°$. There was no measurable difference in indices of refraction of crystals grown from mixes higher or lower in SiO_2. The prisms had negative elongation and were optically negative. Above approximately 830° the crystals formed had

properties similar to those produced in the dry way at high temperatures. The powder X-ray diffraction patterns of the cordierite produced hydrothermally both above and below 830° were identical in every detail with the pattern from crystals produced in the dry way at higher temperatures and from the natural crystals.

From the above data the writer believes that the evidence for solid solution of silica in cordierite is subject to some doubt. In addition, there appears to be evidence for two forms of cordierite even though the X-ray data are inconclusive. The indices of refraction of the hydrothermal cordierite produced below 830° are in accord with the average index of refraction of the μ form of Rankin and Merwin and there is agreement on most of the properties of the α form. The higher indices of refraction of the cordierite prepared hydrothermally below 830° were thought at first to be due to the presence of iron gained from the steel pressure vessel; however, according to Folinsbee's curve (1941, p. 495), this would mean about 15 mol per cent $Fe_2Al_4Si_5O_{18}$ in solid solution. The writer considers the absorption of this much iron most unlikely. The effect of water, believed by a few investigators to be an essential constituent of cordierite, on the indices of refraction would probably be opposite to that observed. It is concluded that the possible existence of two forms of cordierite is worthy of further study.

Forsterite.—Mg_2SiO_4 in the form forsterite grows readily from powdered mixes or from glasses of requisite compositions under an excess of water vapor at about 430° or higher. The mineral grows very quickly in equi-dimensional facetted crystals. It is very resistant to decomposition in regions where it is not a stable phase. For example, runs of several weeks' duration are required for the effects of serpentization to become observable. Other examples are found in runs made on glasses close to Mg_2SiO_4 in composition in which forsterite always appears as the result of the inability to quench such glasses with techniques now available. The optical properties and powder X-ray diffraction pattern are identical with those of synthetic forsterite prepared in the dry way at high temperatures and are similar to those of natural olivines close to Mg_2SiO_4.

Enstatite.—The compound $MgSiO_3$ grows in the presence of an excess of water vapor above about 660° C. from a glass of the proper composition. Within a temperature region extending about 40° above 660° the compound forms as the result of a reaction of the metastable products talc and forsterite which are the stable equivalent below 660°. Above approximately 700° the compound forms directly from its glass within an hour. The crystals usually form a dense fibrous mass. The optical properties are similar to those of a natural enstatite (Bishopville Meteorite) which is close to $MgSiO_3$ in composition. The powder X-ray diffraction pattern is diffuse and not sufficiently resolved to distinguish with certainty whether the compound is enstatite, protoenstatite (= mesoenstatite), or clinoenstatite; however, the X-ray pattern, given in figure 8A, shows greatest similarity to enstatite. X-ray powder diffraction patterns of this diffuse type, commonly obtained in products in the $MgO—Al_2O_3—SiO_2—H_2O$ system, are usually regarded as being the result of very small crystals or of disorder in the structure.

Enstatite, yielding an X-ray pattern identical with that of natural enstatite, has been synthesized with the aid of a LiF, LiCl, or KVO_3 flux by L. M. Atlas (personal communica-

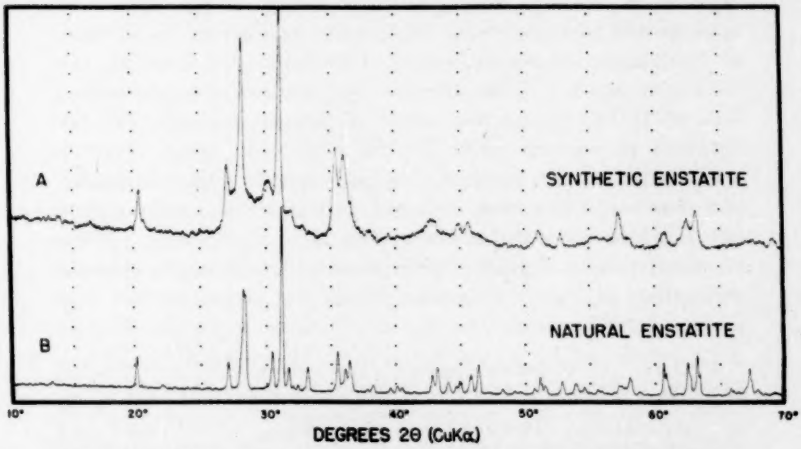

Fig. 8. A. Powder X-ray diffraction pattern of synthetic enstatite prepared at 980°, 1 hour, 15,000 psi, from a glass of the enstatite composition. B. Powder X-ray diffraction pattern of natural enstatite (Bishopville meteorite).

tion, May 1950). Without the aid of a flux he obtained patterns which "resemble those of rhombic enstatite." Schairer and Yoder (Dec., 1950, unpublished) obtained unexpectedly from a glass of pyrope composition heated in the dry way an X-ray pattern of enstatite identical with natural enstatite. The enstatite persisted metastably for as long as 9 days at 1200°, at the end of which time the stable products, cordierite + forsterite + spinel, comprised the charge.

Protoenstatite.—The enstatite ⇌ protoenstatite inversion was found by Atlas (1952, p. 138) to be 985° C. in the presence of alkali fluxes. Schairer and Yoder (unpublished data, 1951) found the inversion to be at least as low as 1125° C. using the dry quenching technique. In this work the inversion appears to take place at 990° ± 10° C. under 15,000 psi water pressure. However, the growth of enstatite above this apparent inversion temperature casts some doubt on this conclusion. For this reason it is more likely that the inversion point lies at a temperature between 985° and 1125°. Protoenstatite was identified by its powder X-ray diffraction pattern.

Spinel.—The compound $MgAl_2O_4$ in the form of spinel crystallizes readily from powdered mixes or glasses of the appropriate composition at least as low as 400° in the presence of an excess of water vapor. Commonly the crystals are distinct octahedra. They are isotropic with an index of refraction of 1.718. Within the error of measurement the crystals obtained in various parts of the region in which spinel is stable are the same as those for pure spinel. Spinel is another compound which is very resistant to decomposition in regions in which it is not a stable phase. The X-ray diffraction pattern of spinel produced under hydrothermal conditions is identical with that of material produced in the dry way at high temperatures.

Brucite. — Crystals having the properties of brucite, $Mg(OH)_2$, were obtained by hydration of MgO in a wide range of temperatures. Hexagonal plates having $\omega = 1.565$ and $\epsilon = 1.1583$ grew rapidly in the two compositions investigated in which brucite was a stable phase.

Periclase.—The isotropic octahedra of periclase, MgO, are obtained only with some difficulty in the presence of water

vapor above about 650° C. Periclase hydrates to brucite rapidly, in fact, even when rapidly cooled. The index of refraction of the periclase was found to be 1.734.

Quartz.—Quartz was readily obtained in the one preparation in which it was a stable phase. The crystals were minute and could be identified with certainty only by the powder X-ray diffraction pattern. In one run a mixture of cristobalite and quartz was obtained. In the work of Bowen and Tuttle (1949, p. 444), silica appeared as cristobalite in most cases. There is the suggestion here that the presence of alumina may promote the formation of quartz and suppress the metastable formation of cristobalite.

Anthophyllite.—Crystals having a powder X-ray diffraction pattern similar to that of a natural anthophyllite from Gouverneur, New York, were obtained from a mixture of corundum, silica glass, and periclase in the proportions of pyrope held 7 days at 670° and 15,000 psi. The intensity of the peaks in the X-ray pattern were smaller for a mixture held 11 days at 670° and 15,000 psi. This is interpreted as the beginning of the decomposition of the anthophyllite to the stable phases. The crystals could not be identified optically because of the fine-grained nature of the product. As will be shown in subsequent sections, the anthophyllite obtained is metastable and on theoretical grounds cannot be obtained in the presence of an excess of water vapor.

EXPERIMENTAL DATA

Demonstration of equilibrium.—Much of the uncertainty in experimental studies of metamorphic rocks will arise over the question of whether or not equilibrium has been obtained. In this experimental work, univariant equilibrium is considered to be demonstrated provided that a slight increase in temperature at a given pressure will produce a change in the mineral assemblage which can be restored by a slight decrease in temperature at the same pressure. It was not always possible to demonstrate this reversibility because the rate of reaction in one direction, usually in the direction of decreasing temperature, is so slow as to be imperceptible in a reasonable time. In practice, divariant equilibrium is established on both the high- and low-temperature sides of a univariant curve and the position of univariant equilibrium interpolated. The only cri-

terion known to the writer of equilibrium in the divariant region is that the number of phases be in accord with the Phase Rule. This is a necessary condition, but not sufficient. It must further be established that the phases present are stable. The recognition of persistent metastable phases, to be discussed shortly, is not always simple and depends on the judgment of the experimenter.

Data.—All of the experiments performed are given in the accompanying tables. The mass of detailed data may appear confusing or contradictory to the geologist not acquainted with the interpretation of experimental data. For this reason an example of interpretation is given in the following section. First, some explanatory notes are required for the data presented in the tables. The symbols used in the tables and figures to follow are defined in table 2.

In table 3a are given the data obtained from a glass of the pyrope composition, $3MgO \cdot Al_2O_3 \cdot 3SiO_2$ ($n = 1.586$); from a portion of the same glass partly devitrified at 1080° for 3 days which consists of cordierite, enstatite, and glass; and from a mix consisting of periclase, quartz, and corundum. From these data it is concluded that the pyrope composition

TABLE 2

Abbreviations Used to Designate Phases

A	Andalusite	M	Montmorillonite
Al-S	Aluminous Serpentine	Mg-C	Magnesian Chamosite
Am	Amesite	Mg-M	Magnesian Montmorillonite
An	Anthophyllite	Mu	Mullite
B	Brucite	P	Periclase
Bo	Boehmite	Pe	Protoenstatite
C	Corundum	Pr	Pyrope
Ce	Clinoenstatite	Py	Pyrophyllite
Cl	Clinochlore	Q	Quartz
Co	Cordierite	S	Serpentine
Cr	Cristobalite	Sa	Sapphirine
D	Diaspore	Se	Sepiolite
E	Enstatite	Sil	Sillimanite
F	Forsterite	Sp	Spinel
G	Gibbsite	T	Talc
K	Kyanite	Tr	Tridymite
Ka	Kaolinite	V	Vapor

TABLE 3

Results of Hydrothermal Treatment of Various Compositions in the $MgO—Al_2O_3—SiO_2—H_2O$ System

Initial Materials	Temp. °C.	Pressure x 10^{-3} psi	Time Hours	Products
(a) Pyrope Composition: $3MgO \cdot Al_2O_3 \cdot 3SiO_2$				
Devit	610	2	125	E + Co + F + Cl
Devit	630	2	124	E + Co + F + Cl
Devit	650	2	128	E + Co + F + glass
Glass	660	2	128	F + Co + T + glass
Glass	500	7.5	208	Al-S + glass
Devit	620	7.5	167	Co + Cl + T
Glass	640	7.5	49	Co + F + Al-S + T
Glass	660	7.5	23	Co + F + Cl + Sp
Glass	680	7.5	20	Co + F + Sp
Glass	450	15	133	Al-S + glass
Glass	475	15	240	Al-S + glass
Natural	500	15	350	Pr + Cl + T + Co
Glass	515	15	16	Al-S + glass
Mix	520	15	115	Al-S + T + Co (?)
Natural	550	15	281	Pr + Cl + Co + T
Glass	550	15	95	Al-S + T + Co
Natural	600	15	188	Pr + Cl + Co + ?
Glass	600	15	22	Al-S + T + Co
Glass	625	15	145	Co + Al-S + Cl + T
Devit	630	15	215	Co + Cl + T
Glass	650	15	22	Co + Cl + T
Glass	650	15	172	Co + Cl + Al-S + T
Devit	655	15	211	Co + Cl + F
Glass	660	15	2	Co + Cl + Al-S + T
Glass	670	15	23	Co + Cl + T
Mix	670	15	167	An + F + C
Glass	670	15	167	Co + Cl + T
Mix	670	15	266	An + F + C + Co
Glass	675	15	23	Cl + F + Co
Glass	680	15	216	Co + Cl + F
Devit	690	15	166	Co + F + Sp
Glass	700	15	18	Co + F + Sp
Glass	750	15	22	Co + F + Sp
Glass	800	15	3	Co + F + Sp
Natural	800	15	66	E + Co + Sp (?)
Mix	500	22.5	117	Al-S + ?
Glass	675	22.5	10	Co + Cl + T + F
Glass	700	22.5	21	Co + Cl + F + Sp
Glass	500	30	120	Al-S + glass
Glass	550	30	120	Co + Cl + T (?)
Glass	650	30	24	Co + Cl + T
Glass	675	30	20	Co + Cl + T
Natural	700	30	65	Pr + Cl + T + Co

TABLE 3 (*Cont.*)

Results of Hydrothermal Treatment of Various Compositions in the $MgO—Al_2O_3—SiO_2—H_2O$ System

Initial Materials	Temp. °C.	Pressure x 10^{-3} psi	Time Hours	Products
Glass	700	30	18	Co + Cl + F
Glass	720	30	22	Co + F + Sp
Glass	740	30	6	Co + F + Sp
Natural	650	60	64	Pr + Cl + T + Co
(b) Clinochlore Composition: $5MgO \cdot Al_2O_3 \cdot 3SiO_2$				
Natural	480	15	327	Cl
Mix A	500	15	16	Al-S
500° Product	525	15	167	Al-S
500° Product	525	15	334	Al-S
Synthetic Cl	550	15	50	Cl
500° Product	550	15	50	Al-S
Mix A	550	15	134	Al-S
Mix B	550	15	165	Al-S + F
Mix A	575	15	164	Al-S
500° Product	600	15	20	Al-S + Cl
500° Product	600	15	115	Al-S + Cl
Natural	650	15	265	Cl
Mix A	650	15	239	Cl + Al-S + F
Mix B	650	15	192	T + F + Al-S + Sp (?)
500° Product	650	15	93	Cl
Mix B	660	15	240	F + C + Cl + T
500° Product	675	15	48	Cl + Al-S
500° Product	675	15	172	Cl + Al-S
500° Product	680	15	166	Cl + F
Natural	680	15	28	Cl + F (trace)
500° Product	690	15	163	Cl + F
Natural	690	15	162	Cl + F
Natural	700	15	94	Cl + F + Co + Sp
Natural	700	15	169	F + Cl + Sp
500° Product	700	15	21	F + Sp + T
500° Product	700	15	167	F + Co + Sp
500° Product	750	15	17	F + Sp + T
500° Product	775	15	24	F + Sp + T + Co (?)
500° Product	800	15	18	F + Sp + T + Co
500° Product	825	15	18	F + Sp + Co
(c) Cordierite Composition: $2MgO \cdot 2Al_2O_3 \cdot 5SiO_2$				
Glass	450	15	138	Al-S + glass
Glass	450	15	335	Al-S + Cl + Py + glass
Glass	470	15	166	Cl + Py + glass
Devit	490	15	233	Co
Glass	490	15	218	Co + Cl + Py + glass
Glass	500	15	335	Co + Al-S + Cl + Py + glass
Glass	510	15	167	Co + Cl(?) + glass
Devit	530	15	167	Co

TABLE 3 (*Cont.*)

Results of Hydrothermal Treatment of Various Compositions in the $MgO—Al_2O_3—SiO_2—H_2O$ System

Initial Materials	Temp. °C.	Pressure x 10^{-3} psi	Time Hours	Products
Devit	700	15	22	Co
Glass	800	15	14	Co
Glass	825	15	26	Co
Glass	840	15	23	α-Co
Glass	850	15	22	α-Co
Glass	875	15	20	α-Co
Glass	900	15	2	α-Co
(d) D-40 Composition: 70 Cordierite 30 Quartz by Weight				
Glass	500	15	260	Q + Py + Cl + glass
Glass	525	15	23	Q + Cr + Py + Cl + glass
Glass	525	15	122	Q + Co + Cl + glass
Glass	570	15	45	Co + Q
Glass	600	15	26	Co + Q
Glass	800	15	52	Co + Q
Glass	850	15	100	α-Co + Q
(e) P-1 Composition: 34.0 MgO 15.5 Al_2O_3 50.5 SiO_2 by Weight				
Glass	630	15	192	T + Cl + glass
Glass	650	15	51	T + Cl + glass
Glass	650	15	191	T + Cl + Co
Glass	670	15	3	T + Cl + glass
Glass	670	15	215	T + Cl + Co
Glass	680	15	1	T + Cl + glass
Glass	700	15	1	T + Cl + glass
Glass	700	15	84	Co + F + T
Glass	700	15	167	Co + F + E
(f) F-34 Composition: 50 Cordierite 50 Enstatite by Weight				
Glass	500	15	24	Al-S + glass
Glass	550	15	217	Cl + Al-S + glass
Glass	600	15	21	T + Co + Cl (?)
Glass	650	15	72	T + Co + Cl (?)
Glass	650	15	162	T + Co + Cl
Devit	650	15	186	Co + T + Cl + Ce
Devit	655	15	185	Co + T + Cl + Ce
Devit	660	15	166	Co + Ce
Devit	670	15	167	Co + Ce
Glass	675	15	19	T + Co + Cl (?)
Glass	680	15	1	T + Co + glass
Glass	700	15	73	Co + T + F
Glass	725	15	14	Co + E + T
Glass	750	15	19	Co + E
Glass	825	15	4	Co + E

TABLE 3 (*Cont.*)

Results of Hydrothermal Treatment of Various Compositions in the $MgO—Al_2O_3—SiO_2—H_2O$ System

Initial Materials	Temp. °C.	Pressure x 10^{-3} psi	Time Hours	Products
Glass	700	30	18	Co + Cl + F
Glass	720	30	22	Co + F + Sp
Glass	740	30	6	Co + F + Sp
Natural	650	60	64	Pr + Cl + T + Co
(b) Clinochlore Composition: $5MgO \cdot Al_2O_3 \cdot 3SiO_2$				
Natural	480	15	327	Cl
Mix A	500	15	16	Al-S
500° Product	525	15	167	Al-S
500° Product	525	15	334	Al-S
Synthetic Cl	550	15	50	Cl
500° Product	550	15	50	Al-S
Mix A	550	15	134	Al-S
Mix B	550	15	165	Al-S + F
Mix A	575	15	164	Al-S
500° Product	600	15	20	Al-S + Cl
500° Product	600	15	115	Al-S + Cl
Natural	650	15	265	Cl
Mix A	650	15	239	Cl + Al-S + F
Mix B	650	15	192	T + F + Al-S + Sp (?)
500° Product	650	15	93	Cl
Mix B	660	15	240	F + C + Cl + T
500° Product	675	15	48	Cl + Al-S
500° Product	675	15	172	Cl + Al-S
500° Product	680	15	166	Cl + F
Natural	680	15	28	Cl + F (trace)
500° Product	690	15	163	Cl + F
Natural	690	15	162	Cl + F
Natural	700	15	94	Cl + F + Co + Sp
Natural	700	15	169	F + Cl + Sp
500° Product	700	15	21	F + Sp + T
500° Product	700	15	167	F + Co + Sp
500° Product	750	15	17	F + Sp + T
500° Product	775	15	24	F + Sp + T + Co (?)
500° Product	800	15	18	F + Sp + T + Co
500° Product	825	15	18	F + Sp + Co
(c) Cordierite Composition: $2MgO \cdot 2Al_2O_3 \cdot 5SiO_2$				
Glass	450	15	138	Al-S + glass
Glass	450	15	335	Al-S + Cl + Py + glass
Glass	470	15	166	Cl + Py + glass
Devit	490	15	233	Co
Glass	490	15	218	Co + Cl + Py + glass
Glass	500	15	335	Co + Al-S + Cl + Py + glass
Glass	510	15	167	Co + Cl(?) + glass
Devit	530	15	167	Co

TABLE 3 (*Cont.*)

Results of Hydrothermal Treatment of Various Compositions in the $MgO—Al_2O_3—SiO_2—H_2O$ System

Initial Materials	Temp. °C.	Pressure x 10^{-3} psi	Time Hours	Products
Devit	700	15	22	Co
Glass	800	15	14	Co
Glass	825	15	26	Co
Glass	840	15	23	α-Co
Glass	850	15	22	α-Co
Glass	875	15	20	α-Co
Glass	900	15	2	α-Co
(d) D-40 Composition: 70 Cordierite 30 Quartz by Weight				
Glass	500	15	260	Q + Py + Cl + glass
Glass	525	15	23	Q + Cr + Py + Cl + glass
Glass	525	15	122	Q + Co + Cl + glass
Glass	570	15	45	Co + Q
Glass	600	15	26	Co + Q
Glass	800	15	52	Co + Q
Glass	850	15	100	α-Co + Q
(e) P-1 Composition: 34.0 MgO 15.5 Al_2O_3 50.5 SiO_2 by Weight				
Glass	630	15	192	T + Cl + glass
Glass	650	15	51	T + Cl + glass
Glass	650	15	191	T + Cl + Co
Glass	670	15	3	T + Cl + glass
Glass	670	15	215	T + Cl + Co
Glass	680	15	1	T + Cl + glass
Glass	700	15	1	T + Cl + glass
Glass	700	15	84	Co + F + T
Glass	700	15	167	Co + F + E
(f) F-34 Composition: 50 Cordierite 50 Enstatite by Weight				
Glass	500	15	24	Al-S + glass
Glass	550	15	217	Cl + Al-S + glass
Glass	600	15	21	T + Co + Cl (?)
Glass	650	15	72	T + Co + Cl (?)
Glass	650	15	162	T + Co + Cl
Devit	650	15	186	Co + T + Cl + Ce
Devit	655	15	185	Co + T + Cl + Ce
Devit	660	15	166	Co + Ce
Devit	670	15	167	Co + Ce
Glass	675	15	19	T + Co + Cl (?)
Glass	680	15	1	T + Co + glass
Glass	700	15	73	Co + T + F
Glass	725	15	14	Co + E + T
Glass	750	15	19	Co + E
Glass	825	15	4	Co + E

TABLE 3 (*Cont.*)

Results of Hydrothermal Treatment of Various Compositions in the $MgO—Al_2O_3—SiO_2—H_2O$ System

Initial Materials	Temp. °C.	Pressure x 10^{-3} psi	Time Hours	Products
(g) Enstatite Composition: $MgO \cdot SiO_2$				
Glass	490	15	45	T + S + F
Glass	500	15	1	T + F
Glass	600	15	1	T + F
Natural	640	15	212	E + T + F
Synthetic "E"	640	15	88	E
Glass	650	15	3	T + F
Natural	650	15	96	E
Glass	660	15	4	E + T + F
Natural	660	15	165	E + T (trace)
Glass	670	15	4	E + T + F
Glass	670	15	172	E + T + F
Natural	670	15	167	E
Glass 700° — 1 hr.	675	15	20	E + T + F
Glass	675	15	2	E + T + F
Glass	700	15	1	E
Glass	700	15	165	E
Glass	800	15	1	E
Glass	900	15	1	E
Glass	900	15	24	E
Glass	980	15	1	E
Glass	1000	15	1	Pe + E
Natural	1020	15	2	E
Glass	1020	15	2	Pe + E
(h) Serpentine Composition: $3MgO \cdot 2SiO_2$				
Mix	400	15	72	S
Mix	450	15	25	S
Mix	480	15	162	S + F (trace)
Mix	500	15	15	S + F + T
Mix	520	15	46	F + T
(i) P-2 Composition: 50 Serpentine 50 Clinochlore by Weight				
Devit	490	15	18	F + Al-S (?)
Devit	490	15	186	F + Al-S (?)
Mix	490	15	190	Al-S + F
Devit	500	15	254	Al-S + F + T
Mix	510	15	211	F + T + Al-S
Mix	530	15	192	Al-S + Cl + F + T
Devit	630	15	116	F + Al-S + Cl + T
Devit	650	15	39	F + Co + T + Cl
Devit	650	15	166	F + Co + Cl
Mix	650	15	69	F + Al-S + T
Devit	660	15	24	F + Co + Cl + T
Mix	670	15	47	F + Co + Cl (?)

TABLE 3 (*Cont.*)

Results of Hydrothermal Treatment of Various Compositions in the $MgO—Al_2O_3—SiO_2—H_2O$ System

Initial Materials	Temp. °C.	Pressure x 10^{-3} psi	Time Hours	Products
Devit	670	15	20	F + Co + Cl
Mix	690	15	44	F + Co + Sp (?)
Devit	700	15	22	F + Co + Sp
(j) P-4 Composition: 50 Forsterite 50 Clinochlore by Weight				
Mix	400	15	38	Cl + S + B
Mix	430	15	20	Cl + S + B
Mix	440	15	120	Cl + F
Mix	480	15	25	Cl + F
Mix	490	15	168	Cl + F
Mix	550	15	92	Cl + F
(k) Magnesian Chamosite Composition: $3MgO \cdot Al_2O_3 \cdot 2SiO_2$				
Mix	500	15	115	Al-S + Sp + Co
Mix	550	15	190	Al-S + Cl + Sp + Co
Devit	650	15	161	Sp + Co + Cl + T
Mix	660	15	169	Cl + Sp + Co
Mix	680	15	3	F + Co + Sp + T
Devit	690	15	288	F + Co + Sp
(l) Amesite Composition: $2MgO; Al_2O_3; SiO_2$				
Mix	480	15	163	Al-S +?
Devit	500	15	144	Al-S + Sp + T
Mix	520	15	139	Al-S + ?
Mix	550	15	173	Al-S + ?
Devit	550	15	114	Al-S + Sp + T
Mix	600	15	116	Al-S + Sp + Co
Devit	600	15	94	Sp + T + Al-S
Mix	650	15	158	Sp + Co + Cl
Devit	650	15	23	Sp + F + Co + T
Devit	650	15	165	Sp + T + Cl
Mix	660	15	165	Sp + F + Co + T
Devit	675	15	72	Sp + T + F
Devit	675	15	172	Sp + T + F
Mix	680	15	159	Sp + F + Co
Devit	700	15	68	Sp + F + Co
Mix	700	15	70	Sp + F + Co
(m) P-3 Composition: 70 MgO 15 Al_2O_3 15 SiO_2 (mol per cent)				
Mix	460	5	68	B + Sp + Al-S
Mix	480	5	63	B + Sp + F + Al-S
Mix	620	7.5	167	B + Sp + F
Mix	400	15	3	B + Sp + Al-S
Mix	440	15	16	B + Sp + Al-S
Mix	470	15	42	B + Sp + Al-S
Mix	480	15	175	B + Sp + Al-S

TABLE 3 (*Cont.*)

Results of Hydrothermal Treatment of Various Compositions in the $MgO—Al_2O_3—SiO_2—H_2O$ System

Initial Materials	Temp. °C.	Pressure x 10^{-3} psi	Time Hours	Products
Mix	490	15	211	B + Sp + Al-S + F
Mix	500	15	23	B + Sp + Al-S + F
Mix	500	15	167	B + Sp + F
Mix	550	15	17	B + Sp + F
Mix	650	15	19	B + Sp + F
Mix	670	15	19	B + Sp + F
Mix	720	15	49	B + Sp + F + P
Mix	810	15	1	B + Sp + F + P
Mix	495	22.5	51	B + Sp + F + Al-S
Mix	490	30	25	B + Sp + Al-S
	(n) Anthophyllite: $7MgO \cdot 8SiO_2 \cdot H_2O$			
Natural	600	15	330	An
Natural	650	15	221	An
Natural	700	15	112	Kupfferite (?)
Natural	800	15	168	Kupfferite (?) + E + Q
Natural	900	15	70	E + Q

would consist of the following stable assemblages under 15,000 psi water vapor:

450°	—	<625°	Al—S + T + Co + V
<625°	—	655°	Co + Cl + T + V
655°	—	680°	Co + Cl + F + V
680°	—	>800°	Co + F + Sp + V

Pyrope was not produced. The metastable assemblages of this and other compositions are discussed on a later page. The natural garnet, very rich in the pyrope molecule, is from Meronitz, Bohemia (U.S.N.M., R-3419), and has an index of refraction of 1.740 ± 0.002, a density of 3.74 ± 0.02, and a unit cell edge of 11.476 ± 0.004 Å. According to the work of Stockwell (1927), the garnet used has properties similar to those very rich in pyrope. Garnets from this locality show little variation in composition and contain approximately $Py_{74}Al_{15}An_5Uv_6$ (Fleischer, 1937, p. 756). No analysis was made. Pure pyrope has not been found in nature.

In table 3b are given the data obtained from mix A of the clinochlore composition, $5MgO \cdot Al_2O_3 \cdot 3SiO_2$, consisting of periclase, silica glass, and γ-alumina; from mix B consisting of periclase, quartz, and corundum; from the product obtained

by heating mix A at 500° overnight under 15,000 psi water vapor; from a synthetic clinochlore; and from a natural leuchtenbergite, supplied by Dr. George Faust from the Nevada Tungsten Mine, New Gabbs, Nevada (analysis in Wells, 1937, p. 106). The following stable assemblages at 15,000 psi water vapor were identified from these data:

480°	—<600°	Al—S + V
<600°	— 680°	Cl + V
680°	— >825°	F + Co + Sp + V

The pressure—temperature diagram obtained from this and other compositions for the equilibrium Cl ⇌ F + Co + Sp + V and the transformation Al-S → Cl are given in figure 9.

In table 3c are given the data obtained from a glass of the

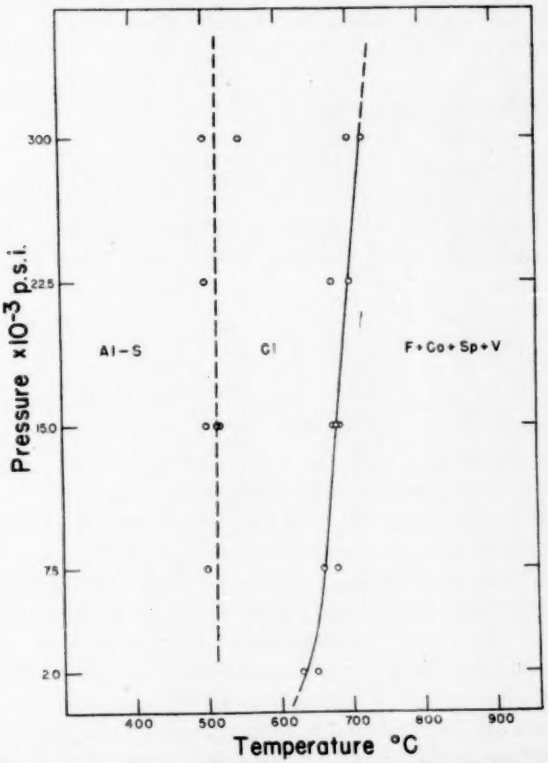

Fig. 9. Pressure—temperature curve of the transformation Al-S → Cl and of the reaction Cl ⇌ F + Co + Sp + V (curve VIII of fig. 10).

cordierite composition, $2MgO \cdot 2Al_2O_3 \cdot 5SiO_2$, and from a portion of the same glass devitrified at 1400° for 2 hours. The index of refraction of the glass was 1.559. The partly devitrified glass consisted of cordierite, spinel, and glass. It is concluded from these data that cordierite is stable at least as low as 490°.

In table 3d are given the data obtained from a glass of the composition 70 per cent cordierite and 30 per cent quartz by weight (D-40). The index of refraction of the glass is 1.525. It is concluded that the assemblage quartz + cordierite is stable at least as low as 525° at 15,000 psi water vapor.

In table 3e are given data for composition P-1 which consists of 34.0 MgO, 15.5 Al_2O_3, 50.5 SiO_2 per cent by weight. In this case all runs were made on a glass of that composition which has an index of refraction of 1.585. It appears as though equilibrium was not obtained with assurance in this composition except in one run at 700° where Co + F + E + V are stable.

In table 3f are given the data for a composition of 50 cordierite 50 enstatite by weight (F-34). A glass, index of refraction = 1.569, and a portion of the same glass devitrified at 1300° for 17 hours were used. The devitrified glass consisted of cordierite + protoenstatite + clinoenstatite. The following assemblages are believed to be stable under 15,000 psi water vapor:

<500°	—	525°	Al—S + Co + T + V
525°	—	650°	Cl + Co + T + V
650°	—	660°	No reliable data.
660°	—	>825°	Co + E + V

In table 3g are given the data obtained from a glass of the enstatite composition, $MgO \cdot SiO_2$, from synthetic "enstatite," and from a natural enstatite. The glass has an index of refraction of 1.580 and was prepared in 1913 by Bowen and Andersen (1914). The natural enstatite, supplied through the courtesy of Dr. W. F. Foshag, is from the Bishopville, South Carolina, meteorite. A published analysis of this material indicates it to be almost pure $MgSiO_3$ (Smith, 1864). The synthetic "enstatite" was prepared by Dr. N. L. Bowen about 1915; no other information is available. The data on these materials indicate that the following assemblages are stable at 15,000 psi water pressure:

<490°	—	500°	S + T + V
500°	—	660°	F + T + V
660°	—	>990°	E + V

The data for the serpentine composition are given in table 3h. All runs were made on a mix of periclase and silica glass in the proper proportions. The following phase assemblages were obtained:

<400°	—	500°	S + V
500°	—	>520°	F + T + V

The data for composition P-2, corresponding with 50 serpentine 50 clinochlore by weight, are given in table 3i. The materials used were a mix of periclase, γ-alumina, and silica glass and a glass devitrified at 1520° for 3 days consisting of forsterite and glass. The assemblages believed to be stable are:

<490°	—	500°	Al-S_{ss} + V
500°	—	520°	Al-S_{ss} + F + T + V
520°	—	655°	Cl + F + T + V
655°	—	680°	Cl + F + Co + V
680°	—	>700°	F + Co + Sp + V

In table 3j are given the data for composition P-4, corresponding with 50 forsterite 50 clinochlore by weight. A mix of the requisite proportions of periclase, silica glass, and the natural leuchtenbergite from Nevada were used. Since the leuchtenbergite did not appear to be affected by the hydrothermal conditions imposed, it can only be concluded that between 430° and 440° the reaction S + B ⇌ F + V takes place.

The magnesian-chamosite composition, $3MgO \cdot Al_2O_3 \cdot 2SiO_2$, was investigated using a glass partly devitrified at 1585° for 2 days. The initial material consisted of spinel, forsterite, and glass. In addition, runs were made on a mix consisting of periclase, γ-alumina, and silica glass. Chamosite was not produced, even though the region was studied in which it is most likely to be stable. The data are given in table 3k.

The data for the amesite composition, $2MgO \cdot Al_2O_3 \cdot SiO_2$, are given in table 3l. A mix, consisting of periclase, γ-alumina, and silica glass, and a glass devitrified at 1580° for 18 hours, consisting of spinel, forsterite, and glass, were used. Amesite was not produced; the assemblages obtained were consistent

with the results obtained from other compositions. The composition readily yielded metastable phases.

In table 3m are given the data for composition P-3 which was prepared with 53.74 periclase, 29.11 γ-alumina, and 17.15 silica glass in per cent by weight. The following assemblages are thought to be stable at 15,000 psi water vapor:

<400°	—	485°	B + Sp + Al-S + V
485°	—	<720°	B + Sp + F + V
<720°	—	>810°	P + Sp + F + V

The data on the decomposition of a natural anthophyllite from Gouverneur, New York, are recorded in table 3n. The cursory investigation suggests that anthophyllite transforms into a monoclinic amphibole, presumably kupfferite, and then decomposes into E + Q + V.

The monoclinic amphibole formed from the natural anthophyllite had an X-ray pattern similar to the monoclinic amphiboles, particularly grunerite, the iron analogue of kupfferite. The indices of refraction are approximately $\gamma = 1.620$ and $\alpha = 1.605$. The monoclinic form was observed as very long needles having positive elongation and a maximum extinction angle of about 18°.

Further study may have an important bearing on the suggested polymorphism of anthophyllite and cummingtonite.

Interpretation of data.—An example of the interpretation of the data is given primarily as a basis for evaluating past and future work and as a guide for geologists interested in the experimental investigation of petrologic problems. The composition $MgSiO_3$ is chosen for discussion because it illustrates the common difficulties of interpretation and the reactions which it exhibits are fairly well established.

First, the data from those runs in which the initial material was glass will be examined. At the lowest temperatures only forsterite + talc are obtained; at the highest temperatures only enstatite is obtained. In general, then, the reaction appears to be talc + forsterite ⇌ enstatite + vapor. However, over a large range of time and intermediate temperatures all three crystalline phases and vapor are obtained. Since divariant equilibrium permits only three phases for a three-component system, equilibrium has not been obtained for the intermediate temperatures. Four phases are possible, but at only one

temperature if the pressure is fixed. Realizing that equilibrium has not been reached, one searches for the lowest temperature at which enstatite begins to form; i.e., 660°. Below this temperature enstatite either is not stable, or insufficient time was given for it to grow, or the energy barrier is too great for it to grow from a glass.

Next, the data from runs in which the initial material was natural enstatite are examined. Long runs show that natural enstatite begins to decompose as low as 660°. No trace of decomposition was observed at the end of a run of equivalent duration only 10° higher.

In view of the agreement of the data, approaching the equilibrium from both the direction of increasing and decreasing temperatures, it is concluded that the equilibrium talc + forsterite ⇌ enstatite + vapor takes place at approximately 660° at 15,000 psi.

Metastable relations.—An assemblage is considered to be metastable if at the same temperature and pressure at which it grew it can be transformed into another assemblage, given sufficient time. The latter assemblage is believed to be *more* stable than the first assemblage. There is no experimental criterion known to this writer which demonstrates conclusively that an assemblage is the *most* stable. Metastable assemblages are known to persist through geologic time. In a few cases a sufficient number of thermodynamic properties have been available to calculate the free energy of an assumed reaction from which may be determined the more stable assemblage.

In view of the large number of metastable assemblages obtained in the $MgO—Al_2O_3—SiO_2—H_2O$ system, a few examples require citation. In the pyrope composition Co + Cl + T + V was shown to be less stable than Co + Cl + F + V above 655°. In addition, the data suggest that An + F + C + V would eventually transform into F + Cl + Co + V. In the clinochlore as well as the amesite compositions the assemblage F + Sp + T + V was demonstrated to transform into F + Co + Sp + V above 680°. The assemblage Co + F + T + V was found to be metastable above 660° in the compositions P-1, and 50 cordierite 50 enstatite. The runs on the enstatite composition showed that this assemblage was not possible above 660°. The assemblage Cl + Sp + T + V obtained in the amesite composition is also prohibited by the results obtained

in several other compositions and is therefore believed to be metastable. Below about 575° the cordierite composition first yields Cl + Py + glass which eventually reacts to give cordierite. The same process occurs in the composition 70 cordierite 30 quartz. In this same composition cristobalite was obtained metastably in one run.

These assemblages have been obtained by other experimenters and recorded as the stable assemblage. It has been shown here that other assemblages are *more* stable. Future work may show that still other assemblages are the *most* stable.

PRESSURE—TEMPERATURE CURVES

The pressure—temperature curves of univariant equilibrium in the system $MgO—Al_2O_3—SiO_2—H_2O$ are given in figure 10. These curves describe the equilibrium conditions at which

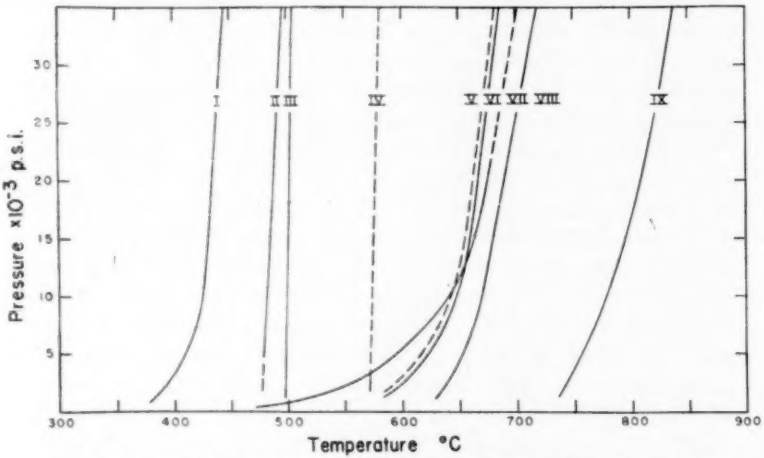

Fig. 10. Some of the pressure—temperature curves (I - IX) of univariant equilibrium in the system $MgO—Al_2O_3—SiO_2—H_2O$.

Curve I.	$S + B \rightleftharpoons F + V$
Curve II.	$B + Al\text{-}S \rightleftharpoons F + Sp + V$
Curve III.	$S \rightleftharpoons F + T + V$
Curve IV.	$Py \rightleftharpoons Mu + Cr + V$
Curve V.	$Cl + T \rightleftharpoons F + Co + V$
Curve VI.	$F + T \rightleftharpoons E + V$
Curve VII.	$B \rightleftharpoons P + V$
Curve VIII.	$Cl \rightleftharpoons F + Co + Sp + V$
Curve IX.	$T \rightleftharpoons E + Q + V$

The assemblages stable in the divariant regions between curves are given in figure 11.

the crystalline phases and water vapor exhibit only one degree of freedom. Where the system can be represented by two, three, or four components, univariancy requires three, four or five phases, respectively. The areas between the curves are regions of divariancy, that is, where two degrees of freedom are exhibited. For example, where the number of components is four, four phases can coexist. If the four components are represented by a tetrahedron, the four phases form a volume within the tetrahedron. This subsidiary tetrahedral volume

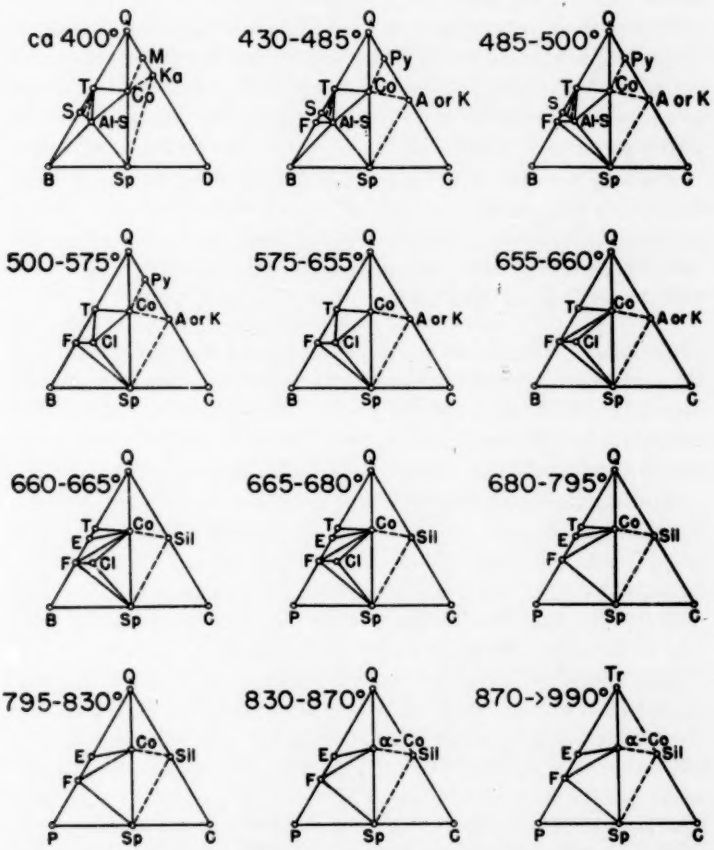

Fig. 11. Assemblages stable in the presence of an excess of water vapor at significant temperature intervals and 15,000 psi in the system MgO—Al_2O_3—SiO_2—H_2O. (The abbreviations are defined in table 2.)

encloses all the compositions for which the four phases, one of which is water vapor, may coexist at the pressures and temperatures represented in the area between the two limiting curves. In figure 11 are given the various four-phase assemblages for the $MgO—Al_2O_3—SiO_2—H_2O$ system which can coexist in the areas between the curves given in figure 10. The assemblages are represented by a one-point projection from the apex H_2O and, although not shown, every four-phase assemblage there designated by a triangle includes the phase water vapor. The great importance of the water as a member of every phase assemblage will be discussed in detail in a later section. Each triangle is labeled with the temperature range at which the assemblages are stable at a pressure of 15,000 psi. The diagrams are essentially the same for all other investigated pressures except for minor variations to be noted later.

Each curve will now be described and some of the details regarding the manner in which the curve was fixed will be presented. Reference will be made continually to figures 10 and 11, starting with the curves at the lowest temperatures and proceeding to those at the highest temperatures.

Curve 1.—The curve at the lowest temperatures represents the temperature and pressure conditions of the equilibrium serpentine + brucite $\rightleftharpoons$ forsterite + vapor. The curve was determined by Bowen and Tuttle (1949, p. 445) and is confirmed by the results obtained from composition P-4.

The equilibrium diagram which describes the four-phase assemblages thought to be stable on the low-temperature side of the curve is labeled *ca.* 400°. The diagram was compiled, not from the results of direct experiment, but mainly from deductions based on the present work at higher temperatures, from the work of Roy and Osborn (1951) on the system $Al_2O_3—SiO_2—H_2O$, and from the work of Bowen and Tuttle. It should be considered only as a reasonable estimate. An exhaustive investigation of this diagram was not undertaken for the reason that at even higher temperatures reliable data could not be obtained because of the tendency for metastable phases to persist in runs of several weeks' duration. An example of this can be seen in the data at low temperatures for the composition cordierite. New techniques will be required to investigate this system in the lowest temperature region.

Between 400° and 430° diaspore breaks down into corundum + vapor; pure montmorillonite transforms into pyrophyllite + vapor; and kaolinite decomposes into pyrophyllite + andalusite or kyanite + vapor (see R. Roy and Osborn, 1951). Each of these reactions would be represented by a specific pressure—temperature curve, not shown in figure 10, below curve I. It should be stated at once that kyanite, andalusite, or sillimanite have not been produced with certainty in the laboratory. In all cases mullite is obtained. The field observations indicate, however, that andalusite or kyanite usually coexist with the minerals designated. Magnesian montmorillonite probably breaks down at a somewhat higher temperature (465°) according to R. Roy (personal communication, 1951). The belief that a complete series of solid solutions exist between serpentine and aluminous serpentine is indicated on the diagram by a family of dashed tie lines radiating from talc. Cordierite is thought to be stable in the presence of an excess of water vapor at these low temperatures. Support for this conclusion is found in the fact that cordierite is one of the first minerals to form in the metamorphism of a sediment. Spotted slates commonly have porphyroblasts of cordierite.

The diagram which describes the four-phase assemblages found to be stable on the high-temperature side of curve I at 15,000 psi is labeled 430° — 485°. Brucite and serpentine can no longer coexist, and forsterite is found to be stable in the presence of an excess of water vapor. In addition pyrophyllite and andalusite or kyanite become stable in the presence of an excess of water vapor.

The tentative join spinel-andalusite or kyanite is given in preference to the join cordierite-corundum. The experimental data available (D.Roy and Osborn, 1951, unpub.) as well as two field occurrences (Comrie Area and Mt. Ascutney, Vt.) suggest that cordierite and corundum are compatible (see Tilley, 1923). The writer is reluctant to accept these data on the following grounds. It is well known that corundum is extremely slow to react in laboratory experiments. Moreover, it crystallizes metastably readily and is resorbed at an extremely slow rate, if at all. The establishment of equilibrium is therefore very uncertain. Similar examples of non-equilibrium are noted in the field evidence. In the Comrie Area, Tilley (1924*b*, p. 49) describes cordierite + corundum + spinel + andalusite

assemblages in addition to the preponderant critical three-phase assemblages cordierite + corundum + spinel and cordierite + corundum + andalusite. This is an indication of non-equilibrium if the number of components remains constant. (However, if the cordierite and spinel contain FeO, then the four phases may be a possible equilibrium assemblage.) In the Mt. Ascutney, Vermont, area described by Daly (1903, p. 30) the common occurrence of corundum as a core of the spinel which clusters in the cordierite may also be cited as evidence of non-equilibrium. The writer prefers, therefore, to rely on the data at high temperatures which show cordierite and corundum as incompatible. This is a prejudice based solely on laboratory experience.

Curve II.—This curve gives the temperature and pressure conditions for the equilibrium brucite + aluminous-serpentine $\rightleftharpoons$ forsterite + spinel + vapor. The runs for the composition P-3 indicate that this reaction takes place at 485° at 15,000 psi. In the diagram, labeled 485° — 500°, representing the stability relations on the high-temperature side of the curve, the line joining brucite and aluminous serpentine has disappeared and the join forsterite-spinel has taken its place. All the other assemblages remain as given in the diagram 430° — 485°.

Curve III.—This curve shows the upper limit of stability of serpentine. The pressure-temperature conditions are for the equilibrium serpentine $\rightleftharpoons$ forsterite + talc + vapor. The four-phase assemblages serpentine solid solutions + forsterite + vapor and serpentine solid solutions + talc + vapor which appear on the left side of the curve are no longer stable. Their place is taken by the four-phase assemblage forsterite + talc + clinochlore + vapor. Although it could not be demonstrated experimentally, there is little doubt that the aluminous-serpentine end member would decompose at a higher temperature than its pure magnesian equivalent. This temperature is estimated to be 520° at 15,000 psi. No further changes were observed to occur between 500° and 575°.

The curve for the three-component boundary system was determined by Bowen and Tuttle (1949, p. 445) and the present experiments on materials of the serpentine and enstatite compositions support their findings at 15,000 psi. The runs

on the clinochlore composition suggest the relations indicated in the four-component system.

Curve IV.—The decomposition of pyrophyllite has been studied by Roy and Osborn (1950, p. 9) and its preliminary pressure—temperature curve is given in figure 10. They found pyrophyllite to break down into mullite and cristobalite. In nature this reaction would probably be represented by: Py $\rightleftharpoons$ Q + A (or K) + V. To the left of curve IV the assemblages quartz + pyrophyllite + cordierite + vapor and cordierite + pyrophyllite + andalusite or kyanite + vapor are possible. To the right of that curve the four-phase assemblage cordierite + quartz + andalusite or kyanite + vapor is stable. No new data were obtained in this region. All other assemblages remain unchanged.

Curve V.—This curve represents the temperature and pressure of the equilibrium talc + clinochlore $\rightleftharpoons$ forsterite + cordierite + vapor. The assemblages stable to the left of the curve are given by the diagram 575° — 655° and those to the right, by the diagram 655° — 660°. The reaction is very sluggish and therefore the equilibrium conditions are known only approximately. The runs on the compositions pyrope and 50 cordierite — 50 enstatite fix this equilibrium. The runs on the composition P-1 do not indicate this reaction, but the assemblage obtained, cordierite + talc + clinochlore + vapor, was found to persist metastably for long periods but not indefinitely in the previously named compositions. It is not uncommon to find different mixtures in the same composition triangle reacting at different rates. It is believed, therefore, that given sufficient time the composition P-1 would exhibit the reaction indicated by curve V.

Curve VI.—The equilibrium talc + forsterite $\rightleftharpoons$ enstatite + vapor is shown by curve VI. On the low-temperature side of the curve enstatite is not stable in the presence of an excess of water vapor, and in the diagram labeled 655° — 660° the join forsterite-talc is stable. On the right side of the curve enstatite becomes a stable member of the assemblages enstatite + talc + cordierite + vapor and enstatite + cordierite + forsterite + vapor. The complete set of assemblages is given in the diagram labeled 660° — 665°. As mentioned earlier, some difficulty was experienced in fixing the conditions for the equilibrium because of the metastable

persistence of talc and forsterite in the region on the right side of the curve. Bowen and Tuttle, whose curve is given in figure 10, experienced this same difficulty (personal communication, 1951). The curve was tested at 15,000 psi and the conditions were duplicated for the compositions enstatite and 50 cordierite — 50 enstatite. Enstatite was not obtained, even with long runs, in the composition P-1 in the region immedately to the right of curve VI. It is believed that curve V is essentially parallel to curve VI and must always lie on the low-temperature side of curve VI. If curve V becomes identical with curve VI, the unlikelihood arises of two reactions taking place at exactly the same temperature and pressure.

It is believed that sillimanite probably begins to grow contemporaneously with the appearance of the pyroxene. This opinion is based on the assumptions that the three minerals which approximate the composition Al_2SiO_5 are polymorphs, and that they are all stable in the designated pressure range. Although the stability relations of kyanite, andalusite, and sillimanite are not known, the field evidence suggests that sillimanite alone survives the higher temperatures.

Curve VII.—The equilibrium brucite $\rightleftharpoons$ periclase + vapor has been investigated by Bowen and Tuttle (1949, p. 446) and more extensively by D. Roy and Osborn (1951, p. 4) whose preliminary curve is given in figure 10. Since only two components are required to express the composition of all the phases, three phases are needed for univariancy. To the left of the curve only brucite is stable; to the right of the curve, periclase + vapor. Similarly, the assemblage at 15,000 psi on the low-temperature side is forsterite + spinel + brucite + vapor; on the high-temperature side, forsterite + spinel + periclase + vapor.

The experiments on composition P-3 do not adequately demonstrate that equilibrium has been approached. The difficulty of quenching periclase without hydration taking place has already been mentioned. Previous workers have experienced this difficulty; however, the technique adopted by Roy and Osborn appears to give reproducible results. The shape of the curve at the lower pressure and temperature conditions may mean that hydration is less effective in that region and would give apparent equilibrium at lower temperatures in the presence of lower pressures. For this reason the curve of Roy and Osborn is accepted with some reservation.

On the assumption that curve VII is correct, the reaction brucite $\rightleftharpoons$ periclase + vapor would take place at lower temperatures than the reactions talc + clinochlore $\rightleftharpoons$ forsterite + cordierite + vapor and talc + forsterite $\rightleftharpoons$ enstatite + vapor below about 10,000 psi. Other than this exception, the series of phase-assemblage diagrams for a pressure of 15,000 psi represent the relations at all pressures in the range investigated (see figure 10). Owing to this conclusion, which is supported by investigations in other systems, the opinion is held that pressure *per se* does not greatly influence the mineralogy of a rock. Pressure, therefore, is relegated to a minor role in considerations of the origin of these metamorphic rocks.

Curve VIII.—This curve gives the equilibrium conditions for the reaction clinochlore $\rightleftharpoons$ forsterite + cordierite + spinel + vapor. The maximum stability limit of clinochlore is, therefore, fixed. The three tetrahedrons having clinochlore and vapor as common apices disappear, and their place is taken by a single volume on the high-temperature side of the curve. The stability of clinochlore at such high temperatures was not anticipated, for it was believed by the writer, and probably by many others, too, that clinochlore was a typical "low-grade" mineral. In other instances clinochlore has been interpreted as characteristic of retrograde metamorphism. As will be seen on a later page, this interpretation is suspect.

Recent intriguing experiments on the thermal decomposition of clinochlore by Brindley and Ali (1950, p. 29) suggest the reaction clinochlore $\rightarrow$ forsterite + spinel + enstatite (?) + vapor. It is worthy of note that even though these results were not obtained under equilibrium conditions the phases obtained are not very different from those at equilibrium. The metastable persistence of enstatite has already been referred to in the present work.

Curve IX.—The curve numbered IX represents the equilibrium talc $\rightleftharpoons$ enstatite + quartz + vapor. This fixes the upper stability limit of talc. The assemblages enstatite + talc + cordierite + vapor and talc + cordierite + quartz + vapor which are stable on the low-temperature side of the curve, as given by the diagram 680° — 795°, cannot exist on the high-temperature side of the curve. Instead the assemblage enstatite

+ cordierite + quartz + vapor is found to be stable as shown in the diagram labeled 795° — 830°. No hydrous phase survives above curve IX.

The curve was carefully determined by Bowen and Tuttle (1949, p. 446) and their curve is given in figure 10. No new data were collected.

Region above Curve IX.—To the right of curve IX there must exist several more pressure—temperature curves. One would represent the inversion of μ-cordierite to α-cordierite (— 830°). Another would represent the inversion of enstatite to protoenstatite. And a possible third curve may represent the temperature and pressure conditions for the formation of mullite which appears as a stable phase on the liquidus (see fig. 2). The appearance of mullite probably takes place at the expense of sillimanite according to the reaction sillimanite $\rightleftharpoons$ mullite + silica (see Greig, 1926). The complete pressure—temperature diagram would also show the inversion curves for the various forms of SiO_2.

The highest temperature curves would give the equilibrium of crystalline phases, all anhydrous, with liquid and vapor. They probably lie at very high temperatures.

The mineral sapphirine which appears on the liquidus (Keith and Schairer, 1952) has been neglected in the phase-assemblage diagrams.

Summary.—The metamorphism of the argillaceous sediments in *the presence of an excess of water* can be summarized in a series of significant mineralogical changes. These are, in the order of increasing temperature:

1. Decomposition of kaolinite
2. Decomposition of diaspore
3. Decomposition of montmorillonite
4. Incompatibility of brucite and aluminous serpentine
5. Appearance of forsterite
6. Decomposition of serpentine
7. Appearance of clinochlore
8. Decomposition of pyrophyllite
9. Incompatibility of talc and clinochlore
10. Appearance of enstatite (and sillimanite?)
11. Decomposition of brucite
12. Decomposition of clinochlore
13. Decomposition of talc

14. Appearance of α-cordierite
15. Appearance of tridymite
16. Appearance of protoenstatite
17. Decomposition of sillimanite

No individual composition could show all of these changes. With introduction of material during metamorphism, the resulting changes of bulk composition would permit such a metasomatized sediment to exhibit many of the changes listed. For reasons to be given later only those steps involving the decomposition of a mineral or a polymorphic transformation should be considered critical to the recognition of the maximum temperature attained during the metamorphism.

The addition of small amounts of iron to the system should not greatly affect the nature of the mineral assemblages. In the past it has been convenient to group iron and magnesia as a single component. (When the number of phases in the divariant region exceeds the number of components, then it is necessary to consider iron and magnesia as individual components.) The diagrams might then be labeled with minerals such as hypersthene, pyrope-almandine garnet, olivine, and chlorite. The addition of a considerable amount of iron would require consideration of such phases as staurolite and chloritoid. With these reservations in mind, the diagrams can be applied to the system $(Mg,Fe)O—Al_2O_3—SiO_2—H_2O$.

STABILITY RELATIONS OF ANTHOPHYLLITE AND PYROPE

Two very important rock-forming minerals, anthophyllite and pyrope, are absent from the diagrams (fig. 11) representing phases in equilibrium with vapor at a large range of temperature. Anthophyllite has been produced in the laboratory by Bowen and Tuttle (1949, p. 450) and by the writer (see table 3a), but only metastably. Pyrope, which has not as yet been synthesized, appears to break down at all temperatures in the presence of an excess of water vapor (see table 3a). It is concluded that neither pyrope nor anthophyllite is stable in the presence of an excess of water. However, these minerals commonly occur with cordierite and chlorite (clinochlore) in nature. For this reason it is believed that anthophyllite and pyrope should appear as stable compounds somewhere in the system $MgO—Al_2O_3—SiO_2—H_2O$.

As has been pointed out, only those assemblages which are

in equilibrium with vapor could be obtained. These assemblages, presented in detail in the preceding section, isolate a region in the tetrahedron which is not accessible by means of the experimental method employed. For brevity this region will be called the water-deficient region since the described experiments indicate that all compositions within the region are incapable of stable coexistence with water vapor at the pressures and temperatures investigated. It is within this region that the compounds pyrope and anthophyllite lie (see fig. 12).

Before proceeding further with the quaternary system, it is instructive first to view the relations presented above in the ternary system $MgO—SiO_2—H_2O$. In figure 13 are given the relations believed to exist at a temperature of about 600° C. The region which is stippled is the water-deficient region. No assemblage in this region can coexist with water vapor. The following assemblages are permissable, in addition to those obtained experimentally (see fig. 11, diagram 575°— 655°) in the excess-water region:

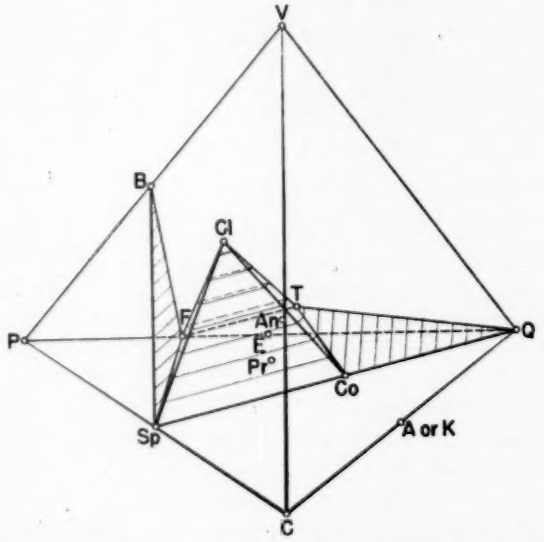

Fig. 12. Tetrahedron illustrating the phases stable in both the water-deficient and excess-water regions at *ca.* 600° and 15,000 psi for the system $MgO—Al_2O_3—SiO_2—H_2O$. The planes which are lined divide the excess-water regions and the water-deficient regions. The points An and T lie on the back face; Pr and Co, on the base; and Cl lies within the tetrahedron.

$$Q + T + An \qquad T + An + F$$
$$Q + An + E \qquad An + E + F$$
$$F + B + P$$

The occurrence of enstatite in the water-deficient region simply means that there was insufficient water present to convert all the material to hydrous compounds. Above 660° enstatite becomes stable in the presence of an excess of water as shown experimentally. The same can be said of forsterite which appears in equilibrium with an excess of water at about 430°. It is stable below this temperature in the water-deficient region. It can be seen, then, that as we pass to higher temperatures the water-deficient phases appear. The question arises as to why anthophyllite does not also appear at higher temperatures in the presence of water vapor. The only reason for its nonappearance is that anthophyllite is no longer stable at that tempera-

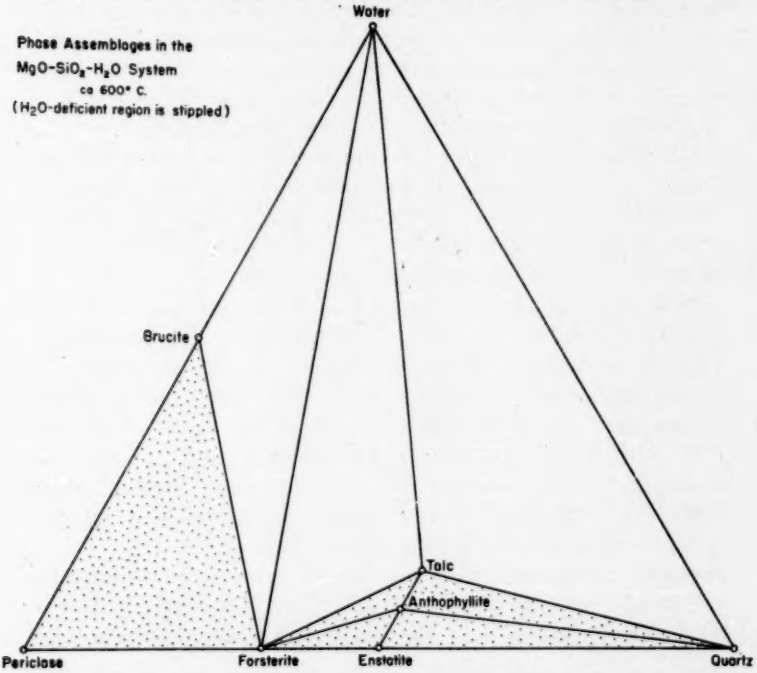

Fig. 13. Assemblages stable in the $MgO—SiO_2—H_2O$ system at *ca.* 600° and 15,000 psi (Bowen and Tuttle, 1949). The water-deficient region is stippled.

ture where its composition becomes exposed to an excess of water vapor, i.e., 660°, the appearance of enstatite. That is to say, anthophyllite apparently decomposes at some temperature below 660°.

Figure 13 is the same as figure 3 given by Bowen and Tuttle (1949, p. 451). They prefer to regard pure magnesian anthophyllite as forming metastably under all circumstances. Their conclusion is based primarily on the metastable appearance of anthophyllite from the decomposition of talc which occurs at a temperature well above the probable upper stability limit of anthophyllite. The *metastable* appearance of a compound above its stability limit is not common, but this is believed to be no serious objection to the *stable* relations proposed. In support of this argument, attention is called to the decomposition products of anthophyllite, E + Q + V, which were obtained (table 3n). This is the stable assemblage above 795°. At an unknown temperature below 660° the decomposition of anthophyllite probably occurs according to the equation An ⇌ E + T in the water-deficient region or An + V → T + F in excess-water region. (There are insufficient data to determine the relationship of kupfferite [?] to anthophyllite.) If for no other reason, the proposed relations are required in the light of the assemblages observed in the field. Therefore, it is believed that anthophyllite occurs stably in the water-deficient region at temperatures below 660°.[2]

Returning now to the four-component system, a similar picture can be constructed. Figure 14 gives the assemblages believed to be stable at 600° at 15,000 psi in both the excess-water and water-deficient regions. The excess-water assemblages were determined by experiment (see fig. 11, diagram 575° — 655°); those in the water-deficient region are based primarily on the common field association of anthophyllite-cordierite, anthophyllite-clinochlore, and anthophyllite-garnet. These joins essentially fix the remaining relations in the water-deficient region but do not preclude other possible assemblages for which the same argument will apply. The solid and dashed lines are those bounding the assemblages in equilibrium with

[2] It will be possible to test these proposed relations experimentally. The sealed-tube technique developed by Adams and Eskola, in which the water content can be fixed at any desired amount, has been briefly described by Goranson (1931, p. 486) and will soon be described in detail by the writer.

vapor; the dotted joins are the boundaries of subsidiary tetrahedrons for compositions which cannot coexist with water in the temperature and pressure range investigated. (The dotted joins appear to cross in the projection, which, of course, does not occur in a three-dimensional model.) The four-phase assemblages possible at *ca.* 600° in the $MgO—Al_2O_3—SiO_2—H_2O$ system at a pressure of 15,000 psi are given in table 4.

The upper stability limit of pyrope would be less than 680°: otherwise it should appear on the diagram 680°—795° as a phase in equilibrium with water vapor.[3] The decomposition of pyrope in the presence of water vapor at all temperatures strongly supports the view that pyrope is stable only in the water-deficient region.

Theoretically it is possible that, at a very low vapor pressure

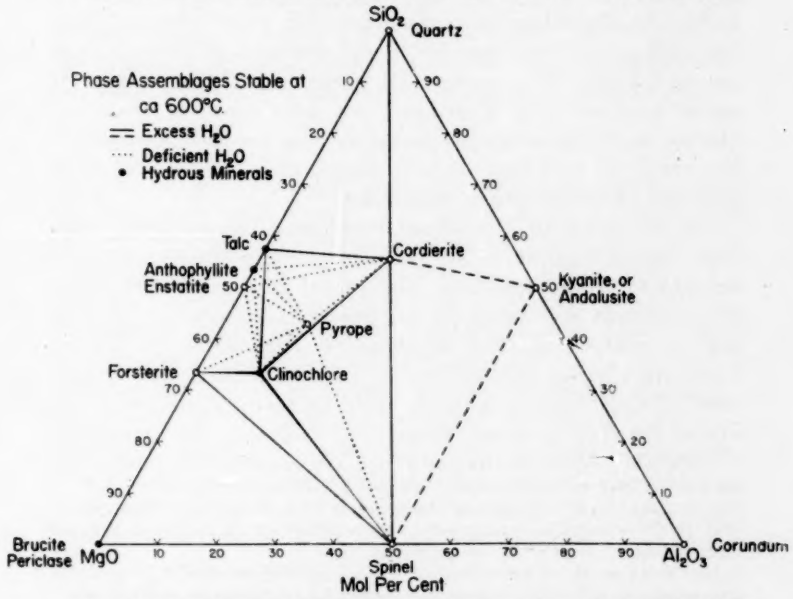

Fig. 14. Assemblages in both the excess-water regions (solid and dashed lines) and water-deficient regions (dotted lines) believed to be stable at *ca.* 600° and 15,000 psi in the system $MgO—Al_2O_3—SiO_2—H_2O$. See table 4 for list of assemblages.

[3] The writer does not wish to be too insistent on this point in view of his experience with the attempted synthesis of grossularite (Yoder, 1950*b*). Even if pyrope failed to appear because its rate of formation is extremely slow above 680°, the relations below 680° are still valid.

(or partial vapor pressure) of water, anthophyllite and pyrope would coexist with water. These relations require the existence of a quintuple point and a sextuple point, respectively, below those pressures investigated. Unfortunately, reactions at these very low pressures, and presumably low temperatures, would be so slow that they could not be realized, if they exist, in a reasonable time. There is no doubt however that, in the pressure range investigated, the water-deficient region exists and that the minerals pyrope and anthophyllite, where stable, lie in this region.

KELYPHITIZATION OF GARNET

It can be seen from figure 14 that a rock of pyrope composition at 600° could consist of pyrope alone, or of pyrope + clinochlore + talc + cordierite, or of clinochlore + talc + cordierite, depending upon the amount of water present. These assemblages in fact represent the stages of a common type of kelyphitization of a garnet. Of great importance is the observation that such a process can take place without any change in temperature or pressure. The process is primarily the result of a change of bulk composition, not a change of pressure or temperature conditions.

On the basis of the above reasoning, the prevalent view that kelyphitization is solely a retrograde process may be subject to serious question. The garnet may react with vapor in subsequent high-grade or low-grade metamorphism yielding only a portion of itself (pyrope + clinochlore + talc + cordierite) or all (clinochlore + talc +cordierite) to hydration.[4] Kelyphitization is most likely to occur where water has access locally, as along fissures, at contacts, or in crushed

[4] This will probably be true of all common garnet except those rich in spessartite and uvarovite. Since spessartite and uvarovite are present at the liquidus in dry equilibrium studies, it is very likely that these garnets will persist above the decomposition temperature of all hydrated minerals and will then coexist with an excess of vapor.

In the presence of an excess of water vapor grossularite is probably converted into a hydrogarnet or decomposes into gehlenite + wollastonite + anorthite, depending on the temperature or pressure (Yoder, 1950*b*, p. 245).

A natural almandine (Alderman, 1935, p. 43) held for 490 hours at 500° and 15,000 psi showed signs of decomposition into unidentified products. According to K. Yagi (personal communication, 1951), the same garnet decomposed in a nitrogen atmosphere at approximately 1000° into iron-cordierite + fayalite + hercynite. An analyzed synthetic glass of the almandine composition held at 600° and 15,000 psi for 83 hours produced only iron-cordierite and magnetite. The decomposition of almandine into cordierite and magnetite has been reported in rocks of the Scottish Highlands (Bailey and Maufe, 1916, p. 199).

TABLE 4

Possible Four-Phase Assemblages in the Excess-Water and Water-Deficient Regions at *ca.* 600° and 15,000 psi

Q + T + Co + V	F + Pr + Cl + E
Q + A or K + Co + V	F + E + An + Cl
T + Co + Cl + V	F + An + Cl + T
T + F + Cl + V	E + Cl + Pr + An
Cl + F + Sp + V	An + Cl + Pr + T
F + B + Sp + V	E + Pr + An + Co
Cl + Co + Sp + V	An + Pr + T + Co
Co + A or K + Sp + V	E + Co + An + Q
A or K + Sp + C + V	T + An + Co + Q
F + Sp + P + B	Co + Pr + Cl + Sp
F + Pr + Cl + Sp	Co + Pr + Cl + T

zones. The process can also take place in garnet-bearing rocks on a regional scale provided the permeability of the rock permits access of water vapor. Both locally and regionally, the process is primarily a change of bulk composition and need not mean a change in pressure or temperature conditions.

METAMORPHIC FACIES

What has just been outlined for a mineral is also true for mineral assemblages. In figure 14 can be found representative mineral assemblages of almost every metamorphic facies as defined by Barth, Correns, and Eskola (1939, p. 345). For example, cordierite + anthophyllite might well represent the amphibolite facies; clinochlore + talc, the green schist facies; enstatite + cordierite, the pyroxene-hornfels facies; and clinochlore + anthophyllite, perhaps the epidote-amphibolite facies. In addition, in the sanidinite facies might be included the assemblages cordierite + spinel, forsterite + spinel, or forsterite + enstatite. And with some reservation, one might be bold enough to suggest that pyrope + enstatite (garnet + pyroxene) could represent the eclogite facies. *At approximately 600° and 15,000 psi, it is possible, therefore, to have assemblages suggestive of every one of the now accepted metamorphic facies in stable equilibrium.* The differences between these facies are the result of variation in bulk composition and need not represent variations of pressure and temperature.

This conclusion, based on experimental fact, appears to be at variance with field observations. The classic view—that for a given composition a change in the pressure and temperature conditions would produce a change in the mineral assemblage—

seems to be questioned. However, the sequence of pressure—temperature curves in figure 10 gives adequate proof that with changes of temperature and, to a lesser extent, of pressure, changes in the mineral assemblages are produced. These curves strongly support the concept of progressive metamorphism. The apparent difficulty lies not in the principle of the facies classification but in the choice of critical assemblages representing the various conditions of pressure and temperature in the progressive metamorphism. In the original exposition of the facies classification, Eskola assumed that the series chosen was isochemical, disregarding the water content (1920, p. 152 and the analyses on p. 153). This assumption can no longer be considered valid in the light of the experimental work. Changes of a few per cent in composition (including the oxide water, H_2O^+) may produce great changes in mineralogy (see fig. 14). What was interpreted by Eskola and others as a change in pressure and temperature conditions may actually be, for the most part, the result of a change in bulk composition. The sequence of progressive metamorphism established in one area, presumably in homogeneous layers, cannot be directly applied to another area as a temperature scale unless the bulk compositions have been established as identical. For example, the temperature of appearance of enstatite in a bed deficient in water will be different from that in a bed containing excess water. It is necessary, therefore, to construct a new facies classification based on a fixed composition, or on several independent compositions, particularly sensitive to temperature and pressure. This project may have to await further experimental work.

In no way should these remarks be construed as detracting from the value of the concept behind the Facies Classification. Eventually sufficient data will be accumulated from which a critical group of assemblages can be selected as indicative of grades of metamorphism. Metamorphic rocks must be treated with the same precision as igneous rocks have been. Until these data have been collected, one should be wary of assigning temperatures and pressures of formation to metamorphic rocks of different bulk compositions which are not contiguous in the same pressure and temperature gradients.

With this new emphasis on bulk composition it is not difficult to accept the occurrence of eclogite with amphibolite or with even "lower grade" rocks. By examining a point mid-

way on the enstatite-pyrope join, it is seen that, as the water content increases the fields of E + Pr + An + Cl, Pr + An + Cl + T, and Cl + T + Co + V are traversed. The sequence is equivalent to eclogite → amphibolite → green schist. No change in pressure or temperature conditions need take place.

The diagram given in figure 14 is only for a temperature of about 600°. Similar joins in the water-deficient region will have to be determined for all the other diagrams given in figure 11. The divariant regions, which these diagrams describe, will be further subdivided by pressure—temperature curves as the reactions in the water-deficient region are established. For example, the equilibrium Pr + Q ⇌ E + Co probably takes place below 600° in the water-deficient region. (See Dunn, 1932, for a description of a natural occurrence and table 3a for an experimental demonstration of Pr → E + Co + Sp. The assemblage E + Co + Sp was shown by other experiments to be metastable; the equilibrium assemblage would be F + Co + Sp.) This reaction will be represented by a pressure—temperature curve on figure 10.

ROLE OF PRESSURE

A few observations should be mentioned in connection with the shape of the pressure—temperature curves. A cursory glance at the curves indicates that the reactions are essentially pressure insensitive. This relation can probably be regarded as extending to the highest pressures in the earth's crust, approximately 150,000 psi. Pressure does not play a significant role in the $MgO—Al_2O_3—SiO_2—H_2O$ system except in the one case involving the decomposition of brucite, the equilibrium relations of which are not as yet fixed with certainty. It is the opinion of the writer that further experimentation in other systems will demonstrate an insensitivity to pressure for most metamorphic reactions except in the very *lowest* pressure regions. Pressure is significant in determining metamorphic assemblages only where polymorphic transition curves, which are essentially vertical, cross the steeply sloping reaction curves (Bowen's petrogenetic grid). Certainly no drastic changes in mineralogy are to be expected even under the maximum pressures available in the crust. As far as the writer knows, there are no minerals common in rocks on the surface of the earth which are stable only at high pressures (high-pressure minerals). Of the three "characteristic high-pres-

sure minerals," diamond, garnet, and jadeite, only diamond is still believed by most other investigators to be stable at high pressures (Yoder, 1950*a*, 1950*b*). Moreover, recent experiments have demonstrated that in the most favorable case, the effect of pressure on the change of free energy of a reaction is very small (Yoder and Weir, 1951). For these reasons pressure should be divested of its mystic powers and relegated to a minor role; temperature and composition are the most important variables in rock metamorphism.

REGIONAL AND CONTACT METAMORPHISM

Fundamentally there should be no difference in the assemblages of minerals obtained under similar conditions, whether the result of regional or of contact metamorphism. The Facies Principle, based on thermodynamics, says that if the pressure, temperature, and composition are fixed, then the mineral assemblage is fixed independent of the manner in which the conditions were applied. Actually, however, contact metamorphism appears to extend to higher temperatures than those attained in regional metamorphism. In this way the assemblages found only in contact metamorphism are usually explained.[5]

[5] Stress itself is a function of temperature, diminishing in effect with increasing temperature, and therefore would not be important in contact metamorphism. At lower temperatures, stress is believed by most petrologists to be the chief factor in accounting for the difference between regional and contact metamorphism. On the other hand, it has not been demonstrated that any mineral common to regional metamorphic rocks requires stress in order for the mineral to be stable. Every mineral common in rocks in the crust of the earth probably has a field of stability on a pressure-temperature diagram. This belief does not preclude the possible enlargement or diminution of the field of stability along the stress coordinate.

Kyanite is perhaps the one mineral which most petrologists regard as a stress mineral. Although its occurrence in veins in kyanite-bearing schists does not invalidate the stress concept (Tilley, 1935), the occurrence of kyanite in veins not associated with kyanite-bearing country rocks (Moore, 1949, p. 1662) causes some uncertainty in the argument. Its occurrence in druses as idiomorphic crystals along with idiomorphic crystals of quartz and muscovite in cavities (Miyashiro, 1951) also throws doubt on the necessity of stress for its growth. There seems to be little doubt that stress may *aid* the formation of some minerals, but their growth is not dependent on stress.

Both Goranson (1930) and Verhoogen (1951) consider hydrostatic pressure as a non-hydrostatic stress where the three principal stresses are equal. Coupling this relation with the belief that hydrostatic pressure is of minor importance in the formation of metamorphic minerals, it is concluded that the stress available in the crust of the earth would contribute a negligible amount of energy to any reaction.

However, an alternative view may be entertained. The "high-temperature "assemblages are stable at low temperatures, even in the presence of water vapor, as they are for compositions in the quartz-spinel-corundum-vapor volume or in the water-deficient region of the quartz-spinel-periclase-vapor volume (see fig. 14). A quartz-cordierite-enstatite gneiss ("granulite facies") may have formed at low temperatures alongside a cordierite-andalusite-spinel rock. In the absence of clear evidence of the temperature gradient, it would not be possible to conclude without doubt, as has been done in the past, that these assemblages were formed only at high temperatures. They may have formed at any temperature. When the conditions of decomposition or polymorphism of minerals are known, some of the assemblages may be fixed on the temperature scale. Without accurate knowledge of the changes of bulk composition, conclusions concerning the temperature gradient based on changes in mineral assemblages are suspect.

The occurrence of "low-grade" minerals at granite contacts has been a baffling puzzle. Some have interpreted this to mean that the granite had formed at low temperatures in the solid state and therefore never had reached the high temperatures required for metamorphism. The upper limit of stability of clinochlore (680°), however, is very close to the temperature at which some granites may have formed from a completely liquid mass (Bowen and Tuttle, personal communication, 1952).[6] The writer prefers the view that "low-grade" metamorphic rocks exist at granite contacts not because the temperature was low, but because the rocks formed in the presence of an excess of water. In the absence of water the so-called "high-grade" minerals would form. One of the chief complications in determining the temperature of formation from field evidence is that the gradient of increasing temperature is also the gradient of decreasing water content, and, on a crustal scale, the gradient of increasing pressure. Fortunately there are minerals which are sensitive to at least the first two variables.

Mention has already been made of structural control of metamorphic assemblages. In those structural features which provide openings, water will have access and an apparent lower grade of metamorphism will take place. For example, the cordierite-anthophyllite rocks at the crests of folds in the

[6] The minimum of the quartz-orthoclase-albite-water system lies close to 695° at 15,000 psi.

Orijärvi leptites seem to be the result of such control (Tuominen and Mikkola, 1950). The crescent-shaped bodies of amphibolite in some gneisses are also probably due to this mechanism.

THE ISOGRAD

The isograd is defined as a plane of constant temperature, or pressure, or both (Tilley, 1924*a*, p. 169). Usually the value of the pressure is arrived at qualitatively, depending upon the field worker's view of an origin near the surface, in the roots of a mountain belt, or in the bottom of a syncline. The temperature gradient is customarily related to the nearest igneous body, or if one is lacking, to an unspecified body at depth, or to the geothermal gradient. Ideally, one would like to find in the field an area similar to that in figure 15a. The plan view depicts a series of vertical, homogeneous sediments cut transversely by a large igneous body. The maximum temperatures reached during the cycle of metamorphism initiated by the invasion of the igneous body are shown schematically in figure 15b. Let us walk along a given sedimentary bed towards the igneous body. In zone E we observe the unmetamorphosed sediment as a metastable collection of minerals, for the most part, which do *not* represent the lowest energy state. As we walk through zone D we search for signs of reconstruction of the sedimentary minerals. At the boundary of zone C the first visual signs of metamorphism appear as knots of poorly formed crystals such as chlorite, garnet, or cordierite, depending on the original composition of the sediment.[7] Here, then, the rate of reaction is sufficient for the more stable minerals to form. (Experimentally, we know that some minerals grow rapidly above a critical temperature and from certain compositions not necessarily near that of the mineral in question.) Continuing along zone C we see that these minerals increase in number and size until the temperature is sufficiently high for the minerals in the sediment to react to form the most stable mineral assemblages at that temperature. At the boundary of zone B a mineral, being in a region above its

[7] In the early stages of metamorphism there is a clear dependence on the original mineralogical composition of the sediment. Unfortunately, there is little known about the exact nature of the minerals in fine-grained sediments. More studies of the type undertaken by Grim, Dietz, and Bradley (1949) are needed.

maximum stability limit, decomposes into phases already present or into new phases. At the boundary of zone A a polymorphic transition may take place. And, finally, at the contact we find the assemblage stable at the highest temperature reached during the metamorphic cycle. The metamorphic rock retains those minerals produced at the highest temperature, since, as the temperature falls to a point at which a reaction is permitted to reverse, the requisite thermal energy level for the reaction to proceed has been passed.

We have described essentially two different types of temperature changes, or, more generally, of isograds. One is dependent on the attainment of a sufficient reaction rate such that a mineral will appear. The other results from the disappearance of a no-longer stable assemblage or from a polymorphic transition. It is believed that the presently accepted

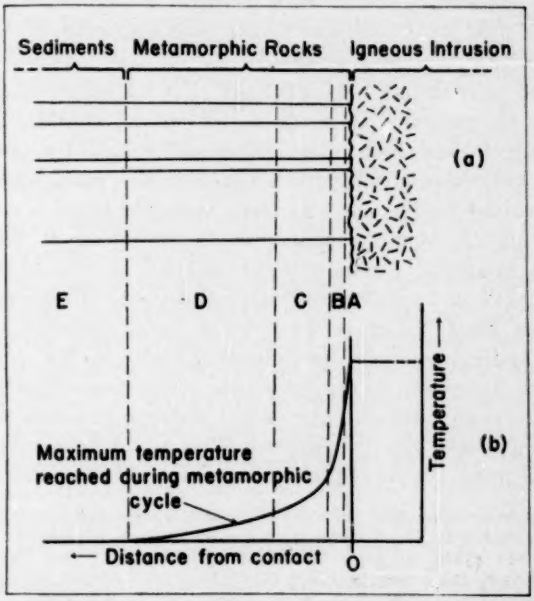

Fig. 15. (a) Plan view depicting a series of vertical sediments cut transversely by a large igneous body.

(b) Graph showing the maximum temperature reached during the metamorphic cycle initiated by the igneous intrusion. Zones A - D are metamorphosed sediments. Zone E represents the unmetamorphosed sediments.

chlorite, biotite, and garnet isograds are of the first type. The sillimanite isograd is of the second type. It may be more critical to base isograds on the disappearance of a previously present mineral or on a polymorphic transition rather than on the first appearance of a mineral which is dependent on variable factors involving rate of growth.[8] Since reaction rates vary with grain size, composition (including volatiles), and temperature, it should not be uncommon to find reversals of the normal sequence of mineral isograds (for example see Goldschmidt, 1920, p. 48). Statistically, however, the normal sequence will obtain. This may be interpreted to mean that, in general, the rate of growth of chlorite > biotite > garnet. It is recommended that the term isograd apply only to univariant equilibrium, and, that the word isograd refer not to a fixed pressure and temperature, but to all the pressures and temperatures on the univariant curve of reference. A new term may be desirable for the conditions under which growth of a phase initiates (for example, isoblast).

In the past it has been assumed that metamorphism takes place in the presence of an excess of water. That is, the sediment which has been metamorphosed originally contained either a collection of anhydrous minerals plus more water than that required by the most hydrous minerals capable of forming during the metamorphism, or, a collection of the most hydrous minerals, presumably formed during the weathering process. Let us consider the latter collection of minerals, the collection most likely to be present in a sediment. For a specific critical example, the assemblage Al-S + Ka + Q + V is chosen. According to the older view, the growth of garnet can only take place provided the excess water is removed and the remaining phases are dehydrated. This might take place at a series of fixed temperatures and pressures below the decom-

[8] Bowen has emphasized the critical nature of the disappearance of a phase assemblage in his paper on the progressive metamorphism of a siliceous dolomite (1940, p. 256). It should also be noted that Bowen has considered only those reactions in which CO_2 is in excess. There must be a CO_2-deficient region in the CaO—MgO—SiO_2—CO_2 system analogous to the H_2O-deficient region in the MgO—Al_2O_3—SiO_2—H_2O system.

It is realized that there are too few natural compounds exhibiting polymorphism which can be used as general temperature indicators. However, the recently discovered relations in the feldspars may prove to be the most useful indicator of temperature in both igneous and metamorphic rocks.

position of kaolinite (~400°). The reaction would be: Al-S + Ka + Q → Pr + V ↑. At the instant this reaction takes place, pyrope would have to grow in the presence of vapor. The experiments performed, however, indicate that pyrope cannot coexist with vapor. Therefore this reaction is most unlikely. It appears, then, that the formation of garnet would not take place by the dehydration of a sediment. Hence, the writer is of the opinion that the garnet "isograd" does not represent the attainment of a specific univariant equilibrium. The alternative view is preferred—that garnet will form in a sediment whose appropriate bulk composition lies in the water-deficient region, at any temperature below the the upper stability limit of garnet, and at any temperature above which its rate of growth is adequate. It is theoretically possible for garnet to grow at room temperature in the water-deficient region. The reason it does not is because the rate of growth at that temperature is negligible. The appearance of garnet in progressive metamorphism is regarded by the writer as being dependent on the rate of growth and not on the attainment of a particular pressure and temperature.

STABILITY OF CORDIERITE

Cordierite commonly occurs in contact aureoles but is usually absent from rocks formed during regional metamorphism. The experimental work indicates that cordierite is stable through a large range of temperature and suggests that it should be found in both contact and regional rocks. The general absence of cordierite in regionally metamorphosed rocks is believed by the writer to be due to the presence of an excess of K_2O (that is, more K_2O than is required to form the micas) which permits the formation of micas instead of cordierite. The presence of water cannot be the controlling factor since cordierite is stable in the presence of an excess of water (at least above approximately 400°).

The metastable growth of clinochlore and pyrophyllite from the cordierite composition demonstrated in the laboratory (table 3c) may correspond closely to the natural situation. Perhaps in the presence of K_2O clinochlore becomes phlogopite, and pyrophyllite is converted into muscovite, thereby providing substance to the reaction usually postulated for the for-

mation of cordierite at high temperatures: biotite + muscovite + quartz = cordierite + orthoclase + water.

If the presence of K_2O is the determining factor, the question immediately arises as to why cordierite is present in aureoles surrounding some granites where K_2O is readily available. It is probable that in those cases where the micas are stable, as in muscovite-biotite-granite, cordierite will not form in the aureole in the presence of an excess of K_2O. The micas in the metamorphosed rock will persist up to the contact. In those cases in which the micas are not stable even in the presence of an excess of K_2O, as in a pyroxene- or amphibole-bearing granite, cordierite would be stable. Near the contact, the micas in the sediment would react, for example, with quartz to give orthoclase and cordierite. An example of the first case may be found in contact phenomena described by Turner (1930, p. 174 ff.) and the second case, by Durrell in California (1940, p. 45) and by Tilley in the Comrie Area (1924*b*).

In the presence of a deficiency of K_2O, it should be possible for cordierite to coexist with the micas below the upper stability limit of the micas. An example of this case might be that of a granite-slate contact at Cape Town (Walker and Mathias, 1947, p. 506).

Additional examples are required to confirm these postulates.

CONCLUSION

The concept of the water-deficient region and the resulting emphasis on changes in bulk composition, particularly the oxide water, is not new to some geologists. This experimental work should give adequate support to their field deductions. The concept is not, however, the answer for all facies problems. Mineralogical problems abound, too. Almost every mineral in the system investigated has peculiarities worthy of further study. The failure to produce some of these minerals in the laboratory always gives rise to uncertainty and ammunition for the skeptic. The concept is not based on these failures, but on the specific assemblages obtained in the presence of an excess of vapor. The investigation of the water-deficient region will not be an easy task. Reactions no doubt will be very slow and the technique tedious. Successful experimentation in this region will open the doors to many problems which have not been solved by present-day technique.

ACKNOWLEDGMENTS

To the many people who have contributed to this work, the writer extends his sincere thanks. Drs. N. L. Bowen and O. F. Tuttle have supplied some compositions and have provided much help and additional information not contained in their paper on the $MgO—SiO_2—H_2O$ system. Dr. J. F. Schairer prepared most of the glasses and supplied some of the constituents of the mixes. Dr. George Faust of the U. S. Geological Survey made the differential thermal analyses and Dr. T. F. Bates made the electron microscopic studies. Drs. W. F. Foshag and George Switzer of the U. S. National Museum provided most of the natural minerals. In addition, Dr. J. B. Thompson supplied a collection of rocks from Mt. Ascutney, Vermont. Dr. and Mrs. R. Roy and Dr. E. F. Osborn gave the writer free access to their data on portions of the $MgO—Al_2O_3—SiO_2—H_2O$ system. Dr. Harry H. Hess supplied some of the mineral standards. Finally, the writer is very grateful to Dr. N. L. Bowen and Prof. C. E. Tilley who critically reviewed the manuscript.

REFERENCES

Alderman, A. R., 1935. Almandine from Botallack, Cornwall: Mineralog. Mag., vol. 24, pp. 42-48.

Atlas, L., 1952. The polymorphism of $MgSiO_3$ and solid-state equilibria in the system $MgSiO_3—CaMgSi_2O_6$: Jour. Geology, vol. 60, pp. 125-147.

Bailey, E. B., and Maufe, H. B., 1916. The geology of Ben Nevis and Glen Coe: Geol. Survey Scotland Memoirs. 247 pp.

Barth, T. F. W., Correns, C. W., and Eskola, P., 1939. Die Entstehung der Gesteine, Julius Springer, Berlin.

Bates, T. F., and Mink J. F., 1951. The morphology and structure of the serpentine minerals antigorite and chrysotile: Am. Mineralogist, vol. 36, pp. 310-311.

Bowen, N. L., 1940. Progressive metamorphism of siliceous limestone and dolomite: Jour. Geology, vol. 48, pp. 225-274.

———, and Andersen, O., 1914. The binary system $MgO—SiO_2$: Am. Jour. Sci., 4th ser., vol. 37, pp. 487-500.

———, and Greig, J. W., 1924. The system $Al_2O_3—SiO_2$: Am. Ceramic Soc. Jour., vol. 7, pp. 238-254.

———, and Tuttle, O. F., 1949. The system $MgO—SiO_2—H_2O$: Geol. Soc. America Bull., vol. 60, pp. 439-460.

Brindley, G. W., and Ali, S. Z., 1950. X-ray study of thermal transformations in some magnesian chlorite minerals: Acta Crystallographica, vol. 3, pp. 25-30.

Daly, R. A., 1903. The geology of Ascutney Mountain, Vermont: U. S. Geol. Survey Bull. 209.

Dittler, E., and Köhler, A., 1938. Neue Beiträge zur Cordieritsynthese: Zentralbl. Mineralogie, Abt. A, pp. 149-159.

Dunn, J. A., 1932. Reaction minerals in a garnet-cordierite gneiss from Mogok: Geol. Survey India Records, vol. 65, pp. 445-456.

Durrell, G., 1940. Metamorphism in the southern Sierra Nevada northeast of Visalia, California: Univ. California Pub., vol. 25, pp. 1-118.

Eskola, P., 1920. The mineral facies of rocks: Norsk geol. tidsskr., vol. 6, pp. 143-193.

Fleischer, M., 1937. The relation between chemical composition and physical properties in the garnet group: Am. Mineralogist, vol. 22, pp. 751-759.

Folinsbee, R. E., 1941. Optic properties of cordierite in relation to alkalies in the cordierite-beryl structure: Am. Mineralogist, vol. 26, pp. 485-500.

Foster, W. R., 1950. Synthetic sapphirine and its stability relations in the system $MgO—Al_2O_3—SiO_2$: Am. Ceramic Soc. Jour., vol. 33, pp. 73-84.

———, 1951. High-temperature X-ray diffraction study of the polymorphism of $MgSiO_3$: Am. Ceramic Soc. Jour., vol. 34, pp. 255-259.

Goldschmidt, V. M., 1920. Geologisch-Petrographische Studien im Hochgebirge des Südhchen Norwegens: Vidensk. Skr. I, Mat.-Naturv. Klasse, No. 10.

Goranson, R. W., 1930. Thermodynamic relations in multi-component systems: Carnegie Inst. Washington Pub. 408.

———, 1931. The solubility of water in granite magmas: Am. Jour. Sci., 5th ser., vol. 22, pp. 483-502.

Greig, J. W., 1926. Formation of mullite from cyanite, andalusite, and sillimanite: Am. Jour. Sci., 5th ser., vol. 11, pp. 1-26.

Grim, R. E., Dietz, R. S., and Bradley, W. F., 1949. Clay mineral composition of some sediments from the Pacific Ocean off the California coast and the Gulf of California: Geol. Soc. America Bull., vol. 60, pp. 1785-1808.

Gruner, J. W., 1934. The crystal structures of talc and pyrophyllite: Zeitschr. Kristallographie, vol. 88, pp. 412-419.

Hendricks, S. B., 1938. On the crystal structure of talc and pyrophyllite: Zeitschr. Kristallographie, vol. 99, pp. 264-274.

Hess, H. H., Smith, R. J., and Dengo, G., 1952. Antigorite from the vicinity of Caracas, Venezuela: Am. Mineralogist, vol. 37, pp. 68-75.

Keith, M. L., and Schairer, J. F., 1952. The stability field of sapphirine in the system $MgO—Al_2O_3—SiO_2$: Jour. Geology, vol. 60, pp. 181-186.

McMurchy, R. C., 1934. The crystal structure of the chlorite minerals: Zeitschr. Kristallographie, vol. 88, pp. 420-432.

Miyashiro, A., 1951. Kyanites in druses in kyanite-quartz-veins from Saiho-ri in the Fukushinzan District, Korea: Geol. Soc. Japan Jour., vol. 57, pp. 59-63.

Moore, G. E., 1949. Structure and metamorphism of the Keene-Brattleboro area, New Hampshire-Vermont: Geol. Soc. America Bull., vol. 60, pp. 1613-1670.

Rankin, G. A., and Merwin, H. E., 1918. The ternary system $MgO—Al_2O_3—SiO_2$: Am. Jour. Sci., 4th ser., vol. 44, pp. 301-325.

Roy, D. M., and Osborn, E. F., 1951. The system $MgO—Al_2O_3—H_2O$: Fourteenth Progress Report, School of Mineral Industries, Pennsylvania State College, pp. 1-23.

Roy, Rustum, and Osborn, E. F., 1950. Studies in the system $Al_2O_3—SiO_2—H_2O$: Eleventh Progress Report, School of Mineral Industries, Pennsylvania State College, pp. 1-8.

Scheerer, Th., 1851. Beiträge zur näheren Kenntniss des polymeren Isomorphismus: Ann. der Physik u. Chemie, vol. 84, pp. 321-410.

Selfridge, G. C., 1936. An X-ray and optical investigation of the serpentine minerals: Am. Mineralogist, vol. 21, pp. 463-503.

Shand, S. J., 1943. Notes on cordierite: (A) Cordierite crystals from a glass furnace; (B) cordierite from Horns Nek, Transvaal: Am. Mineralogist, vol. 28, pp. 391-395.

Smith, J. L., 1864. Chladnite of the Bishopville Meteoric Stone proved to be a magnesian pyroxene: Am. Jour. Sci., 2nd ser., vol. 38, pp. 225-226.

Stockwell, C. H., 1927. An X-ray study of the garnet group: Am. Mineralogist, vol. 12, pp. 327-344.

Tilley, C. E., 1923. Paragenesis of the minerals of the three component system MgO—Al_2O_3—SiO_2 in thermal metamorphism: Geol. Mag., vol. 60, pp. 101-107.

———, 1924*a*. The facies classification of metamorphic rocks: Geol. Mag., vol. 61, pp. 167-171.

———, 1924*b*. Contact-metamorphism in the Comrie area of the Perthshire Highlands: Geol. Soc. London Quart. Jour., vol. 80, pp. 22-71.

———, 1925. Metamorphic zones in the Southern Highlands of Scotland: Geol. Soc. London Quart. Jour., vol. 81, pp. 100-112.

———, 1935. The rôle of kyanite in the "hornfels zone" of the Carn Chuinneag granite (Ross-shire): Mineralog. Mag., vol. 24, pp. 92-97.

Tu, K C., 1950. Ph.D. Thesis, Department of Geology, University of Minnesota. Unpublished.

Tuominen, H. J., and Mikkola, T., 1950. Metamorphic Mg—Fe enrichment in the Orijärvi region as related to folding: Comm. géol. Finlande Bull., vol. 23, pp. 67-92.

Turner, F. J., 1930. The metamorphic and ultrabasic rocks of Lower Cascade Valley, South Westland: New Zealand Inst. Trans., vol. 61, pp. 170-201.

Tuttle, O. F., 1948. A new hydrothermal quenching apparatus: Am. Jour. Sci., vol. 246, pp. 628-635.

———, 1949. Two pressure vessels for silicate-water studies: Geol. Soc. America Bull., vol. 60, pp. 1727-1729.

Verhoogen, J., 1951. The chemical potential of a stressed solid: Am. Am. Geophys. Union Trans., vol. 32, pp. 251-258.

Walker, F., and Mathais, M., 1947. The petrology of two granite-slate contacts at Cape Town, South Africa: Geol. Soc. London Quart. Jour., vol. 102, pp. 499-521.

Wells, R. C., 1937. Analyses of rocks and minerals: U. S. Geol. Survey Bull. 878.

Winchell, A. N., 1951. Elements of optical mineralogy, Part II, John Wiley & Sons, Inc., New York.

Yoder, H. S., Jr., 1950*a*. The jadeite problem: Am. Jour. Sci., vol. 248, pp. 225-248, 312-334.

———, 1950*b*. Stability relations of grossularite: Jour. Geology, vol. 58, pp. 221-253.

———, and Weir, C. E., 1951. Change of free energy with pressure of the reaction nepheline + albite = 2 jadeite: Am. Jour. Sci., vol. 249, pp. 683-694.

Geophysical Laboratory
Carnegie Institution of Washington
Washington, D. C.